UC Davis

UC Davis Electronic Theses and Dissertations

Title

Quantum Aspects of Rotating Near-Extremal Black Holes

Permalink

https://escholarship.org/uc/item/6ck5d56d

ISBN

9798193263425

Author

Rakic, Ilija

Publication Date

2026-09-08

Peer reviewed|Thesis/dissertation

eScholarship.org Powered by the California Digital Library
University of California

Quantum Aspects of Rotating Near-Extremal Black Holes

By

ILIJA RAKIĆ
DISSERTATION

Submitted in partial satisfaction of the requirements for the degree of

DOCTOR OF PHILOSOPHY

in

Physics

in the

OFFICE OF GRADUATE STUDIES

of the

UNIVERSITY OF CALIFORNIA

DAVIS

Approved:

Mukund Rangamani, Chair

Veronika Hubeny

Jaroslav Trnka

Committee in Charge

2026

Copyright © 2026 by Ilija Rakić

All rights reserved.

To my mother, Tatjana Rakić.

Abstract

This dissertation studies various quantum aspects of near-extremal black holes, utilizing recent developments in low-dimensional models of quantum gravity and gravitational path integral techniques. In chapter 2, the one-loop determinant of metric fluctuations for the Kerr black hole is computed in its near-horizon region. The zero modes of the fluctuation operator are regulated by turning on a temperature-dependent correction to the background geometry, which leads to important low-temperature corrections to the thermodynamics of these black holes. In chapter 3, this technique is extended beyond the near-horizon region and is applied analytically to the BTZ black hole and numerically to other examples. In chapter 4, the JT gravity effective theory is used to model the process of Hawking radiation, which leads to quantum corrections to the emission spectra of near-extremal black holes. Specifically, the emission of charged radiation by the Reissner-Nordström and Kerr black holes is studied. One thread that runs through all chapters is the appearance of rotating black holes, which present their own unique challenges and tests for these techniques.

Acknowledgments

To my family and family friends - Thank you for bringing joy to my every trip home. Hvala, Djordje, Edita, Milane, Jovana, Gorane, Ivo, Dora, Ivana, Stipo, Irina, Nina, Ana, Petra, Zorane, i Zoro.

To my friends - Thank you for always being there. Hvala, Igore, Ivana, Luka (M.), Luka (V.), Marko (D.), Marko (V.), Mihajlo, Milane, Milice, Nikola, Stefane, i Vuče.

To Nada Rakić and Robert Whallon - Thank you for providing me with a home away from home. And to Nada - Thank you for always being a true friend. Hvala, Nado!

To my collaborators, Gustavo Joaquin Turiaci, Maciej Kolanowski, and Lorenzo Toni - It has been a pleasure learning from you, and a privilege discovering and creating with you.

And lastly, to my advisor, Mukund Rangamani - Thank you for the opportunities you have given me and for your patience and understanding. It has been an inspiration working with you, as you have shown me what it means to be a true physicist. I hope to carry those same principles into my future work. Thank you, Mukund.

Contents

Abstract **iii**

Acknowledgments **iv**

List of Publications **viii**

1 Introduction **1**

1.1 Thermodynamics of near-extremal black holes 2

1.2 Emission spectra of near-extremal black holes 6

1.3 Outline of dissertation 9

2 Thermodynamics of the near-extremal Kerr black hole **11**

2.1 The Kerr black hole and its extremal limit 14

2.1.1 The Kerr spacetime 15

2.1.2 A low temperature expansion 18

2.1.3 A two-dimensional perspective on the extremal limit 21

2.2 The low temperature thermodynamics 23

2.2.1 The classical action 23

2.2.2 Adding quantum effects 24

2.2.3 The extremal zero modes 26

2.2.4 Regularization of zero modes 35

2.2.5 The entropy of near-extremal Kerr 40

2.3 Generalizations 41
2.3.1 The Kerr-Newman black hole 42
2.3.2 The Kerr-AdS black hole in four dimensions 46
2.4 Discussion 48

3 Looking at near-extremal black holes from far away 55
3.1 Extending the nearly-gapless modes to the full geometry 61
3.1.1 The BTZ black hole 61
3.1.2 The hyperbolic black hole 71
3.1.3 The Reissner-Nordström (AdS) black hole 87
3.2 The role of rotational modes 111
3.2.1 Rotational modes in Kerr AdS_4 112
3.2.2 Rotational modes in Kerr-Newman 114
3.2.3 Rotational modes in the near-horizon of extremal Kerr spacetime . . 118
3.2.4 Rotational modes in BMPV 120
3.3 Low-temperature thermodynamics of the BTZ black hole 122
3.4 Discussion 128

4 Charged particle emission by near-extremal black holes 130
4.1 Emission by a Reissner-Nordström black hole 138
4.1.1 Near-extremal Reissner-Nordström background 138
4.1.2 Solving the wave equation 142
4.1.3 Semiclassical emission rate 150
4.1.4 Quantum-corrected emission rate 155
4.2 Radiation from small charged black holes 163
4.2.1 Classification of charged radiation 164
4.2.2 Neutral-like regime 170
4.2.3 Superradiant-dominated regime 174

4.3 Radiation from large charged black holes 178
4.3.1 Greybody factor from WKB theory 179
4.3.2 Wave equation with complex Delta 182
4.4 Emission by a Kerr black hole 191
4.4.1 Near-extremal Kerr Background 191
4.4.2 Wave equation and emission rate 194
4.4.3 Real Delta 201
4.4.4 Complex Delta 207
4.5 Discussion 212

5 Appendix **221**
5.1 Rotational zero mode: compensating diffeomorphism 221
5.2 Wave equation: hypergeometric and gamma functions 226
5.3 Wave equation: alternative solution using the CFT technique 227
5.3.1 Reissner-Nordström wave equation 230
5.3.2 Kerr wave equation 231
5.4 Emission rate: determining the normalization constant in the quantum rate . 231

References **235**

List of Publications

The following is a list of publications [1, 2, 3, 4] of the author at the time of writing this dissertation. Chapters two, three, and four of this dissertation are based on articles one, two, and four. The introductory sections of these articles have been rewritten - a part of them serves as the basis for the introduction of this dissertation. The remainder of the articles has mostly been left unchanged. Article three does not appear in this dissertation.

- **Ilija Rakic**, Mukund Rangamani, and Gustavo J. Turiaci. "Thermodynamics of the near-extremal Kerr spacetime". In: *JHEP* 06 (2024), p. 011. DOI: 10.1007/JHEP06(2024)011. arXiv: 2310.04532 [hep-th].

- Maciej Kolanowski, Donald Marolf, **Ilija Rakic**, Mukund Rangamani, and Gustavo J. Turiaci. "Looking at extremal black holes from very far away". In: *JHEP* 04 (2025), p. 020. DOI: 10.1007/JHEP04(2025)020. arXiv: 2409.16248 [hep-th].

- **Ilija Rakic**, and Lorenzo Toni. "One-loop determinants in AdS_3 supergravity with extended supersymmetry". In: *JHEP* 07 (2026), p. 257. DOI: 10.1007/JHEP07(2026)257. arXiv: 2508.15701 [hep-th].

- **Ilija Rakic**. "The evaporation of near-extremal black holes through charged particle emission". In: arXiv: 2512.18895 [hep-th].

Chapter 1

Introduction

A quantum theory of gravity continues to be developed after more than a half century. This time scale reflects the difficulty of this endeavor, but also represents an invitation to one of the most alluring problems in all of physics. With a lack of experimental evidence to guide this search, it has mostly been left to the imagination of the theorist.

One thread in this search, which also consists of one of the earliest attempts at obtaining this theory, is the program of quantization of gravitational fluctuations on top of a fixed curved background spacetime. Although this approach does not result in a full theory, it continues to yield important new insights into the quantum nature of gravity to this day. The indispensable tool upon which it is built is the Euclidean gravitational path integral pioneered by Gibbons and Hawking [5].

The quintessential object in General Relativity, the classical theory of gravity, is the black hole. From the early days of their study, black holes have been recognized to have a thermal nature [6] with a temperature set by their surface gravity and an entropy given by the famous Bekenstein-Hawking formula [7, 8, 9, 10] as one quarter of their horizon area in Planck units. The use of path integral methods in the study of black hole thermodynamics has led to predictions such as Hawking radiation [9, 10, 11] which was the first convincing evidence to point to an underlying quantum nature. A thermodynamic entropy further motivated

the search for a microscopic origin, which in part led to the development of holography [12, 13, 14] with its most vivid realization, the AdS/CFT correspondence [15, 16, 17, 18]. Furthermore, many puzzles were encountered, such as the Hawking information paradox [19, 20, 21] that questioned the unitarity of black hole evolution and whose recent resolution led to various refinements and corrections to the path integral formalism [22]. What is common to all of these developments and what stands as one of the motivating pillars of this field is the fundamental question of the degree to which and the sense in which a black hole can be understood as any other common quantum system.

1.1 Thermodynamics of near-extremal black holes

The central focus of this thesis is the specific class of near-extremal black holes, those with their mass near an extremal limit determined by their angular momentum and charge or, equivalently, black holes that have a low temperature. Quantum gravity research has recognized their importance only in more recent decades due to their role as a natural setting for holography. Furthermore, because quantum effects start to show up at low temperatures, they are valuable in their own right as laboratories for understanding these effects. They also possess an emergent symmetry near their horizon that allows for extra calculational convenience.

The thermodynamic description of black holes is obtained by using the gravitational path integral as follows. The metric, and possibly other fields, are broken up into a dominant background plus a small fluctuation. The action of the theory is evaluated on the background fields, i.e. "on shell", resulting in the leading order contribution to the partition function, from which the free energy and other thermodynamic quantities follow. The sub-leading quantum corrections come from the fluctuations via the well-known method of the one-loop determinant. The action is expanded to second order in the fluctuations and written in terms of a quadratic differential operator. The eigenvalue problem of this operator is solved, and

its determinant gives the one-loop corrections. This usually results in an infinite answer, and therefore a crucial final step is regularization and renormalization.

The first attempt at systematically understanding this computation for near-extremal black holes was undertaken by Sen et. al. [23, 24, 25, 26, 27]. Their analysis showed that instead of working in the full black hole spacetime, which is usually calculationally intractable, one can focus on a region near the horizon of the black hole - the near-horizon region. This region geometrically factorizes into a factor of the two-dimensional maximally symmetric AdS_2 spacetime and an internal space such as a sphere in the simplest case. The boundary of this region is determined by the black hole temperature, and beyond this boundary it smoothly connects to the surrounding spacetime. Sen et. al. showed that at low-temperature, the quantum effects are fully captured by the fluctuations in this near-horizon region. Their calculation is based on a key property of the AdS_2 spacetime, which is that it has enhanced symmetry represented by the $SL(2,\mathbb{R})$ group [28]. This extra symmetry enables the determination of the explicit eigenmodes of the quadratic fluctuation operator, which are then used to compute the one-loop determinant. Among these modes are contained a peculiar set of modes which require special treatment. These are elements of the kernel of this operator, meaning that their eigenvalue is zero, and hence they are referred to as zero modes. They are associated with Killing isometries of the black hole near-horizon geometry and are generated by large diffeomorphisms and possibly large gauge transformations (associated with for example a U(1) Maxwell gauge field). In particular, a set of modes associated with the emergent $SL(2,\mathbb{R})$ symmetry is always found. These are now referred to as the Schwarzian modes and they play an important role in the low-temperature thermodynamics. Set et. al. accounted for only a part of the contribution of the zero modes, and the rest was argued away. The fact that these are zero modes implies that they are strongly coupled, which therefore means that they needed to be given a full quantum-mechanical treatment before their full contribution could be determined.

The study of near-extremal black hole thermodynamics raised some puzzles long before

these quantum effects were calculated. One major puzzle relates to the entropy of these black holes. At extremality, meaning zero temperature, these black holes have a horizon area, which implies a non-zero entropy. For an ordinary quantum system, one would either expect a unique ground state at zero temperature, which would then imply zero entropy, or, to explain a non-zero entropy, i.e. a degenerate ground state, one would require a high amount of symmetry, which for the extremal black hole does not show up in its geometry. This puzzle and others (see, for example, [29] and [30]) were outlined in [31] where a list of assumptions was made that could resolve these puzzles, but no physical mechanism was provided. This mechanism would have to wait for the calculations of Sen et. al. [23, 24, 25, 26, 27] to be revised in more recent years.

The past decade has seen the development of an effective quantum theory of gravity, a two-dimensional dilaton-gravity theory called Jackiw-Teitelboim gravity, or JT gravity for short [32, 33, 34, 35, 36, 37]. This theory naturally emerges in the description of near-extremal black holes after dimensionally reducing the metric and possibly other higher-dimensional fields to the AdS_2 part of the near-horizon region. It describes the dynamics of a mode that physically corresponds to fluctuations of the boundary of AdS_2, and originates from the breaking of the $\mathrm{SL}(2,\mathbb{R})$ symmetry due to the geometry starting to transition to the asymptotic domain. This mode can be identified with the Schwarzian zero modes mentioned above, which are generated exactly by the diffeomorphisms that lead to fluctuations of the near horizon boundary. The mode has a coupling constant that is inverse to temperature, so it is strongly coupled near extremality. Fortunately, this theory can be quantized and solved exactly, as described and reviewed in [38]. The result turns out to be one-loop-exact [39]. The quantum fluctuations of this mode give important temperature dependent contributions to the thermodynamics of near-extremal black holes. This was first worked out for the BTZ black hole in [40], and then for the Reissner-Nordström black hole in [41]. For earlier applications to the thermodynamics of near-extremal black holes, see [42, 43, 44, 45, 46], who reproduced the leading order temperature corrections to the semiclassical thermodynamics.

Before reviewing the results of [41], we present an alternative approach to the calculation of quantum corrections, which more closely parallels the original treatment of near horizon fluctuations by Sen et. al. [23, 24, 25, 26, 27]. In more recent years, a more direct and general computation has been performed by [47], which does not rely on dimensional reduction but instead evaluates the gravitational path integral directly in the higher-dimensional spacetime as follows. The near horizon region is not taken to be extremal, but instead a small temperature-dependent correction is added to the geometry, which is derived from the original full black hole geometry. This acts as an IR regulator for the aforementioned Schwarzian and other zero modes, promoting their eigenvalue from zero to a non-zero temperature-dependent value and enabling an estimate of their contribution to the one-loop determinant.

Both the two-dimensional JT gravity approach and the higher-dimensional temperature-corrected near-horizon approach result in the same one-loop determinant for all near-extremal black holes to which they have both been applied. From this a clean prediction can be made for the low-temperature thermodynamics to one-loop order. We quote here the general result for specifically the entropy to summarize the origin of the various terms

$$S = S_0 + c_{\rm cl}\, r_+\, T + c_{\rm q}\, \log S_0 + \frac{3}{2}\, \log \frac{T}{T_q}\,. \tag{1.1}$$

The first two terms are obtained from the classical geometry through the Bekenstein-Hawking formula. S_0 is the naive extremal entropy, i.e. what the entropy would have been if extremality could be reached. The linear in T term is its lowest order near-extremal correction, with r_+ being the radial position of the horizon, which makes $r_+\, T$ unitless, and $c_{\rm cl}$ being a unitless number that depends on the type of black hole, i.e. how much mass, charge and angular momentum it has. The logarithmic correction in S_0 arises from the one-loop determinant of gravitons and other matter fields fluctuating around the black hole, with the coefficient $c_{\rm q}$ depending on the type of black hole and the exact matter content - these are the corrections that were obtained by Sen et. al. [23, 24, 25, 26, 27]. Finally, the $\log T$ corrections come from

the earlier-unaccounted zero mode contribution. The famous $\frac{3}{2}$ coefficient comes specifically from the Schwarzian modes. Other zero modes can also contribute, resulting in a different numerical factor. The quantum temperature scale T_q is an emergent IR scale that sets the temperature below which these quantum zero mode corrections become important.

As explained in [41], this provides a resolution to the decades-old puzzle mentioned earlier with the desired upshot: equation (1.1) implies that at low enough temperatures, the ground state degeneracy is removed in the absence of an underlying symmetry principle. This implies that near-extremal black holes behave rather as ordinary quantum systems, providing affirmative evidence for the fundamental question of their quantum nature raised at the beginning. If their temperature is taken to be too low, non-perturbatively small in the extremal entropy, then the entropy becomes negative, signaling that equation (1.1) is not the end of the story[1].

1.2 Emission spectra of near-extremal black holes

Another sense in which black holes behave as ordinary matter is that they radiate field quanta as shown by Hawking [9, 10]. As a result, they lose energy and possibly charge and angular momentum. It also turns out that through this emission process they eventually evaporate, i.e. they have a finite lifetime determined by the rate at which they radiate.

Their emission spectrum is such as that of a black-body up to a frequency-dependent term called the greybody factor. This factor is found by solving the problem of scattering the field in question against the black hole background. This was done for the Reissner-Nordström charged black hole emitting charged scalar radiation by Gibbons in [51]. For the Kerr rotating black hole, the scattering problem involving a scalar field was solved by Starobinskii [52] in the context of classical wave scattering and was later extended to electromagnetic and gravitational radiation [53] (this work was based on the analysis of fields with spin in the Kerr background by Press & Teukolsky in [54, 55, 56]). The analytical results in these works

[1] A possible resolution to this issue is to interpret equation (1.1) as an ensemble average - see [48, 49, 50].

were performed under various approximation conditions on the black hole and radiation parameters, but were subsequently extended numerically to the full range of parameters in a series of papers by Page [57, 58, 59], which resulted in the first attempt at a full evaporation history of these black holes based on the field content of our Universe.

Recent work [60], which analyzed the spectra of neutral radiation, has shown that there is more to this story for near-extremal black holes (for earlier work, see [61], and for extensions to supergravity, see [62]). Their work uses the effective JT gravity theory in the near horizon region to model the process of Hawking radiation. If the theory is coupled to other fields in the 4D, then dimensional reduction gives rise to additional matter fields in the 2D in addition to the strongly coupled Schwarzian mode that dominates at low temperature. The interaction of the Schwarzian mode with the other 2D matter fields gives corrections to processes such as the decay of the black hole through emission of field quanta, the scattering of fields by the black hole, and others. Using this effective theory, [60] worked out the quantum-corrected emission spectra and resulting evaporation rates of near-extremal Reissner-Nordström for the most dominant modes of the neutral scalar, and the electromagnetic and gravitational fields. It was found that these rates are different from the semi-classical ones predicted by Hawking's theory. In a low energy regime, the quantum evaporation rates are suppressed compared to the semi-classical ones, while at energies beyond this regime, it was shown that the quantum rates reduce to the semi-classical ones.

Computing the evaporation rate for these neutral radiation fields using the effective theory involves input from the same wave scattering problem used to compute the greybody factors for the semi-classical rate, and therefore we will refer to this as the wave method. For charged radiation being emitted by a large black hole (large compared to the charge and mass of the particle being emitted), one can employ a completely different technique for computing the rate, which we will refer to as the instanton method. The decay rate to a lower energy state through the emission of a charged particle-antiparticle pair involves finding a geometry called the instanton and comparing it to the original black hole geometry [63, 64, 65]. This results in

an exponentially suppressed decay rate, analogous to the Schwinger rate for pair production in a strong electric field [66]. It was shown in [60] that adding quantum corrections coming from the Schwarzian mode to the black hole and instanton geometries does not change the decay rate, implying that it is fully captured by the original theory.

These rates (corrected for neutral and unchanged for charged) were then used by [60] to give an evaporation history of the large black hole, different from the one based on the semi-classical Hawking rates. The story goes as follows. A black hole in our Universe emits quanta of all of these fields, with the neutral quanta being the photon and graviton, and the charged quanta being the electron or positron. All higher mass fields can safely be ignored for black holes at low temperatures, because their rates are suppressed due to their higher mass. Since the electron emission rate is highly suppressed, most of the radiation being emitted is neutral, and this causes the black hole to lose energy, and drives it closer to the extremal mass. Eventually, the black hole enters the low-energy quantum regime, and the neutral rates become small, smaller than predicted by the semi-classical theory. Every once in a while, on time scales of order the exponentially suppressed electron emission rate, the electron is emitted carrying both energy and charge. Since the extremal mass bound for the charged black hole is determined by its charge, when the electron is emitted, both the mass and the bound are lowered. It was shown that in this process more charge is carried away than mass, meaning that the black hole moves away from the extremal bound. In fact, this disparity is large enough that the black hole is launched out of the quantum regime. From this point onward, the story repeats itself until all of the charge is exhausted. Since the charged particle rate is unaffected by the corrections from the quantum effective theory, it takes the same amount of time for the black hole to emit all of its charge, but once it reaches that point, it will have emitted less energy (through neutral radiation) than the semi-classical theory would have predicted. Therefore, the lifetime of the black hole is longer, as there is more mass left over to be radiated. This also implies that the black hole spends a larger fraction of its lifetime in the near-extremal regime than the semi-classical theory would have predicted.

These developments motivate the question of whether the same wave method treatment can be given to charged radiation that is not large, i.e. where the instanton method would fail, and whether this would lead to novel quantum corrections in the spectrum of charged radiation, which would further imply a different evaporation history for a black hole emitting that radiation.

1.3 Outline of dissertation

One goal of this dissertation, which will be treated in Chapters 2 and 3, is to compute the low-temperature corrections of other examples of near-extremal black holes using the higher-dimensional gravitational path integral technique and to further develop this technique, i.e. to extend it beyond the near-horizon region. Another goal, treated in Chapter 4, will be to go beyond thermodynamics and to apply the JT gravity effective theory to the study of the emission spectra of Hawking radiation. One major theme common to all chapters is the study of rotating black holes, which offer less symmetry than those treated thus far in the literature, requiring extra calculational care. At the same time, this makes them a more stringent test for the techniques outlined above. We proceed to give more details of the contents of each chapter and briefly describe the results that are attained.

In Chapter 2, we go beyond the spherically symmetric Reissner-Nordström and extend the analysis to the Kerr spacetime, the simplest non-spherical black hole in vacuum Einstein gravity. Although, its near horizon region possesses extra $\mathrm{SL}(2,\mathbb{R})$ symmetry, the near-horizon region does not exactly factorize into AdS_2 and a compact internal space as in the case of spherically symmetric backgrounds, and thus dimensional reduction and the JT gravity method cannot be cleanly used, which calls for the 4D gravitational path integral technique. This results in equation (1.1) for the Kerr spacetime. This chapter is based on [1].

The success of the 4D path integral technique in the near-horizon region motivates the search for the zero modes in the full 4D spacetime. In chapter 3, we identify among the

eigenspectrum of the quadratic fluctuation operator in the full spacetime, modes which we argue correspond to the Schwarzian zero modes encountered in the near-horizon geometry, as they contribute a factor of $T^{\frac{3}{2}}$ to the one-loop determinant universally. Due to the lack of $\mathrm{SL}(2,\mathbb{R})$ in the full geometry, we do not expect these to be zero modes, which we confirm, but they have the property that their eigenvalues scale linearly with the regulating temperature, implying that they reduce to zero at extremality. Furthermore, we find that they have the property that their support descends into the near-horizon throat as extremality is approached. This computation is done analytically for the BTZ black hole and numerically for other examples. This chapter is based on [2].

In chapter 4, we turn to an application of the JT gravity effective theory in the description of black hole Hawking radiation. The quantum-corrected emission spectra were worked out for neutral radiation by [60] for the Reissner-Nordström spacetime. We extend this analysis to charged radiation. One motivation is to unite the two approaches discussed above, the wave and instanton methods. Another is to generalize this to the Kerr black, where field modes with angular momentum can be thought of as being charged, due to the similarities between charged modes and modes with angular momentum in the 2D near horizon region. This chapter is based on [4].

Given that the chapters deal with fairly different topics, we leave a discussion and summary of the obtained results to the individual chapters, where we also point out possible future directions in which they can be taken. Finally, the dissertation ends with chapter 5, where the appendices to the previous chapters are collected. These involve calculations that are either too heavy or not too relevant to the main development in the chapters. Their exact content is summarized in their corresponding chapters.

Chapter 2

Thermodynamics of the near-extremal Kerr black hole

In this chapter, we perform an analysis of the near horizon fluctuations of the near-extremal Kerr spacetime with the goal of obtaining low-temperature corrections to its thermodynamics, i.e. deriving equation (1.1) for the Kerr spacetime[1]. There are two broad reasons for attempting this exercise:

- At a technical level, one can use the Kerr solution to test the general principles away from the spherically symmetric situation[2]. Although the dimensional reduction to JT gravity continues to apply at the classical level [46], there are complications arising from the reduced symmetry. For one, the dimensional reduction to AdS_2 is not quite natural, as the near horizon region of the Kerr spacetime, the NHEK of [70], includes an AdS_2 that is warped and fibered over a compact base space. For another, the low temperature corrections to the near-horizon region are complicated to describe in this language. We therefore seek a direct computation of the quantum corrections, without relying directly

[1]The analysis of quantum effects in the near-extremal Kerr geometry was also undertaken in [67], concurrently with [1]. See also [68] for a subsequent analysis in higher dimensions.

[2]A situation without spherical symmetry was considered in [69], where it is assumed, based on symmetry arguments, that the low energy behavior is described by a Schwarzian mode, even though it was not derived from first principles.

on the connection to JT gravity used by [40, 41, 71].

- The extremal Kerr entropy has been argued to be captured by a 2d chiral CFT, per the Kerr/CFT correspondence [72]. The near-extremal thermodynamics was analyzed in [73] and the developments in this area are reviewed in [74]. The logic here was to leverage the near-horizon geometry of extreme Kerr spacetime [70], which has a $\mathrm{SL}(2,\mathbb{R})\times\mathrm{U}(1)$ isometry. By exploiting a particular set of large diffeomorphism modes, determined by suitable fall-off conditions, an asymptotic Virasoro algebra emerges from the diffeomorphisms of the azimuthal circle. The central charge is fixed by the black hole's angular momentum, and the extremal entropy is reproduced by the Cardy formula. The status of this approach deserves to be investigated in light of recent developments.

To contextualize our discussion, we start by recalling the first attempt at systematically understanding the semiclassical quantum corrections around an extremal Kerr black hole in pure Einstein-Hilbert gravity by [27], who argued that the quantum corrected entropy of this black hole, with no additional matter degrees of freedom, is given by

$$S = \frac{A}{4\,G_N} + \frac{64}{180}\,\log\frac{A}{4\,G_N}\,. \tag{2.1}$$

The logarithmic correction arises from the one-loop determinant of gravitons around the semiclassical black hole saddle.[3]

To compute the logarithmic in temperature corrections to (2.1), we use the second, more general approach outlined in the introduction and inspired by [47][4], where the zero mode gravitational path integral is evaluated after a small non-vanishing temperature correction is added to the near horizon geometry, which generates a non-vanishing action for these zero

[3]One can analogously extract the leading correction for non-extremal black holes [75], obtaining instead $\frac{334}{180}\log A$. The two calculations do not have to agree on the coefficient of the $\log A$ term, as the near-extremal calculation is an asymptotic expansion at small temperatures (in the appropriate ensemble). A comparison with the non-extremal calculation would require a resummation of perturbative corrections in the temperature.

[4]Which is somewhat akin to the recent discussion of [76] who undertake a similar exercise in the spherically symmetric context

modes, enabling a clean estimate of their contribution to the determinant.

The zero modes in question were identified by [27] and are associated with two sets of large diffeomorphisms that respect the near-AdS_2 asymptotics: one set of zero modes corresponds to the Schwarzian dynamics of the AdS_2 asymptopia, and the other set to the fluctuations of the black hole angular velocity. This can be motivated by dimensional reduction along the deformed two-sphere; the former modes correspond to gravitational fluctuations in AdS_2, while the latter is a zero mode of the U(1) Maxwell field, coming from the four-dimensional metric, obtained in the reduction.

The method of [47] requires us to work directly in the NHEK geometry. Doing so, and examining the eigenspace of the spin-2 fluctuation operator (with a harmonic gauge fixing term), we are only able to identify the Schwarzian zero modes. The other mode, the rotational zero mode, whose form can be guessed from its physical effect, we find to be singular.[5] This poses an interesting puzzle, impacting the analysis of semi-classical corrections to rotating black hole thermodynamics.

Accounting for the Schwarzian modes alone as the only zero modes leads to the following result for the near-extremal entropy. In the canonical ensemble with fixed angular momentum we find

$$S = S_0 + 4\pi^2 \frac{T}{T_q} + \frac{154}{180} \log S_0 + \frac{3}{2} \log \frac{T}{T_q} \,. \tag{2.2}$$

Here $S_0 = \frac{A_0}{4G_N}$ is the naive extremal entropy,[6] and T_q is the emergent scale in the IR coming from the Schwarzian dynamics. The $\frac{3}{2} \log T$ term confirms a naive application of the general philosophy of [41]. The discrepancy in the $\log S_0$ term relative to (2.1) is due to our only being able to identify the Schwarzian zero modes. We have chosen to present the result

[5]The spectrum of fluctuations about the NHEK geometry was carefully analyzed in [77, 78]. However, these works focus on physical spin-2 fluctuations, which are best analyzed in terms of gauge-invariant degrees of freedom (the Teukolsky scalars adapted to the near-horizon). These gauge-invariant fields, however, do not capture the full set of large diffeomorphisms, which must be analyzed separately (for an illustration see Appendix E of [79]).

[6]While it is helpful to view the result in terms of the entropy, note that the more natural presentation is directly in terms of the partition function, where it is clear that the result has to break down at very low temperatures owing to competition from other saddle point configurations.

consistent with what we are able to conclusively establish in this chapter. In the course of our analysis, we explain how the zero mode contribution affects the logarithmic corrections, and elucidate the sensitivity on the ensemble choice. Finally, the result (2.2) applies to four dimensional pure gravity, but it is easy to incorporate light matter fields in the evaluation of the quantum corrections; they only affect the coefficient of the $\log S_0$ term and not the temperature dependence.

In the next chapter, we will show that the harmonic gauge is always problematic when studying quantum effects on a Ricci-flat background. In non-Ricci flat rotating black holes, e.g, Kerr-Newman and Kerr-AdS black holes, we indeed find rotational zero-modes. The problem for Kerr black holes in flat space persists (since it is the only of these geometries that is Ricci flat).

Outline of the chapter: We review the geometry and the classical thermodynamics of the Kerr black hole in section 2.1. In particular, we emphasize the choice of ensemble we use, as this will be crucial in ascertaining the low temperature corrections. Following this in section 2.1.2 we describe the geometry at low temperatures holding the angular momentum fixed. In section 2.2, using the Gibbons-Hawking on-shell prescription, we review how the classical thermodynamics is derived. We then calculate in the near-horizon region and present our central result for the quantum corrections to the Kerr black hole low temperature thermodynamics. In section 2.3 we generalize our results to other rotating black holes in four dimensions. Finally, we conclude in section 2.4 with a broader discussion, focusing on the puzzles associated with the rotational zero modes, interpretation á la the Kerr/CFT correspondence, etc., and outline some future directions for further investigation.

2.1 The Kerr black hole and its extremal limit

We begin with a brief review of some basic features of the classical thermodynamics of Kerr black holes, primarily to set our conventions. We will work with the simplest gravitational

dynamics dictated by the Einstein-Hilbert action. In Euclidean signature, relevant for the evaluation of the gravitational path integral that computes the black hole free energy, the action is given by

$$I_{\text{EH}} = -\frac{1}{16\pi G_N}\left[\int_{\mathcal{M}} \mathrm{d}^4x\,\sqrt{g}R + 2\int_{\partial\mathcal{M}} \mathrm{d}^3x\,\sqrt{\gamma}\,K\right]. \tag{2.3}$$

In addition to the bulk Einstein-Hilbert action, we have included the Gibbons-Hawking-York (GHY) boundary term. This is required when imposing Dirichlet boundary conditions on the metric (we will consider other boundary conditions, whence this boundary term will be appropriately modified). One can add to this action contributions from minimally coupled matter fields. As we are going to study only geometric backgrounds, such matter fields will not affect the classical thermodynamics.

2.1.1 The Kerr spacetime

The general stationary axisymmetric black hole solution with a Killing horizon, is the Kerr black hole. The geometry has a non-vanishing ADM mass and angular momentum. In Boyer-Lindquist coordinates it is given by

$$\mathrm{d}s^2 = -\frac{\rho^2\Delta}{\Xi}\,\mathrm{d}t^2 + \frac{\rho^2}{\Delta}\,\mathrm{d}r^2 + \rho^2\,\mathrm{d}\theta^2 + \frac{\Xi}{\rho^2}\,\sin^2\theta\left(\mathrm{d}\varphi - \frac{2\,m\,a\,r}{\Xi}\,\mathrm{d}t\right)^2, \tag{2.4}$$

with

$$\rho^2 = r^2 + a^2\cos^2\theta\,, \qquad \Delta = r^2 - 2mr + a^2\,, \qquad \Xi = (r^2+a^2)^2 - a^2\Delta\,\sin^2\theta\,. \tag{2.5}$$

The coordinates (θ,φ) parametrize a space that is topologically a sphere – we have $\theta\in[0,\pi]$ while $\varphi\sim\varphi+2\pi$. The Euclidean geometry is obtained by Wick rotation $t\to -\mathrm{i}t_{\text{E}}$ and

keeping $a \in \mathbb{R}$.[7] The metric is asymptotically flat since at large r it approaches the Minkowski line element, with suitable subleading corrections.

To fully specify the boundary conditions, we need to decide a range for Euclidean time. Fixing temperature and angular velocity corresponds to the following identification

$$(t_{\text{E}}, \varphi) \sim (t_{\text{E}} + \beta, \varphi + \mathrm{i}\beta\Omega) \sim (t_{\text{E}}, \varphi + 2\pi). \tag{2.6}$$

These boundary conditions fix the asymptotic metric, and the variational problem is well-defined with the GHY boundary term. As we will see later, fixing the angular momentum J requires a different choice of boundary terms.

The relation between the thermodynamic data $\{T, \Omega\}$ and the parameters $\{m, a\}$ specifying the solution can be determined directly from the geometry. The radius of the outer horizon (i.e., the largest root of Δ) is given by

$$r_+ = m + \sqrt{m^2 - a^2}. \tag{2.7}$$

The Euclidean path integral requires a smooth geometry. At the horizon radius $r = r_+$, a combination of thermal and spatial circles becomes contractible. The resulting geometry has to be capped off smoothly, which fixes r_+ and a in terms of the thermodynamic potentials.

Expanding the line element close to the horizon using $r = r_+ + \frac{(r_+^2 - a^2)\varepsilon^2}{4r_+(r_+^2 + a^2\cos^2\theta)}$, for small ε, we find the metric

$$\mathrm{d}s^2 = -\frac{(a^2 - r_+^2)^2\varepsilon^2\mathrm{d}t^2}{4r_+^2(a^2 + r_+^2)^2} + \mathrm{d}\varepsilon^2 + (r_+^2 + a^2\cos^2\theta)\mathrm{d}\theta^2 + \frac{(a^2 + r_+^2)^2\sin^2\theta}{r_+^2 + a^2\cos^2\theta}(\mathrm{d}\varphi - \frac{a}{r_+^2 + a^2}\mathrm{d}t)^2 + \cdots, \tag{2.8}$$

where the ellipses indicate terms in the metric that are subleading in the near-horizon expansion. The smoothness at the poles of the sphere is guaranteed if we define $\widetilde{\varphi} = \varphi - \frac{a}{r_+^2 + a^2}\mathrm{d}t$ and periodically identify $\widetilde{\varphi} \sim \widetilde{\varphi} + 2\pi$. Working at θ and $\widetilde{\varphi}$ the thermal circle contracts at

[7] Thus, the Euclidean metric we have has a complex line element, which is indeed the correct saddle for the problem, cf. [80].

the horizon without a conical singularity when the Euclidean time is periodically identified, determining the temperature to be

$$T = \frac{r_+^2 - a^2}{4\pi\, r_+\, (a^2 + r_+^2)} = \frac{r_+ - m}{4\pi\, m\, r_+}\,. \tag{2.9}$$

The coordinate identifications are $(t_{\scriptscriptstyle \rm E}, \widetilde{\varphi}) \sim (t_{\scriptscriptstyle \rm E} + \beta, \widetilde{\varphi})$. Reverting to the original coordinates this translates into $(t_{\scriptscriptstyle \rm E}, \varphi) \sim (t_{\scriptscriptstyle \rm E} + \beta, \varphi + \mathrm{i}\frac{a}{r_+^2 + a^2}\beta)$, which determines the angular velocity

$$\Omega = \frac{a}{r_+^2 + a^2} = \frac{a}{2\, m\, r_+}. \tag{2.10}$$

Finally, the ADM mass and angular momentum evaluated for the Kerr metric (2.4) are given by

$$M = \frac{m}{G_N}, \qquad J = \frac{m\, a}{G_N}\,. \tag{2.11}$$

Ensemble choices: The action (2.3) evaluated on the Kerr black hole with Dirichlet boundary conditions satisfies the quantum statistical relation

$$I_{\scriptscriptstyle \rm EH} = -S + \beta\, M + \beta\, \Omega\, J\,, \tag{2.12}$$

where the Bekenstein-Hawking entropy is given by the familiar formula

$$S = \frac{A}{4G_N} = \frac{2\pi\, m\, r_+}{G_N}\,. \tag{2.13}$$

From this expression we can derive the thermodynamic interpretation of the quantities appearing in the r.h.s. of (2.12). This describes the physics in the grand canonical ensemble, holding β and Ω fixed, and letting r_+ (or equivalently m) and a to be adjusted accordingly. In this ensemble, the macroscopic charges M and J, are derived quantities and can fluctuate.

In the rest of this chapter, we will work instead in an ensemble of fixed angular momentum. The importance of being explicit with the choice of ensemble can be made clear by reviewing

the coordinate identifications. Recall that our the boundary conditions are specified by the identification (2.6). This implies that $\mathrm{i}\beta\Omega$ is only defined modulo 2π in a theory without fermions, and modulo 4π in a theory with fermions. The Kerr black hole solution, however, does not respect this symmetry. The resolution is that, when working at fixed angular velocity, there is actually an infinite family of solutions related by $\mathrm{i}\beta\Omega \to \mathrm{i}\beta\Omega + 2\pi\mathbb{Z}$ (for a theory without fermions) or $\mathrm{i}\beta\Omega \to \mathrm{i}\beta\Omega + 4\pi\mathbb{Z}$ (for a theory with fermions). These are genuinely different saddles with the same boundary conditions and should all be included in the evaluation of the partition function, as emphasized in [81].

In an ensemble of fixed J, the canonical ensemble, this issue does not appear (there is a similar sum over saddles with the only effect of imposing the restriction that $2J \in \mathbb{Z}$). At the level of the classical analysis, the canonical ensemble requires a different boundary term in (2.3) which we specify later. Its effect will essentially be to remove the $\beta\,\Omega\,J$ term on the r.h.s of (2.12).

2.1.2 A low temperature expansion

Let us examine the low temperature behavior of the Kerr black hole at fixed angular momentum J. We will take $J > 0$ for concreteness. To simplify some expressions below, we introduce

$$\mathsf{J} = \sqrt{G_N\, J}\,, \qquad \mathsf{T} = 2\pi T. \tag{2.14}$$

From (2.7) and (2.9) in the extremal limit the mass and entropy are given by

$$M_0 = \frac{\mathsf{J}}{G_N}\,, \qquad S_0 = \frac{2\pi \mathsf{J}^2}{G_N}. \tag{2.15}$$

Here and henceforth, we adhere to the convention that the extremal values are indicated by a subscript '0'. At non-vanishing temperature the mass and entropy receive corrections,

$$\begin{aligned} M &= \frac{\mathsf{J}}{G_N} + \frac{\mathsf{J}^3}{G_N}\,\mathsf{T}^2 + \cdots\,, \\ S &= \frac{2\pi\,\mathsf{J}^2}{G_N} + \frac{4\pi\,\mathsf{J}^3}{G_N}\,\mathsf{T} + \cdots\,. \end{aligned} \tag{2.16}$$

The ellipses indicate higher-order terms suppressed by additional factors of JT. The temperature dependence of the leading correction to the extremal entropy and energy is quite universal. In particular, the fact that the mass approaches the extremal value quadratically leads precisely to the breakdown of the statistical mechanical interpretation of the black hole pointed out in [29]. More precisely, at low enough temperatures, the excitation energy of the black hole above extremality becomes comparable to the average energy of a Hawking quantum. This happens at a temperature scale

$$T_q = \frac{G_N}{2\,\mathsf{J}^3} \quad\Longrightarrow\quad \mathsf{T}_q = \frac{\pi\,G_N}{\mathsf{J}^3}. \tag{2.17}$$

For temperatures $\mathsf{T} \gg \mathsf{T}_q$, the classical picture of the black hole is correct. At low temperatures $\mathsf{T} \sim \mathsf{T}_q$, quantum effects near the horizon become important, and the thermodynamic behavior has to be revisited. This will be the focus of the rest of the article.

A different perspective on the results (2.16) can be obtained by looking at the Kerr geometry near-extremality. It is convenient to parametrize the coordinates by

$$r = r_+ + 2\,\mathsf{J}^2\mathsf{T}(\cosh\rho - 1)\,, \qquad \tau = \frac{t_{\scriptscriptstyle \mathrm{E}}}{\mathsf{T}}\,. \tag{2.18}$$

To leading order in $\mathsf{T} \to 0$ and keeping ρ fixed, we obtain the NHEK geometry [70]

$$\mathrm{d}s_0^2 = (1+\cos^2\theta)\mathsf{J}^2\left[\mathrm{d}\rho^2 + \sinh^2\rho\,\mathrm{d}\tau^2 + \mathrm{d}\theta^2\right] + \frac{4\,\mathsf{J}^2\,\sin^2\theta}{1+\cos^2\theta}(\mathrm{d}\varphi + \mathrm{i}(\cosh\rho - 1)\,\mathrm{d}\tau)^2\,. \tag{2.19}$$

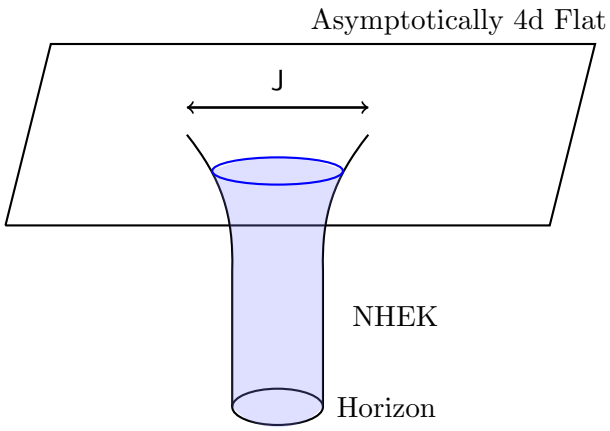


Figure 2.1: A sketch of a spatial slice of the near-extremal Kerr black hole. The blue region is well approximated by the NHEK metric for low enough temperatures. Far from the horizon, the approximation breaks down and the metric transitions to the asymptotically flat extremal Kerr geometry.

Importantly, this is a fibration of AdS_2 over $\mathbf{S}^2$. This is an exact solution of Einstein's equation [70] but gets corrections of order JT coming from the full Kerr metric.

From this perspective, the result (2.16) arises from studying the breaking of the symmetries AdS_2, deforming it by an irrelevant operator to connect to the asymptotically flat region. In fact, a quantum mechanical theory with an emergent conformal symmetry broken by finite temperature effects is described by the Schwarzian theory; it leads to the behavior (2.16). At the classical level, the connection between the near-extremal Kerr black hole and the Schwarzian theory was analyzed in [46]. We will justify the connection at the quantum level.

It will be convenient to introduce another radial coordinate y related to ρ by $y = \cosh\rho$. In these coordinates, the NHEK metric becomes

$$\mathrm{d}s_0^2 = (1+\cos^2\theta)\mathsf{J}^2\left[(y^2-1)\mathrm{d}\tau^2 + \frac{\mathrm{d}y^2}{y^2-1} + \mathrm{d}\theta^2\right] + \frac{4\,\mathsf{J}^2\,\sin^2\theta}{1+\cos^2\theta}(\mathrm{d}\varphi + \mathrm{i}(y-1)\mathrm{d}\tau)^2\,. \quad (2.20)$$

In the rest of the article we will go between (2.19) and (2.20) depending on which form is most convenient.

The NHEK geometry is obtained by keeping the radial coordinate ρ (or equivalently

y) fixed in the low temperature limit, and the conformal boundary of AdS_2 is located at $\rho = \infty$. When analyzing quantum effects, it is important to work at a small but non-vanishing temperature. In this case, the approximations behind the NHEK geometry break down at $\rho_c \sim -\log(\mathsf{T})$ before reaching the conformal boundary of AdS_2. When $\rho \sim \rho_c$ the near horizon geometry transitions to the extremal asymptotically flat Kerr metric. This behaviour is illustrated in fig. 2.1.

2.1.3 A two-dimensional perspective on the extremal limit

For completeness, and to connect with the Schwarzian dynamics alluded to above, it is useful to recast the near-horizon solution in two-dimensional terms. Focus first on the following metric ansatz

$$\mathrm{d}s^2 = \frac{1+\cos^2\theta}{2\Phi}\, g_{\mu\nu}\mathrm{d}x^\mu \mathrm{d}x^\nu + \frac{1+\cos^2\theta}{2}\Phi^2 \mathrm{d}\theta^2 + \Phi^2 \frac{2\sin^2\theta}{1+\cos^2\theta}(\mathrm{d}\varphi - \mathrm{i}A)^2. \tag{2.21}$$

Here $x^\mu = (\tau, \rho)$ and $g_{\mu\nu}$ is a two-dimensional metric along these directions alone. The 'dilaton' $\Phi(\tau,\rho)$, the one-form $A = A_\mu \mathrm{d}x^\mu$ specifying a U(1) connection, and the metric $g_{\mu\nu}$ depend only on time and radial coordinates. The dependence on the polar coordinate θ is fixed by the ansatz, and ∂_φ is a Killing field.

The four dimensional Einstein-Hilbert action can be reduced to a two-dimensional dynamical system along τ and y. Focus, in particular, on the fields, appearing in (2.21).[8] The two-dimensional metric, dilaton and gauge field have their dynamics specified by

$$I_{\text{EH}} = -\frac{1}{4}\int_{\mathcal{M}_2} \mathrm{d}^2x\,\sqrt{g}\left[\Phi^2\, R + \frac{1}{\Phi} + \frac{1}{2}\Phi^5\, F^2\right] - \frac{1}{2}\int_{\partial\mathcal{M}_2} \sqrt{h}\,\Phi^2 K. \tag{2.22}$$

This is a two-dimensional dilaton-gravity theory with a particular dilaton potential. The boundary term corresponds to fixing the boundary two-dimensional metric and U(1) gauge

[8] Any mode that does not fall in this category, can be viewed as a matter field in two dimensions, as long as they respect the polar angle dependence specified by the ansatz. This issue will be important in the sequel.

connection.

It is easy to verify that the NHEK line element (2.20) is a solution of (2.22), with the two-dimensional metric reducing to the constant negative curvature metric on AdS_2, viz.,

$$g^{(0)}_{\mu\nu}\mathrm{d}x^\mu \mathrm{d}x^\nu = \Phi_0^{3/2}(\mathrm{d}\rho^2 + \sinh^2\rho\,\mathrm{d}\tau^2)\,. \tag{2.23}$$

The dilaton is constant $\Phi_0 = 2\mathsf{J}^2$ and the U(1) connection is a left-invariant one-form on AdS_2

$$A^{(0)} = -(\cosh\rho - 1)\,\mathrm{d}\tau. \tag{2.24}$$

The two-dimensional perspective is useful to define more precisely what we mean by a fixed angular momentum ensemble, at least in the NHEK region. The angular momentum is proportional to the conserved charge that couples to the U(1) gauge field A. Fixing the angular momentum is then equivalent to fixing the charge of the gauge field at the boundary. To make the variational problem of the action (2.22) well-defined, it is necessary to add a new boundary term given by

$$I_{\text{EH}} \to I_{\text{EH}} + \frac{1}{2}\int_{\partial\mathcal{M}_2} \sqrt{h}\, n^\mu\, \Phi^5\, F_{\mu\nu}A^\nu\,, \tag{2.25}$$

where n^μ is a normal to the two-dimensional boundary and h the induced metric. One can verify that in the NHEK solution this term is precisely $\beta\Omega J$. Upon integrating over the boundary holonomy it implements the Legendre transform required to go to fixed charge ensemble. This boundary term can be directly written in four dimensional language using the results from [82].

2.2 The low temperature thermodynamics

2.2.1 The classical action

We start by evaluating the classical contribution to the thermodynamics of the Kerr black hole. Following [5], we compute the on-shell action for the Kerr solution (2.4). Since this geometry is Ricci flat, there is no bulk contribution to the action. Therefore, all the information is in the Gibbons-Hawking-York term evaluated on the boundary cut-off surface. One finds

$$\begin{aligned} K &= \frac{1}{2\sqrt{\Delta}\,\rho^3}\,\frac{\mathrm{d}}{\mathrm{d}r}\big(\rho^2\,\Delta\big) = \frac{2}{r} - \frac{M}{r^2} + \cdots\,, \\ \sqrt{\gamma} &= \sin\theta\,\sqrt{\Delta}\,\rho\,. \end{aligned} \tag{2.26}$$

Rather than include counterterms in the asymptotically flat region, we perform a background subtraction, and evaluate

$$I_{\text{EH,on-shell}} = -\frac{2}{16\pi\,G_N}\int_0^\beta \mathrm{d}t\int_0^\pi \mathrm{d}\theta\int_0^{2\pi}\mathrm{d}\phi\,\sqrt{\gamma}\,[K-K_0] \tag{2.27}$$

where K_0 is the extrinsic curvature trace for the solution with $M=0$ (flat space). This procedure leads to a finite result for the grand canonical free energy G

$$\mathcal{Z}[\beta,\Omega] = e^{-\beta\,G} = e^{-I_{\text{EH,on-shell}}}\,, \qquad I_{\text{EH,on-shell}} = \frac{M\,\beta}{2\,G_N}\,. \tag{2.28}$$

The canonical free energy F in turn is obtained by a Legendre transform

$$F = G - \Omega\,J = \frac{r_+ - M}{2\,G_N}\,. \tag{2.29}$$

As a sanity check note that as $a\to 0$, $r_+\to 2\,M$ and we obtain correctly the Schwarzschild free energy. Since this calculation is valid for a generic Kerr black hole, we can easily evaluate the near-extremal result simply by expanding (2.29) for small T using our parameterization

in (2.58) to find

$$F = \frac{\mathsf{J}^2\,\mathsf{T}}{2\,G_N}(1 + \mathsf{J}\,\mathsf{T} + \cdots)\,. \tag{2.30}$$

We note in passing that the grand canonical free energy also has a sensible low T expansion, since $G \propto M$.

This calculation was performed in the full Kerr solution (2.4) retaining the asymptotically flat region. An alternative route consists of zooming into the near-horizon region and performing the calculation there. We describe this calculation in 2.2.4 after we introduce the low-temperature corrections to the near-horizon region.

2.2.2 Adding quantum effects

We now turn to the evaluation of quantum corrections to the black hole entropy of the (near) extremal Kerr black hole. In order to do so, we will follow Sen and focus on the path integral in the near horizon region (see [26] for a nice presentation for the case of charged black holes). We shall begin our analysis by considering the zero temperature $\mathsf{T} = 0$ black hole, and subsequently incorporate temperature corrections.

Let us focus on the near-horizon NHEK geometry (2.20) of the extremal Kerr spacetime. The quantum effects we want to compute are captured by the one-loop determinant of the graviton and matter fields around this background geometry.

We begin by explaining the general strategy to compute the quantum corrections around this (or any) geometry. Let $x = (\tau, y, \theta, \varphi)$ denote the four dimensional coordinates. The one-loop determinant may be evaluated by expanding the metric fluctuations (or those of other matter fields) in a complete orthonormal basis of normalizable modes $f_n^{(i)}(x)$. Here i runs over a complete set of degrees of freedom at each spacetime point.

Consider then the heat kernel $K^{ij}(x, x'; s)$ defined using the eigenspectrum of the kinetic operator

$$K^{ij}(x, x'; s) = \sum_n e^{-\lambda_n s}\, f_n^{(i)}(x)\, \bar{f}_n^{(j)}(x')\,. \tag{2.31}$$

The basis has been suitably chosen to diagonalize the kinetic operator for the fluctuations (derived from the Gaussian approximation of the action) with eigenvalues λ_n. For bookkeeping purposes it is convenient to include in this sum potential zero modes with $\lambda_n = 0$, and correct for their effect at the end of the calculation. The contribution to the one-loop determinant of all fluctuations is then given by

$$\log Z_{1-\text{loop}} = \frac{1}{2}\int_{\Lambda_{\text{UV}}}^{\infty} \frac{\mathrm{d}s}{s} \int \mathrm{d}^4x\, \sqrt{g}\, K(x,x;s)\,. \tag{2.32}$$

The integral over s requires a UV cut-off Λ_{UV}. The heat kernel admits a Laurent series expansion in powers of $\sqrt{s}$ around $s = 0$. In even dimensions, only even powers of $\sqrt{s}$ appear, while in odd dimensions only odd powers of $\sqrt{s}$ appear. Let $K_0(x)$ the constant term in this expansion, following [27] – it only appears in even dimensions, which is the case of interest for us ($d = 4$). $K_0(x)$ is an important quantity, since it leads to a term in the one-loop determinant that grows logarithmically with the area of the black hole, or equivalently in our case with J. To see this we can replace the contribution from K_0 in equation (2.32) and notice that the s integration region $\Lambda_{\text{UV}} \ll s \ll \mathsf{J}^2$ leads to $\log(\mathsf{J}^2/\Lambda_{\text{UV}}) = \log(S_0) + \mathcal{O}(1)$, using that the UV cut-off is of order G_N. Therefore, in the macroscopic limit, the logarithmic correction is the leading quantum effect to the entropy.

For pure gravitational background such as the NHEK geometry, it is easy to compute $K_0(x)$ even in the presence of matter fields. Since the matter fields are not turned on the background (2.20), there is no kinetic mixing to quadratic order between the matter fields and the graviton. In the presence of n_S minimally coupled massless scalar fields, n_V minimally coupled massless vector fields, n_F minimally coupled massless Dirac fields, and a single spin-2 field, K_0 is given by [83, 84, 85, 86, 87]

$$K_0(x) = -\frac{1}{90\pi^2}\,(n_S + 62\,n_V + 11\,n_F)E - \frac{1}{30\pi^2}\,(n_S + 12\,n_V + 6\,n_F + \frac{424}{3})\,I\,, \tag{2.33}$$

where

$$E = \frac{1}{64}(R_{\mu\nu\rho\sigma}R^{\mu\nu\rho\sigma} - 4R_{\mu\nu}R^{\mu\nu} + R^2), \tag{2.34}$$

$$I = -\frac{1}{64}(R_{\mu\nu\rho\sigma}R^{\mu\nu\rho\sigma} - 2R_{\mu\nu}R^{\mu\nu} + \frac{1}{3}R^2). \tag{2.35}$$

The invariants appearing in K_0 are straightforward to compute, as only the Kretschmann scalar $R_{\mu\nu\rho\sigma}R^{\mu\nu\rho\sigma}$ is non-vanishing on solutions of vacuum Einstein's equations. Integrating $K_0(x)$ over the spacetime geometry, we are left with the s integral, which produces a logarithmic term in J, as explained in [27] and recalled in the previous paragraph. The final answer is

$$\log Z'_{1-\text{loop}} = \frac{1}{180}\,(2\,n_S - 26\,n_V + 7\,n_F + 424)\log S_0 + \cdots\,, \tag{2.36}$$

where the prime indicates that in this result we haven't yet accounted for the zero modes. The ellipses correspond to terms that are either order one or decay in the large S_0 limit and are therefore sub-leading. In particular, note that the contribution from gravitons gives a factor of $\frac{424}{180}\log S_0$. We have to correct this by accounting for the graviton zero modes of the background.

2.2.3 The extremal zero modes

Our main goal is to revisit the zero mode contributions. In order to do so, we should first understand how they arise, and then characterize them explicitly. On general grounds in the extremal Kerr metric, one expects two sets of such modes [27], which can be distinguished by their transformation under $\mathrm{SL}(2,\mathbb{R})$ isometry, cf., [88]. The first of these are usually referred to as the tensor zero modes in the literature. They are associated with the asymptotic symmetry of AdS_2. We will therefore refer to them as the *Schwarzian modes*. The second set of modes are associated with the U(1) gauge field obtained under the dimensional reduction to AdS_2. They are usually referred to as the vector zero modes in the literature, but since they respect the axisymmetry of the Kerr solution, we will refer to them as the *rotational modes*.

It is worth emphasizing that both these modes are associated with metric perturbations in the four dimensional NHEK geometry.

In order to determine the modes in question, we need to construct the quadratic fluctuation operator for the Einstein-Hilbert theory. We will do so following [85], by explicitly including a gauge fixing term, and expanding the resulting action to Gaussian order in perturbations about the NHEK geometry. We pick the harmonic gauge fixing term and let

$$I_{\rm grav} = I_{\rm EH} + I_{\rm gf}\,, \qquad I_{\rm gf} = \frac{1}{32\pi G_N}\int {\rm d}^4x\,\sqrt{g}\left(\nabla_\mu h^\mu{}_\nu - \frac{1}{2}\,\nabla_\nu h\right)\left(\nabla_\rho h^{\rho\nu} - \frac{1}{2}\,\nabla^\nu h\right), \tag{2.37}$$

where $I_{\rm EH}$ was given earlier in (2.3). Expanding this to quadratic order, we obtain

$$I^{(2)}_{\rm grav} = \frac{1}{16\pi G_N}\int {\rm d}^4x\,\sqrt{g}\,\frac{1}{4}\,\widetilde{h}^{\mu\nu}\Delta_L\,h_{\mu\nu}\,, \tag{2.38}$$

with $\widetilde{h}_{\mu\nu} = h_{\mu\nu} - \frac{1}{2}\,g_{\mu\nu}\,h$. The operator Δ_L is the spin-2 Lichnerowicz operator, which maps symmetric rank-2 tensors to symmetric rank-2 tensors via[9]

$$\Delta_L h_{\mu\nu} = -\nabla_\rho\nabla^\rho h_{\mu\nu} + 2\,R_{\mu\rho}\,h^\rho{}_\nu - 2\,R_{\mu\rho\nu\sigma}\,h^{\rho\sigma} - 4\left(R_{\nu\sigma} - \frac{1}{4}\,g_{\nu\sigma}\,R\right)h^\sigma{}_\mu\,. \tag{2.39}$$

Since the Kerr spacetime is Ricci-flat, we can simplify the operator to

$$\Delta_L = -\nabla_\rho\nabla^\rho h_{\mu\nu} - 2\,R_{\mu\rho\nu\sigma}\,h^{\rho\sigma}\,. \tag{2.40}$$

We can now give a mathematical characterization of the problem. The construction of the heat kernel proceeds by finding a complete set of eigenmodes for this Lichnerowicz operator. However, as detailed above, we circumvent the explicit analysis of the eigenspectrum by using the fact that the leading large charge correction to the entropy can be extracted from the conformal anomaly. Since we have included the zero modes in that analysis, we need to

[9]If we have a non-vanishing cosmological constant, then $\widetilde{h}^{\mu\nu}(\Delta^\Lambda_L h_{\mu\nu}) = \widetilde{h}^{\mu\nu}(\Delta_L h_{\mu\nu}) - 2\,\Lambda\widetilde{h}^{\mu\nu}h_{\mu\nu}$.

isolate their contribution. The zero modes in question are metric perturbations that lie in the kernel of Δ_L. We will also require that such perturbations be normalizable with respect to the ultralocal measure $\mathrm{D}h$, which is defined by the property

$$\int \mathrm{D}h\, e^{-\int \mathrm{d}^4x\, \sqrt{g}\, \widetilde{h}_{\mu\nu}\, h^{\mu\nu}} = 1\,. \tag{2.41}$$

The Faddeev-Popov ghosts that come with the gauge fixing action I_{gf} are implicitly included in the derivation of (2.36). As noted in the literature, cf., [26], there are no zero modes arising from the ghost sector. For our discussion, which seeks to revisit the zero mode contribution to the one-loop determinant, we do not have to worry about the ghost modes. For further details the reader should consult the aforementioned earlier literature.

The Schwarzian zero modes

First, let us consider the Schwarzian zero modes, whose presence owes to the AdS_2 asymptotics. The fastest way to find them is by direct computation of a metric perturbation that is annihilated by the Lichnerowicz operator. Consider a linear fluctuation of the NHEK line element by $\mathrm{d}s^2_{\mathrm{Sch}}$, viz.,

$$\mathrm{d}s^2 = \mathrm{d}s^2_0 + \mathrm{d}s^2_{\mathrm{Sch}}\,. \tag{2.42}$$

By plugging in an ansatz for the fluctuation to have no components along the angular directions, and the fields to be functions only of the AdS_2 coordinates, one can directly solve for the modes in question. One finds that the Schwarzian modes takes the following form:

$$\mathrm{d}s^2_{\mathrm{Sch}} = \mathsf{J}^2\,(1+\cos^2\theta)\left[H_{\tau\tau}(\tau,y)\,\mathrm{d}\tau^2 + 2\,H_{\tau y}(\tau,y)\,\mathrm{d}\tau\,\mathrm{d}y + H_{yy}(\tau,y)\,\mathrm{d}y^2\right], \tag{2.43}$$

where the functions $H_{\mu\nu}(\tau, y)$ are given explicitly by

$$\begin{aligned} H_{\tau\tau}(\tau, y) &= -\left(\frac{y-1}{y+1}\right)^{\frac{n}{2}} \left(\delta_+ e^{\mathrm{i}n\tau} + \delta_- e^{-\mathrm{i}n\tau}\right), \\ H_{\tau y}(\tau, y) &= \mathrm{i}\frac{1}{y^2-1}\left(\frac{y-1}{y+1}\right)^{\frac{n}{2}} \left(\delta_+ e^{\mathrm{i}n\tau} - \delta_- e^{-\mathrm{i}n\tau}\right), \\ H_{yy}(\tau, y) &= \frac{1}{(y^2-1)^2}\left(\frac{y-1}{y+1}\right)^{\frac{n}{2}} \left(\delta_+ e^{\mathrm{i}n\tau} + \delta_- e^{-\mathrm{i}n\tau}\right). \end{aligned} \tag{2.44}$$

Within the linearized ansatz the parameters $\delta_\pm$ are in principle arbitrary. To ensure reality of the metric fluctuation, we impose $\delta_+ \propto \xi_n$ and $\delta_- \propto \bar{\xi}_n = \xi_{-n}$. The normalization of the modes can be determined by demanding orthonormality of the eigenfunctions of the spin-2 Laplace operator, which we shall specify precisely in the following section, cf., (2.65). We will also shortly argue that $n \in \mathbb{N}/\{0, 1\}$.

A simpler way to determine these modes is to realize that arise from large diffeomorphisms in AdS_2. They correspond precisely to the Schwarzian boundary graviton of [35, 37, 36], see [38] for a review. Picking an ansatz for the vector field generating the diffeomorphism that exploits the underlying symmetry of the NHEK geometry, say (for simplicity focusing on the positive frequency modes)

$$\zeta_T = e^{\mathrm{i}n\tau}\left(f_1(y)\,\frac{\partial}{\partial y} + f_2(y)\frac{\partial}{\partial t} + f_3(y)\frac{\partial}{\partial \varphi}\right), \tag{2.45}$$

one can again directly solve for the resulting metric perturbation to lie in the $\ker(\Delta_L)$. This fixes

$$f_2(y) = \frac{\mathrm{i}\, f_1'(y)}{n}, \qquad f_3(y) = \frac{(y-1)\, f_1'(y) - f_1(y)}{n}, \tag{2.46}$$

and leads to a ODE for $f_1(y)$, which is solved straightforwardly and determines

$$f_1(y) = \left(\frac{y-1}{y+1}\right)^{\frac{n}{2}} (n+y)\,\frac{\delta_+}{2\,(n^2-1)}. \tag{2.47}$$

This solution is actually the unique smooth vector zero mode generated by a diffeomorphism

of the form (2.45).

Since this is an important fact (in particular in regard to the discussion in the next section) we explain this in some detail before moving on. First, one can evaluate

$$\Delta_L h_{\theta\theta}|_{\theta=0} - \Delta_L h_{\theta\theta}|_{\theta=\frac{\pi}{2}} = -6(f_1'(y) + \mathrm{i}n f_2(y)) = 0,$$

imposing the first relation above. To find the solution for $f_3(y)$, we can write $f_3(y) = \frac{(y-1)\, f_1'(y) - f_1(y)}{n} + \delta f_3(y)$ and evaluate then the following component of the Lichnerowicz operator

$$\partial_\theta(\Delta_L h_{\theta y})|_{\theta=0} + \frac{1}{2}\partial_\theta(\Delta_L h_{\theta y})|_{\theta=\frac{\pi}{2}} = 14ne^{\mathrm{i}n\tau}(y^2-1)^{-1}\delta f_3(y),$$

which automatically implies that $\delta f_3(y) = 0$. Inserting this in any of the remaining non-trivial components of $\Delta_L h$ produces a second order differential equation for $f_1(y)$. One solution was quoted in (2.47) while the other (obtained by replacing $n \to -n$) is singular at the horizon $y = 1$ for $n > 0$. Therefore, the Schwarzian zero mode is the only one of the form (2.45).

The vector field generating our large diffeomorphisms is

$$\zeta_T = \frac{1}{\mathrm{i}\, n}\left(\partial_t \Phi_T \,\frac{\partial}{\partial y} - \partial_y \Phi_T \,\frac{\partial}{\partial t} + \mathrm{i}\,((y-1)\,\partial_y - 1)\Phi_T \,\frac{\partial}{\partial \varphi}\right), \tag{2.48}$$

with

$$\Phi_T(y,\tau) = f_1(y)\, e^{\mathrm{i}n\tau}\,. \tag{2.49}$$

Note that the vector field is non-normalizable. It acts non-trivially on the boundary, and thus should not to be treated as pure gauge modes. To see this, we note that near the conformal boundary of AdS_2 these fluctuations are generated by diffeomorphisms along the vector field

$$\zeta_T \sim -\xi(\tau)\,\partial_\tau + \xi'(\tau)\, y\,\partial_y\,, \qquad \xi(\tau) = \sum_n \xi_n\, e^{\mathrm{i}n\tau}. \tag{2.50}$$

Therefore, these modes act as time reparametrizations $\tau \to \tau - \varepsilon(\tau)$ while the y or radial

component ensures that the boundary curve is of fixed length [37]. The integration space is

$$\mathcal{M}_{\rm Sch} = {\rm Diff}(\mathbf{S}^1)/{\rm PSL}(2,\mathbb{R})\,. \tag{2.51}$$

The quotient is by the isometries of AdS_2; curves related by such transformations should not be over counted. In the space of small fluctuations displayed in (2.44), the generators of the isometries correspond to $n = -1, 0, 1$. Consequently, for we only integrate over $|n| \geq 2$ modes.

As determined above, at exact extremality with $\mathsf{T} = 0$, these modes have vanishing action by virtue of being exact zero modes. In JT gravity this corresponds to working on a background with a constant (spacetime independent) dilaton.

If we focus on the asymptotia, these large diffeomorphisms are solely determined by their behavior near the conformal boundary of AdS_2. In writing (2.44) or (2.45) we have picked a particular way to propagate the modes to the interior of the NHEK geometry. This is determined implicitly by the way that diffeomorphism invariance was fixed in the calculation. One way to implement this is to work with a gauge fixing term for fluctuations, demanding that they satisfy the harmonic gauge condition. Demanding that the large diffeomorphisms are zero modes in the presence of this gauge-fixing term imposes the precise form of (2.44). One can indeed alternately have determined the modes by solving for the harmonic gauge fixing term $I_{\rm gf}$, since any pure diffeomorphism (with a normalizable metric perturbation) would have left $I_{\rm EH}$ invariant.

The rotational zero mode: a puzzle

On general grounds, it is expected that in addition to these Schwarzian space of zero modes, there is a second set of zero modes associated to fluctuations in the angular velocity of the black hole. One way to motivate them, as for instance argued in [27], is to consider dimensionally reducing to two dimensions. Since the 4d solution is only axisymmetric,

the reduction gives a Maxwell gauge field (2.24). In the language of section 2.1.3, where we describe the NHEK geometry as a two-dimensional dilaton gravity coupled to a U(1) gauge field and to matter, these are large gauge transformations acting on the U(1) sector. Consequently, we anticipate that the vector fields in AdS_2 admit a set of zero modes associated with a large gauge transformation of the form $A \to A + \mathrm{d}H$ with

$$H(y,\tau) = \left(\frac{y-1}{y+1}\right)^{\frac{n}{2}} \left(\delta\lambda_+ \, e^{\mathrm{i}n\tau} + \delta\lambda_- \, e^{-\mathrm{i}n\tau}\right). \tag{2.52}$$

Again, these zero modes are determined by their behavior at large y, and their profile in the interior should be fixed by our gauge fixing term. In the two-dimensional dilaton gravity theory, it is natural to use a Lorenz gauge fixing term for the U(1) gauge field. One can then check that this then is a zero mode with these choices. Once this is determined, we can parametrize these modes by $\delta\lambda_+ \propto v_n$ and the reality condition implies that $\delta\lambda_- \propto \overline{v}_n$. The moduli space of these zero modes is denoted as $\mathcal{M}_{\mathrm{U}(1)}$, but its details depend on the choice of the ensemble. For example, in a fixed angular velocity ensemble, it is given by $\mathcal{M}_{\mathrm{U}(1)} = \mathrm{Loop}(\mathrm{U}(1))/\mathrm{U}(1)$.

However, part of our motivation was to not rely on the dimensional reduction, but to rather work directly in the NHEK spacetime in four dimensions. To this end, we should examine if we can find a metric perturbation that could correspond to such a gauge transformation upon reduction. We realize that one can achieve the desired effect by a diffeomorphism $\mathrm{d}\varphi \to \mathrm{d}\varphi + \mathrm{d}H$ or equivalently by a vector field

$$\xi^\mu_R = H(y,\tau)\,(\partial_\varphi)^\mu \,. \tag{2.53}$$

Carrying out this exercise, we find that the metric perturbation generated by ξ^μ_R, viz., $h_{\mu\nu} = 2\nabla_{(\mu}\xi^R_{\nu)}$, fails to be annihilated by the Lichnerowicz operator Δ_L. In fact,

$$\Delta_L h_{\mu\nu} \neq 0\,, \qquad \sqrt{g}\frac{1}{4}\widetilde{h}^{\mu\nu}\Delta_L\, h_{\mu\nu} = \frac{64\ n^2}{y^2-1}\,\frac{\sin^5\theta}{(1+\cos^2\theta)^4}\left(\frac{y-1}{y+1}\right)^n \delta\lambda_+\,\delta\lambda_-\,. \tag{2.54}$$

Tracing through the calculation, we ascertain that the reason for this failure is that the diffeomorphism fails to satisfy the harmonic gauge condition. This is indeed the only way for it to have failed, for I_{EH} would be unchanged by any diffeomorphism resulting in a normalizable metric perturbation.

One attempt to fix this would be by modifying ξ^μ_R to bring the perturbation back into the harmonic gauge. We can look for ξ^μ_H such that $\xi^\mu_{R,H} = \xi^\mu_R + \xi^\mu_H$ has the same asymptotic behaviour, but the resulting metric perturbation does satisfy the harmonic gauge condition. This again turns out to be tractable, but the resulting vector field is no longer smooth. An example of an explicit solution is

$$\xi^H_\mu = \left[c_1 + c_2 \left(\cos\theta + 2\,\log\tan\frac{\theta}{2}\right) - 4\,\log\sin\theta\right]\left(\partial_y H(y,\tau)\,\mathrm{d}y + \partial_\tau H(y,\tau)\,\mathrm{d}\tau\right). \quad (2.55)$$

Here c_1 and c_2 are integration constants, which can be picked at will. Clearly, however, there is no choice of them that ensures that the vector field $\xi^\mu_{R,H}$ is regular at the poles ($\theta = 0, \pi$) of the deformed $\mathbf{S}^2$. This solution is somewhat reminiscent of the singular modes recently obtained in [89]. We explain how we arrive at this result in section 5.1, where we rule out a number of other possible ansatz for the compensating diffeomorphism.

At this point, we find ourselves at an impasse. On the one hand, there does not appear to be a metric fluctuation that is in the kernel of the Lichnerowicz operator, and has the right structure to be called a rotational zero mode. In fact, our attempts to solve for a general diffeomorphism associated to a zero mode has not yielded any physically interesting solutions.

On the other hand, we have identified a putative zero mode, albeit one generated by a diffeomorphism that is singular at the poles of the sphere. Even if this were not physically acceptable, one could use the intuition from 2d dilaton gravity coupled to matter, to argue for a different gauge fixing term for the rotational zero mode, viz., one obtained by uplifting Lorenz gauge condition of the U(1) gauge field to one for the 4d metric. This choice would break spacetime covariance, as we would impose different gauge choices for the Schwarzian

and rotational modes.

Clearly, neither of these is satisfactory. For now, we will proceed with the rest of the analysis, deferring a more detailed discussion to section 2.4.

Incorporating the zero modes

We are now ready to write a formal expression for the complete one-loop determinant around the extremal Kerr geometry, after incorporating these two sets of zero modes. The contribution is of two types. The first, comes from the fact that a diffeomorphism produces a change in the metric of order $h_{\mu\nu} \sim \mathcal{O}(\mathsf{J}^2)$. Therefore, we need to compute the Jacobian between the integration measure over metric fluctuations, and the measure over the large diffeomorphisms themselves. This Jacobian factor was carefully computed by Sen in [27]. It was found that each gravitational zero mode[10] contributes a factor of $\frac{1}{2}\log S_0$ to $\log Z$. Including for a moment, both the Schwarzian and the rotational zero modes, we would obtain a total contribution of $-2\log S_0$. In addition, we have a remaining integral over such large diffeomorphisms that still needs to be performed.

The total one-loop determinant, accounting for the Schwarzian and rotational zero modes, would therefore update (2.36) to

$$\log Z_{1-\text{loop}} = \frac{1}{180}\,(2\,n_S - 26\,n_V + 7\,n_F + 64)\log S_0 + \log \underbrace{\int_{\mathcal{M}_{\text{Sch}}} \mathrm{d}\xi \int_{\mathcal{M}_{\text{U(1)}}} \mathrm{d}v}_{\text{Large diffeos}} \,. \tag{2.56}$$

Ignoring the matter fluctuations and the integral over the large diffeomorphisms, we reproduce the result quoted in (2.1). The previous work on this problem such as [27] stops here. The assumption was that the final term on the r.h.s. is independent of J and T. This is not a well-defined procedure, since the moduli space of zero modes is non-compact and would formally lead to divergent answers. Therefore, these zero modes need regulating. The physical

[10]Take for example the Schwarzian modes. There are an infinite number of them. Nevertheless, the important quantity in the one-loop determinant is the zeta-function regularized number of zero modes, which is -3. A similar calculation for the rotational zero modes gives -1.

way to do this, proposed in [47], is to turn on a small temperature and use it as an IR regulator. Specifically, one works with a background that is not just NHEK, but includes small $\mathcal{O}(\mathsf{T})$ corrections. Then we can compute the action over the zero modes and take $\mathsf{T} \to 0$ limit at the end of the calculation. We will tackle this in the next subsection.

However, given our issues with the rotational zero mode, if we were to only include the Schwarzian zero modes, then we would rewrite (2.56) as

$$\log Z_{1-\text{loop}} = \frac{1}{180}\,(2\,n_S - 26\,n_V + 7\,n_F + 154)\log S_0 + \log \underbrace{\int_{\mathcal{M}_{\text{Sch}}} \mathrm{d}\xi}_{\text{Large diffeos}} \,. \tag{2.57}$$

As we will discuss below, in the canonical ensemble the functional integral over the rotational zero mode has no effect. The main change is the coefficient of the $\log S_0$ contribution. In any event, we will simply evaluate (2.57) in what follows. This will suffice to demonstrate that the remaining functional integral over the large diffeomorphisms gives us the suppression of density of states at low temperatures.

2.2.4 Regularization of zero modes

Following [47], we first obtain the corrected background around which we re-evaluate the one-loop determinants. The procedure consists in keeping T non-zero but small, and including the leading correction to the NHEK limit. Solving the equation for the temperature in the small T limit, we find the parameters a and r_+ behave as

$$\begin{aligned} a &= \mathsf{J} - \mathsf{J}^3\,\mathsf{T}^2 - 4\,\mathsf{J}^4\,\mathsf{T}^3 + \cdots\,, \\ r_+ &= \mathsf{J} + 2\,\mathsf{J}^2\,\mathsf{T} + 5\,\mathsf{J}^3\,\mathsf{T}^2 + \cdots\,. \end{aligned} \tag{2.58}$$

To motivate the correction to the metric at leading order, similar to the derivation of the

NHEK geometry in section 2.1.2, let us define

$$r - r_+ = 2\,\mathsf{J}^2\,\mathsf{T}\,(y-1)\,, \qquad \tau = \frac{t_{\scriptscriptstyle \mathrm{E}}}{\mathsf{T}}\,. \tag{2.59}$$

Proceeding with this ansatz, and taking $\mathsf{T} \to 0$ first, we find the metric functions reduce to

$$\begin{aligned} \Delta(r) &= 4\,\mathsf{J}^4\,\mathsf{T}^2\left[(y^2-1) + 4\,\mathsf{J}\,\mathsf{T}\,(y-1) + \cdots\right], \\ \rho^2(r,\theta) &= \mathsf{J}^2\left[1 + \cos^2\theta + 4\,\mathsf{J}\,\mathsf{T}\,y + \cdots\right], \\ \Xi(r,\theta) &= 4\,\mathsf{J}^4\left[1 + 4\,\mathsf{J}\,\mathsf{T}\,y + \cdots\right]. \end{aligned} \tag{2.60}$$

Plugging this into the line element and retaining terms to linear order in T (note that so far we have made no assumption about the range of y), we find the NHEK geometry and its leading temperature correction

$$\begin{aligned} \mathsf{J}^{-2}\,\mathrm{d}s_0^2 &= g_1\left[(y^2-1)\,\mathrm{d}\tau^2 + \frac{\mathrm{d}y^2}{y^2-1} + \mathrm{d}\theta^2\right] + 4\,g_2\,(\mathrm{d}\varphi + \mathrm{i}\,(y-1)\,\mathrm{d}\tau)^2\,, \\ \mathsf{J}^{-2}\,\mathrm{d}s_1^2 &= \mathsf{J}\,\mathsf{T}\Bigg(g_1\left[(y-1)\,\left(1-(y^2+y-1)\,c\right)\mathrm{d}\tau^2 + \frac{(y^2+y-1-c)\,\mathrm{d}y^2}{(y^2-1)\,(y+1)} + y\,\mathrm{d}\theta^2\right] \\ &\quad + g_2\,(\mathrm{d}\varphi + \mathrm{i}\,(y-1)\,\mathrm{d}\tau)\left[\frac{4\,c}{g_1}\,y\,(\mathrm{d}\varphi + \mathrm{i}\,(y-1)\,\mathrm{d}\tau) - \mathrm{i}\,(y^2-1)\,(1-c)\,\mathrm{d}\tau\right]\Bigg). \end{aligned} \tag{2.61}$$

To simplify the expressions we defined the functions of the polar angle θ

$$c(\theta) = \cos^2\theta\,, \qquad g_1(\theta) = 1 + c(\theta)\,, \qquad g_2(\theta) = \frac{1-c(\theta)}{1+c(\theta)}\,. \tag{2.62}$$

Note that the leading temperature correction has a different dependence on the polar angle. In particular, the line element $\mathrm{d}s_1^2$ does not conform to the ansatz used for the two-dimensional reduction (2.21).

Given this, following [47], we should evaluate the one-loop determinant around a background metric that includes the finite temperature correction computed above, viz., compute

the determinant around

$$\mathrm{d}s^2_{\text{background}} = \mathrm{d}s^2_0 + \mathrm{d}s^2_1. \tag{2.63}$$

Further corrections are subleading in the low temperature expansion.

The on-shell action

Before moving on to the one-loop determinant, we briefly describe the calculation of the classical on-shell action contribution in the corrected near-horizon region (2.61). The extremal near-horizon has AdS_2 asymptotics, however, the leading temperature correction is an irrelevant deformation of these asymptotics, as is clear from the line element $\mathrm{d}s^2_1$. Therefore, the evaluation will require careful regulating of the divergences, i.e. the inclusion of additional counterterms.

Let us consider the canonical ensemble with fixed asymptotic charge. We have to implement the Legendre transformation as in (2.29) to fix the charge, as opposed to the holonomy of the gauge field. This is easy to do: we include a counterterm that changes the boundary condition for the gauge field from Dirichlet (fixed holonomy) to Neumann (fixed charge). Naively, we would include this counterterm in the asymptotically flat region, but in the case of the fixed charge ensemble, the radial Gauss law implies that the selfsame counterterm suffices in the near-horizon region. In fact, this Neumann boundary condition is natural from the near-horizon AdS_2 perspective, since the gauge potential grows linearly, $A_t \sim y$, as $y \to \infty$.[11] In short, once we zoom into the near-horizon region, in the canonical ensemble, we fix the metric and the field strength at a fixed constant y hypersurface.

While this Neumann boundary term suffices at strict extremality to regulate the on-shell action, one must further regulate the divergence arising from the irrelevant deformation of AdS_2 asymptotics. Since we are holding the metric fixed, we have the freedom to include counterterms built from the induced first metric on the fixed y hypersurface. Following

[11] As discussed in [47] one can work in the grand canonical ensemble by imposing a mixed boundary condition.

usual AdS counterterm analysis we can see that the natural counterterms are a hypersurface cosmological constant, and a hypersurface Einstein-Hilbert term. Putting all this together, we have

$$I_{\text{EH}}^{\text{reg}} = I_{\text{EH}} - \frac{1}{16\pi G_N}\int \mathrm{d}^3x\,\sqrt{\gamma}\,\left(\alpha\, n_\mu\, A_\nu\, F^{\mu\nu} + c_1 + c_2\,{}^{\gamma}R\right) \tag{2.64}$$

The coefficient of the Neumann boundary term α is fixed by demanding that the zero temperature calculation in the near-horizon region lead to a finite result. This determines $\alpha = \frac{8}{\pi}$. It also imposes a linear relation between c_1 and c_2, since each of these terms gives a linearly divergent action. Including the leading temperature correction, we find a quadratically divergent result from I_{EH}. At this stage we exploit the freedom to the constant mode of the gauge potential A_μ at $\mathcal{O}(\mathsf{T})$ (which does not affect the field strength), and tune the relation between c_1 and c_2. The specific values of the counterterms and the shift of the background gauge potential are not particularly illuminating, and so we refrain from quoting them. The upshot of this analysis is the same result quoted in (2.30).

The one-loop determinant

Moving onto the one-loop determinant and starting with the non-zero modes, we note that incorporating the correction at linear order in temperature correction to the background is an easy task for the evaluation of the one-loop determinant of these modes – the result agrees with (2.36) up to corrections that are subleading in the small T limit. Therefore, we do not need to worry about repeating that calculation and can simply borrow the result. The situation is completely different for the modes that have vanishing action at $\mathsf{T} = 0$, they now have an action of order T, which we determine next.

We begin with the Schwarzian modes. We normalize the Schwarzian modes given in (2.44) as determined in [88]

$$\delta_+ = \sqrt{\frac{n(n^2-1)}{2\pi}}\,\xi_n\,, \qquad \delta_- = \sqrt{\frac{n(n^2-1)}{2\pi}}\,\xi_n^*\,. \tag{2.65}$$

This is also the normalization used originally in [27], but differs from that used in [90]. The latter work fixes the coefficients $\delta_\pm$ to unity (up to the amplitude factor), and instead incorporates suitable factors in the integration measure that they compute. These choices do not modify the final answer at the level of approximation we are working. They only affect the order one contribution to the entropy, viz., contributions that do not grow with the horizon area or the temperature.

We can now compute the on-shell action for the Schwarzian modes, by evaluating (2.3) at quadratic order in $\delta_\pm$ from the total metric $\mathrm{d}s_0^2 + \mathrm{d}s_1^2 + \mathrm{d}s_\epsilon^2$. The calculation, while straightforward, still requires the subtle treatment of counterterms and boundary terms related to the choice of ensemble described earlier in this subsection. We find at the end of the day, for a single mode of a given value of n, an action to quadratic order for the Schwarzian modes:

$$I_{\text{EH}} = \frac{2\pi\,\mathsf{J}^2}{G_N} + \frac{4\pi\,\mathsf{J}^3\,\mathsf{T}}{G_N} - \frac{4\pi\,\mathsf{J}^3\,\mathsf{T}}{G_N}\,\frac{\delta_+\,\delta_-}{4\,(n^2-1)}\,. \tag{2.66}$$

Using the given values of $\delta_\pm$ in (2.65) and including the sum over all Fourier modes, we end up with

$$I_{\text{EH}} = \frac{2\pi\,\mathsf{J}^2}{G_N} + \frac{4\pi\,\mathsf{J}^3\,\mathsf{T}}{G_N} - \frac{4\pi^2\mathsf{T}}{\mathsf{T}_q}\,\sum_{|n|>1}\frac{n}{8\pi}\,\xi_n\,\xi_n^*\,. \tag{2.67}$$

As advertised, the Schwarzian modes have been lifted with the leading temperature correction. This is the same as the result obtained in the spherically symmetric solutions examined hitherto [41, 90, 47], despite the non-trivial dependence on the polar angle in the temperature corrected background.

Evaluating the one-loop determinant around the near-extremal Kerr geometry gives a small action to these modes, of order $\mathsf{J}^3\mathsf{T}$. Now the evaluation of the path integral over these Schwarzian modes is well-defined. Using zeta-function regularization these modes lead to a contribution

$$\log Z_{\text{Sch}} = \log\prod_{n=2}^{\infty}\frac{2G_N}{\mathsf{J}^3\,\mathsf{T}\,n} = \frac{3}{2}\log\frac{\mathsf{T}}{\mathsf{T}_q} + \mathcal{O}(1)\,. \tag{2.68}$$

We emphasize that the order one term in the r.h.s. is not reliable. For example, even the

non-zero modes would also contribute at this order, and we have not included them in our temperature corrected analysis.

Finally, let us comment on the rotational modes. Even if they were genuine zero modes of the NHEK background, we expect them to have an action of order T in the fixed angular velocity ensemble. Their quantization nevertheless is simpler. Since U(1) is compact, the quantum mechanics of these modes are gapped. In particular, if we work in a fixed charge sector, viz., fixing the angular momentum in our case, then their contribution can only at most shift the ground state energy.

2.2.5 The entropy of near-extremal Kerr

We are now ready to put all the pieces together and compute the final form of the free energy of the Kerr black hole, in an ensemble of fixed angular momentum. The first ingredient is the on-shell classical action on the near-extremal (finite but small T) background. It is given by

$$\log Z_{\text{tree}} = S_0 + 2\pi^2 \frac{T}{T_q} + \mathcal{O}(T^2)\,. \tag{2.69}$$

We keep the leading order correction at finite temperature. The second ingredient is the one-loop determinant, including the Schwarzian mode contribution. The answer, combining (2.68) and (2.57), is given by

$$\log Z_{1-\text{loop}} = \frac{1}{180}\left(2\,n_S - 26\,n_V + 7\,n_F + 154\right)\log S_0 + \frac{3}{2}\,\log\frac{T}{T_q} + \mathcal{O}(1). \tag{2.70}$$

We emphasize again that the order one correction is not reliable since we have not kept track of it in the heat kernel expansion. Putting these two results together, we obtain the total free energy

$$-\beta F = S_0 + 2\pi^2 \frac{T}{T_q} + \frac{1}{180}\left(2n_S - 26n_V + 7n_F + 154\right)\log S_0 + \frac{3}{2}\,\log\frac{T}{T_q} + \mathcal{O}(1)\,. \tag{2.71}$$

From this expression we can compute the entropy as a function of temperature using thermodynamic identities. We obtain the final answer,

$$S = S_0 + \frac{1}{180}\left(2\,n_S - 26\,n_V + 7\,n_F + 154\right)\log S_0 + 4\pi^2\frac{T}{T_q} + \frac{3}{2}\,\log\frac{T}{T_q} + \mathcal{O}(1). \tag{2.72}$$

This is our prediction for the quantum entropy of black hole microstates of the Kerr black hole, without the contribution from the rotational zero mode. For the Standard Model the light fields relevant to the one-loop determinant at energies lower than electroweak scale, and for black holes smaller than the Hubble scale, is the photon and three neutrinos, and $n_V = 1$, $n_F = 3/2$ leading to

$$S_{\rm SM} = S_0 + \frac{277}{360}\log S_0 + 4\pi^2\frac{T}{T_q} + \frac{3}{2}\,\log\frac{T}{T_q} + \mathcal{O}(1)\,. \tag{2.73}$$

On the other hand, for pure gravity $n_S = n_V = n_F = 0$, and thus we arrive at the result quoted in the opening of this chapter, viz.,

$$S_{\text{pure grav}} = S_0 + \frac{154}{180}\log S_0 + 4\pi^2\frac{T}{T_q} + \frac{3}{2}\,\log\frac{T}{T_q} + \mathcal{O}(1)\,. \tag{2.74}$$

This calculation does not take into account instabilities of the Kerr black hole in flat space that would appear as imaginary components to $\log Z$ that determine the lifetime of the black hole. We comment on this in section 2.4.

2.3 Generalizations

In this section we will generalize our analysis to more complicated near-extremal rotating black hole. We first consider in section 2.3.1 the extremal limit of a charged rotating black hole in asymptotically flat space. Next in section 2.3.2 we analyze an uncharged rotating black hole in asymptotically AdS_4. Even though the results are quantitatively different, we

find qualitatively the same behavior as the extremal limit of the Kerr black hole.

2.3.1 The Kerr-Newman black hole

In this section we consider near-extremal black hole geometries which are solutions to a gravity theory including at least an Einstein-Maxwell sector

$$I_{\text{EM}} = -\frac{1}{16\pi G_N}\int_{\mathcal{M}} \mathrm{d}^4x\,\sqrt{g}\,[R - F_{\mu\nu}F^{\mu\nu}] + I_{\text{GHY}}, \tag{2.75}$$

where $F_{\mu\nu} = \partial_\mu A_\nu - \partial_\nu A_\mu$ and A_μ is a U(1) Maxwell potential. When imposing Dirichlet boundary conditions on all fields, the boundary terms include the Gibbons-Hawking-York term and also an electromagnetic boundary term $\oint \mathrm{d}\Sigma^\mu F_{\mu\nu}A^\nu$ [91, 92]. The black hole solution of this theory is the Kerr-Newman black hole. We work instead in an ensemble where we fix J, the angular momentum, and Q, the electric charge. Following a similar notation as in the uncharged case, we label the black hole by the parameter $a = J/M$ and by the location of the outer horizon which at extremality becomes $r_+ = \sqrt{Q^2 + a^2}$.

To compute the near-extremal entropy of Kerr-Newman black hole we follow a similar procedure as in the previous section. First, we can take the zero temperature limit after performing a change of coordinates as in (2.20) to zoom into the near horizon region. The generalization of the NHEK geometry when charge is present is

$$\mathrm{d}s_0^2 = \Gamma(\theta)\left[(y^2-1)\mathrm{d}\tau^2 + \frac{\mathrm{d}y^2}{y^2-1} + \mathrm{d}\theta^2 + \gamma(\theta)^2(\mathrm{d}\varphi + \mathrm{i}\,k\,(y-1)\,\mathrm{d}\tau)^2\right]. \tag{2.76}$$

where we define the functions

$$\Gamma(\theta) = r_+^2 + a^2\cos^2\theta\,, \qquad \gamma(\theta) = \frac{(r_+^2+a^2)\sin\theta}{r_+^2 + a^2\cos^2\theta}\,, \qquad k = \frac{2ar_+}{r_+^2+a^2}\,. \tag{2.77}$$

These functions implicitly depend on (Q, J) through the variables (r_+, a). Finally, we also

need to perform the same transformation of the gauge potential, which becomes

$$A_\mu \, \mathrm{d}x^\mu = f(\theta) \, (\mathrm{d}\varphi + \mathrm{i} \, k \, (y-1) \mathrm{d}\tau) - \frac{e}{k} \, \mathrm{d}\varphi \, , \tag{2.78}$$

where

$$f(\theta) = Q \frac{r_+^2 + a^2}{2 r_+ a} \, \frac{r_+^2 - a^2 \cos^2\theta}{r_+^2 + a^2 \cos^2\theta} \, , \qquad\qquad e = \frac{Q^2}{r_+^2 + a^2} . \tag{2.79}$$

The extremal horizon area of this black hole, in our conventions, is given by

$$S_0 = \frac{A_{\text{extremal}}}{4 G_N} = \frac{\pi \, (2a^2 + Q^2)}{G_N} . \tag{2.80}$$

The extremal mass is $M_0 = \sqrt{a^2 + Q^2}$ and $a = J/M_0$. The one-loop determinant around this geometry was computed in [93]. The calculation is similar to [27]; it uses the Seeley-de Witt expansion to evaluate the temperature independent correction, and ignores the temperature dependent effects from zero modes. To apply this formalism one needs to take Q to be large and work with a fixed ratio

$$Q \to \infty \, , \qquad b = a/Q \text{ fixed.} \tag{2.81}$$

That way Q represents the overall scale of the metric and sources logarithmic corrections computed by the Seeley-de Witt expansion.

We want to correct this last step described in the previous paragraph, just as done for Kerr above. We will mention some salient features compared to the previous treatment, in particular, mainly focusing on the contribution from the gravitational mode. Once again we consider gauge fixing to the harmonic gauge, including the same I_{gf} contribution (2.37) to the action (2.75). We have to keep track of the metric dependence from the Maxwell term. Including this, the kernel of the quadratic action for metric fluctuations $h_{\mu\nu}$ becomes

$$\Delta_L^{\text{EM}} h_{\mu\nu} = \Delta_L h_{\mu\nu} + \frac{1}{2} F^2 g_{\mu\nu} h^\rho{}_\rho - F^2 h_{\mu\nu} + 4 F_{(\mu\rho} F_{\nu\sigma)} h^{\rho\sigma} + 8 F_{(\mu\rho} F_\sigma{}^\rho h^\sigma{}_{\nu)} + 4 F_{(\mu\rho} F_{\nu)}{}^\rho h^\sigma{}_\sigma , \tag{2.82}$$

where $F^2 = F_{\mu\nu}F^{\mu\nu}$ and the parenthesis between indices indicates symmetrization of the pair $T_{(ab)} = \frac{1}{2}(T_{ab} + T_{ba})$. The superscript EM indicates this kernel applies to a solution of Einstein-Maxwell equations.

Similar to the uncharged case, we find a robust Schwarzian zero mode labeled by an integer $n \in \mathbb{Z}$ different from $n \neq 0, \pm 1$. We can construct it by implementing a large diffeomorphism

$$\zeta_T = e^{\mathrm{i}n\tau}\left(f_1(y)\,\frac{\partial}{\partial y} + f_2(y)\frac{\partial}{\partial t} + f_3(y)\frac{\partial}{\partial \varphi}\right), \tag{2.83}$$

where now the functions become

$$\begin{aligned} f_2(y) &= \frac{\mathrm{i}\, f_1'(y)}{n}\,, \qquad f_3(y) = \frac{2ar_+ f_1'(y)(y-1) - 2ar_+ f_1(y)}{n(r_+^2 + a^2)}\,, \\ f_1(y) &= \left(\frac{y-1}{y+1}\right)^{\frac{n}{2}}\,(n+y)\,\frac{\delta_+}{2\,(n^2-1)}. \end{aligned} \tag{2.84}$$

The change in the metric generated by this diffeomorphism is an obvious generalization of (2.44), namely

$$\mathrm{d}s^2_{\mathrm{Sch}} = \Gamma(\theta)\left[H_{\tau\tau}(\tau, y)\,\mathrm{d}\tau^2 + 2\,H_{\tau y}(\tau, y)\,\mathrm{d}\tau\,\mathrm{d}y + H_{yy}(\tau, y)\,\mathrm{d}y^2\right], \tag{2.85}$$

and the functions $H_{\mu\nu}(\tau, y)$ are the same that appeared in (2.44). One can check by explicit calculation that

$$\Delta_L^{\mathrm{EM}} \nabla_{(\mu}\zeta_{T\nu)} = 0, \tag{2.86}$$

making it an exact zero mode of the action.

To treat this zero mode we will raise the temperature of the black hole, which amounts to keeping the first correction to the low temperature limit that produced (2.76). This gives an action to this mode proportional to T/T_q and produces a $\frac{3}{2}\log\frac{T}{T_q}$ correction to the entropy. T_q is now a generalization of the quantity introduced in section 2.1.2, that now also depends on the charge, and can be extracted from the classical term in entropy that is linear in T. It

is given by

$$T_q = \frac{\pi}{G_N\, M_0\, S_0}\,. \tag{2.87}$$

This relation is valid for any charge and angular momentum, see [94]. Therefore, quantum effects from the Schwarzian mode become large for temperatures smaller than this scale.

The other expected zero mode is the rotational mode which we can write again as

$$\xi^\mu_R = H(y,\tau)\,(\partial_\varphi)^\mu\,. \tag{2.88}$$

Just as for Kerr, we find this mode has a non-vanishing action since

$$\Delta_L^{\rm EM}\nabla_{(\mu}\xi^R_{\nu)} \neq 0. \tag{2.89}$$

More specifically, the right hand side does vanish when $a = 0$, and it is of order a when $a \ll r_+$. Our calculations are consistent with the fact that we do find a rotational zero mode in Reissner-Nordström that is actually enhanced to a set of SU(2) modes. We do not attempt to find a compensating diffeomorphism that puts this mode in our preferred gauge in this chapter, but we will do so in 3.2.2.

To summarize, we find the near-extremal entropy of the Kerr-Newman black hole to be

$$S_{\rm Kerr-Newman}(T) = S_0 + f(b)\log S_0 + \frac{3}{2}\log\frac{T}{T_q}, \tag{2.90}$$

The first term is the classical Bekenstein-Hawking area, the second term comes from the temperature independent contribution to the heat kernel, including the zero mode correction, and the last term comes from a proper treatment of the Schwarzian mode. The temperature independent contribution has two pieces $f(b) = f_0 + f_{hk}(b)$: one from the zero modes, f_0, and

another, f_{hk}, from the direct heat kernel calculation ignoring zero modes. These are in turn

$$f_0 = -\frac{3}{2}\,,$$
$$f_{hk} = \frac{1233\,(2\,b^2+1)^2\tan^{-1}\left(\frac{b}{\sqrt{b^2+1}}\right) - b\,\sqrt{b^2+1}(-463+3080\,b^2+7960\,b^4+3184\,b^6)}{720\,b\,(b^2+1)^{5/2}\,(2\,b^2+1)}\,. \tag{2.91}$$

Due to the fact that we did not find a rotational zero mode for $b \neq 0$ our result for $f(b)$ differs from the result in [93]. According to [93] the zero mode contribution is $f_0 = -2$ since they argue for a total of -4 zero modes. This is the same puzzle raised for Kerr in section 2.2.3. For $b = 0$ we recover the Reissner-Nordström result found in [95] and [47], and the puzzle disappears.

2.3.2 The Kerr-AdS black hole in four dimensions

A second generalization we can consider is the rotating AdS_4 black hole [96], which for simplicity we dub the Kerr-AdS black hole.[12] In standard Boyer-Lindquist coordinates takes the form:

$$\begin{aligned}
\mathrm{d}s^2 &= -\frac{\Delta_r}{\rho^2}\left(\mathrm{d}t - \frac{a}{\Xi}\,\sin^2\theta\,\mathrm{d}\varphi\right)^2 + \frac{\rho^2}{\Delta_r}\,\mathrm{d}r^2 + \frac{\rho^2}{\Delta_\theta}\,\mathrm{d}\theta^2 + \frac{\Delta_\theta\,\sin^2\theta}{\rho^2}\left(a\,\mathrm{d}t - \frac{r^2+a^2}{\Xi}\,\mathrm{d}\varphi\right)^2\,,\\
\Delta_r(r) &= (r^2+a^2)\left(1+\frac{r^2}{\ell^2_{\mathrm{AdS}}}\right) - (r_+^2+a^2)\left(1+\frac{r_+^2}{\ell^2_{\mathrm{AdS}}}\right)\frac{r}{r_+}\,,\\
\Delta_\theta(\theta) &= 1-\frac{a^2}{\ell^2_{\mathrm{AdS}}}\,\cos^2\theta\,, \qquad \rho^2(r,\theta) = r^2+a^2\,\cos^2\theta\,, \qquad \Xi = 1-\frac{a^2}{\ell^2_{\mathrm{AdS}}}\,.
\end{aligned} \tag{2.92}$$

The Euclidean solution is obtained by $t \to \mathrm{i}\,t_{\mathrm{E}}$. The solution is parameterized by two parameters which we have taken to the horizon size r_+ and the rotation parameter a. The

[12] This is an interesting case to consider since in some situations BPS rotating (charged) black holes in AdS in four and five dimensions can be matched with the boundary CFT results, such as [97, 98, 99], particularly in light of [69].

intensive thermodynamic parameters are

$$T = \frac{r_+ \left(1 + a^2\, \ell_{\rm AdS}^{-2} + 3\, r_+^2\, \ell_{\rm AdS}^{-2} - a^2\, r_+^{-2}\right)}{4\pi \left(r_+^2 + a^2\right)}\,, \qquad \Omega = a\, \frac{1 + \frac{r_+^2}{\ell_{\rm AdS}^2}}{r_+^2 + a^2}\,, \tag{2.93}$$

while the extensive quantities are

$$M = \frac{m}{2\, G_N\, \Xi^2}\,, \qquad J = \frac{m\, a}{2\, G_N\, \Xi^2}\,, \qquad m \equiv \frac{r_+^2 + a^2}{r_+} \left(1 + \frac{r_+^2}{\ell_{\rm AdS}^2}\right). \tag{2.94}$$

The extremal Kerr-AdS$_4$ solution is attained along a codimension-1 locus in parameter space (setting $T = 0$). It is clearly characterized by a single scale, r_0, which sets the size of the near-horizon AdS$_2$ length scale, viz.,

$$r_+ = r_0\,, \qquad a_0 = r_0 \sqrt{\frac{\ell_{\rm AdS}^2 + 3\, r_0^2}{\ell_{\rm AdS}^2 - r_0^2}}\,. \tag{2.95}$$

The line element of this near-horizon solution is of the general form given in (2.76), albeit with different angular dependence, cf., [100] for the explicit geometry.

In the non-extremal solution (2.92) the physical charges (2.94) are extensive, but there is a second length scale set by the background cosmological constant $\ell_{\rm AdS}$, which may not scale homogeneously with the charges. Consequently, in analyzing the logarithmic contribution from the heat kernel (2.36), one will end up with $\log S_0 + \log F(M\ell_{\rm AdS}, J)$, where the function F cannot be determined without detailed knowledge of the eigenspectrum. However, in the near-horizon geometry is characterized by a single macroscopic length scale. Inspired by this, [101] analyzes the Seeley-de Witt expansion and extracts the logarithmic correction in the area for rotating AdS$_4$ black holes.

Focusing instead on the temperature corrections, we need to only examine the gravitational zero modes. The analysis in the near-horizon geometry proceeds as in the previous examples. Including the contribution from the Schwarzian mode, we predict a low temperature entropy

of the form quoted in (2.2) with

$$S_0 = \frac{\pi}{G_N}\,\frac{r_0^2+a_0^2}{1-\frac{a_0^2}{\ell_{\rm AdS}^2}}\,, \qquad T_q = \left(1-\frac{a_0^2}{\ell_{\rm AdS}^2}\right)\frac{\ell_{\rm AdS}^2+6\,r_0^2+a_0^2}{r_0\,\ell_{\rm AdS}^2\,(r_0^2+a_0^2)}\,, \tag{2.96}$$

and the $\log S_0$ coefficient as determined in the aforementioned reference.

2.4 Discussion

The main result of this chapter is an explicit demonstration that near-extremal Kerr black holes do not have a macroscopic ground state degeneracy, in contrast to the leading classical expectation. As presaged at the outset, this is indeed what one might expect based on the general arguments given in [41]. The suppression of the classical entropy arises due to geometric zero modes supported in the near-horizon. These modes are to be treated quantum mechanically, and their functional integral induces a power-law suppression at low temperatures. The analysis we undertake is valid for low, but not arbitrarily low, temperatures. In particular, we expect the result (2.2) to hold for $T \leq T_q$, but not for temperatures that are exponentially (in S_0) below this scale. To ascertain effects in this regime would require control over other saddle point configurations to the quantum gravity path integral, which at the moment one does not have.

The primary motivation for undertaking the exercise, whose result one might have viewed as a foregone conclusion, was to test the general principles directly in four dimensional gravity, without reducing to two-dimensional dilaton gravity. At a technical level we are led to examining the kernel of the spin-2 fluctuation operator about the near-horizon of the extremal Kerr geometry. This turns out to be a feasible, though non-trivial, exercise thanks in part to the enhanced symmetry. Curiously, we only find three zero modes in the NHEK geometry. These Schwarzian modes would correspond in the 2d dilaton gravity description of section 2.1.3 to AdS_2 boundary graviton modes.

Naively, one also expects another zero mode associated with the fluctuation of the

angular velocity. From the perspective of section 2.1.3 this is associated with the large gauge transformation of the Maxwell field, arising from the fibration structure. Note that in a spherically symmetric solution, one would have obtained a SO(3) gauge field, but the axisymmetric background only has a U(1). The putative zero mode which can be identified using the result of [88] satisfies the Lorenz gauge condition in 2d. However, when lifted to the full 4d NHEK geometry we find that it is not annihilated by the spin-2 fluctuation operator. While the mode in question is generated by a diffeomorphism, it violates the gauge condition chosen to simplify the quadratic fluctuations (harmonic gauge). Furthermore, attempting to bring it into our preferred gauge leads to a vector field that is singular at the poles of the $\mathbf{S}^2$. We emphasize that this issue is particular to the rotating solutions; for spherically symmetric black holes we recover the expected zero modes associated with the isometries of the sphere.

We adhere to the philosophy that the physical zero modes should correspond to large diffeomorphisms along smooth vector fields. We will find in the next chapter that this is true and that the issue is with the harmonic gauge choice. There are several alternatives one could then consider: allow for the vector field to be singular while staying within the gauge, or make different gauge choices (breaking covariance in the action) for different modes. Either of the alternatives would have given us a rotational zero mode, whose presence a-priori seems sensible on physical grounds. In our final result for the entropy, the presence or absence of this rotational zero mode does not affect the temperature dependent terms in the canonical ensemble[13], but we are led to a different coefficient for the $\log S_0$ contribution than that ascertained in the earlier analysis of [27].

The issue with the rotational zero mode is stark if we consider supersymmetric solutions like the five-dimensional BMPV geometry.[14] In that case, the semiclassical path integral computation can be contrasted against a microscopic counting. As demonstrated in [27] one

[13]This is perhaps the most clear in the context of JT gravity coupled to gauge fields. While quantum effects from the gauge fields lead to temperature-dependent corrections in the grand-canonical ensemble, the Laplace transform necessary to evaluate the canonical fixed charge partition function removes them, leaving solely the Schwarzian contribution, see [102].

[14]We thank Ashoke Sen for emphasizing this point to us.

has exact agreement between the two approaches vis-á-vis the $\log S_0$ correction to the entropy, once one correctly accounts for the zero modes. The count goes as follows: the BMPV solution preserves $\mathrm{SU}(2) \times \mathrm{U}(1)$ isometry. The near-horizon solution (see for instance [103]) is then expected to have 3 Schwarzian zero modes, 3 zero modes from the SU(2) isometry, and a rotational zero mode for a total of 7 gravitational zero modes. Indeed, it is only with these 7 zero modes, one does match with the microscopic calculation. The structure of the near-horizon geometry is similar to the BTZ case, and as in that case, we have been unable to identify a suitable candidate for the rotational zero mode (we do recover the remaining six zero modes). For completeness, we note that the solution also has zero modes associated to Maxwell fields sourcing the background (depending on the string theory embedding), which one can find quite directly. To fix this issue one should therefore either explain why the rotational mode is indeed a zero-mode, or find another mode (perhaps fermionic), assumed in [27] to be a zero mode, to have an action such that the $\log S_0$ is modified in a way that the final answer matches the microsocopic result from string theory.

The puzzle of the rotational zero mode notwithstanding, one has a clear statement for the low temperature thermodynamics of rotating black holes. For simplicity, we have only described the results for four dimensional black holes in asymptotically flat (and AdS) spacetimes. The analysis can be readily generalized to other dimensions. The only ingredients one needs are the near-horizon region and the leading thermal correction. The former is readily available, thanks to the classification of extremal near-horizon geometries, cf., [104] for a review of this program (for known vacuum black holes explicit near-horizon geometries were compiled in [105]). It would be interesting to complete the zero mode analysis and deduce their lifting at low temperatures.

We now turn to some other outstanding issues and comment on ideas in the literature for understanding Kerr entropy, the physical interpretation of the zero modes in the near-horizon geometry, and other physical consequences their presence could have.

Comments on Kerr/CFT: We recall that in [72] it is argued that diffeomorphisms of the NHEK geometry generated by the vector field

$$\zeta_{\mathfrak{f}} = \mathfrak{f}(\varphi)\,\frac{\partial}{\partial\varphi} - \mathfrak{f}'(\varphi)\,\frac{\partial}{\partial y}\,, \tag{2.97}$$

leads to an enhancement of the $\mathrm{SL}(2,\mathbb{R}) \times \mathrm{U}(1)$ isometry to a chiral Virasoro algebra. The central charge of the Virasoro algebra is fixed by the angular momentum, $c_L = 12\,J$. Exploiting the fact that the natural ground state has temperature $T_L = \frac{1}{2\pi}$ and using Cardy asymptotics, one reproduces the extremal entropy $S = 2\pi\,J$. An extension to the near-extremal situation identifies another chiral Virasoro symmetry [73] with $c_R = 12\,J$, and recovers the classical correction to the near-extremal entropy (the linear T correction).

There are two observations to be made regarding this proposal in light of our analysis. Firstly, from the perspective of the gravitational path integral the diffeomorphisms (2.97) lead to non-normalizable deformations of the AdS_2 asymptotics. Indeed, implementing a diffeomorphism with some profile function $\mathfrak{f}(\varphi)$ we find

$$\delta_{\mathfrak{f}}\,\mathrm{d}s^2 = 2\,g_1\left(\left[\frac{\mathrm{d}y^2}{(y^2-1)^2} - y^2\,\mathrm{d}t^2 + \frac{4\,g_2}{g_1}\left(y(y-1)\,\mathrm{d}t^2 + \mathrm{d}\varphi^2 - \mathrm{i}\,\mathrm{d}t\,\mathrm{d}\varphi\right)\right]\mathfrak{f}' - \frac{\mathrm{d}y\,\mathrm{d}\varphi}{y^2-1}\,\mathfrak{f}''\right). \tag{2.98}$$

This asymptotic behaviour was indeed an input in ascertaining which class of diffeomorphisms to admit in [72]. However, the vector field (2.97) is not distinguished in any way in the analysis of the near-horizon fluctuation spectrum, and the resulting deformation has a divergent on-shell action.

A second perspective is offered by the insight of [40] who demonstrate a universal Schwarzian sector in 2d CFTs. Assuming that the CFT has a non-vanishing twist gap (viz., there are no conserved currents), and a large central charge $c \gg 1$, in the canonical ensemble

with $T \sim \mathcal{O}(c^{-1})$ and $J \sim \mathcal{O}(c^3)$, one finds

$$Z_{\rm CFT}(T,J) \sim (c\,T)^{\frac{3}{2}}\, J^{-\frac{3}{4}}\, \exp\left[2\pi\sqrt{\frac{c\,J}{6}} + \frac{\pi\,c}{12}\,T - \frac{1}{T}\left(J - \frac{1}{12}\right)\right]. \tag{2.99}$$

This result which follows from the vacuum dominance in a dual channel, can be demonstrated to hold for $T \ll c^{-1}$ rigorously [106]. This universal high-spin regime is not attained if the central charge scales like the angular momentum. One could attempt to match the result obtained from the path integral computation extrapolating (2.99) past its regime of validity. Doing so would appear to give us the desired result (assuming as earlier that the left movers contribute to the extremal entropy and the right movers to the thermal excitations), but requires further justification.

An asymptotically flat perspective: Here, we have computed the quantum corrections to the entropy of near-extremal Kerr black holes. The calculation consisted in an evaluation of the one-loop determinants around the extremal geometry. We found the presence of exact zero modes localized in the NHEK throat. These zero modes need to be quantized. Making this problem well-defined requires turning on a small temperature, and thus going away form the extremal limit. Other than this IR regulator, most of the calculation was mainly performed in the NHEK throat. Therefore, it is worth thinking about the role of these zero modes in the full, asymptotically flat, geometry. What are these zero modes in the asymptotically flat extremal solution?

To answer this question one needs to look carefully at the topology of the extremal black hole. While a non-extremal black hole has the topology of a cigar, the extremal black hole bears closer resemblance to a cylinder (although the size of the thermal circle becomes infinite) since the horizon has been pushed infinitely far down the throat. When studying gravitational fluctuations on a space with boundary we need to impose boundary conditions to separate diffeomorphisms that are gauged from those that physically act on the boundary. The choice at the asymptotically flat (or AdS) boundary can be made once and for all at

the spacetime asymptopia. Nevertheless, in the extremal background we need to decide how to treat the diffeomorphism which becomes non-vanishing as we approach the horizon. The physical answer is that they should not be gauged. Instead, they can be glued smoothly to the large diffeomorphisms we study in the NHEK throat. Consequently, they should be treated as exact zero modes at zero temperatures, which get a non-vanishing action once temperature is turned on.

Instabilities of the Kerr black hole: The extremal limit of Kerr or Kerr-Newman black hole suffers from instabilities, such as superradiance in the uncharged case and Schwinger pair production (in addition) in the charged case, which we did not incorporate in this analysis[15]. From an estimate of the lifetime of the black hole, one concludes that the imaginary piece which sets the decay time is comparable to the one-loop contribution at temperatures of order $T_q \sim J^{-3}$. It would therefore appear that the near-extremal Kerr black hole radiates spin-2 gravitons and gets further from extremality before entering the regime where the quantum corrections kick in. This has an implication for the interpretation of our result as a statement concerning low-temperature thermodynamics.

A different type of instabilities was recently discovered in [107] when higher derivative corrections to the Einstein-Hilbert action are included (such as in string theory). In the presence of matter, the Aretakis instability [108], which owes to additional conserved charges at the horizon, is yet another possibility. Similar issues for persist for the solutions with negative cosmological constant, where there are interesting implications for the dual holographic CFT [109, 110].

All these mechanisms take place close to the horizon. They can therefore can be analyzed directly in the NHEK throat (or generalizations thereof). In particular, it is useful to follow the approach of section 2.1.3 and describe the dynamics near the horizon in terms of an AdS_2 gravity theory. From this vantage point the instabilities can be viewed as arising due the

[15]One can view our analysis as focusing on the absolute value of the one-loop effective action, whereas superradiance is reflected as an imaginary contribution to the effective action.

presence of tachyonic matter modes in AdS_2 coupled to Jackiw-Teitelboim gravity. In this way of thinking about the problem, it does not matter whether the 2d fields arise from a higher dimensional geometric or matter degree of freedom. Some physical applications such as the one proposed in [107] (and essentially any of the other instabilities mentioned in the previous paragraph) require being arbitrarily close to extremality and therefore quantum effects from the Schwarzian mode should be taken into account if one wants to work at temperatures smaller than T_q. This is an interesting open problem.

Chapter 3

Looking at near-extremal black holes from far away

So far, our gravitational path integral analysis of near-extremal black holes has been situated in the near-horizon region, where we have been evaluating one-loop determinants of fluctuations of gravitons and matter. The enhanced $\mathrm{SL}(2,\mathbb{R})$ symmetry of this region resulted in the presence of zero modes associated with large diffeomorphisms or gauge transformations of the geometry, of which the large diffeomorphisms, referred to as the *Schwarzian* modes, played a crucial role in correcting the low temperature thermodynamics of these black holes. Despite the success of this approach, there are a few outstanding questions which we hope to clarify. The aims of this chapter are twofold:

- First, we wish to provide a perspective on the quantum corrections without referring to the near-horizon geometry directly, but rather working in the full near-extremal black hole spacetime.[1] Relatedly, we would like to reproduce the modes responsible for such quantum effects by working at finite temperature, and not strictly in a small temperature perturbation expansion.

[1]The original analysis of [41] or [40] was carried out in the full geometry, but relied on a split between the near-horizon, analyzed in a low-temperature expansion, and an external part. These two contributions were glued together to evaluate the functional integral. We will instead work directly in the near-extremal solution, and not make particular use of the near-horizon region.

- Second, we would like to clarify aspects of the large gauge transformations associated with abelian rotational isometries, clearing up the puzzle encountered in the previous chapter.

In the rest of the opening of this chapter, we elaborate on these two points and highlight the salient results of our analysis.

The Schwarzian mode in the black hole spacetime: The infinite AdS_2 throat of extremal black holes is not truly decoupled from the asymptotic region. Indeed, it is this lack of decoupling that activates the near-horizon strongly coupled modes. As articulated in [23, 24, 25, 26] one may nevertheless use this AdS_2 region to probe quantum effects. In particular, the $SL(2,\mathbb{R})$ symmetry enables determination of explicit eigenspectrum of the quadratic fluctuation operators. Contained herein are the zero modes, elements in the kernel of the associated operator, generated by large gauge transformations of the near-horizon geometry.

How do the fluctuations in the full geometry manifest the physical effect of these near-horizon zero modes? Generically, there cannot be zero modes in the entire black hole spacetime (away from extremality). In the case of near-extremal black holes, based on the near-horizon analysis, we should expect to see a set of nearly-gapless modes. One might guess that the eigenspectrum of the quadratic fluctuation operator contains modes whose eigenvalues scale linearly with the regulating temperature. Ideally, the support of such modes should also descend into the near-horizon throat as we approach extremality. We demonstrate this picture explicitly in several examples below, showing that the near-horizon zero modes of the extremal solution arise from very light off-shell modes in the full geometry.

The analysis of the eigenspectrum in the full black hole geometry is more involved than in the near-horizon. Nevertheless, we will explicitly verify this picture in a couple of examples: (a) analytically in the near-extremal rotating BTZ geometry, and (b) numerically in the hyperbolic AdS_4 black hole, and the Reissner-Nordström-AdS_4 black hole, respectively. Specifically, we will exhibit eigenmodes of the spin-2 fluctuation operator that exhibit this

linear in T scaling. Based on their properties, we will argue they correspond to the Schwarzian modes encountered in the near-horizon geometry. They contribute a factor of $T^{\frac{3}{2}}$ to the one-loop determinant universally. In addition, we will also find low-lying modes corresponding to gauge field, and rotational isometries. Using these results, we shall reproduce the near-extremal BTZ partition function originally obtained in [40]. Specifically, we will confirm that the result scales as $T^{\frac{3}{2}}\, e^{S_0}$, with S_0 being the (naive) extremal entropy, irrespective of the choice of ensemble (see below).

Before turning to other zero modes, we should highlight a technical result that we derive and use in our analysis. It is well known that the Euclidean Einstein-Hilbert action is sign indefinite, owing to the wrong sign kinetic term for the conformal mode. The standard prescription to deal with this issue is to integrate along purely imaginary conformal factors [111]. A similar prescription for electrically charged black holes in Einstein-Maxwell theory is, to the best of our knowledge, not available in the literature. Taking inspiration from recent analyses [112, 113] we provide a prescription for linearized Einstein-Maxwell theory, and demonstrate its efficacy. Our prescription to deal with modes with non-positive definite action in short amounts to integrating the Maxwell fluctuations along an imaginary contour (along with rotating negative norm eigenmodes of the quadratic fluctuation operator).

Rotational and gauge zero modes: Isometries of the black hole, as well as higher-dimensional gauge fields present in the theory, result in additional zero modes in the near-horizon [26]. For example, spherically symmetric solutions have non-abelian zero modes. These can be identified by dimensionally reducing the solution onto AdS_2 whence one encounters non-abelian gauge fields, whose large gauge transformations constitute the aforesaid modes, see [41] for an explicit analysis in Reissner-Nordström. Likewise, one expects axisymmetric solutions to have abelian rotational zero modes.

Note that rotational and gauge zero modes are closely related. For one, should one uplift black holes to solutions in string or M-theory in 10 or 11 dimensions, then most gauge fields

become geometric.[2] For isometries generated by vector fields with a constant norm, this identification is immediate. However, the dimensional reduction to AdS_2 gravity to identify rotational zero modes is not always fully justified.

A case in point is the Kerr solution, where the near-horizon geometry [70] is non-trivially warped over the polar angle of the $\mathbf{S}^2$. In the previous chapter, we attempted to directly construct the rotational zero mode in the four-dimensional near-horizon extremal Kerr geometry, and encountered a curious puzzle. The putative rotational zero mode failed to satisfy the harmonic gauge condition chosen to carry out the calculation, which one would have intuitively expected it to do. Specifically, we demonstrated that the large diffeomorphism which would have led to such a zero mode, is not generated by a vector field that is smooth everywhere, should we have demanded the harmonic gauge be respected.

We provide a prosaic resolution to this puzzle, by pointing out the breakdown of the harmonic gauge for any Ricci flat near-horizon geometry (which, in particular, includes Kerr). In such cases, one encounters a gauge redundancy, by demonstrating the existence of normalizable diffeomorphisms that preserve the gauge choice. In particular, we show that there are indeed perturbations such as the rotational zero mode that cannot be brought into the harmonic gauge. Relatedly, the ghost one-loop determinant vanishes, confirming the failure of the gauge choice. We show that this problem does not exist for non-Ricci flat near-horizon geometries, such as Kerr-Newman and Kerr AdS black holes.

This simple resolution to the puzzle clarifies issues raised in the previous chapter, where we also pointed out that the absence of rotational zero modes would be a serious problem for supersymmetric black holes. In particular, the matching of the BMPV black hole entropy with the microscopic count carried out in [27] is contingent on such modes being present. We demonstrate that the BMPV black hole near-horizon indeed supports the requisite number of bosonic zero modes.

In the process of resolving this puzzle, we also check for additional zero-modes in the

[2]We thank Ashoke Sen for emphasizing this point and for extensive discussions regarding zero modes.

near-horizon of the extremal BTZ black hole. In line with the above argument, we find one associated with the rotational isometry. However, such a zero mode should not contribution to the low-temperature thermodynamics. Using the dual CFT partition function [40] argued for a low-temperature behavior $T^{\frac{3}{2}}\, e^{S_0}$, irrespective of the choice of ensemble; viz., this result holds whether we study the system at finite angular momentum (canonical) or angular velocity (grand canonical). Addressing how the gravitational computation remains consistent with the CFT analysis, requires a careful analysis of boundary conditions and ensemble choices, which we elaborate on next.

Boundary conditions and ensemble choices: While we motivated the study of low-temperature corrections using the full geometry, we were incomplete in our specification of the problem. One has to be cognizant of the boundary conditions for the two scenarios. The most natural boundary conditions in the AdS_2 throat involve fixing all the macroscopic conserved charges [23], including the energy. However, the subtle quantum effects captured by the Schwarzian modes and its gauge and isometry cousins are better understood in the grand canonical ensemble, where we fix temperature and all chemical potentials. (One can revert back to the fixed charge ensemble upon a Laplace transform.) This choice of boundary conditions is, in fact, more appropriate for the comparison with the full geometry. In higher dimensions the non-normalizable modes, which are more natural to fix, correspond to chemical potentials.[3]

An additional wrinkle in making the comparison is that, while the near-horizon zero modes are derived in the fixed-charge ensemble (from the perspective of the throat), their contribution to the one-loop determinant has hitherto been estimated by passing to the grand canonical ensemble as an intermediate step. The essential idea facilitating this is that the temperature-regulated zero mode action reduces to the quantum mechanics of a particle moving on a group manifold (this perspective is natural if one dualizes the gauge field

[3]This statement largely holds for both flat and AdS asymptotics. There are some exceptional cases, like AdS_4 where both the fixing charge and chemical potentials are admissible [114, 115], but even in these cases we imagine fixing the latter.

dynamics to a topological BF theory). Nevertheless, this analysis does not always guarantee that these modes will (a) extend smoothly away from the throat, (b) be appropriately regulated by the finite temperature solution within the throat. These two questions are not unrelated, since the finite temperature correction to the metric in the throat is equivalent to the leading correction to the decoupling limit involved in gluing back to the exterior spacetime. We will analyze some examples where the modes do not extend outside the throat, making them unphysical. We will also argue in favor of the following criterion to identify this phenomenon. *Whenever a gauge or rotational mode has a singular susceptibility*[4] *(rate of change of charge against chemical potential) at zero temperature, the light mode associated to this symmetry will not extend to the full geometry.*

Outline of the chapter: We begin in section 3.1 with an analysis of the Schwarzian mode in the full black hole spacetime. We present our analytic results for BTZ, and numerical results for the hyperbolic and Reissner-Nordström black holes in AdS_4 in section 3.1. We also comment on the asymptotically flat Reissner-Nordström solution along the way. A detailed discussion of our contour prescription for dealing with the sign indefiniteness of Einstein-Maxwell theory can be found in section 3.1.3. We then examine the rotational modes in section 3.2, demonstrating their existence in Kerr-Newman and Kerr AdS spacetimes, and explain the reason for the issues encountered in the case of Kerr. After explaining how to deduce analogous zero modes for BMPV and BTZ, we turn in section 3.3 to the case of the low-temperature BTZ thermodynamics. We argue that in some cases the light modes (corresponding to rotation or gauge modes) found in the throat do not extend to the full geometry, and that one can identify when this happens from singularities in certain thermodynamic functions in the classical limit.

[4]In some parts of the literature this has been referred to as the compressibility [116], but here we adhere to the more traditional thermodynamic definition, viz., variation of an extensive parameter with respect to its intensive conjugate.

3.1 Extending the nearly-gapless modes to the full geometry

We begin our discussion by demonstrating how the zero modes, localized in the near-horizon throat of the extremal black holes, uplift to the full geometry in the near-extremal solution. We will first discuss the rotating BTZ spacetime, where one has analytic control. We then describe other examples, such as the hyperbolic AdS_4 solution. Finally, we find the Schwarzian and rotational modes in the full Reissner-Nordström solution in AdS_4.

3.1.1 The BTZ black hole

In this section, we consider a theory of 3d gravity with a negative cosmological constant coupled to matter, with an action of the form

$$I = -\frac{1}{16\pi G_N}\int \mathrm{d}^3x\,\sqrt{g}\left(R+\frac{2}{\ell_{\mathrm{AdS}}^2}\right) - \frac{1}{8\pi G_N}\oint \mathrm{d}^2x\,\sqrt{\gamma}\,K + I_{\mathrm{matter}}\,. \tag{3.1}$$

For simplicity, we work in units where $\Lambda = -1$, or equivalently, set the AdS_3 radius to unity $\ell_{\mathrm{AdS}} = 1$. The matter sector can be arbitrary and will not be important for the discussion here, as we argue below. We are interested in studying quantum corrections around the asymptotically AdS_3 rotating BTZ geometry, specifically in the near-extremal limit, and identifying the Schwarzian modes originating from metric fluctuations.

The classical BTZ solution has the following line element [117] in Euclidean signature

$$\mathrm{d}s^2 = f(r)\,\mathrm{d}t_{\mathrm{E}}^2 + \frac{\mathrm{d}r^2}{f(r)} + r^2\left(\mathrm{d}\varphi + \frac{\mathrm{i}\,r_+\,r_-}{r^2}\,\mathrm{d}t_{\mathrm{E}}\right)^2, \tag{3.2}$$

where

$$f(r) = \frac{(r^2-r_+^2)(r^2-r_-^2)}{r^2}\,. \tag{3.3}$$

The solution is written in terms of r_+ and r_-, the outer and inner horizon radii, respectively.

t_{E} corresponds to Euclidean time and $\varphi \sim \varphi + 2\pi$ the spatial coordinate of the conformal boundary with metric $\mathrm{d}s^2|_{\text{bdy}} = \mathrm{d}t_{\text{E}}^2 + \mathrm{d}\varphi^2$. After imposing smoothness at the horizon, the parameters r_+ and r_- are related to temperature and angular velocity by

$$T = \frac{r_+^2 - r_-^2}{2\pi r_+}\,, \qquad \Omega = \frac{r_-}{r_+}\,, \tag{3.4}$$

or equivalently the left-moving and right-moving temperatures

$$T_L = \frac{r_+ - r_-}{2\pi}\,, \qquad T_R = \frac{r_+ + r_-}{2\pi}\,. \tag{3.5}$$

In the grand canonical ensemble, these potentials enter the boundary geometry through the identifications $(t_{\text{E}}, \varphi) \sim (t_{\text{E}} + \beta, \varphi + \mathrm{i}\,\beta\Omega)$ together with $\varphi \sim \varphi + 2\pi$. The charges of the solution are the mass and angular momentum

$$M = \frac{r_+^2 + r_-^2}{8\,G_N}\,, \qquad J = \frac{r_+ r_-}{4\,G_N}\,. \tag{3.6}$$

Finally, the Brown-Henneaux derivation of the asymptotic symmetry implies a boundary central charge [118]

$$c = \frac{3}{2\,G_N}\,. \tag{3.7}$$

The near-extremal limit we are interested in can be characterized in multiple ways, see [40] for more details. In terms of left- and right-moving temperatures, we want to take T_R fixed but with

$$T_L \ll T_R\,. \tag{3.8}$$

This limit also corresponds to low temperatures $T = 2\,\frac{T_L T_R}{T_L + T_R} \sim 2\,T_L$ and fixed spin since $T_R \sim \sqrt{J/c}$ (or in terms of angular velocity $\Omega \sim 1$).

The classical on-shell action predicts a temperature-dependent mass and entropy in the

near-extremal limit

$$M - J \sim 2\pi^2 \frac{T^2}{T_q}\,, \qquad S \sim 2\pi\sqrt{\frac{c\,J}{6}} + 4\pi^2 \frac{T}{T_q}\,. \tag{3.9}$$

The temperature T_q is the scale at which the classical approximation is argued to breakdown [29, 30] and is given by

$$T_q = \frac{24}{c}\,. \tag{3.10}$$

The precise origin and consequences of the quantum corrections appearing at $T \lesssim T_q$ was explained in [40] for BTZ, and more generally in [41]. We should emphasize that T_q is a dimensionful scale, and the fact that we are working in units where the length of the spatial circle is 2π is implicit in (3.10).

In fact, the quantum effects coming from the metric (as well as matter fluctuations) were computed in [119]. As already stated, the purpose of this section is not to reproduce the final answer, which is already known, but to identify the precise profile (in some convenient gauge) of the metric fluctuations in the full asymptotically AdS_3 geometry corresponding to the so-called Schwarzian modes that live near the horizon.

Let us begin by reviewing some generalities which will be useful in the rest of the article. We consider quantum fluctuations $h_{\mu\nu}$ around the BTZ metric $g_{\mu\nu}$ in (3.2)

$$g_{\mu\nu} \to g_{\mu\nu} + h_{\mu\nu}\,. \tag{3.11}$$

It will also prove useful to introduce the (partial) trace reversed fluctuation

$$\widetilde{h}_{\mu\nu} = h_{\mu\nu} - \frac{1}{2} g_{\mu\nu} h\,. \tag{3.12}$$

We would like to integrate over all metric fluctuations. To do so, one needs to implement a

gauge-fixing procedure. We do this by adding the following two terms to the action:

$$I_{\rm gf} = \underbrace{\frac{1}{32\pi\, G_N}\int \mathrm{d}^3x\,\sqrt{g}\,\nabla^\mu\widetilde{h}_{\mu\sigma}\,\nabla^\nu\widetilde{h}_\nu{}^\sigma}_{\text{gauge fixing term}} + \underbrace{\frac{1}{32\pi\, G_N}\int \mathrm{d}^3x\,\sqrt{g}\,\bar{\eta}_\mu\,(-g^{\mu\nu}\nabla^2 - R^{\mu\nu})\,\eta_\nu}_{\text{ghost action}}\,. \quad (3.13)$$

The first one corresponds to our choice of gauge-fixing term, while the second corresponds to the action for the ghosts η_μ needed to introduce to carry out the Faddeev-Popov procedure. Since we aim to identify the Schwarzian modes, we focus on the quadratic action for $h_{\mu\nu}$ which is given by [84, 85]

$$I \supset \frac{1}{16\pi G_N}\int \mathrm{d}^3x\sqrt{g}\,\widetilde{h}^{\mu\nu}(\Delta_L h)_{\mu\nu} \quad (3.14)$$

The kernel appearing in this action is the spin-2 Lichnerowicz operator, which is

$$(\Delta_L h)_{\mu\nu} = -\frac{1}{4}\nabla_\rho\nabla^\rho h_{\mu\nu} + \frac{1}{2}\,R_{\rho(\mu}\,h_{\nu)}{}^\rho - \frac{1}{2}\,R_{\mu\rho\nu\sigma}\,h^{\rho\sigma} - \left(R_{\sigma(\nu} - \frac{1}{4}\,g_{\sigma(\nu}\,R\right)h_{\mu)}{}^\sigma - \frac{\Lambda}{2}h_{\mu\nu}\,. \quad (3.15)$$

This expression is actually valid in any dimension. Let us recall the exact result for the one-loop quantum corrections originating from the metric in the grand canonical ensemble [119]

$$\begin{aligned}\log Z^{\text{1-loop}}_{\text{graviton}} &= \log\left[\prod_{n=2}^{\infty}\frac{1}{(1-e^{-4\pi^2 T_L n})(1-e^{-4\pi^2 T_R n})}\right] \\ &\sim \underbrace{\frac{1}{24\,T_L}}_{\text{Shift of extremal energy}} + \underbrace{\frac{3}{2}\log T_L}_{\text{Schwarzian mode}}\end{aligned} \quad (3.16)$$

Since the expression is naturally written in terms of left- and right-moving temperatures,[5] in the second line we took the near-extremal limit by keeping T_R fixed and taking T_L to be small. The first term in $\log Z^{\text{1-loop}}_{\text{graviton}}$ in the expression above corresponds to a renormalization of the

[5]This expression for $Z^{\text{1-loop}}_{\text{graviton}}$ is nothing else than the product of left- and right-moving vacuum Virasoro characters. This was important in [40] but will not play a crucial role in our present discussion.

extremal mass of the black hole, and will not be important for our purposes. What we are after is to identify the modes responsible for the second term in $\log Z^{\text{1-loop}}_{\text{graviton}}$ which, for obvious reasons, are referred to as the Schwarzian modes. In [40] it was explained how to reproduce such modes from analyzing quantum effects in the $\text{AdS}_2\times\mathbf{S}^1$ throat of the near-extremal BTZ black hole. Our goal here is to identify them in the full geometry, without restricting to the throat.[6]

We shall immediately present our result for the precise Schwarzian profiles, analyze their physical properties, and then mention how they were derived (and how the possibility of further zero modes for this system is excluded). In the harmonic gauge we are using to gauge-fix, the Schwarzian profiles are given by,

$$\begin{aligned} h^{(n)}_{\mu\nu}\,\mathrm{d}x^\mu\,\mathrm{d}x^\nu = H_n(r)\,\Bigg[&\left(r^2\,f(r)^2(\mathrm{d}\varphi-\mathrm{i}\,\mathrm{d}t_{\text{E}})^2+(r_+ + r_-)^2\,\mathrm{d}r^2\right)\cos\left(\frac{2\pi\,n\,t_{\text{E}}}{\beta}\right)\\ &-2\,\mathrm{i}\,(r_+ + r_-)\,r\,f(r)\,\mathrm{d}r\,(\mathrm{d}\varphi-\mathrm{i}\,\mathrm{d}t_{\text{E}})\sin\left(\frac{2\pi\,n\,t_{\text{E}}}{\beta}\right)\Bigg], \end{aligned} \tag{3.17}$$

where the function appearing in front of the metric is given by

$$H_n(r) = N_n\,2\,r^2\left(\frac{r^2-r_+^2}{r^2-r_-^2}\right)^{\frac{|n|}{2}-2}\left(\frac{r_+^2-r_-^2}{r^2-r_-^2}\right)^{4-\frac{|n|}{2}\frac{r_+-r_-}{r_+}}. \tag{3.18}$$

The temporal dependence is fixed in terms of Matsubara frequencies given the identification $t_{\text{E}}\sim t_{\text{E}}+\beta$. Looking at the full profile for $h^{(n)}_{\mu\nu}$ and how it behaves near the horizon shows that fluctuations with $|n|<2$ are singular, while fluctuations with $|n|\geq 2$ are smooth. The range for n therefore excludes $n=0$ and $n=\pm 1$. N_n is a normalization constant we will fix imminently. Let us first record some special properties of these fluctuation profiles:

[6] An attentive reader might be surprised that (3.16) presents a $\frac{3}{2}\log T$ correction coming solely from the Schwarzian mode. The isometries of the throat are $\text{SL}(2,\mathbb{R})\times\text{U}(1)$ which suggest the presence of another contribution $\frac{1}{2}\log T$ from angular momentum fluctuations in the grand canonical ensemble. We will explain in section 3.3 the reason for the rotational modes being absent in the full geometry.

- All these modes are both transverse and traceless

$$\nabla^\mu h_{\mu\nu} = h^\mu{}_\mu = 0, \tag{3.19}$$

guaranteeing that it corresponds indeed to a spin-2 tensor. These two conditions imply that it also satisfies the harmonic gauge $\nabla^\mu \widetilde{h}_{\mu\nu} = 0$. Representations of the modes in other gauge-fixing implementations are related by diffeomorphisms.

- These modes are eigenmodes of the Lichnerowicz operator. Specifically, they satisfy

$$(\Delta_L h)_{\mu\nu} = \underbrace{\frac{|n|\, T_L}{T_L + T_R}\Big(1 - |n|\frac{T_L}{T_L + T_R}\Big)}_{=\lambda_n} h_{\mu\nu}\,. \tag{3.20}$$

The main property making these modes special is that the eigenvalue of the Lichnerowicz operator vanishes linearly as $T \sim T_L \to 0$, with T_R fixed. Moreover, in the low-temperature limit the eigenvalues are proportional to the Matsubara frequency n[7]. These are the defining property of the Schwarzian modes, spin-2 fluctuations that are nearly zero-modes near extremality.

- We argued earlier that we should not include $n = 0$ and $n = \pm 1$. We mentioned below Eq. (3.17) that the metric fluctuation for these modes is divergent. This can be quantified by evaluating their norm, as appears in the definition of the path integral ultralocal measure. One can check that the $n = 0, \pm 1$ modes have a divergent norm and therefore do not contribute to the path integral. More explicitly, the ultralocal measure is[8]

$$\int \mathrm{D}h_{\mu\nu}\, e^{-\|h\|^2} = 1\,, \qquad \|h\|^2 = \int \mathrm{d}^3x\sqrt{g}\,\widetilde{h}^{\mu\nu}h_{\mu\nu}\,. \tag{3.21}$$

[7]We remind the reader that the Schwarzian modes, when properly normalized by their natural symplectic measure, also have an action proportional to their Matsubara frequency, see for example [120] or [90].

[8]In writing this formula we used the fact that we are working in units with $\ell_{\mathrm{AdS}} = 1$, otherwise some powers of ℓ_{AdS} should be included by dimensional analysis.

We can expand metric fluctuations as

$$h_{\mu\nu} = \sum_n \alpha_n h^{(n)}_{\mu\nu} + h^{\perp}_{\mu\nu}, \tag{3.22}$$

where $h^{\perp}_{\mu\nu}$ denotes metric fluctuations perpendicular to all $h^{(n)}_{\mu\nu}$ according to the inner product introduced above. Moreover, all $h^{(n)}_{\mu\nu}$ are perpendicular to each other since their eigenvalues are different. To determine the measure, we normalize the profiles $h^{(n)}_{\mu\nu}$ according to

$$\left\|h^{(n)}\right\|^2 = N_n^2 \, \frac{16\,\pi^2\, r_+\,(r_+ + r_-)^8\,(r_+ - r_-)^4\,\Gamma\left(3 - |n| + |n|\frac{r_-}{r_+}\right)}{\Gamma\left(2 + |n|\frac{r_-}{r_+}\right)}\,\Gamma(|n| - 1)\,. \tag{3.23}$$

The final term on the right-hand side makes it clear that the norm diverges when $n = 0$ or ± 1, indicating that the mode is non-normalizable and should not be included in the path integral. We can fix the normalization constant α_n for $n \neq 0, \pm 1$ such that $\left\|h^{(n)}\right\|^2 = 1$. The integration measure is then

$$\int \mathrm{D}h_{\mu\nu} = \int \mathrm{D}h^{\perp}_{\mu\nu} \int \prod_{|n|\geq 2} \frac{\mathrm{d}\alpha_n}{\sqrt{\pi}}, \tag{3.24}$$

including solely normalizable modes. A similar restriction on n occurs in the evaluation of the one-loop determinant based on the $\mathrm{AdS}_2 \times \mathbf{S}^1$ throat. In that case, this restriction is due to the isometries of AdS_2 making the $n = 0, \pm 1$ modes unphysical.

- As we approach extremality, the modes are localized near the horizon.[9] We can first show that the normalized modes vanish at a fixed value of $r > r_+$, in the limit $r_- \to r_+$. To see this, notice that $H_n(r) \sim N_n(r_+ - r_-)^4$ while $N_n \sim (r_+ - r_-)^{-2}$ implying that $H_n(r) \sim (r_+ - r_-)^2 \to 0$ as $r_+ \to r_-$ at fixed r. This implies that either the modes disappear completely at extremality, or they become localized near the horizon. To show

[9]We will give an explicit mapping to the Schwarzian modes of the near-horizon region in section 3.3,

that the second option is correct, we consider the following observable, the regularized length of the throat

$$L = \int_{r_+}^{\infty} \mathrm{d}r\, \sqrt{g_{rr} + h_{rr}} \approx \underbrace{\int_{r_+}^{\infty} \mathrm{d}r\, \sqrt{g_{rr}}}_{\text{BTZ length of the throat}} + \underbrace{\int_{r_+}^{\infty} \mathrm{d}r\, \frac{h_{rr}}{2\sqrt{g_{rr}}}}_{\text{fluctuation } \delta L} + \cdots . \tag{3.25}$$

The BTZ answer is strictly divergent. We can, however, regulate the result by subtracting off this divergence and focusing instead on the change in length δL. Explicit integration leads, for one mode $\alpha_{n\geq 2}$, to

$$\delta L = \alpha_n \cos\left(\frac{2\pi n t_{\mathrm{E}}}{\beta}\right) \frac{N_n (r_+ - r_-)^2\, (r_+ + r_-)^4\, \Gamma\left(\frac{n-1}{2}\right) \Gamma\left(2 - \frac{n}{2}(1 - \frac{r_-}{r_+})\right)}{4\, \Gamma\left(\frac{3}{2} + \frac{n}{2}\frac{r_-}{r_+}\right)} . \tag{3.26}$$

Importantly, now the effect of the fluctuation mode on the length remains finite at zero temperature since $N_n \sim (r_+ - r_-)^{-2}$, leading to $\delta L \sim \alpha_n \cos\left(\frac{2\pi n t_{\mathrm{E}}}{\beta}\right)$. This shows that at extremality the zero-mode corresponds precisely to fluctuations in the length of the throat, which is the same geometric interpretation as the Schwarzian modes in the AdS_2 description.

- We can also see that the modes are localized at a finite proper distance from the horizon. (We focus on $n \geq 2$ for simplicity; analogous formulas apply for $n \leq -2$.) To do so, let us change coordinates from r to the proper distance from the horizon z:

$$z = \operatorname{arctanh}\left(\sqrt{\frac{r^2 - r_+^2}{r^2 - r_-^2}}\right) . \tag{3.27}$$

Notice that for any $r > r_+$, in the extremal limit the proper distance blows up. We now may consider wavefunction density, the integrand of $\|h\|^2$, which is

$$\left\|h^2\right\|_{\mathrm{den}} = \sqrt{g}\, h^{\mu\nu} h_{\mu\nu} . \tag{3.28}$$

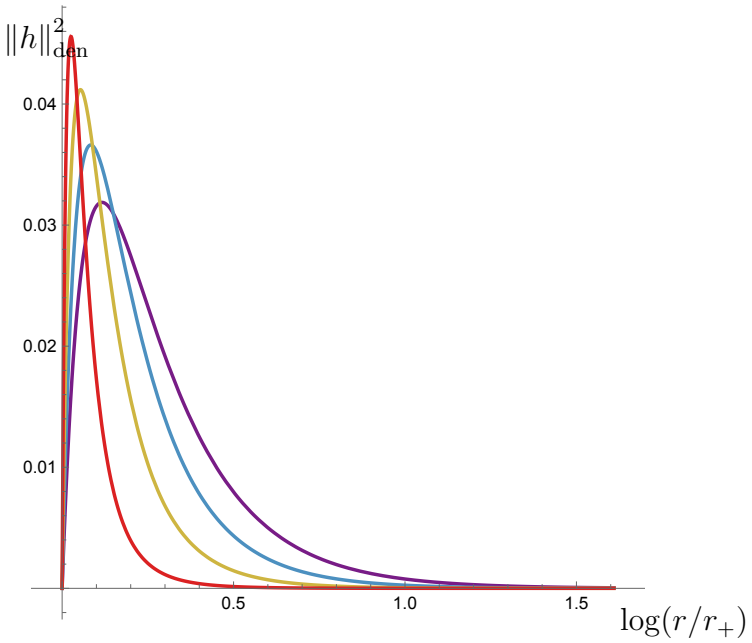


Figure 3.1: Plot of the norm density defined in (3.28) as a function of the proper radial distance $\log(r/r_+)$ for the $n = 3$. The figure shows the result for $r_-/r_+ = 0.6$ (purple), 0.7 (blue), 0.8 (yellow), 0.9 (red). We see that, for a fixed r, the amplitude of the fluctuation becomes smaller as the black hole becomes colder. Instead, the maximum of $\sqrt{g}h^{\mu\nu}h_{\mu\nu}$ increases but progressively localizes closer to the horizon. Indeed, in the extremal limit the maximum amplitude takes place at a finite proper distance from the horizon, which is infinite proper distance down the throat from the boundary.

It is quite a lengthy function but easy to analyze. In particular, it vanishes both on the horizon ($z = 0$) and at infinity ($z \to \infty$). Moreover, it has only one maximum at

$$z = \operatorname{arctanh}\left(\sqrt{\frac{(2\,n-3)\,r_+}{2\,n\,r_- + 3\,r_+}}\right). \tag{3.29}$$

In particular, in the extremal limit $r_- \to r_+$, it has a finite limit

$$z = \operatorname{arctanh}\left(\sqrt{\frac{2\,n-3}{2\,n+3}}\right) < \infty. \tag{3.30}$$

Moreover, if we evaluate the density,

$$\int_0^\beta \mathrm{d}t_{\text{E}} \int_0^{2\pi} \mathrm{d}\varphi\, \sqrt{g}\, h^{\mu\nu}\, h_{\mu\nu}, \tag{3.31}$$

it is easy to check that it is finite at the maximum found above, even in the $r_- \to r_+$ limit. This is consistent with the solution vanishing for any $r > r_+$ because we need to 'zoom' into the near-horizon region to see this result. At extremality all points with $r > r_+$ are located at an infinite proper distance from the horizon. This strongly suggests that these modes are indeed localized deep in the AdS_2 throat.

- We can now add up the contributions from all these modes, after properly normalizing the eigenvalues of the Lichnerowicz operators according to the Einstein action.

$$\frac{1}{16\pi\, G_N}\int \mathrm{d}^3x\,\sqrt{g}\,\widetilde{h}^{\mu\nu}(\Delta_L h)_{\mu\nu} = \sum_{n\neq -1,0,1}\frac{1}{16\pi\, G_N}\,\lambda_n\,\alpha_n^2 + (\text{orthogonal modes}) \quad (3.32)$$

The orthogonal modes include $h^{\perp}_{\mu\nu}$. Assuming Δ_L is non-degenerate, there is no mixing between $h^{\perp}_{\mu\nu}$ and the $h^{(n)}_{\mu\nu}$.[10] Since no matter field is turned on in the background apart from the metric, all other matter fluctuations are automatically orthogonal as well. The properly normalized contribution to the one-loop determinant from $h^{(n)}_{\mu\nu}$ is

$$\begin{aligned}
\log Z^{1-\text{loop}}_{\text{graviton}} &\supset -\frac{1}{2}\sum_{n\neq 0,\pm 1}\log\Big(\frac{\lambda_n}{16\pi\, G_N}\Big)\\
&= -\frac{1}{2}\sum_{n\neq 0,\pm 1}\log\Big[\frac{1}{16\pi\, G_N}\,\frac{|n|\,T_L}{T_L+T_R}\Big(1-|n|\,\frac{T_L}{T_L+T_R}\Big)\Big]\\
&= -\sum_{n\geq 2}\log\Big(\frac{c}{24}\frac{n\,T}{\sqrt{J/c}}\Big)\Big(1+\cdots\Big)\\
&= \frac{3}{2}\log\Big(\frac{T}{T_q}\Big)+\cdots\,.
\end{aligned} \quad (3.33)$$

The answer is written in terms of the left and right temperatures (3.5) in the second line and in terms of the temperature (3.4) and angular momentum (3.6) in the third line. In the third line, we also replace Newton's constant with the central charge (3.7). The final steps follows via zeta-function regularization as described in [121, 47], where we have also used the quantum scale (3.10). The ellipsis denotes terms that are finite

[10] This can be verified in BTZ but will need to be assumed in the higher-dimensional cases.

in both the small temperature and in the large c limits. This contribution reproduces the Schwarzian limit of the exact answer (3.16).

Therefore, (3.17) is the desired result. For our choice of gauge-fixing, we have found the precise profile of the Schwarzian mode away from the throat region. In the rest of this section, we will extend this to black holes in four or higher-dimensions, although the analog of the mode functions such as $H_n(r)$ will have to be found numerically. For this reason, we discussed the BTZ case first.

Our strategy for solving for the modes was straightforward. We parameterized the metric fluctuation in terms of arbitrary axisymmetric functions. We use tracelessness and the divergence free condition to eliminate some functions, and then massage the eigenvalue equation for the Lichnerowicz operator $(\Delta_L h)_{\mu\nu} = \lambda\, h_{\mu\nu}$ to arrive at a second order ODE in the radial coordinate, which we then solved (for the explicit strategy see section 3.1.2). The analysis was aided in part by the results of [122] and [123]. In fact, the result we seek is implicitly present in the latter work. We verified that our analysis agrees with theirs by direct computation.

Before continuing, two comments are in order. First, this is only one specific contribution to the full answer $Z^{1-\text{loop}}_{\text{graviton}}$. Thanks to the solvability of the eigenvalue problem around the BTZ metric, cf., [122, 123], one can verify these are the full set of modes with eigenvalue vanishing with the temperature. Any other mode contributes a temperature independent correction at extremality. Second, this should be surprising since one might expect zero-modes due to the rotational symmetry of BTZ. The exact result (3.16) suggests these modes are not present, and we will analyze this problem further in section 3.3.

3.1.2 The hyperbolic black hole

Before we dive into the physically most interesting case of Reissner-Nordström black hole, let us consider a simpler pure gravity background also in four dimensions – the Schwarzschild-AdS4 solution with a hyperbolic horizon. Lack of both matter and rotation will allow us

to identify relevant modes with greater ease. The geometry in question is a solution of Einstein-Hilbert theory with action

$$I = -\frac{1}{16\pi\, G_N}\int \mathrm{d}^4x\,\sqrt{g}\,(R-2\Lambda) + I_{\rm bdy} + I_{\rm matter}. \tag{3.34}$$

The hyperbolic AdS black hole metric is

$$ds^2 = f(r)\,\mathrm{d}t_{\rm E}^2 + \frac{\mathrm{d}r^2}{f(r)} + r^2\,\mathrm{d}\Sigma_H^2\,, \qquad f(r) = \frac{r^2}{\ell_{\rm AdS}^2} - 1 - \frac{r_+}{r}\left(\frac{r_+^2}{\ell_{\rm AdS}^2} - 1\right). \tag{3.35}$$

and $\mathrm{d}\Sigma_H^2$ is a line element on any 2d surface with the Ricci curvature -2. Since we expect that Schwarzian modes should be in 's-wave' sector, the choice of the surface is not relevant.[11] The horizon is located at $r = r_+$. It is easy to check that (3.35) satisfies Einstein equations with the cosmological constant $\Lambda = -\frac{3}{\ell_{\rm AdS}^2}$. The surface gravity of the horizon, which is proportional to the black hole temperature, reads:

$$\kappa := 2\pi\, T = \frac{1}{2}\,f'(r_+) = \frac{3\,r_+}{2\,\ell_{\rm AdS}^2} - \frac{1}{2r_+}\,. \tag{3.36}$$

We may proceed exactly as in the previous section with the expansion of the action and land on the same operator as in (3.15). It is our task to diagonalize that operator.

This black hole has a near-extremal limit not too different from the one relevant for charged black holes. The reason is that the surface gravity can vanish at a finite value of r_+ given by

$$\kappa = 0 \quad \Rightarrow \quad r_+ = r_{\rm ext} = \frac{\ell_{\rm AdS}}{\sqrt{3}}. \tag{3.37}$$

The fact that the zero-temperature limit retains a macroscopic horizon suggests similar conceptual problems as the one identified in [29, 30, 31] and solved in [40, 41, 71] by

[11] A priori, we could take the 2d geometry to be a compact Riemann surface with genus $g > 1$. However, holographic CFTs on compact hyperbolic spaces often have energies unbounded from below owing to the presence of conformally coupled scalars. We will therefore work with the non-compact space $\mathbb{H}_2$ with an IR regulator.

identifying the Schwarzian modes. Indeed, the near-extremal near-horizon geometry develops an AdS_2 throat. The near-horizon version of that problem may be found in [124]. The goal of this section is to identify the Schwarzian modes in the full asymptotically AdS_4 higher-dimensional geometry.

At the classical level, we can verify the Schwarzian behavior by computing the low-temperature energy and entropy

$$S \sim \frac{\ell_{\rm AdS}^2\, V_H}{12\, G_N} + 4\pi^2 \frac{T}{T_q}\,, \qquad E \sim \frac{\ell_{\rm AdS}^3}{12\sqrt{3}\,\pi} \frac{V_H}{G_N} + 2\pi^2\, \frac{T^2}{T_q}, \tag{3.38}$$

where V_H is the (dimensionless) volume of the hyperbolic 2d surface Σ_H. This has precisely the form predicted by JT gravity and allows us to identify the temperature scale

$$T_q = \frac{G_N}{V_H}\, \frac{12\sqrt{3}\pi}{\ell_{\rm AdS}^3}, \tag{3.39}$$

at which the classical approximation breaks down and quantum effects are crucial.

Schwarzian modes

As already noted, we anticipate the Schwarzian modes should be homogeneous in the hyperbolic space. We can therefore preserve the 2d hyperbolic symmetry, and pick as our ansatz for the perturbation the following line-element:

$$h_{\mu\nu}\, \mathrm{d}x^\mu\, \mathrm{d}x^\nu = e^{\frac{2\pi \mathrm{i}\, n}{\beta}\, t_{\rm E}} \left(f_1(r)\, f(r)\, \mathrm{d}t_{\rm E}^2 + f_2(r)\, \frac{\mathrm{d}r^2}{f(r)} + 2\,\mathrm{i}\, f_3(r)\, \mathrm{d}t_{\rm E}\, \mathrm{d}r + r^2\, f_4(r)\, \mathrm{d}\Sigma_H^2 \right), \tag{3.40}$$

where, as indicated, the functions $f_i(r)$ for $i \in \{1, \cdots, 4\}$ depend only on the radial coordinate. We have inserted factors of $f(r)$ and r^2 for convenience. They ensure that this perturbation will be in L_2 with respect to the ultralocal measure set by $\|h\|^2$ as defined by

$$\int \mathrm{D}h_{\mu\nu}\, e^{-\|h\|^2} = 1\,, \qquad \|h\|^2 = \frac{1}{\ell_{\rm AdS}^4} \int \mathrm{d}^4x \sqrt{g}\, \widetilde{h}^{\mu\nu} h_{\mu\nu}\,, \tag{3.41}$$

provided f_i are in L^2 (i.e., square-integrable) with respect to the uniform measure on $[r_+, \infty)$. We have also used the periodicity of the Euclidean time circle $t_{\scriptscriptstyle \rm E} \sim t_{\scriptscriptstyle \rm E} + \beta$ to expand in Matsubara modes in time. Since we are not restricting ourselves to the near-horizon, we expect Schwarzian modes to be physical (as opposed to pure gauge). Therefore, they should be traceless and transverse. It follows that we want to solve the following system,

$$\Delta_L h_{\mu\nu} = \frac{\lambda}{\ell^2_{\rm AdS}}\, h_{\mu\nu}\,, \qquad \nabla^\mu h_{\mu\nu} = 0\,, \qquad g^{\mu\nu}\, h_{\mu\nu} = 0\,. \tag{3.42}$$

The tracelessness condition allows us to eliminate $f_4(r)$ algebraically

$$f_4 = -\frac{1}{2}\,(f_1 + f_2)\,, \tag{3.43}$$

The transversality condition can be used to eliminate f_1,

$$\begin{aligned} f_1 = \frac{1}{\beta\,(\ell^2_{\rm AdS}(2\,r - 3\,r_+) + 3\,r_+^3)}\Big[&\beta\, f_2\,\big(\ell^2_{\rm AdS}\,(5\,r_+ - 6\,r) + 8\,r^3 - 5\,r_+^3\big) \\ &+ 2\,r\,\big(\beta\, f_2'\,(r_+ - r)\,\big(\ell^2_{\rm AdS}\, - r^2 - r\,r_+ - r_+^2\big) - 2\pi\ \ell^2_{\rm AdS}\, n\, r\, f_3\big)\Big] \end{aligned} \tag{3.44}$$

Finally, f_2 and f_3 can themselves be expressed in terms of a scalar potential $u(r)$

$$f_2 = u - \frac{\beta}{4\pi\,\ell^2_{\rm AdS}\, n\, r^2}\ \big(\ell^2_{\rm AdS}\,(2\,r - 3\,r_+) + 3\,r_+^3\big)\, f_3\,, \tag{3.45}$$

and

$$f_3 = -\frac{4\pi\,\beta\,\ell^2_{\rm AdS}\, n\, r^2\,\big(\big(\ell^2_{\rm AdS}\,(6\,r - 5\,r_+) - 8\,r^3 + 5\,r_+^3\big)\,u + 2\,r\,\big(\ell^2_{\rm AdS}\,(r - r_+) - r^3 + r_+^3\big)\,u'\big)}{4\,\ell^2_{\rm AdS}\, r^4((2\pi\ell_{\rm AdS}\, n)^2 - \beta^2) + \beta^2\, r_+\,(r_+^2 - \ell^2_{\rm AdS})\,(\ell^2_{\rm AdS}\,(4\,r - 3\,r_+) - 12\,r^3 + 3\,r_+^3)}. \tag{3.46}$$

With these changes, the eigenvalue equation, the first equation in (3.42), becomes a second order generalized eigenvalue problem for $u(r)$. Its explicit form is not very illuminating, so instead of writing it down, we only note a few salient properties. Before doing so, it is helpful

to change variables from r to z by the map,

$$r = \frac{4\, r_+}{4 - (1+z)^2}\,. \tag{3.47}$$

This makes the domain of integration compact, $z \in [-1, 1]$. The two end-points $z = \pm 1$ end up being regular singular points of the eigenvalue equation. Let us examine the solutions near the boundaries.

Near the asymptotic boundary, i.e., in the neighborhood of $z = 1$, we find

$$u(z) \sim (1-z)^{s_\pm}\,, \qquad s_\pm = \frac{1}{2}\left(7 \pm \sqrt{9 - 16\,\lambda}\right). \tag{3.48}$$

We require the solutions to preserve the asymptotic form of the metric, viz., obey Dirichlet boundary conditions. This is only achieved by the local solution that decays faster, viz., $(1-z)^{s_+}$.

Near the horizon, viz., in the vicinity of $z = -1$, we find

$$u(z) \sim (1+z)^{s'_\pm}\,, \qquad s'_\pm = -2 \pm n\,. \tag{3.49}$$

The solution will be regular[12] at the horizon, only if we pick the faster decay; this requires the choice $s' = -2 + |n|$. This, however, is not enough, we must also impose $|n| \geq 2$.

All told, from the local Frobenius analysis, we are led to a further substitution

$$u(z) = (z+1)^{|n|-2}\,(1-z)^{\frac{5}{2}}\,w(z)\,. \tag{3.50}$$

Now the function $w(z)$ must be merely regular at the horizon and vanish at $z = 1$. (Note that w will be C^2 but not C^3 at that boundary). With this set of boundary conditions, our eigenvalue problem is well-posed as long as $\lambda < \frac{5}{16}$. For larger values, both solutions decay at

[12]To be precise, for regularity we demand that the solutions be sufficiently smooth to lie in L^2 with respect to the ultralocal measure. We will use this definition of regularity in the rest of this section.

$z = 1$.

In the numerical analysis, we tracked the lowest set of eigenvalues of Δ_L as a function of temperature (for a fixed Matsubara frequency labeled by $n \in \mathbb{Z}$). The generalized eigenvalue problem for u may be written using (3.50) as the following ODE for $w(z)$:

$$\mathcal{D}w = \lambda\, \mathcal{G}\, w, \tag{3.51}$$

where

$$\mathcal{D} = A(z)\, \partial_z^2 + B(z)\, \partial_z + C(z) \tag{3.52}$$

and $\mathcal{G}(z)$ is a specific multiplicative factor in the source term proportional to the eigenvalue, fixed in terms of our choice of the Sturm-Liouville operator $\mathcal{D}$. We discretized the interval $[-1, 1]$ into Gauss-Lobatto grid, (z_i) with $i \in \{1, \cdots, N+1\}$, on which we used a spectral collocation method. Writing the unknown function w as a vector of values on the grid $\vec{w} = (w(z_i))$, we may approximate derivatives of w by matrix multiplication by a certain matrix $\mathcal{D}_{\text{discretized}}$.[13] Then, the operators $\mathcal{D}$ and $\mathcal{G}$ takes the discretized form:

$$\mathcal{D}_{\text{discretized}} = A(\vec{z})\, D^2 + B(\vec{z})\, D + C(\vec{z}) \tag{3.53}$$

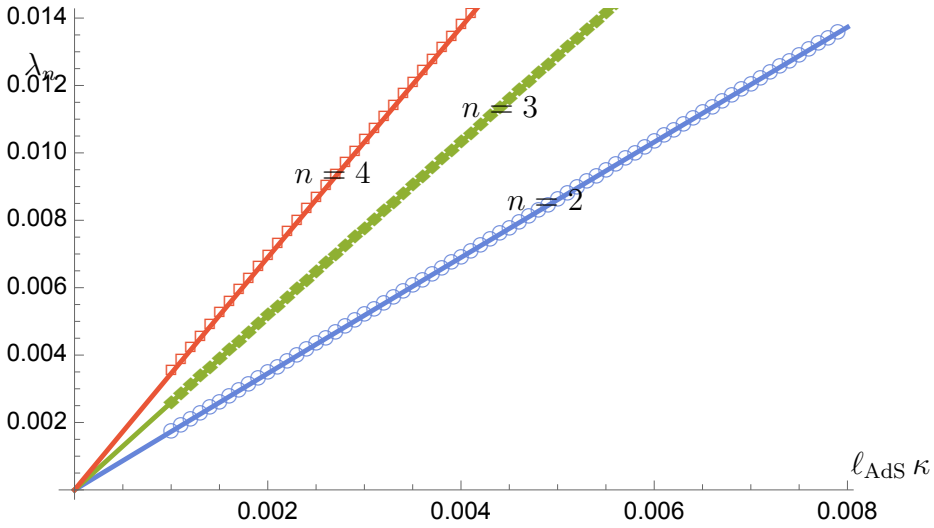
and

$$\mathcal{G}_{\text{discretized}} = \mathcal{G}(\vec{z}), \tag{3.54}$$

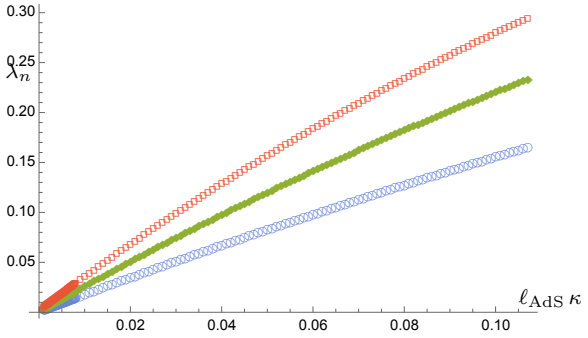
where $A(\vec{z})$ denotes a diagonal matrix with the diagonal entries given by values of $A(z)$ on the grid points and the same *mutatis mutandis* holds for $B(\vec{z})$, $C(\vec{z})$, and $\mathcal{G}(\vec{z})$. To implement the boundary conditions at infinity, we simply replace the row in $\mathcal{D}_{\text{discretized}}$ corresponding to $z = 1$ with zeroes. The functions A and $\mathcal{G}$ vanish at $z = -1$. The conditions at $B(-1)$ and $C(-1)$ ensure that the solution is regular (and not blowing up) at the horizon, so no further change is needed. Having done all that, we may just ask for the eigenvalues for

[13] For more details on spectral methods and explicit implementations, see [125]. For the review of using them in gravity, see [126].

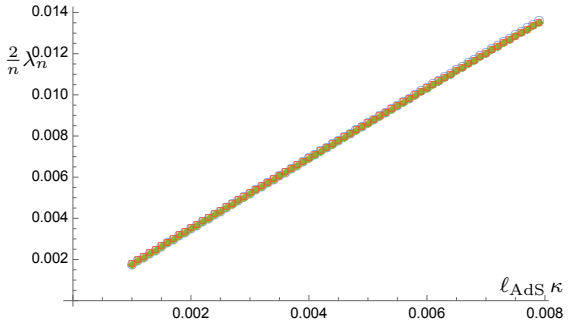
this generalized eigenvalue problem using built-in functions in Mathematica. We found that already at $\kappa\,\ell_{AdS} = O(10^{-2})$ machine precision was not sufficient, and so we had to work with extended precision. The results of this numerical analysis for the lowest three positive frequency Matsubara modes ($n = 2, 3, 4$) is illustrated in fig. 3.2.



(a) The eigenvalue spectrum at low temperatures.



(b) The eigenvalue spectrum over an extended range.



(c) Rescaled eigenvalues demonstrating scaling.

Figure 3.2: The uplift of Schwarzian modes to the full hyperbolic AdS_4 black hole geometry. We show the data for very low temperatures in the top panel, fig. 3.2a, demonstrating linear behavior with temperature. In the bottom left panel, fig. 3.2b, we show the behavior over a greater range of temperatures, making the departures from linear growth manifest. Finally, in the bottom right panel fig. 3.2c, we plot the eigenvalues rescaled by the overtone number $\frac{2}{n}\,\lambda_n$ to demonstrate that $\lambda_n \sim n\,T$ (notice the three curves are overlapping, which was achieved by working with extended precision numerics).

The numerical data for the eigenvalues for $n = 2, 3, 4$ fit well to a quadratic polynomial

for low values of surface gravity, $\kappa\,\ell_{\rm AdS} \in [0.001, 0.008]$. Letting,

$$\lambda_n = a_n + b_n\,\kappa\,\ell_{\rm AdS} + c_n\,(\kappa\,\ell_{\rm AdS})^2\,, \tag{3.55}$$

we find

$$\begin{aligned} &b_2 = 1.73195\,, && c_2 = -1.97407\,, && a_2 \sim \mathcal{O}\big(10^{-7}\big)\,,\\ &b_3 = 2.59772\,, && c_3 = -4.40843\,, && a_3 \sim \mathcal{O}\big(10^{-7}\big)\,.\\ &b_4 = 3.46369\,, && c_4 = -7.82459\,, && a_4 \sim \mathcal{O}\big(10^{-7}\big)\,. \end{aligned} \tag{3.56}$$

This is indeed consistent with these modes becoming zero modes as we attain extremality, i.e., at $\kappa = 0$. In particular, as expected, at very low temperatures, we have a set of modes whose eigenvalues scale linearly with temperature. Furthermore,

$$\frac{b_3}{b_2} = \frac{2.59772}{1.73195} \approx \frac{3}{2} - 0.000012\,, \qquad \frac{b_4}{b_3} = \frac{3.46369}{2.59772} \approx \frac{4}{3} - 0.000021\,. \tag{3.57}$$

This illustrates that the eigenvalues have a slope that scales linearly with the overtone number n, consistent with them being the extension of the Schwarzian mode onto the full geometry.[14] The upshot of this numerical results is that one has[15]

$$\lim_{T\to 0} \frac{\lambda_n\,\ell^2_{\rm AdS}}{16\pi G_N} \approx \alpha\,n\,\frac{T}{T_q} + \mathcal{O}\big(T^2\big)\,, \qquad |n| \geq 2\,, \tag{3.58}$$

in excellent agreement with our expectation based on the near-horizon analysis (for explicit investigation in the case of the hyperbolic black hole, cf. [124]). This result implies that the graviton one-loop determinant around the near-extremal hyperbolic black hole is

$$\log Z^{1-\rm loop}_{\rm graviton} \supset -\sum_{n\geq 2} \log\left(\frac{\lambda_n \ell^2_{\rm AdS}}{16\pi G_N}\right) = \frac{3}{2}\log\frac{T}{T_q} + \mathcal{O}(1), \tag{3.59}$$

[14]The discrepancy of $\mathcal{O}\big(10^{-5}\big)$ is mainly because we truncated the Taylor expansion at quadratic order.

[15]A factor of $\ell^{-2}_{\rm AdS}$ arises from our normalization of the Lichnerowicz operator eigenvalue, while another factor of $\ell^4_{\rm AdS}$ arises from the normalization of the inner product $\|h\|^2$.

consistent with the result obtained by gluing the near-horizon throat to the far-away region, and applying 2d gravity techniques on the throat.

Probe gauge fields

The analysis in section 3.1.2 focused on the fluctuation of gravitons. It is also interesting to analyze the one-loop determinant of matter around this geometry. One class of matter that is interesting to examine is a probe gauge field. Owing to the associated gauge invariance, one expects to see a set of large gauge transformations being manifested as zero modes in the near-horizon of the extremal solution.[16]

In fact, the analysis of a probe Maxwell field, which we now undertake, will provide a useful guide for the analysis around the Reissner-Nordström geometry later in the sequel. We will examine the dynamics in a U(1) theory, with the standard Maxwell action supplemented by the Lorenz gauge fixing term. To wit,

$$\begin{aligned} I = I_{\rm Max} + I_{\rm gf} &= \int {\rm d}^4x\, \sqrt{g}\, \left[F_{\mu\nu}\, F^{\mu\nu} + 2\, (\nabla^\mu A_\mu)^2 \right] \\ &= 2 \int {\rm d}^4x\, \sqrt{g}\, A^\mu \left(-\delta_\mu{}^\nu\, \nabla^2 + R_\mu{}^\nu \right) A_\nu \end{aligned} \tag{3.60}$$

In the second line we have integrated by parts, discarding the boundary term, and thereby extracted the operator whose fluctuation determinant we wish to compute, viz.,

$$\det \left(-\delta^\nu{}_\mu\, \nabla^2 + R^\nu{}_\mu \right). \tag{3.61}$$

The gauge field vanishes in the background geometry (3.35), and the measure of integration for fluctuations A_μ are normalized with respect to the ultralocal measure on the space of

[16] Per se, we do not expect the Klein-Gordon operator associated to scalar fields to have low-lying eigenvalues. We have verified this numerically for some reasonably small values of κ.

fluctuations defined through the norm, i.e.,

$$\|A\|^2 = \int \mathrm{d}^4x\,\sqrt{g}\,A^\mu A_\mu\,. \tag{3.62}$$

As for the Schwarzian modes, potential light fluctuations should be physical (not gauge) modes in the full geometry. As such, we may require that they are divergence-free. It follows that we want to solve the following system of equations

$$-\nabla^2 A_\mu + R^\nu{}_\mu A_\nu = \frac{\lambda}{\ell^2_{\mathrm{AdS}}}\,A_\mu\,, \qquad \nabla^\mu A_\mu = 0\,. \tag{3.63}$$

Based on the intuition from the near-horizon analysis, we expect to find the low-lying eigenmodes to be homogeneous on $\mathbb{H}_2$. Therefore, we pick the ansatz

$$A_\mu\,\mathrm{d}x^\mu = e^{\frac{2\pi\,\mathrm{i}\,n}{\beta}\,t_{\mathrm{E}}}\,\sqrt{f}\left(\mathrm{i}\,a_t(r)\,\mathrm{d}t_{\mathrm{E}} + a_r(r)\,\frac{\mathrm{d}r}{f}\right), \tag{3.64}$$

parameterized by functions $a_t(r)$ and $a_r(r)$. The factors of $\sqrt{f}$ are inserted for convenience alone. They ensure that A is in L^2 with respect to the ultralocal measure if a_t, a_r are in L^2 with respect to the $r^2\,\mathrm{d}r$ measure on $[r_+,\infty)$.

The condition that fluctuations are divergence-free allows us to eliminate a_t:

$$a_t = \beta\frac{\left(\ell^2_{\mathrm{AdS}}\,(4\,r-3\,r_+) - 6\,r^3 + 3\,r_+^3\right)a_r + 2\,r\left(\ell^2_{\mathrm{AdS}}\,(r-r_+) + r_+^3 - r^3\right)a_r'}{4\pi\,\ell^2_{\mathrm{AdS}}\,n\,r^2}\,. \tag{3.65}$$

We are then left with a single radial ODE to solve

$$\begin{aligned}
0 &= \left(\ell^2_{\mathrm{AdS}}\,(r_+ - r) + r^3 - r_+^4\right)a_r''(r) - 2\,(\ell^2_{\mathrm{AdS}} - 3\,r^2)\,a_r'(r) + V_A(r)\,a_r(r)\,,\\
V_A(r) &\equiv -\frac{\ell^4_{\mathrm{AdS}}\left(16\pi^2\,n^2\,r^4 + \beta^2\,\left[4\,\lambda\,r^4 - 4\,\lambda\,r^3\,r_+ + 8\,r^2 - 24\,r\,r_+ + 15\,r_+^2\right]\right)}{4\,\beta^2\,r^2\,(r-r_+)}\\
&\quad - \frac{2\,\ell^2_{\mathrm{AdS}}\left(-2\,\lambda\,r^6 + 6\,r^4 + 2\,\lambda\,r^3\,r_+^3 + 12\,r\,r_+^3 - 15\,r_+^4\right) + 3\,\beta^2\left(5\,r_+^6 - 8\,r^6\right)}{4\,r^2\,(r-r_+)}\,.
\end{aligned} \tag{3.66}$$

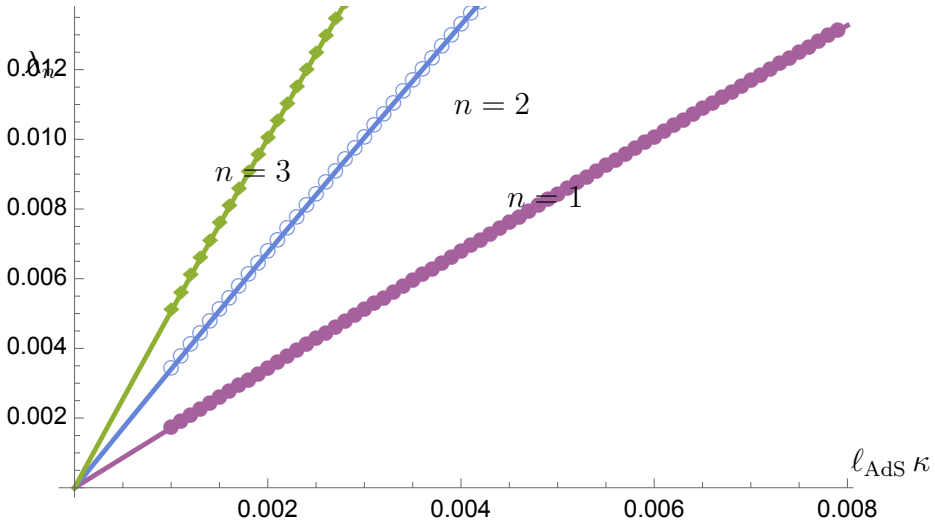
To analyze the equation, we again pass to the z-coordinate introduced in (3.47) to compactify the domain of integration. As before, both $z = \pm 1$ are regular singular points of (3.66). Analyzing the behavior near the horizon and asymptopia, we learn

$$a_r(z) \sim \begin{cases} (1-z)^{s_\pm}\,, & s_\pm = \frac{5}{2} \pm \sqrt{\frac{1}{4} - \lambda}\,, \qquad z \lesssim 1\,, \\ (1+z)^{s'_\pm}\,, & s'_\pm = \pm n - 1\,, \qquad z \gtrsim -1\,. \end{cases} \tag{3.67}$$

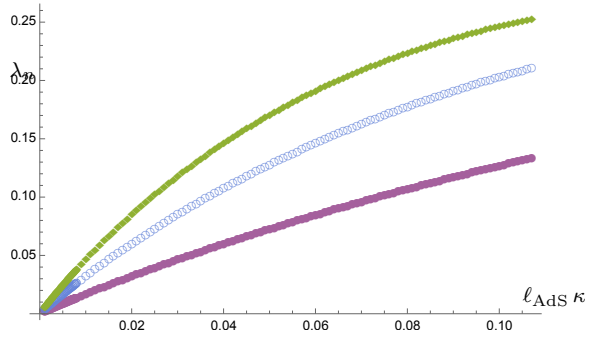
We learn that the s_+ solution is normalizable and preserves Dirichlet boundary conditions at $z = 1$, while at the horizon we need $s' = |n| - 1$. As for the Schwarzian modes earlier, this is not enough and one must impose, in this case, $|n| \geq 1$. Redefining, $a_r(z)$ in favor of a new function $w(z)$ through,

$$a_r(z) = (1+z)^{|n|-1}\,(1-z)^{\frac{5}{2}}\,w(z)\,, \tag{3.68}$$

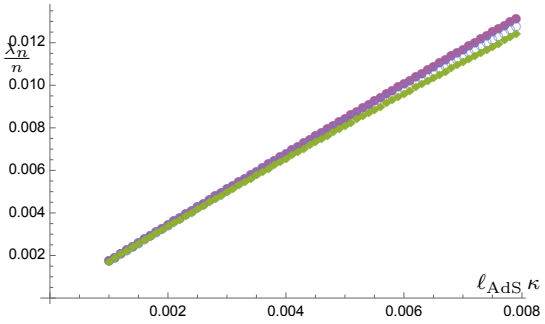
we conclude that $w(z)$ must be regular at $z = -1$ (horizon) and vanish at $z = 1$ (infinity). The function $w(z)$ will only be C^0 at the latter boundary. We now have a well-posed eigenvalue problem. We solved it numerically in the same way as for the Schwarzian modes. The only difference being that we found machine precision to be sufficient for our purposes. This explains why the data presented below matches the near-horizon analysis with less precision. That may be best seen by comparing fig. 3.2c and fig. 3.3c for temperatures of order $\kappa\,\ell_{\text{AdS}} \sim 10^{-2}$.



(a) The eigenvalue spectrum at low temperatures.



(b) The eigenvalue spectrum over an extended range.



(c) Rescaled eigenvalues demonstrating scaling.

Figure 3.3: The uplift of probe Maxwell field zero modes to the full hyperbolic AdS_4 black hole geometry. We show the data for very low temperatures in the top panel fig. 3.3a, demonstrating linear behavior with temperature. In the bottom left panel fig. 3.3b, we show the behavior over a greater range of temperatures, making the departures from linear growth manifest. Finally, in the bottom right panel fig. 3.3c, we plot the eigenvalues rescaled by the overtone number $\frac{1}{n}\,\lambda_n$ to demonstrate that $\lambda_n \sim n\,T$.

This analysis illustrates the presence how the gauge field zero modes in the near-horizon are manifest in the full geometry at low temperatures. The mechanics of the computation is similar in the spirit to the Schwarzian discussion, and much simplified in the present case, by the decoupling between the gauge field and metric perturbations.

The contribution to the one-loop determinant from this set of gauge (near) zero modes

would be

$$\log Z^{1-\text{loop}}_{\text{gauge}} \supset -\sum_{n\geq 1} \log\left(\frac{\lambda_n\, \ell^2_{\text{AdS}}}{16\pi G_N}\right) = \frac{1}{2}\log\frac{T}{T_q} + \mathcal{O}(1)\,. \tag{3.69}$$

Unlike the Schwarzian modes, this answer is not by itself the complete story. These zero modes exist with fixed asymptotic chemical potential μ, viz., in the grand canonical ensemble. Owing to charge quantization, we should sum over boundary conditions with shifted chemical potentials, $\beta\mu \to \beta\mu + 2\pi\,\mathrm{i}\,\mathbb{Z}$. The full partition function is given by the sum over these shifts, weighted by the classical action, which will itself receive corrections from the backreaction of the gauge fields. Every such configuration can be viewed as a new saddle, and as such, if the above backreaction is ignored each of them will have a one-loop contribution given by (3.69). A simple application of Poisson resummation (see, for example, [102, section 2] or [41, section 3]) suggests that the fixed charge partition function is temperature independent near-extremality. To give a complete argument for this feature, without using the throat, would require accounting for the backreaction of the gauge field in the presence of these integer fluxes (although one can already notice the backreaction will be small at low temperatures since the shift in the chemical potential vanishes linearly with temperature).

Rotations – a formal detour

For asymptotically flat, or asymptotically globally AdS black holes, we also expect another family of gravitational zero modes. These arise from the background isometries. For spherically symmetric black holes such as Reissner-Nordström they originate from the rotations of the sphere (or, more geometrically, from the Killing fields of the sphere). Similar statements apply for the case of axisymmetric solutions like Kerr.

It is interesting to ask if the black holes with hyperbolic horizons, which we are currently examining, allow for an analog of such modes. If so, they should be easier to analyze. The answer to this question depends on the nature of the horizon spatial cross-section. If the spatial cross-section was a compact hyperbolic space, then there would generically be no Killing vectors, and thus we won't encounter an analog of the rotational zero modes. On

the other hand, on $\mathbb{H}_2$, which is a maximally symmetric space, we do have Killing vector fields. These are, however, not normalizable. Consequently, the associated modes in the full spacetime will also not be normalizable as well.

For the present, we will study this $\mathbb{H}_2$ model as an illustrative example. To analyze the modes, we will simply ignore the issue of normalizablity by working with an IR regulator. One should keep in mind that these solutions will disappear from our functional space if we remove the regulator. Hence, one should treat this part as a rather formal (but useful) exercise.

Let $\mathfrak{v}$ be a Killing (co)-vector in $\mathbb{H}_2$. We pick an ansatz for the metric perturbations around (3.35)

$$h_{\mu\nu}\,\mathrm{d}x^\mu\,\mathrm{d}x^\nu = 2\,e^{\frac{2\pi\mathrm{i}\,n}{\beta}\,t_{\mathrm{E}}}\,\mathfrak{v}\,r\,\sqrt{f}\left(\mathrm{i}\,g_1(r)\,\mathrm{d}t_{\mathrm{E}} + g_2(r)\,\frac{\mathrm{d}r}{f}\right). \tag{3.70}$$

The inspiration for this is similar to the rationale behind the choice for the gauge field analysis, cf. the discussion around (3.64). The sprinkling of factors of $\sqrt{f}$ ensure that as long as $\{f_1, f_2\}$ are in L^2 with respect to the uniform measure on $[r_+, \infty)$, the metric perturbation has a finite ultralocal norm. We now aim to solve (3.42).

We have ensured that the perturbation is trace free, so only have to impose the divergenceless condition, which helps eliminate g_1

$$g_1 = -\beta\,\frac{\left(\ell_{\mathrm{AdS}}^2\,(6\,r - 5\,r_+) - 8\,r^3 + 5\,r_+^3\right)g_2 + 2\,r\left(\ell_{\mathrm{AdS}}^2\,(r - r_+) - r^3 + r_+^3\right)g_2'}{4\pi\,\ell_{\mathrm{AdS}}^2\,n\,r^2}\,. \tag{3.71}$$

The eigenvalue equation itself is a second order ODE for g_2, which we report here for

completeness

$$
\begin{aligned}
0 &= \left(\ell_{\text{AdS}}^2\,(r-r_+) - r^3 + r_+^3\right) g_2''(r) + 2\left(\ell_{\text{AdS}}^2 - 3\,r^2\right) g_2'(r) + \ell_{\text{AdS}}^2\, V_{f_2}(r)\, g_2(r)\,, \\
V_{g_2} &\equiv \frac{\ell_{\text{AdS}}^2\left(\beta^2\left(16\,\lambda\,r^3\,(r_+ - r) - 24\,r^2 + 60\,r\,r_+ - 35\,r_+^2\right) - 16\,\pi^2\,n^2\,r^4\right)}{4\,\beta^2\,r^2\,(\ell_{\text{AdS}}^2(r-r_+) - r^3 + r_+^3)} \\
&\quad + \frac{\left(8\,\lambda\,r^6 + 6\,r^4 - 2\,r^3\,r_+\left(4\,\lambda\,r_+^2 + 7\right) - 30\,r\,r_+^3 + 35\,r_+^4\right) + \beta^2\left(16\,r^6 + 28\,r^3\,r_+^3 - 35\,r_+^6\right)}{2\,r^2\,(\ell_{\text{AdS}}^2(r-r_+) - r^3 + r_+^3)}\,,
\end{aligned}
\tag{3.72}
$$

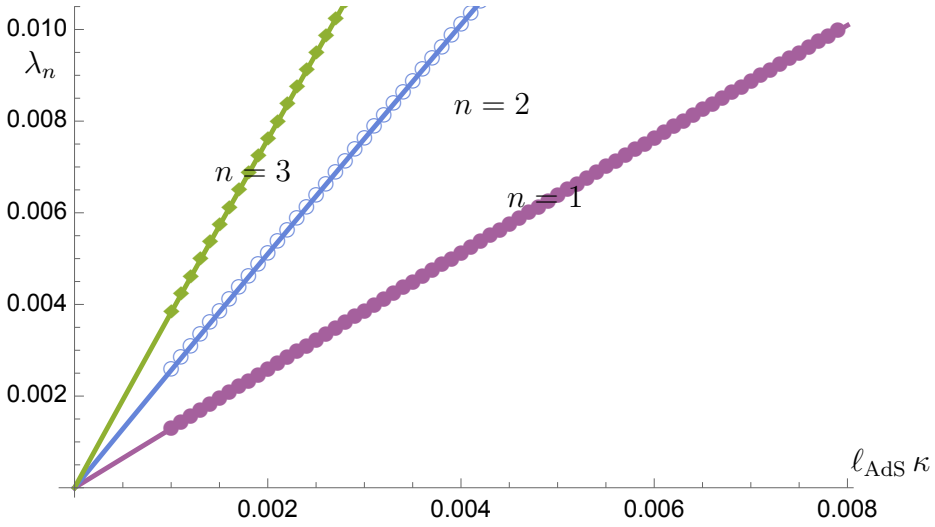
where λ is the eigenvalue we seek. Passing, as before, to the compactified domain of the z-coordinate (3.47), we learn of the asymptotic behavior

$$
g_2(z) \sim \begin{cases} (1-z)^{s_\pm}\,, \quad s_\pm = \dfrac{5}{2} \pm \sqrt{\dfrac{9}{4} - 4\,\ell_{\text{AdS}}^2\lambda}\,, & z \lesssim 1\,, \\ (1+z)^{s'_\pm}\,, \quad s'_\pm = \pm n - 1\,, & z \gtrsim -1\,. \end{cases}
\tag{3.73}
$$

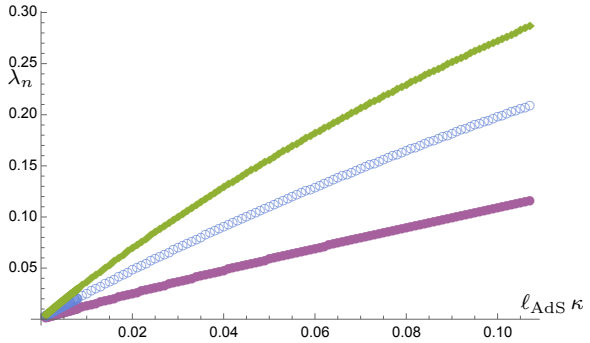
This suggests trading $g_2(z)$ in favor of $w(z)$, which is related by

$$
g_2(z) = (1+z)^{|n|-1}\,(1-z)^{\frac{3}{2}}\,w(z)\,,
\tag{3.74}
$$

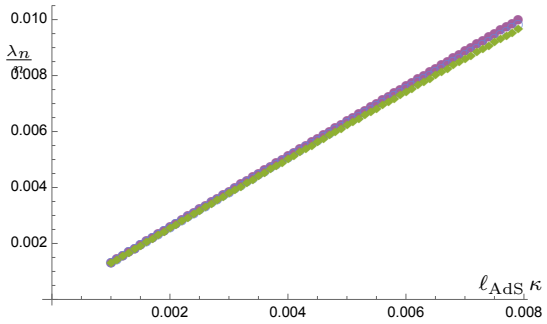
which again requires us to consider only $|n| \geq 1$ just like the gauge modes. The function $w(z)$ is required to be regular at $z = -1$ (horizon) and vanish at $z = 1$ (asymptopia). At the latter boundary $w(z)$ is C^2 but not C^3. We now have a well-posed eigenvalue problem, which we can solve numerically in the same way as for the Schwarzian modes. The main difference from that case is that we found machine precision to be sufficient for our purposes. This explains why the data presented below matches the near-horizon analysis with less precision. That may be best seen by comparing fig. 3.2c and fig. 3.3c for temperatures of order $\kappa\ell_{\text{AdS}} \sim 10^{-2}$.



(a) The eigenvalue spectrum at low temperatures.



(b) The eigenvalue spectrum over an extended range.



(c) Rescaled eigenvalues demonstrating scaling.

Figure 3.4: The uplift of the (formal) rotational field zero modes to the full hyperbolic AdS_4 black hole geometry. We show the data for very low temperatures in the top panel, fig. 3.4a, demonstrating linear behavior with temperature. In the bottom left panel, fig. 3.4b, we show the behavior over a greater range of temperatures, making the departures from linear growth manifest. Finally, in the bottom right panel, fig. 3.4c, we plot the eigenvalues rescaled by the overtone number $\frac{1}{n}\,\lambda_n$ to demonstrate that $\lambda_n \sim n\,T$. While the plot very closely resembles that of the probe Maxwell field fig. 3.3, there are subtle differences in the numerical data.

These rotational zero modes will also give rise to a factor of $\frac{1}{2}\,\log T$ to $\log Z^{1-\mathrm{loop}}_{\mathrm{graviton}}$. This is, as in the discussion at the end of section 3.1.2, the contribution from a single saddle. We still have to sum over the configurations related by the shifts of the rotational chemical potential $\beta\Omega \to \beta\Omega + 2\pi\,\mathrm{i}\,n$ (or $4\pi\,\mathrm{i}\,n$ in theories with fermionic degrees of freedom), which will additionally entail computing the shifted value of the classical on-shell action. The expectation,

based on a calculation done at the level of the throat, is that Poisson resummation will again remove the temperature dependence of the quantum correction near extremality. This might be harder to verify since the backreacted solutions involve a rotating version of the hyperbolic black hole.

3.1.3 The Reissner-Nordström (AdS) black hole

We are now ready to attack the most interesting problem – the one-loop determinant for the Reissner-Nordström solution. For technical reasons, it is easier to work with AdS asymptotics, which simplifies imposition of boundary conditions. So we will initially work with a finite cosmological scale ℓ_{AdS}, and subsequently comment on the limit $\ell_{\text{AdS}} \to \infty$ in section 3.1.3.

The background metric for the spherically symmetric static solution reads

$$\mathrm{d}s^2 = f(r)\,\mathrm{d}t_{\text{E}}^2 + \frac{\mathrm{d}r^2}{f(r)} + r^2\,\mathrm{d}\Omega_2^2\,, \qquad f(r) = \frac{r^2}{\ell_{\text{AdS}}^2} + 1 - \frac{2m}{r} + \frac{Q^2}{r^2}. \tag{3.75}$$

We consider an electrically charged black hole and so the Maxwell potential is

$$A = \mathrm{i}\left(\frac{Q}{r} - \frac{Q}{r_+}\right)\mathrm{d}t_{\text{E}}\,. \tag{3.76}$$

It will prove useful to parameterize the solution in terms of the outer and inner horizon radii, which we achieve via

$$Q^2 = r_+\,r_-\left(1 + \frac{r_+^2 + r_-^2 + r_+\,r_-}{\ell_{\text{AdS}}^2}\right), \qquad 2\,m = r_+\left(\frac{r_+^2}{\ell_{\text{AdS}}^2}\right) + \frac{Q^2}{r_+}\,. \tag{3.77}$$

The black hole solution is a saddle point for the gravitational action with fixed temperature

and chemical potential, which are in turn

$$\begin{aligned}\kappa &:= \frac{T}{2\pi} = \frac{r_+ - r_-}{2\,r_+^2}\left(1 + \frac{r_-^2 + 2\,r_+\,r_- + 3\,r_+^2}{\ell_{\rm AdS}^2}\right), \\ \mu &= \sqrt{\frac{r_-}{r_+}}\,\sqrt{1 + \frac{r_+^2 + r_-^2 + r_+\,r_-}{\ell_{\rm AdS}^2}}\,.\end{aligned} \tag{3.78}$$

We will be interested in the near-extremal limit as before. If we take the limit $r_- \simeq r_+$, keeping $\ell_{\rm AdS}$ fixed, then we obtain a solution with AdS_4 asymptotics. On the other hand, taking the limit with $r_+ \simeq r_- \ll \ell_{\rm AdS}$ allows us to make contact with black holes in flat spacetime. For later reference, note that setting $r_+ = r_0 + \mathsf{T}$ and $r_- = r_0 - \mathsf{T}$, we have

$$\kappa = \frac{\mathsf{T}}{r_0^2}\left(1 + 6\,\frac{r_0^2}{\ell_{\rm AdS}^2}\right) + \mathcal{O}(\mathsf{T}^2)\,, \qquad \mu = \sqrt{1 + 3\,\frac{r_0^2}{\ell_{\rm AdS}^2}} + \mathcal{O}(\mathsf{T})\,, \tag{3.79}$$

which implies

$$\kappa \sim \frac{3\,\mathsf{T}}{\ell_{\rm AdS}^2}\,\frac{2\,\mu^2 - 1}{\mu^2 - 1}\,. \tag{3.80}$$

From the near-horizon analysis, we expect three families of low-lying modes. These modes were identified using the heat kernel in [26], or rewriting the theory in the throat as a theory of 2d gravity coupled to matter in [44, 41]. These should correspond to the Schwarzian diffeomorphisms, the SO(3) rotations, and the U(1) gauge transformations, respectively. While the Schwarzian and the U(1) modes are decoupled in the near-horizon region, there is a priori no reason why they should do so in the full spacetime. Both would be expected to behave as scalars under SO(3) rotations, and therefore can mix. We will see that the modes indeed mix, and thus will treat them on the same footing in our analysis.

A contour prescription for linearized Einstein-Maxwell dynamics

The Reissner-Nordstr̈om AdS_4 solution is a solution to the Einstein-Maxwell theory, with Euclidean action

$$\begin{aligned} I &= -\frac{1}{16\pi\, G_N}\int \mathrm{d}^4x\,\sqrt{g}\left(R+\frac{6}{\ell^2_{\rm AdS}}-F_{\mu\nu}F^{\mu\nu}\right)-\frac{1}{8\pi\, G_N}\oint \mathrm{d}^3x\,\sqrt{\gamma}\,K+I_{\rm bdy}\,,\\ I_{\rm bdy} &= \frac{1}{8\pi\, G_N}\oint \sqrt{\gamma}\,\left[\frac{2}{\ell_{\rm AdS}}+\ell_{\rm AdS}\,{}^{\gamma}R\right]. \end{aligned} \tag{3.81}$$

We will discuss gauge fixing terms in the sequel. Due to the background Maxwell field, contrary to the hyperbolic example discussed above, we cannot decouple the conformal and transverse traceless modes. As a result, after expanding the action to the quadratic order, we obtain a non-positive definite quadratic form $I^{(2)}$ (or, to put it simply, the Euclidean action is not bounded from below).[17] The general strategy of dealing with such problems was presented in [112, 113]. For the reader's convenience, we will briefly recapitulate the salient points.

On the space of fluctuations, parameterized by elements X and Y, we need to introduce an auxiliary inner product

$$\langle X|Y\rangle = (X_i)^\star\ \mathbb{G}^{ij}\,Y_j \tag{3.82}$$

that is not positive-definite (but non-degenerate). As already mentioned, the quadratic action is a quadratic form:

$$I^{(2)} = X_i\,\mathbb{S}^{ij}\,X_j. \tag{3.83}$$

Using $\mathbb{G}$ and $\mathbb{S}$, we may now introduce an operator $\hat{L}$ such that

$$\hat{L} = \mathbb{G}^{-1}\cdot\mathbb{S}. \tag{3.84}$$

[17] For Einstein-Hilbert theory, this is the well-known statement that the conformal mode has the wrong sign kinetic term. In Einstein-Maxwell theory, the conformal mode mixes with the photons (and gravitons), but there is nevertheless a direction in field space where the action is unbounded below.

By construction, $\hat{L}$ will be self-adjoint with respect to $\langle\cdot|\cdot\rangle$, and then we may write[18]

$$I^{(2)}(X) = \langle X|\,\hat{L}\,|X\rangle\,. \tag{3.85}$$

Hence, it is an operator $\hat{L}$ that we would like to study, in particular to find its spectrum. The rule of thumb of [112, 113] is that whenever we encounter an eigenvector of negative norm, we Wick rotate the inner product (and thus, also the contour of integration in the path integral) to make it positive.[19] Then, it is $\det\left(\hat{L}\right)$ that computes the one-loop corrections to the partition function. Due to the gauge and diffeomorphism invariance of the Einstein-Maxwell action, $\hat{L}$ is going to have a large kernel. To deal with it, one needs to introduce gauge fixing terms that we should introduce promptly. In the following we will denote by $\hat{L}_0$ the operator without gauge-fixing terms and by $\hat{L}$ the full operator.

Before that, let us try to apply the prescribed procedure to the problem at hand. The simplest choice of the inner product is given by the ultralocal measure on the graviton and photon fluctuations,

$$\|X\|^2 = \ell_{\rm AdS}^{-4}\int \mathrm{d}^4x\,\sqrt{g}\,\left(\tilde{h}^{\mu\nu}h_{\mu\nu} + a^\mu a_\mu\right), \tag{3.86}$$

where $\tilde{h}_{\mu\nu}$ is defined in (3.12). The metric and Maxwell fluctuations are $h_{\mu\nu}$ and a_μ, respectively. We will also use $h = g^{\mu\nu}h_{\mu\nu}$ (as before) and $f = \mathrm{d}a$. Then, we should expand the action to the second order in $h_{\mu\nu}$ and a_μ. In this expansion, we encounter the first problem. The terms describing mixing between gravitons and photons are schematically of the form

$$\int \mathrm{d}^4x\,\sqrt{g}\,h\,F\,f\,, \tag{3.87}$$

with appropriate index contractions. However, since F is clearly imaginary, these terms will evaluate to something imaginary as well for real h and a. It follows, that the quadratic form

[18]This expression presumes that the complex conjugations $\star$ does not change X. As we will see presently, it is a slightly subtle assumption.

[19]For Einstein-Hilbert dynamics this is the original prescription of [111].

$\mathbb{S}$ is not real-valued and so $\hat{L}_0$ will not be self-adjoint with respect to $\mathbb{G}$.

There are a few ways out of this impasse. The most common one is to analytically continue the black hole charge Q to imaginary values. Then, all the background fields are real, and we do not have to worry about these problems. However, it is easy to check that the Reissner-Nordström black hole with imaginary charge at very low temperatures must have complex r_+. Thus, we could not be able to probe the regime we are most interested in. Another possibility is to work with magnetically charged black holes (and perhaps use the electromagnetic duality at the end of the day). Then, the background Maxwell field is real. This approach was successfully applied in the previous calculations of certain one-loop quantities (see for example [127, 128, 129]). However, this is a choice that can only be made in four dimensions. It does have an additional unsavory feature of needing multiple coordinate patches to describe the gauge potential. Therefore, we will not pursue this strategy either.

Instead, we proceed by simply declaring that we integrate the Maxwell fluctuations along the imaginary axis and write[20]

$$a = \mathrm{i}\,\overline{a}\,. \tag{3.88}$$

Then, $I^{(2)}$ will be real for $h, \overline{a} \in \mathbb{R}$. There is a price to pay for this choice of contour. Kinetic terms for $\overline{a}$ have wrong signs. As a result, even the purely Maxwell part of $I^{(2)}$ is not bounded from below. Since we are already using a formalism that is supposed to take care of these sorts of problems, we need not be troubled by this particular development. Indeed, let us notice that the inner product now reads

$$\|X\|^2 = \ell_{\mathrm{AdS}}^{-4} \int \mathrm{d}^4x\, \sqrt{g}\, \left(\tilde{h}^{\mu\nu} h_{\mu\nu} - \overline{a}^{\mu}\, \overline{a}_{\mu} \right). \tag{3.89}$$

Thus, we do not expect that this choice of contour should introduce (or remove) any additional negative modes in $\hat{L}_0$.

As explained at the beginning of this section, this choice of inner product and contour

[20]Note, that this is different from just applying Wick rotations to real Lorentzian fluctuations. In this case, only $a_{t_{\mathrm{E}}}$ would be imaginary.

(after fixing the gauge invariance of the theory, which we do next) leads to an operator $\hat{L}$ that is non-negative and self-adjoint. This is enough for our purpose of identifying the nearly zero-modes characteristic of an AdS_2 throat. To complete the calculation of the partition function, one would need to evaluate the norm of the eigenfunctions of $\hat{L}$ using the inner product and further rotate the contour of any mode with negative norm (which would otherwise lead to a negative action). We will not attempt to give a complete characterization of this last step, although it is straightforward.

We are now ready to discuss the thorny issue of the gauge invariance. We need to break it explicitly in the action to remove the degeneracy of $\hat{L}_0$. In general, all choices are allowed. However, as we will see, only some of them are convenient. Let us start by naively repeating the analysis of the previous sections and trying to impose Lorenz and harmonic gauge. The relevant terms read

$$I'_{\rm gf} = \frac{1}{16\pi\, G_N} \int \mathrm{d}^4x\, \sqrt{g} \left(2\,(\nabla^\mu a_\mu)^2 + \frac{1}{2}\, \nabla^\mu \tilde{h}_{\mu\nu}\, \nabla_\rho \tilde{h}^{\rho\nu} \right). \tag{3.90}$$

Treating $I'_{\rm gf}$ as a quadratic form, we obtain a modified operator $\hat{L}'$ from $\hat{L}_0$. One can explicitly check that the eigenvalue equation

$$\hat{L}' X = \lambda X \tag{3.91}$$

for $X = (h, \overline{a})$ is inconsistent with the gauge conditions

$$\nabla_\mu \tilde{h}^{\mu\nu} = 0\,, \qquad \nabla_\mu a^\mu = 0\,. \tag{3.92}$$

Thus, if we wanted to continue along this line, we would have to deal with pure gauge degrees of freedom, which would make our life unnecessary hard (for one, we would have to then also compute the eigenspectrum of the ghost operators). Instead, we use the method of [112] to find a more convenient choice of gauge.

The idea is to enforce a gauge where all physical fluctuations (viz., the ones satisfying

gauge conditions) are orthogonal to pure gauge modes. The space of gauge parameters in our case is parametrized by a vector field ξ and a scalar field χ. Pure gauge configurations are described by a map $\mathcal{P}$

$$\mathcal{P}(\xi,\chi) = (\mathcal{L}_\xi g_{\mu\nu},\ \mathcal{L}_\xi A_\mu + \nabla_\mu \chi) = (h_{\mu\nu}, a_\mu) \tag{3.93}$$

from the gauge parameters to the space of fluctuations. Hence, the physical fluctuations must be orthogonal to the image of $\mathcal{P}$. If we equip the gauge parameter space (which is automatically a vector space) with the inner product to make it a Hilbert space, we will have a well-defined notion of $\mathcal{P}^\dagger$:

$$\langle X|\mathcal{P}(\xi,\chi)\rangle = \left\langle \mathcal{P}^\dagger X \middle| (\xi,\chi)\right\rangle, \tag{3.94}$$

where the first inner product is in the space of fluctuations, and the other one in the space of gauge parameters. Hence, our gauge condition reads[21]

$$\mathcal{P}^\dagger X = 0. \tag{3.95}$$

The gauge-fixing term can then be taken to be (up to a constant)

$$I_{\rm gf} \sim \langle X|\, \mathcal{P}\mathcal{P}^\dagger\, |X\rangle\ . \tag{3.96}$$

It follows that the eigenvalue equation

$$\hat{L}X = \frac{\lambda}{\ell^2_{\rm AdS}} X\,, \tag{3.97}$$

is consistent with the gauge condition. This choice will thus simplify the analysis by allowing us to focus on physical fluctuations (and therefore simplify the number of degrees of freedom

[21]There are certain subtleties connected to this procedure, which are discussed in [113].

in the equations).

Note that the choice of $\mathcal{P}^\dagger$ will depend on the choice of the auxiliary inner product on the space of gauge parameters. The simplest choice is

$$\|(\xi,\chi)\|^2 = \ell_{\text{AdS}}^{-4}\int \mathrm{d}^4x\,\sqrt{g}\,\left(\,\xi_\mu\xi^\mu + \chi^2\right). \tag{3.98}$$

Then, our gauge conditions now read[22]

$$\nabla^\mu\tilde{h}_{\mu\nu} - \frac{1}{2}\,F_{\nu\mu}\,a^\mu + A_\nu\,\frac{1}{2}\nabla^\mu a_\mu = 0\,, \tag{3.99a}$$

$$\nabla^\mu a_\mu = 0\,. \tag{3.99b}$$

One can explicitly check that they are indeed consistent with the eigenvalue problem.

We could now proceed by expanding the action and finding operator $\hat{L}$ explicitly. However, it is easy to make a mistake while trying to establish if various terms with abstract indices correspond to Hermitian operators.[23] As an alternative, we will decompose the perturbations with respect to different representations of time-translations and SO(3). In this way, we reduce the problem to one dimension in which it is much easier to explicitly find the form of the operator $\hat{L}$. Before dealing with the details of this procedure, let us point out that the background fields (g, F) are even and odd under time-reversal,[24] respectively. It follows that we may decompose the perturbations with respect to their time-reversal parity. We will have two sectors: in which the metric fluctuations are even and the Maxwell field is odd or vice versa.

[22] In deriving the form of $\mathcal{P}^\dagger$ one should keep in mind that it is $\overline{a}$ that is invariant under complex conjugation, not a. Nevertheless, if we considered real background fields and real fluctuations, we would obtain the same form of the gauge conditions.

[23] As an example, one can check that even the Lichnerowicz operator as given in (3.15) is not Hermitian unless the background metric is Einstein.

[24] Or, more precisely, what a quantum field theorist would call CT.

The Schwarzian and U(1) gauge modes

As noted above, the Schwarzian and the U(1) modes should preserve the background SO(3) rotation isometry. So we can focus on a spherically symmetric ansatz, and use time-translational invariance to decompose them into Matsubara modes. We may additionally decompose metric and Maxwell fluctuations into even and odd parity modes, respectively, under time-reversal. All in all, we can motivate the following general ansatz to parameterize the perturbation:

$$\begin{aligned} h_{\mu\nu}\mathrm{d}x^\mu \mathrm{d}x^\nu &= \frac{1}{\sqrt{\pi\beta} r}\left[\cos\left(\frac{2\pi n\, t_{\scriptscriptstyle \mathrm{E}}}{\beta}\right)\left(f_1\, f\, \mathrm{d}t_{\scriptscriptstyle \mathrm{E}}^2 + f_2\, \frac{\mathrm{d}r^2}{f} + \frac{r^2\, f_4}{4}\, \mathrm{d}\Omega_2^2\right) + \sin\left(\frac{2\pi n\, t_{\scriptscriptstyle \mathrm{E}}}{\beta}\right) f_3\, \mathrm{d}t_{\scriptscriptstyle \mathrm{E}}\mathrm{d}r\right], \\ a_\mu\, \mathrm{d}x^\mu &= \frac{\mathrm{i}}{\sqrt{2\pi\beta}\, r}\left(\cos\left(\frac{2\pi n\, t_{\scriptscriptstyle \mathrm{E}}}{\beta}\right)\sqrt{f}\, a_t\, \mathrm{d}t_{\scriptscriptstyle \mathrm{E}} + \sin\left(\frac{2\pi n\, t_{\scriptscriptstyle \mathrm{E}}}{\beta}\right) a_r\, \frac{\mathrm{d}r}{\sqrt{f}}\right), \end{aligned} \tag{3.100}$$

where f_i with $i = 1, \cdots 4$, a_t, and a_r are functions of r alone. The inner product written in terms of these read:

$$\int \mathrm{d}^4x\sqrt{g}\left(\tilde{h}^{\mu\nu}\, h_{\mu\nu} + a_\mu\, a^\mu\right) = \int_{r_+}^{\infty} \mathrm{d}r\left((f_1 - f_2)^2 + f_3^2 - (f_1 + f_2)\, f_4 - a_t^2 - a_r^2\right). \tag{3.101}$$

It follows that for perturbations to land in our Hilbert space, they should be sufficiently regular around $r = r_+$ and vanish sufficiently fast around $r = \infty$.[25]

After some integration by parts, we arrive at the desired quadratic fluctuation operator $\hat{L}$. Its form is too long to write down here, instead we mention a few properties.

- As advertised, we may decouple gauge degrees of freedom. Imposing (3.99) allows us to

[25]Note that if we act on the fluctuations with the isometry $t_{\scriptscriptstyle \mathrm{E}} \mapsto t_{\scriptscriptstyle \mathrm{E}} + \frac{\beta}{2n}$, we obtain a perturbation with reversed parity properties. Hence, we do not have to consider them separately.

eliminate a_t, f_1 and f_2. Specifically,

$$\begin{aligned}
a_t &= \frac{\beta}{4\pi\, n\, r}\left((r\, f' + 2f)\, a_r + 2\, r\, f\, a_r'\right), \\
f_1 &= \frac{\sqrt{2}\, Q\, \beta\, a_r\, \sqrt{f} + 2\, r\left(\beta\, f_3\, \frac{\mathrm{d}}{\mathrm{d}r}(rf) + \beta\, r\, f\, f_3' + 2\pi\, n\, r\, f_2 + \pi n\, r\, f_4\right)}{4\pi\, n\, r^2}, \\
f_2 &= \frac{1}{8\pi n\, \beta\, r^2 f}\left[\beta^2\, r\left(r^2\, f_3\, f'^2 + r\, f\,(r\, f_3\, f'' + f'\,(3\, r f_3' + f_3)) + f^2\left(r^2\, f_3'' - 2\, f_3\right)\right)\right. \\
&\qquad \left. + \pi n\, \beta\, r^3\,(f_4\, f' + 2\, f\, f_4') - 4\,\pi^2 n^2\, r^3\, f_3 + \sqrt{2}\, Q\, \beta^2\, \sqrt{f}\,(r\, f\, a_r' + a_r\,(r\, f' - f))\right].
\end{aligned} \tag{3.102}$$

- Eliminating the above functions, the eigenvalue problem becomes a system of three second-order ODEs for f_3, f_4, and a_r.

- To solve this, we pass over to the coordinate z introduced in (3.47), and deduce that $z = \pm 1$ are regular singular points of this eigenvalue problem.

- Near the AdS boundary ($z = 1$) we find the behavior of f_3 and f_4 to be correlated, and a set of six decays in addition. Specifically, parameterizing

$$f_3 \sim (1-z)^{s_3}, \qquad f_4 \sim (1-z)^{s_4}, \qquad a_r \sim (1-z)^{s_r}, \tag{3.103}$$

we find $s_4 = s_3 - 1$ and

$$\begin{aligned}
s_3 &= \frac{3}{2} \pm \sqrt{\frac{9}{4} - 4\,\lambda}, \qquad & s_3 &= \frac{3}{2} \pm \sqrt{\frac{33}{4} - 4\,\lambda}, \qquad & s_3 &= \frac{7}{2} \pm \sqrt{\frac{1}{4} - \frac{1}{2}\,\lambda}, \\
s_r &= \frac{7}{2} \pm \sqrt{\frac{9}{4} - 4\,\lambda}, \qquad & s_r &= \frac{7}{2} \pm \sqrt{\frac{33}{4} - 4\,\lambda}, \qquad & s_r &= \frac{3}{2} \pm \sqrt{\frac{1}{4} - \frac{1}{2}\,\lambda}.
\end{aligned} \tag{3.104}$$

These fall-offs correspond to the decays of massive gravitons, photons, and scalars (conformal mode) near the AdS boundary. Since we impose Dirichlet boundary conditions at infinity, we should choose positive signs everywhere in (3.104).

- At the horizon (near $z = -1$), we require the perturbations to be smooth. This leads to

demanding

$$f_3 \sim (1+z)^{|n|-2}\,, \qquad f_4 \sim (1+z)^{|n|-1}\,, \qquad a_r \sim (1+z)^{|n|-2}\,. \tag{3.105}$$

Just as at the boundary, this behavior can be identified with that of a mixture of decays of gravitons and photons for neutral black holes.[26]

Since there is no a priori reason why the different modes should decouple, we must take all of these fall-offs into account. We do so by redefining the perturbations after stripping off some leading factors at the horizon and boundary with the ansatz

$$\begin{aligned} f_3(z) &= (1-z)^{\frac{1}{2}}\,(1+z)^{|n|-2}\,U_3(z)\,, \\ f_4(z) &= (1-z)^{-\frac{1}{2}}\,(1+z)^{|n|-1}\,U_4(z)\,, \\ a_r(z) &= (1-z)^{\frac{3}{2}}\,(1+z)^{|n|-2}\,U_r(z)\,. \end{aligned} \tag{3.106}$$

The Dirichlet boundary conditions at the AdS asymptopia translate to $U_3(1) = U_4(1) = U_r(1) = 0$, as long as

$$\lambda < \frac{5}{16}\,. \tag{3.107}$$

We can now use this eigensystem to solve for the uplift of the Schwarzian and the U(1) gauge modes. We will begin with the former, and then tackle the latter.

The Schwarzian modes: Let us first record a useful observation from (3.106). Owing to the factors of $(1-z)^{|n|-2}$, the metric and gauge field perturbations will fail to be in L^2 with respect to the ultralocal measure and thus will not have finite action for $|n| \leq 1$. Hence, for now, we shall consider only $n \geq 2$ (without loss of generality, we may take n to be positive). This is already suggestive of the Schwarzian modes from our preceding analyses.

[26]There are also additional asymptotics near $z = -1$ corresponding to the behavior of scalars. However, they decay faster at the horizon, and therefore are automatically included as subleading terms in the provided expressions.

Using the numerical method described in section 3.1.2, we were able to track the lowest-lying eigenvalue for different n. For example, working with $\mu = 10$ we examine the behavior within the interval $\kappa\,\ell_{\rm AdS} \in (0.000975, 0.1)$.[27] Sample results of this numerical analysis for the lowest three overtones are illustrated in fig. 3.6. The numerical data for the eigenvalues for $n = 2, 3, 4$ fit well to a quadratic polynomial for low values of surface gravity. Parameterizing the eigenvalues in the low-temperature regime $\kappa\,\ell_{\rm AdS} \in [0.000975, 0.001]$ as

$$\lambda_n = a_n + b_n\,\kappa\,\ell_{\rm AdS} + c_n\,(\kappa\,\ell_{\rm AdS})^2\,, \tag{3.108}$$

we find

$$\begin{aligned} &b_2 = 0.17408\,, \qquad c_2 = -0.01512\,, \qquad a_2 \sim \mathcal{O}\big(10^{-10}\big)\,,\\ &b_3 = 0.26112\,, \qquad c_3 = -0.03021\,, \qquad a_3 \sim \mathcal{O}\big(10^{-9}\big)\,.\\ &b_4 = 0.34815\,, \qquad c_4 = -0.05022\,, \qquad a_4 \sim \mathcal{O}\big(10^{-9}\big)\,. \end{aligned} \tag{3.109}$$

This is indeed consistent with these modes becoming zero modes as we attain extremality, i.e., at $\kappa = 0$. In particular, as expected, at very low temperatures, we have a set of modes whose eigenvalues scale linearly with temperature. Furthermore,

$$\frac{b_3}{b_2} = \frac{0.26112}{0.17408} \approx \frac{3}{2} - 9.9\times 10^{-7}\,, \qquad \frac{b_4}{b_3} = \frac{0.34815}{0.26112} \approx \frac{4}{3} - 3.715\times 10^{-6}\,. \tag{3.110}$$

This illustrates that the eigenvalues have a slope that scales linearly with the overtone number n, consistent with them being the extension of the Schwarzian mode onto the full geometry.[28] The upshot of our numerical results is that one has for a near-extremal Reissner-Nordström AdS_4 black hole, a set of eigenmodes with eigenvalues

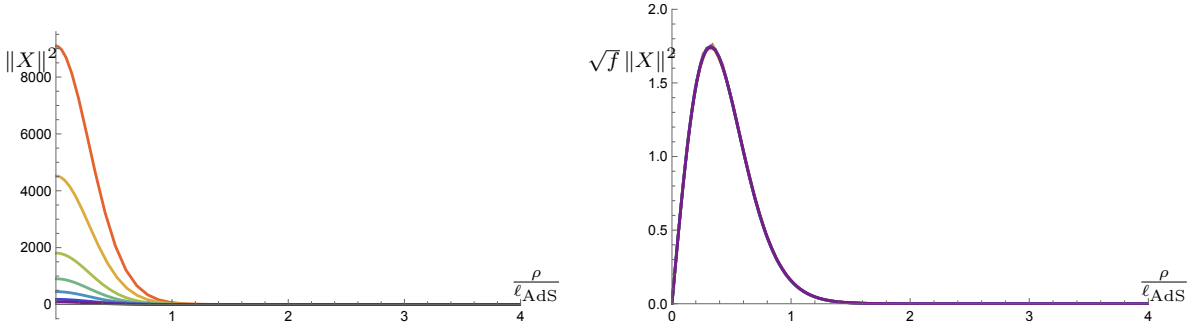
$$\lim_{T\to 0} \frac{\lambda_n \ell_{\rm AdS}^2}{16\pi G_N} \approx \alpha\, n\, \frac{T}{T_q} + \mathcal{O}\big(T^2\big)\,, \qquad |n| \geq 2\,, \tag{3.111}$$

[27] The choice of μ was dictated by convergence of the numerics for low temperatures. We find that one needs to go to even lower temperatures at as we lower μ.

[28] As before, the discrepancy of $\mathcal{O}\big(10^{-6}\big)$ is because we truncated the Taylor expansion at the quadratic order.

in excellent agreement with the expectation based on the near-horizon analysis.

We can also find eigenfunctions from our numerical analysis.[29] To get a sense of how the modes behave, we examine the norm of the perturbations, which is the integrand of (3.101). We depict the result in fig. 3.5. It is clear that for the range of temperatures considered, these fluctuations are localized near the horizon, thus confirming the fact that they are indeed the uplift of the Schwarzian modes onto the full geometry. Moreover, one can check that the metric contributions to the norm are a few orders of magnitude larger than the Maxwell ones, and so we may see these modes as being "mainly metric" (as one would expect from the near-horizon analysis). However, at large r, the norm density becomes negative (albeit very small). This is connected with the fact that a_r decays slower at infinity than f_3, f_4 and does not seem to have any physical significance.

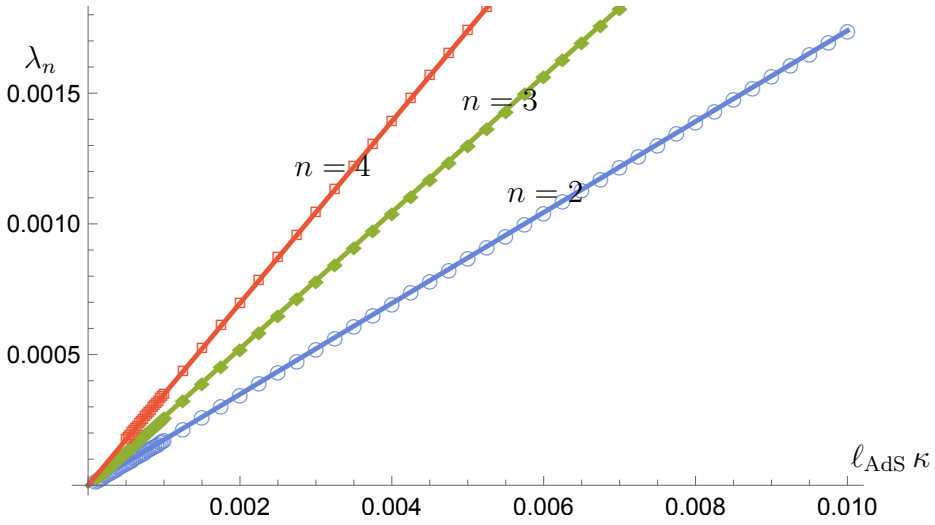


(a) Norm against the proper distance from horizon.

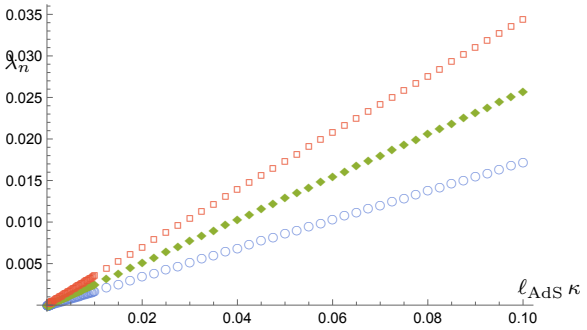
(b) Norm density versus proper distance from horizon

Figure 3.5: The behavior of the norm of the perturbations, with $n = 2$, as a function of proper distance $\rho \sim \ell_{\text{AdS}} \log(r/r_+)$ from the horizon. As with earlier results, this is for a Reissner-Nordström-AdS$_4$ black hole geometry with $\mu = 10$. The norm $\|X\|^2$ defined as the integrand of (3.101), viz., the specific combination of the functions f_i, a_t and a_r. The data is shown for $\kappa\ell_{\text{AdS}} \in \{0.01, 0.005, 0.002, 0.001, 0.0005, 0.0002, 0.0001\}$. On the left panel fig. 3.5a we show the bare norm which increases in amplitude as we go to lower temperature, similar to the feature seen in the BTZ case fig. 3.1. However, the norm density, which is normalized to integrate to unity, displays data collapse as depicted in fig. 3.5b.

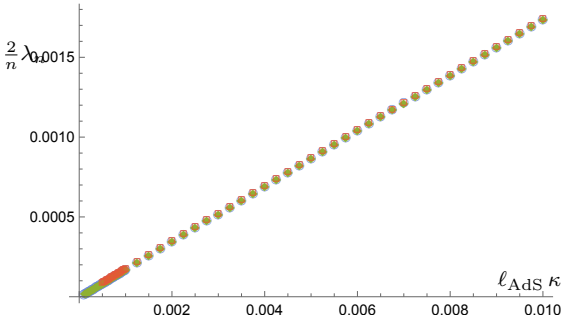
[29] Obtaining them, however, requires a larger grid than the eigenvalue computation.



(a) The eigenvalue spectrum at low temperatures.



(b) The eigenvalue spectrum over an extended range.



(c) Rescaled eigenvalues demonstrating scaling.

Figure 3.6: The uplift of Schwarzian modes to the full Reissner-Nordström-AdS$_4$ black hole geometry with $\mu = 10$. We show the data for very low temperatures in the top panel, fig. 3.6a, demonstrating linear behavior with temperature. In the bottom left panel, fig. 3.6b, we show the behavior over a greater range of temperatures, making the (mild) departures from linear growth manifest. Finally, in the bottom right panel fig. 3.6c, we plot the eigenvalues rescaled by the overtone number $\frac{2}{n}\lambda_n$ to demonstrate that $\lambda_n \sim n\,T$ (notice the three curves are overlapping, which was achieved by working with extended precision numerics).

The U(1) **modes:** Since we already have the spherically symmetric fluctuations of the Maxwell field, we also ought to find the modes associated with the U(1) gauge symmetry. These should be part of the same eigensystem, and we ought to have all the necessary ingredients at hand to find them.

Thus far, we tracked the lowest-eigenvalue and detected the Schwarzian modes. Now,

we instead can track the second lowest-lying eigenvalue[30] for a given Matsubara frequency. Unfortunately, one needs to go to significantly lower temperatures to see the linear scaling properly. Since at lower temperatures, gradients near the horizon are larger, this makes the numerics more challenging. Sample results of this numerical analysis for the lowest three overtones are illustrated in fig. 3.7. The numerical data for the eigenvalues for $n = 1, 2, 3$ (see below) fit well to a quadratic polynomial for low values of surface gravity. For example, for $\mu = 10$ we may look at $\kappa\,\ell_{\rm AdS} \in [9.75 \times 10^{-4}, 10^{-3}]$. Letting,

$$\lambda_n = a_n + b_n\,\kappa\,\ell_{\rm AdS} + c_n\,(\kappa\,\ell_{\rm AdS})^2\,, \tag{3.112}$$

we find

$$\begin{aligned} &b_1 = 0.61238\,, && c_1 = -0.56216\,, && a_1 \sim \mathcal{O}\big(10^{-8}\big)\,,\\ &b_2 = 1.22216\,, && c_2 = -1.75035\,, && a_2 \sim \mathcal{O}\big(10^{-7}\big)\,.\\ &b_3 = 1.18378\,, && c_3 = -4.19197\,, && a_3 \sim \mathcal{O}\big(10^{-5}\big)\,. \end{aligned} \tag{3.113}$$

This is indeed consistent with these modes becoming zero modes as we attain extremality, i.e., at $\kappa = 0$. In particular, as expected, at very low temperatures, we have a set of modes whose eigenvalues scale linearly with the Matsubara frequency. Furthermore,

$$\frac{b_2}{b_1} = \frac{1.22216}{0.612376} \approx 2 - 0.0042\,, \qquad \frac{b_3}{b_1} = \frac{1.85748}{0.612376} \approx 3 + 0.001\,. \tag{3.114}$$

This illustrates that the eigenvalues have a slope that scales linearly with the overtone number n, consistent with them being the extension of the U(1) mode onto the full geometry.[31] The upshot of these numerical results is that one has

$$\lim_{T\to 0} \frac{\lambda_n \ell_{\rm AdS}^2}{16\pi G_N} \approx \alpha\, n\, \frac{T}{T_q} + \mathcal{O}\big(T^2\big)\,, \qquad |n| \geq 1\,, \tag{3.115}$$

[30]Here the operator has an additional factor of two relative to the operator that was considered for gauge modes in the hyperbolic AdS black hole. The eigenvalues are therefore a factor of two larger.

[31]The numerical discrepancies in this case are slightly higher, but for similar reason as before.

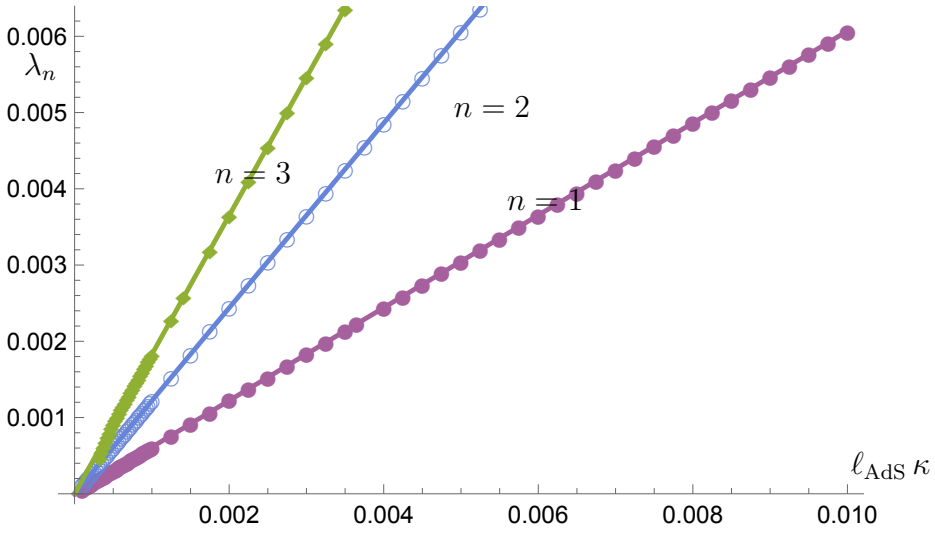
in excellent agreement with our expectation based on the near-horizon analysis.

There is one issue that we need to explain, for the astute reader ought to be surprised by the inclusion of $|n| = 1$ mode. As argued around (3.106) such a mode should lead to singular behavior at the horizon. However, just as for Schwarzian modes, we can find the form of the eigenfunctions. In particular, we learn that $U_3(1) = U_r(1) = 0$ for $n = 1$, and thus, f_3, f_4, a_r are smooth, when we consider the second lowest-eigenvalue (but not for the lowest one). We illustrate this explicitly by plotting the norm for the $n = 1$ mode for $\kappa\,\ell_{\rm AdS} = 0.01$ in fig. 3.8.

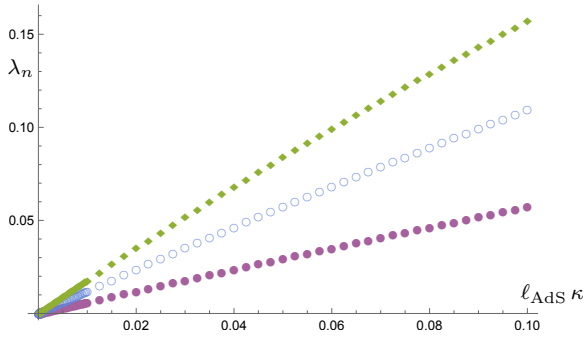
From these plots, it may seem surprising that f_3 and a_r are of the same magnitude. One might have naively hoped that the U(1) modes have dominant support on gauge field fluctuations. However, this is not the case, unlike for the Schwarzian which was supported dominantly on graviton perturbations. The reason for this mixing turns out to be connected with our choice of gauge. For divergence free vectors we have

$$\nabla^\mu \tilde{h}_{\mu\nu} = \frac{1}{2} F_{\nu\mu} a^\mu. \tag{3.116}$$

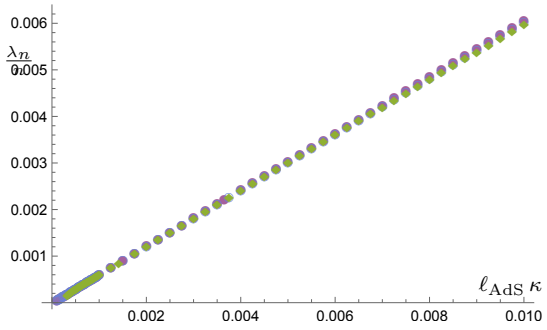
Hence, as long as $F_{\nu\mu}a^\mu \neq 0$ (which here is equivalent to $a^\mu \neq 0$), $h_{\mu\nu}$ cannot vanish as well. However, let us emphasize that fluctuations $(h_{\mu\nu}, a_\mu)$ and $(h_{\mu\nu} + \mathcal{L}_\xi g_{\mu\nu}, a_\mu + \mathcal{L}_\xi A_\mu)$ give the same contribution to the quadratic action (ignoring gauge fixing terms) and we can always choose ξ in such a way $\nabla^\mu \tilde{h}_{\mu\nu} = 0$.



(a) The eigenvalue spectrum at low temperatures.



(b) The eigenvalue spectrum over an extended range.



(c) Rescaled eigenvalues demonstrating scaling.

Figure 3.7: The uplift of U(1) gauge zero modes to the full Reissner-Nordström-AdS$_4$ black hole geometry with $\mu = 10$. We show the data for very low temperatures in the top panel fig. 3.7a, demonstrating linear behavior with temperature. In the bottom left panel fig. 3.7b, we show the behavior over a greater range of temperatures, making the departures from linear growth manifest. Finally, in the bottom right panel fig. 3.7c, we plot the eigenvalues rescaled by the overtone number $\frac{1}{n}\,\lambda_n$ to demonstrate that $\lambda_n \sim n\,T$.

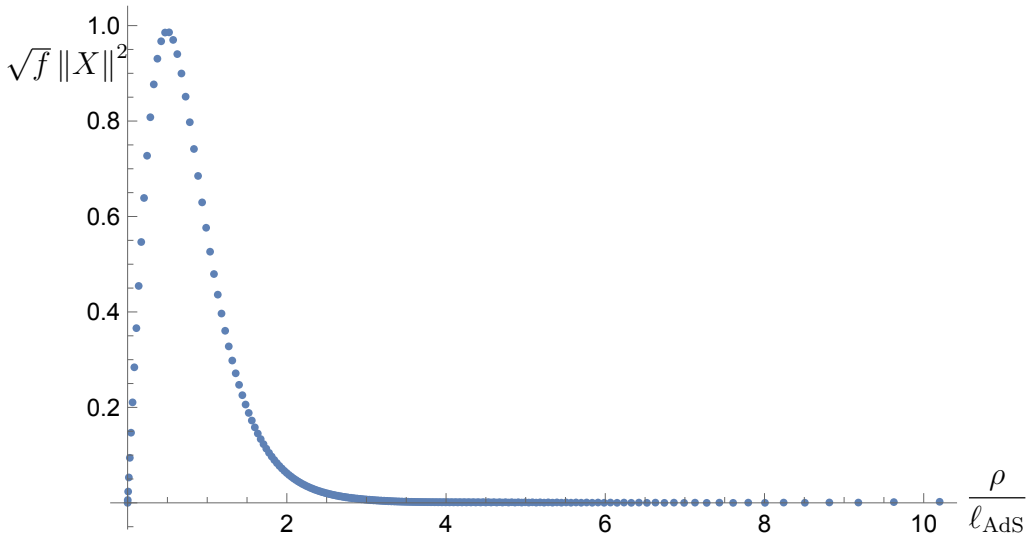


Figure 3.8: The behavior of the norm density of the $n = 1$ mode for $\kappa\,\ell_{\rm AdS} = 0.001$ to illustrate that the U(1) gauge modes remain well-behaved. The conventions are as in fig. 3.5b.

The rotational modes

The final piece of our analysis is to unearth the modes corresponding to the SO(3) rotations, which we know exist in the near-horizon geometry. The incarnation of these modes in the full spacetime should lie in the vector sector of the theory. In particular, they should be built out of the Killing vectors of the $\mathbf{S}^2$. Exploiting this intuition, and accounting for the time-reversal properties, we can motivate the following ansatz for these modes:

$$\begin{aligned} h_{\mu\nu}\,\mathrm{d}x^\mu\,\mathrm{d}x^\nu &= \sqrt{\frac{3}{2\pi\,\beta}}\,\mathfrak{v}\,\left(\cos\left(\frac{2\pi n\,t_{\rm E}}{\beta}\right)\,g_2\,\frac{\mathrm{d}r}{\sqrt{f}} - \sin\left(\frac{2\pi n\,t_{\rm E}}{\beta}\right)\,g_1\,\sqrt{f}\,\mathrm{d}t_{\rm E}\right)\,, \\ a_\mu\,\mathrm{d}x^\mu &= \mathrm{i}\sqrt{\frac{3}{4\pi\,\beta}}\,\mathfrak{v}\,\sin\left(\frac{2\pi n t_{\rm E}}{\beta}\right)\,g_3\,. \end{aligned} \tag{3.117}$$

Here $\mathfrak{v}$ is a covector on $\mathbf{S}^2$ and g_i for $i = 1, 2, 3$ are functions of r alone. The norm of these fluctuations reads:

$$\ell_{\rm AdS}^{-2}\int \mathrm{d}^4x\,\sqrt{g}\,\left(\tilde{h}^{\mu\nu}\,h_{\mu\nu} + a_\mu\,a^\mu\right) = \int_{r_+}^{\infty}\mathrm{d}r\,\left(g_1^2 + g_2^2 - g_3^2\right)\,. \tag{3.118}$$

Hence, we see that g_i must be sufficiently regular around $r = r_+$ and vanish sufficiently fast around $r = \infty$ for the perturbation to be an element of the Hilbert space we wish to consider.

The Maxwell perturbations are automatically divergent-free. Moreover, they also satisfy $F_{\mu\nu}a^\nu = 0$. Therefore, the only non-trivial gauge constraint is

$$0 = \nabla^\mu \tilde{h}_{\mu\nu} = \nabla^\mu h_{\mu\nu}. \tag{3.119}$$

In other words, we simply need the metric perturbation to respect the harmonic gauge. This (one) equation may be immediately solved to obtain

$$g_1 = \beta \, \frac{(r\, f' + 4\, f)\, g_2 + 2\, r\, f\, g_2'}{4\pi\, n\, r}. \tag{3.120}$$

With this in mind, the eigenvalue problem becomes a system of two second-order ODEs for g_2 and g_3.

Passing to the z-coordinate (3.47), and examining the fall-offs near the boundary and horizon, should yield insights about field redefinitions. Assuming,

$$g_2 \sim (1-z)^{s_2}\,, \qquad g_3 \sim (1-z)^{s_3}\,, \tag{3.121}$$

we find the following four decays near the horizon $z = 1$,

$$\begin{aligned} s_2 &= \frac{3}{2} \pm \sqrt{\frac{9}{4} - 4\,\lambda}\,, \qquad & s_2 &= \frac{3}{2} \pm \sqrt{\frac{1}{4} - \frac{1}{2}\,\lambda}\,, \\ s_3 &= \frac{5}{2} \pm \sqrt{\frac{9}{4} - 4\,\lambda}\,, \qquad & s_3 &= \frac{1}{2} \pm \sqrt{\frac{1}{4} - \frac{1}{2}\,\lambda}\,, \end{aligned} \tag{3.122}$$

which can be identified with graviton and photon asymptotics. The choice of positive signs ensures that we get to impose Dirichlet boundary conditions at infinity. Smoothness at the horizon leads to

$$g_2 \sim (1+z)^{|n|-1}\,, \qquad g_3 \sim (1+z)^{|n|}. \tag{3.123}$$

At the end of the day, we can motivate the following reparameterization:

$$\begin{aligned} g_2(z) &= (1+z)^{|n|-1}\,(1-z)\,V_2(z)\,, \\ g_3(z) &= (1+z)^{|n|}\,(1-z)^{\frac{1}{2}}\,V_3(z)\,, \end{aligned} \tag{3.124}$$

supplemented with the boundary conditions $V_2(1) = V_3(1) = 0$, which imposes Dirichlet BCs as long as

$$\lambda < \frac{7}{16}\,. \tag{3.125}$$

Due to the factors of $(1-z)^{|n|-1}$, the perturbations will fail to be smooth for $n = 0$. Hence, we shall consider only $n \geq 1$ (without loss of generality, we may take n to be positive).

Tracking once again the lowest-lying eigenvalue, using the numerical scheme described in section 3.1.2, for different n we obtain our rotational modes. Sample results of this numerical analysis for the lowest three Matsubara modes are illustrated in fig. 3.10 for $\mu = 10$. The numerical data for the eigenvalues for $n = 1, 2, 3$ fit well to a quadratic polynomial for low values of surface gravity. For example, for $\mu = 10$ we may look at $\kappa\,\ell_{\rm AdS} \in [10^{-3}, 10^{-2}]$. Letting,

$$\lambda_n = a_n + b_n\,\kappa\,\ell_{\rm AdS} + c_n\,(\kappa\,\ell_{\rm AdS})^2\,, \tag{3.126}$$

we find

$$\begin{aligned} &b_1 = 0.51382\,, && c_1 = -0.669075\,, && a_1 \sim \mathcal{O}\big(10^{-6}\big)\,, \\ &b_2 = 1.02451\,, && c_2 = -2.286737\,, && a_2 \sim \mathcal{O}\big(10^{-6}\big)\,. \\ &b_3 = 1.53324\,, && c_3 = -4.363498\,, && a_3 \sim \mathcal{O}\big(10^{-5}\big)\,. \end{aligned} \tag{3.127}$$

This is indeed consistent with these modes becoming zero modes as we attain extremality, i.e., at $\kappa = 0$. In particular, as expected, at very low temperatures, we have a set of modes whose eigenvalues scales linearly with temperature. Furthermore,

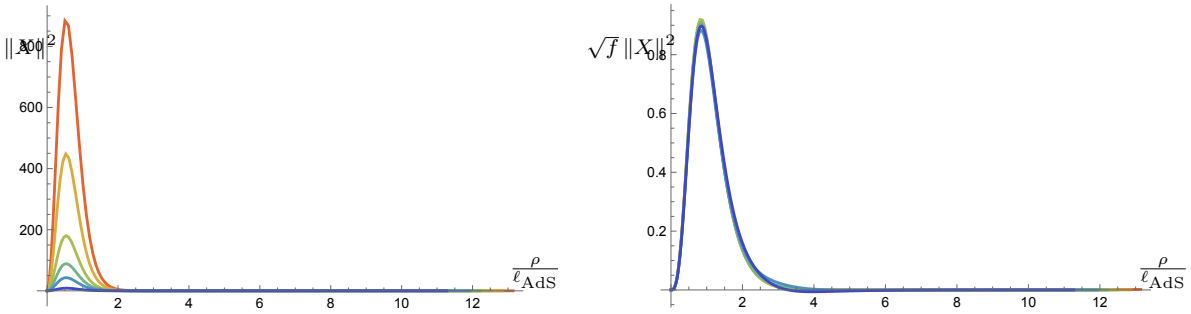
$$\frac{b_2}{b_1} = \frac{1.02451}{0.51382} \approx 2 - 0.00450\,, \qquad \frac{b_3}{b_2} = \frac{1.53324}{1.02451} \approx \frac{3}{2} - 0.00344\,. \tag{3.128}$$

This illustrates that the eigenvalues have a slope that scales linearly with the overtone number n, consistent with them being the extension of the Schwarzian mode onto the full geometry. The upshot of this numerical results is that one has

$$\lim_{T\to 0} \frac{\lambda_n \ell_{\text{AdS}}^2}{16\pi G_N} \approx \alpha\, n\, \frac{T}{T_q} + \mathcal{O}\big(T^2\big)\,, \qquad |n| \geq 1\,, \tag{3.129}$$

in excellent agreement with our expectation based on the near-horizon analysis.

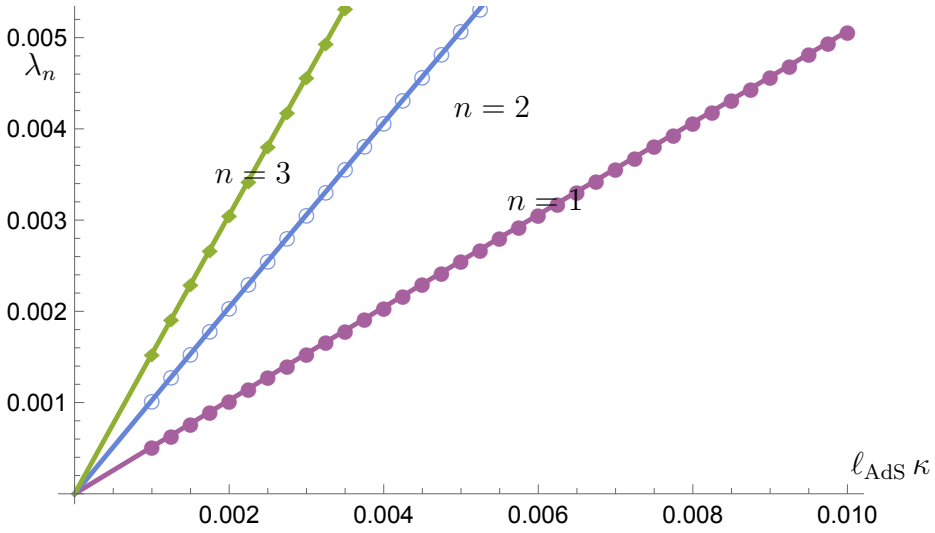
We can also find eigenfunctions, see fig. 3.9. Moreover, for the considered temperatures, these fluctuations are localized near the horizon, thus confirming the fact that they are connected to the rotational modes in the near-horizon region.



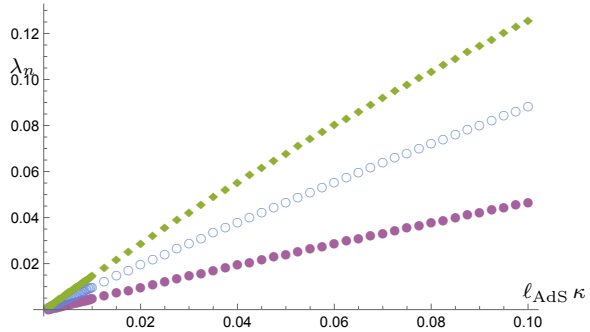
(a) Norm against the proper distance from horizon.

(b) Norm density versus proper distance from horizon

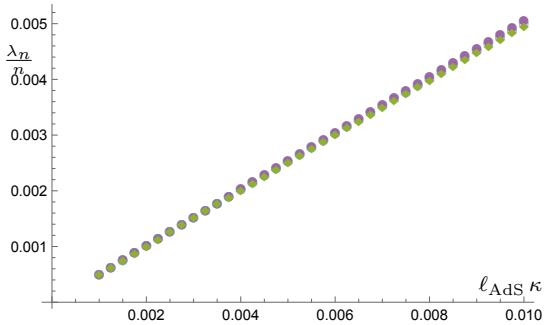
Figure 3.9: The behavior of the norm of the perturbations, with $n = 2$, as a function of proper distance $\rho \sim \ell_{\text{AdS}} \log(r/r_+)$ from the horizon. As with earlier results, this is for a Reissner-Nordström-AdS$_4$ black hole geometry with $\mu = 10$. The norm is defined as the integrand of (3.118). The data is shown for $\kappa\ell_{\text{AdS}} \in \{0.01, 0.005, 0.002, 0.001, 0.0005, 0.0002, 0.0001\}$. On the left panel fig. 3.9a we show the bare norm which increases in amplitude as we go to lower temperature, similar to the feature seen in the BTZ case fig. 3.1. However, the norm density, which is normalized to integrate to unity, displays data collapse as depicted in fig. 3.9b.



(a) The eigenvalue spectrum at low temperatures.



(b) The eigenvalue spectrum over an extended range.



(c) Rescaled eigenvalues demonstrating scaling.

Figure 3.10: The uplift of the rotational field zero modes to the full Reissner-Nordström-AdS$_4$ black hole geometry ($\mu = 10$). We show the data for very low temperatures in the top panel fig. 3.10a, demonstrating linear behavior with temperature. In the bottom left panel fig. 3.10b, we show the behavior over a greater range of temperatures, making the departures from linear growth manifest. Finally, in the bottom right panel fig. 3.10c, we plot the eigenvalues rescaled by the overtone number $\frac{1}{n}\,\lambda_n$ to demonstrate that $\lambda_n \sim n\,T$.

Flat space limit

Thus far, we have discussed only black holes with AdS asymptotics. The presence of the timelike conformal boundary makes the analysis significantly easier because, as we have seen, infinity is a regular singular point of the eigenvalue equations at hand. Instead of trying to solve a significantly harder problem in the asymptotically flat context, we can try to take the

limit with $\ell_{\rm AdS} \to \infty$. Of course, out of the discussed examples, only Reissner-Nordström admits this limit.[32] However, there are a few subtleties involved in the process:

- Extremal Reissner-Nordström-AdS has $\mu > 1$ whereas asymptotically flat solution must have $\mu = 1$. This follows from (3.78) when we take $\ell_{\rm AdS} \to \infty$ (equivalently, take $r_+ \simeq r_- \ll \ell_{\rm AdS}$). For concreteness, we will do in such a way that the black hole's charge at extremality remains constant. We will see important consequences of the constraint $\mu = 1$ in section 3.3.

- The quadratic fluctuation operators (e.g., the Lichnerowicz operator and its charged analogue) being dimensionful, the eigenvalues have mass dimension +2. Hitherto, we took this into account by using $\ell_{\rm AdS}$ to supply the dimensions, by defining

$$\hat{L}X = \frac{\lambda}{\ell_{\rm AdS}^2} X \,. \tag{3.130}$$

  In order to take the limit, we will instead use the black hole size to set the dimensions. Hence, the analog of the parametrization (3.108) should be rather (ignoring for simplicity the constant and quadratic deviation terms characterized by a_n and c_n)

$$\lambda_n \frac{r_0^2}{\ell_{\rm AdS}^2} = \tilde{b}_n \left(\kappa\, r_0\right), \qquad \tilde{b}_n \equiv b_n \frac{r_0}{\ell_{\rm AdS}} \,, \tag{3.131}$$

  where r_0 is the black hole radius at extremality. We expect $\tilde{b}_n$ to have a sensible limit as we take $\ell_{\rm AdS} \to \infty$.

- The final complication we need to deal with is the following. In our analysis, we have focused on eigenmodes of the quadratic fluctuation operator that are in L^2, which placed an upper bound on the dimensionless eigenvalue λ_n, cf. (3.107). As we make the black hole smaller in AdS units, we wish to ensure that this is respected. In addition, we are

[32] A Ricci-flat black hole with a hyperbolic horizon would fail to be asymptotically flat, and does not seem to be of particular physical interest.

interested in ensuring that we are in the regime where the eigenvalues scale linearly with temperature. Both of these are satisfied only when the black hole is sufficiently cold, which demands

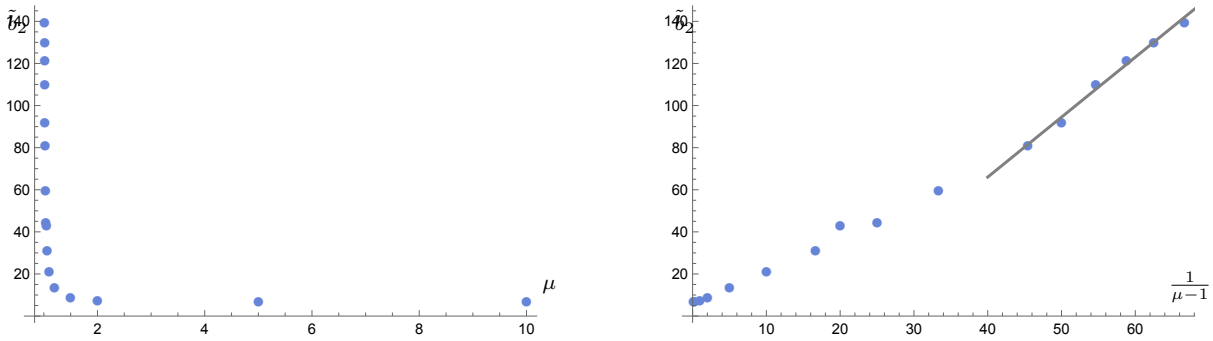
$$\kappa\, r_0 = \mathcal{O}\left(\frac{r_0^2}{\ell_{\text{AdS}}^2}\right). \tag{3.132}$$

This makes the numerical analysis much more challenging. We were nevertheless able to attain low enough temperatures to see the effect we describe below with $\frac{r_0}{\ell_{\text{AdS}}} \sim \mathcal{O}(10^{-1})$.

Having explained all these subtleties, we are ready to investigate the limits themselves. Note that since (with reasonable precision) $b_n = \frac{n}{2} b_2$, we may restrict ourselves to studying $\tilde{b}_2$. Our numerical analysis for the L^2 normalizable modes reveals the following:

- For the Schwarzian and rotational family of eigenmodes, the rescaled fit parameter $\tilde{b}_2$ remains constant as we take $r_0 \ll \ell_{\text{AdS}}$. This suggests that modes robustly survive the limit $\ell_{\text{AdS}} \to \infty$, and should therefore contribute to the quantum effects around the asymptotically flat Reissner-Nordström black hole.

- On the other hand for the U(1) modes we find something surprising; $\tilde{b}_2$ blows up as we go with $\ell_{\text{AdS}} \to \infty$ as depicted in fig. 3.11. In particular, we find that $\tilde{b}_2 \to (\mu - 1)^{-1}$ as $\mu \to 1$. Recall that we are using the chemical potential (which is dimensionless in our convention) to characterize the limit where the cosmological scale diverges. This strongly suggests that these modes should not contribute in the $\ell_{\text{AdS}} \to \infty$ limit. We will reconcile this conclusion with the near-horizon analysis in section 3.3, and propose a criterion to identify when this can happen.



(a) Divergence of $\tilde{b}_2$ as $\mu \to 1$.

(b) The rate of divergence: $\tilde{b}_2 \sim (\mu - 1)^{-1}$.

Figure 3.11: The behavior of the U(1) modes in a Reissner-Nordström black hole as a function of the (dimensionless) chemical potential. We use the chemical potential as a proxy to take the flat space limit, since $\mu \to 1$ as $r_+ \simeq r_- \ll \ell_{\rm AdS}$. In the limit, we see that the linear fit coefficient $\tilde{b}_2$ diverges as $(\mu - 1)^{-1}$ strongly suggesting that these modes are absent in the asymptotically flat black hole spacetime.

3.2 The role of rotational modes

The Schwarzian mode is universally present in all near-extremal black hole geometries. As we explained earlier, one also expects isometries of the background geometry to generate a set of zero modes. We indeed saw their avatars in the full geometry in section 3.1 for the neutral hyperbolic AdS_4 and the charged Reissner-Nordström-AdS_4 black holes. We now turn to the question of understanding these zero modes from the near-horizon perspective.

The reason for doing so is to address a puzzle raised in the previous chapter, where the rotational zero mode in the near-horizon geometry of the extremal Kerr black hole was examined using the harmonic gauge fixing condition for gravitational perturbations. It was demonstrated that in this gauge, the putative zero mode associated with the rotational isometry was not regular at the poles of the deformed $\mathbf{S}^2$. The lack of smoothness suggested a potential absence of such rotational zero modes in axisymmetric spacetimes.[33] Other geometries were not examined closely, but two facts regarding the absence of such rotational

[33] In the cases we have analyzed the issue arises for axisymmetric solutions (viz., for abelian rotations). For example, in the spherically symmetric case, one can dimensionally reduce in the near-horizon region to JT gravity with the isometries realized as non-abelian gauge fields.

zero modes were noted: a) the result was consistent with the expectation of low-temperature behavior of the extremal BTZ geometry, and b) if true, and moreover if one insisted on working in harmonic gauge, this result could have serious consequences for supersymmetric black holes such as the BMPV solution.

We now turn to a detailed analysis of the situation by working in the near-horizon geometry. As a first step, we examine axisymmetric solutions supported by matter or cosmological constant. For the Kerr AdS_4 black hole, we demonstrate the presence of a rotational zero mode, satisfying the harmonic gauge condition, as required. We also check that something similar occurs in the presence of background matter fields by examining the Kerr-Newman solution. These two examples suffice to reveal the problem in the Kerr geometry – the harmonic gauge condition breaks down! We explain why this is the case, and argue that there is indeed a rotational zero mode in the Kerr geometry, thereby resolving our puzzle. For completeness, we then also demonstrate that the supersymmetric BMPV solution does indeed have all the zero modes expected from the analysis of [27]. The content of this section addresses fact b) from the previous paragraph. We will also clarify the physics behind fact a) in section 3.3.

3.2.1 Rotational modes in Kerr AdS_4

We now turn to our first example, the Kerr AdS_4 black hole. We will work in the near-horizon geometry, which is obtained by zooming into the AdS_2 throat region, cf. [100]. The line element is given by (nb: we use $x = \cos\theta$ instead of the polar angle)

$$ds^2 = F(x)\left(\left(y^2-1\right)\mathrm{d}\tau^2 + \frac{\mathrm{d}y^2}{y^2-1} + G(x)\frac{\mathrm{d}x^2}{1-x^2}\right) + H(x)(\mathrm{d}\phi + \mathrm{i}\Omega\,(y-1)\,\mathrm{d}\tau)^2\,. \quad (3.133)$$

The functions appearing in the metric are

$$F(x) = \frac{a^2\,x^2 + r_+^2}{V}\,, \quad G(x) = \frac{V}{1 - \frac{a^2\,x^2}{\ell_{\rm AdS}^2}}\,, \quad H(x) = (1-x^2)\,\frac{\ell_{\rm AdS}^2\left(a^2 + r_+^2\right)^2\left(\ell_{\rm AdS}^2 - a^2\,x^2\right)}{\left(\ell_{\rm AdS}^2 - a^2\right)^2\left(a^2 x^2 + r_+^2\right)}\,, \tag{3.134}$$

with

$$\Omega = \frac{2\,a\,r_+\left(1 - \frac{a^2}{\ell_{\rm AdS}^2}\right)}{V\left(a^2 + r_+^2\right)}\,, \qquad a = \frac{r_+\sqrt{\ell_{\rm AdS}^2 + 3r_+^2}}{\sqrt{\ell_{\rm AdS}^2 - r_+^2}}\,, \qquad V = \frac{a^2 + \ell_{\rm AdS}^2 + 6\,r_+^2}{\ell_{\rm AdS}^2}\,. \tag{3.135}$$

The idea as in Chapter 2 is to seek a zero-mode generated by a large diffeomorphism along the Killing field ∂_ϕ. We will need to add a compensating vector field to ensure that the resulting perturbation lies in harmonic gauge. Therefore, consider the following vector field

$$\xi^\mu \partial_\mu = H(\tau, y)\,\partial_\phi + \alpha(x)\,\nabla^\mu H\,\partial_\mu\,, \qquad H(\tau, y) = e^{{\rm i}\,n\,\tau}\left(\frac{y-1}{y+1}\right)^{\frac{|n|}{2}}\,. \tag{3.136}$$

This choice is suggested by the structure of the gauge field zero modes that arise in the AdS_2 throat, were we to ignore the warping along the x direction, and dimensionally reduce to a 2d gravity theory. In particular, since $H(\tau, y) \to e^{{\rm i}\,n\,\tau}$ as $y \to \infty$, this vector field is not normalizable. It therefore generates a large diffeomorphism (and not just a gauge transformation). The second piece involving the yet to be determined function $\alpha(x)$ is a compensating (normalizable) diffeomorphism, which is included to here to bring the resulting perturbation into harmonic gauge.

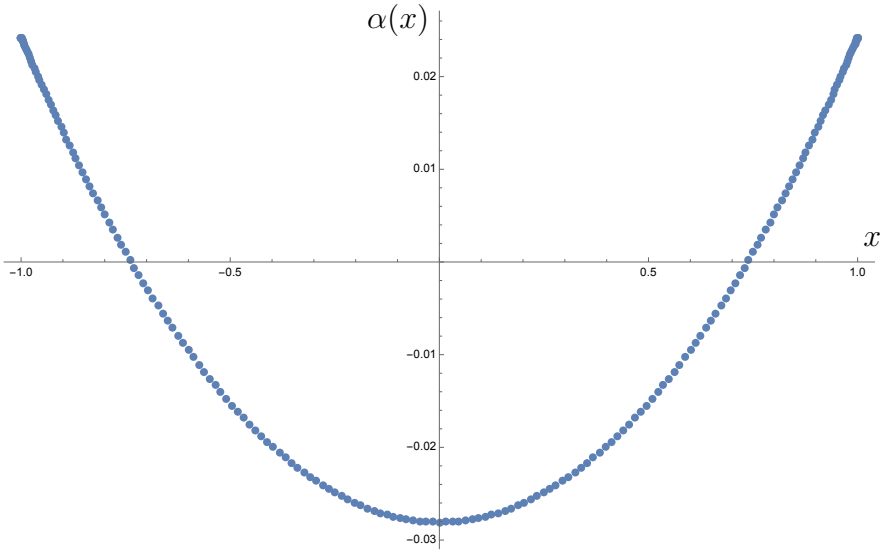


Figure 3.12: The solution for the profile of the function $\alpha(x)$ in rotational zero mode ξ defined in (3.136) at $r_+ = 0.2\,\ell_{\rm AdS}$. Note importantly, that the function is well-behaved at the poles of the $\mathbf{S}^2$, $x = \pm 1$.

The resulting metric perturbation $h_{\mu\nu} = 2\,\nabla_{(\mu}\xi_{\nu)}$ is automatically trace-free $h_\mu{}^\mu = 0$. Thus, to ensure it preserves the harmonic gauge, we only need to require it is divergence-free $\nabla^\mu h_{\mu\nu} = 0$ as well. This leads to a simple (but long) equation for α. It is a second order, linear inhomogeneous ODE. As such, it is straightforward to solve this equation numerically. We depict an illustrative solution for a particular choice of r_+ in fig. 3.12. Perhaps surprisingly, this equation does not depend on n. One can also check directly that the metric perturbation thus generated lies in the kernel of the spin-2 Lichnerowicz operator (3.15).

The upshot of this calculation is that there is a smooth solution as long as $\Lambda = -\frac{3}{\ell_{\rm AdS}^2} \neq 0$. We will shortly see that this suggests that something singular occurs in the Ricci-flat limit, which will be relevant for the Kerr solution.

3.2.2 Rotational modes in Kerr-Newman

Next we turn to the Kerr-Newman geometry as a solution in Einstein-Maxwell theory. In Chapter 2, we examined the near-horizon geometry for zero modes and in particular constructed the explicit form of the Schwarzian mode. The line-element of the near-horizon

spacetime takes the form

$$\mathrm{d}s^2 = \Gamma(x)\left(\left(y^2-1\right)\mathrm{d}\tau^2 + \frac{\mathrm{d}y^2}{y^2-1} + \frac{\mathrm{d}x^2}{1-x^2} + \left(1-x^2\right)\gamma(x)^2\left(\mathrm{d}\phi + \mathrm{i}\,\Omega\,(y-1)\,\mathrm{d}\tau\right)^2\right), \tag{3.137}$$

and is supported by a Maxwell field, which in turn is

$$A = \mathrm{i}f(x)\,\Omega\,\mathrm{d}\tau + \left(f(x) - \frac{e}{\Omega}\right)\mathrm{d}\phi\,. \tag{3.138}$$

The functions appearing above are

$$\Gamma(x) = r_+^2 + a^2\,x^2\,, \qquad \gamma(x) = \frac{r_+^2 + a^2}{r_+^2 + a^2\,x^2}\,, \qquad f(x) = Q\frac{r_+^2 + a^2}{2\,r_+\,a}\frac{r_+^2 - a^2x^2}{r_+^2 + a^2\,x^2}\,. \tag{3.139}$$

The physical parameters, Ω, e, and r_+ are themselves

$$\Omega = \frac{2\,a\,r_+}{r_+^2 + a^2}\,, \qquad e = \frac{Q^3}{r_+^2 + a^2}\,, \qquad r_+ = \sqrt{a^2 + Q^2}\,. \tag{3.140}$$

Note that the gauge field has a finite expression as $a \to 0$, despite the factors of Ω^{-1} the expression.

As in the vacuum case, we work with the harmonic gauge for the metric and Lorentz gauge for Maxwell perturbations. In Chapter 2, the Schwarzian mode was exhibited as an element in the kernel of the Lichnerowicz operator, which for Einstein-Maxwell theory is given by[34]

$$\begin{aligned}(\Delta_L^{\mathrm{EM}}h)_{\mu\nu} = (\Delta_L h)_{\mu\nu} - \frac{1}{2}\,g_{\mu\nu}\,g^{\alpha\beta}\,(\Delta_L h)_{\alpha\beta} \\ + \frac{1}{4}\left[-F^2\left(h_{\mu\nu} - \frac{g_{\mu\nu}}{2}\,h\right) - 4\,h\,F_{\mu\rho}F_\nu{}^\rho + 4\,F_{\mu\rho}\,F_{\nu\sigma}\,h^{\rho\sigma} + 8\,F_{\mu\rho}\,F_\sigma{}^\rho\,h_\nu{}^\sigma\right].\end{aligned} \tag{3.141}$$

[34]We define the operator by the kinetic term for the gravitons parameterized as $h^{\mu\nu}\,(\Delta_L^{\mathrm{EM}}h)_{\mu\nu}$ in harmonic gauge, which is slightly different from the presentation in (3.14). We are also employing the harmonic and Lorenz gauge choices instead of the one used in section 3.1.3 in the near-horizon geometry.

Furthermore, it was also pointed out that a putative rotational zero mode, which one would expect to be generated by the diffeomorphism along the Killing field ∂_ϕ, fails to be in the kernel of (3.141).

We will now examine the latter statement closely, and verify that there is indeed a rotational zero mode. We will consider an ansatz identical to what we chose in Kerr AdS_4. Imagine generating a large diffeomorphism of the near-horizon geometry (3.137) along the vector field ξ introduced in the Kerr AdS_4 context in (3.136), reproduced below for convenience

$$\xi = H(\tau, y)\,\partial_\phi + \alpha(x)\,\nabla^\mu H\,\partial_\mu\,, \qquad H(\tau, y) = e^{\mathrm{i}\,n\,\tau}\left(\frac{y-1}{y+1}\right)^{\frac{|n|}{2}}\,. \tag{3.142}$$

The component along ∂_ϕ is the part that was considered in in Chapter 2.

Since we want the perturbation generated by ξ to be a physical zero mode, it must satisfy the harmonic and Lorenz gauge conditions. It is immediate to see that the latter cannot be satisfied as written, since ξ also Lie drags the gauge field. Per se, this is not a problem because we may accompany the diffeomorphism along ξ by a gauge transformation by a scalar χ. Thus, the Maxwell perturbation is

$$\delta A = \mathrm{d}\chi + \mathcal{L}_\xi A. \tag{3.143}$$

We wish to choose χ in such a way that this expression is divergence-free, i.e., $\nabla^\mu \delta A_\mu = 0$. The structure of ξ leads to the following choice:

$$\chi = -\mathrm{i}\,e\frac{\partial_\tau H}{1+y}\,\frac{\alpha}{\Gamma}\,. \tag{3.144}$$

Then, we are left with the task of imposing the harmonic gauge condition on $\mathcal{L}_\xi g$. This leads

to an inhomogeneous second order ODE for $\alpha(x)$

$$\Gamma\frac{\mathrm{d}}{\mathrm{d}x}\left((x^2-1)\,\gamma\,\frac{\mathrm{d}\alpha}{\mathrm{d}x}\right)+\left[2\,\Gamma\,\gamma+\Omega^2\,(x^2-1)\,\gamma^3\,\Gamma-\frac{\mathrm{d}}{\mathrm{d}x}\big((x^2-1)\,\gamma\,\Gamma'\big)\right]\alpha=(1-x^2)\,\Omega\,\gamma^3\,\Gamma^2\,. \tag{3.145}$$

This equation is easy to solve numerically, and the result is exhibited in fig. 3.13. In particular, we find a unique smooth solution as long as $Q\neq 0$. In the $Q\to 0$ limit, however, the coefficient in front of α in (3.145) vanishes. It then follows that the homogeneous equation has a solution $\alpha(x)=$ constant. For that reason, a smooth solution to the inhomogeneous equation of interest ceases to exist.

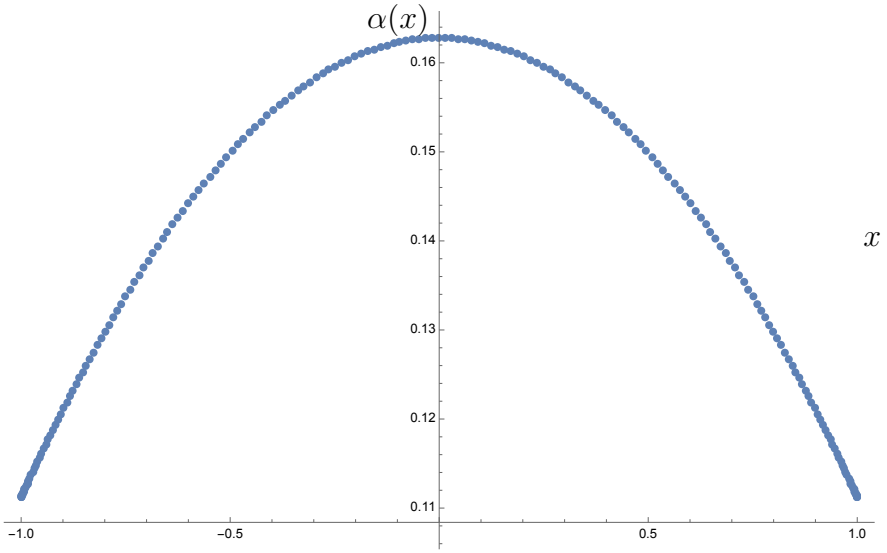


Figure 3.13: The solution for the profile of the function $\alpha(x)$ in rotational zero mode ξ defined in (3.145) at $a=0.2\,r_+$ (thus $Q=0.98\,r_+$). As in fig. 3.12 we note that the function is well-behaved at the poles of the $\mathbf{S}^2$, $x=\pm 1$.

We have thus established a near-horizon large diffeomorphism that respects the gauge conditions chosen for the metric and the gauge field. It then follows that the perturbation has vanishing on-shell action. We verified this statement by explicit calculation of the on-shell Einstein-Maxwell action. Notice, however, that owing to the mixing with the gauge field, as evidenced by the gauge transformation along χ, the resulting metric perturbation, $h_{\mu\nu}=2\,\nabla_{(\mu}\xi_{\nu)}$, will not be annihilated by (3.141). In Chapter 2, we did not analyze the structure of the compensating diffeomorphism and gauge transformation, but only noted that

the diffeomorphism along $H(\tau, y)\,\partial_\phi$ is not annihilated by the Lichnerowicz operator, which, while true, is insufficient to conclude anything about the zero modes of the kinetic operators.

3.2.3 Rotational modes in the near-horizon of extremal Kerr spacetime

As presented above, there are various rotating black holes that admit rotational zero modes in their near-horizon region. On the other hand, it was observed in Chapter 2 that this is not the case for the Kerr black hole in the harmonic gauge. We will argue that this is a failure of the harmonic gauge on the NHEK background rather than any physical phenomenon.

There are two ways in which a gauge choice may fail: either there exist perturbations that cannot be transformed into the chosen form, or there are non-zero perturbations satisfying all the gauge conditions that may not be transformed to zero. For the harmonic gauge, these two notions are essentially equivalent. Indeed, let us consider a perturbation $h_{\mu\nu}$ and let

$$\mathsf{GF}_\mu = \nabla^\nu \left(h_{\mu\nu} - \frac{1}{2}\, g_{\mu\nu}\, h \right). \tag{3.146}$$

We will assume that $h_{\mu\nu}$ is smooth and decays sufficiently fast at infinity to ensure that it is normalizable with respect to the ultralocal measure. It follows that GF_μ is also normalizable.

Now we note that $h_{\mu\nu}$ is in the harmonic gauge if and only if $\mathsf{GF}_\mu = 0$. If this is not the case, we may modify it by a gauge transformation

$$h_{\mu\nu} \mapsto h_{\mu\nu} + \nabla_\mu \zeta_\nu + \nabla_\nu \zeta_\mu \,, \tag{3.147}$$

for a normalizable vector field ζ^μ. To ensure that the new perturbation is in the harmonic gauge, ζ^μ must satisfy the following equation:

$$\left(\delta^\mu{}_\nu\, \nabla^2 + R_\nu{}^\mu\right) \zeta_\mu = -\mathsf{GF}_\nu \,. \tag{3.148}$$

This is an elliptic problem for the compensating diffeomorphism generated by ζ^μ. It has a solution for all GF_μ only if the cokernel of the operator defined by the left-hand side vanishes. But this operator is self-adjoint, and so the condition is equivalent to the requirement that its kernel be zero.[35] We thus see that for the harmonic gauge, the two possible modes of failure are equivalent.

The only thing that is left is to prove that the operator $\delta^\mu{}_\nu\,\nabla^2 + R_\nu{}^\mu$ on the near-horizon extreme Kerr (NHEK) geometry indeed has a non-zero kernel. Of course, since the NHEK is Ricci flat, the operator reduces to the Laplacian, $\delta^\mu{}_\nu\,\nabla^2$.

Let us start by inspecting a hyperbolic disk:

$$\mathrm{d}s^2_{\mathrm{AdS}_2} = (y^2-1)\,\mathrm{d}\tau^2 + \frac{\mathrm{d}y^2}{y^2-1}\,. \tag{3.149}$$

The spectral theory on this background is well-known [88]. In particular, the (co)vector Laplacian has one series of normalized eigenstates, namely [36]

$$\zeta = \mathrm{d}H\,, \qquad H(\tau,y) = e^{\mathrm{i}n\,\tau}\left(\frac{y-1}{y+1}\right)^{\frac{|n|}{2}}\,. \tag{3.150}$$

It is an easy exercise to check that ζ pull-backed to the NHEK background, which has the line element [70]

$$\mathrm{d}s^2_{\mathrm{NHEK}} = \left(1+x^2\right)\left(\left(y^2-1\right)\,\mathrm{d}\tau^2 + \frac{\mathrm{d}y^2}{y^2-1} + \frac{\mathrm{d}x^2}{1-x^2}\right) + 4\frac{1-x^2}{1+x^2}\left(\mathrm{d}\phi + \mathrm{i}\,(y-1)\,\mathrm{d}\tau\right)^2\,, \tag{3.151}$$

satisfies

$$\nabla^2\zeta_\mu = \nabla_\mu\nabla^2 H + R_\mu{}^\nu\,\nabla_\nu H = 0\,. \tag{3.152}$$

Thus, as promised, $\nabla^2\,\delta_\mu{}^\nu$ has a non-zero kernel and the harmonic gauge cannot be imposed.

[35] As such, due to i factors in the (complex Euclidean) metric, the Laplacian does not have to be self-adjoint. However, it is easy to see that is when restricted to axisymmetric perturbations, it does, which suffices for the argument.

[36] This should be familiar from the structure of gauge field zero modes encountered in the near-horizon AdS_2 geometry.

That resolves the puzzle encountered in Chapter 2.

Let us add a couple more remarks to close out this discussion. Firstly, we can consider a more general near-horizon geometry which is a warped bundle with a AdS_2 factor, such as, for example, any d-dimensional black hole with $\mathrm{U}(1)^{d-3}$ symmetry group, cf [28]. Then, ζ is still well-defined as a pull-back. Moreover, $\nabla^2 H = 0$ and the first equality of (3.152) still holds. It follows that in general ζ satisfies,

$$\left(\delta^{\mu}{}_{\nu}\,\nabla^2 - R^{\mu}{}_{\nu}\right)\zeta_{\mu} = 0. \tag{3.153}$$

One may recognize that this is the operator that describes Maxwell fluctuations (around an uncharged saddle). That shows that ζ is universally a zero mode for $U(1)$ theory. Moreover, on any Ricci-flat background, ζ is in the kernel of the Laplacian and the harmonic gauge is invalid. Thus, not only do we have an issue for the Kerr spacetime, but similar problems will also persist for the higher-dimensional Myers-Perry solutions. Secondly, the one-loop determinant for the ghost associated with the diffeomorphism is exactly $\det\left(-\delta^{\mu}{}_{\nu}\,\nabla^2 - R^{\mu}{}_{\nu}\right)$. As we have seen, this determinant vanishes on the Ricci-flat backgrounds, thus providing yet another sign of the failure of the harmonic gauge. Finally, a compactification of the theory to two-dimensional JT gravity, coupled to a rotational U(1) gauge field and matter, suggests that the rotational modes are present. An explicit calculation can be made in the two-dimensional harmonic gauge combined with the Lorenz gauge for the gauge field (this is *not* the dimensional reduction of the 4d harmonic gauge condition for Kerr!). This observation would be more convincing if there were an improvement of the 4d harmonic gauge that led to the same answers.

3.2.4 Rotational modes in BMPV

In Chapter 2 we noted that we were unable to determine any rotational zero modes in the near-horizon geometry of the five-dimensional BMPV black hole. We pointed out that

this would be a serious problem because these modes needed to be present to match the macroscopic gravitational computations with the microscopic result obtained from string theory [27]. In light of the above, it behooves us to re-examine the solution, and fill this gap.

The near-horizon geometry of the BMPV black hole reads (cf. [103])

$$\mathrm{d}s^2 = \left(y^2-1\right)\mathrm{d}\tau^2 + \frac{\mathrm{d}y^2}{y^2-1} + \mathrm{d}\psi^2 + \sin^2\psi\,\mathrm{d}\chi^2 + \cos^2\omega\left(\mathrm{i}\,(y-1)\,\tan\omega\,\mathrm{d}\tau + \cos\psi\,\mathrm{d}\chi + \mathrm{d}\phi\right)^2, \tag{3.154}$$

where $\psi \in [0,\pi], \chi \in [0,2\pi], \phi \in [0,4\pi]$. The parameter $\omega \in [0,\frac{\pi}{2}]$ measures the angular momentum in units of the mass. The solution has $\mathrm{SU}(2)\times\mathrm{U}(1)$ rotational isometry. From the gravitational fluctuations one expects 7 zero modes; 3 from the Schwarzian set of modes, 3 associated with the SU(2) rotations, and 1 associated with the U(1) isometry. The former six are easy to find, as already mentioned in Chapter 2. We will focus on the U(1) rotational zero mode. Notice that this metric corresponds to the very near horizon, near AdS_2, regime of the BMPV black hole, not the larger AdS_3 throat.

Let us borrow the ansatz from the previous subsections and choose a vector field,

$$\xi = H(\tau,y)\,\partial_\phi + \alpha\,\nabla^\mu H\,\partial_\mu\,. \tag{3.155}$$

Here $H(\tau,y)$ is the same function encountered in (3.136). The perturbation generated by ξ is $\mathcal{L}_\xi g$. It is straightforward to check that it is traceless. Moreover, its divergence reads

$$\nabla^\mu\left(\nabla_\mu\xi_\nu + \nabla_\nu\xi_\mu\right) = -\frac{1}{2}\left(3\,b + b\,\cos 2\omega + \sin 2\omega\right)\nabla_\nu H. \tag{3.156}$$

Hence, we see that ξ with

$$\alpha = -\frac{\sin 2\omega}{3+\cos 2\omega} \tag{3.157}$$

is indeed a zero mode. For the non-rotating solution, where $\omega = 0$, this is indeed a rotational zero mode associated with the $\mathbf{S}^3$. In this case, we have a set of SO(4) zero modes, of which this is a part. For $\omega \neq 0$, however, the U(1) zero mode identified above does not mix with

the other rotations. This is in perfect agreement with the predictions of [27].

3.3 Low-temperature thermodynamics of the BTZ black hole

Here, we continue the discussion from the previous section, and focus on the case of the BTZ spacetime, for reasons that will become clear shortly.

Let us recall the puzzle regarding the low-temperature thermodynamics of BTZ, alluded to in the previous section. To sharpen the puzzle, it is useful to import some results reviewed in section 3.1.1. The one-loop determinant for gravitons around the BTZ geometry can be computed from first principles, in an ensemble of fixed temperature and angular velocity, either using the heat-kernel method [119] or with a formal argument using the asymptotic symmetries [130]. In the low-temperature limit, up to a possible shift in the extremal limit, leads to [40]

$$Z^{1-\text{loop}}_{\text{graviton}} \sim T^{\frac{3}{2}} \,. \tag{3.158}$$

At low temperatures, the prefactor of $T^{3/2}$ is consistent with the presence of Schwarzian modes but not with the rotational ones. The latter are expected, in an ensemble of fixed angular velocity, to produce another factor of $T^{1/2}$ around an individual saddle.[37] Contrary to the expectation in Chapter 2, the BMPV analysis from the previous section suggests that indeed there should be a rotational zero mode in the near-horizon region of the BTZ geometry, leading to an extra $T^{1/2}$ factor. Why is the one-loop determinant around an individual near-extremal BTZ geometry $T^{3/2}$ and not T^2?

We shall first show that the extremal BTZ geometry does indeed have a rotational zero-mode in the near-horizon region. Consider the BTZ solution (3.2). In the near-extremal

[37] To obtain full one-loop determinant, one should sum over integer shifts of the chemical potential for rotations at infinity, which is the subset of the $\text{SL}(2,\mathbb{Z})$ transformed black hole. The scaling with temperature is the same, both with and without performing the sum.

limit, we work at fixed J and expand around the extremal value $r_+ = r_-$ with the scaling

$$r_+ = r_0 + \frac{\mathsf{T}}{4} + \frac{\mathsf{T}^2}{32\, r_0} + \mathcal{O}\big(\mathsf{T}^3\big)\,, \qquad r_- = r_0 - \frac{\mathsf{T}}{4} - \frac{3\,\mathsf{T}^2}{32\, r_0} + \mathcal{O}\big(\mathsf{T}^3\big)\,. \tag{3.159}$$

Plugging (3.159) into the BTZ line element (3.2) together with

$$\varphi \to \varphi - \mathrm{i}\, t_{\scriptscriptstyle \mathrm{E}}\,, \qquad r = r_0 + \frac{\mathsf{T}}{4}\, y\,, \qquad t_{\scriptscriptstyle \mathrm{E}} \to \frac{\tau}{\mathsf{T}}\,, \tag{3.160}$$

we zoom into the extremal near-horizon metric, which is a fibration of a circle over AdS_2,

$$\mathrm{d}s^2 = \frac{1}{4}\left((y^2-1)\,\mathrm{d}\tau^2 + \frac{\mathrm{d}y^2}{y^2-1} + 4\, r_0^2\left(\mathrm{d}\varphi - \mathrm{i}\,\frac{y}{2\, r_0}\,\mathrm{d}\tau\right)^2\right). \tag{3.161}$$

Before tackling the rotational mode, let us confirm analytically that the off-shell modes identified in section 3.1.1 are indeed the Schwarzian modes. These modes should be in the kernel of the Lichnerowicz operator in the extremal near-horizon geometry (3.161). By direct computation, one finds

$$\mathrm{d}s^2_{\mathrm{Sch}} = \left(\frac{y-1}{y+1}\right)^{\frac{|n|}{2}}\left[\left(-\mathrm{d}\tau^2 + \frac{\mathrm{d}y^2}{(y^2-1)^2}\right)\cos(n\tau) - 2\,\mathrm{i}\,\frac{\mathrm{d}\tau\,\mathrm{d}y}{y^2-1}\sin(n\tau)\right] \tag{3.162}$$

Here $n \geq 2$ and the amplitude of the modes can be normalized by demanding the modes be suitably orthonormal. Now consider the off-shell modes $h^{(n)}_{\mu\nu}$ obtained in (3.17), and apply the scaling (3.160). It is not hard to show that the line element reduces to

$$h^{(n)}_{\mu\nu}\,\mathrm{d}x^\mu\,\mathrm{d}x^\nu = 8\, r_0^4\,\mathsf{T}^2\,\mathrm{d}s^2_{\mathrm{Sch}} + \mathcal{O}\big(\mathsf{T}^3\big)\,. \tag{3.163}$$

This adds to the list of checks that all we find in the full geometry are the uplift of the Schwarzian modes.

Let us now return to the question of the rotational mode. We can borrow the ansatz from

the analysis in section 3.2 and choose a vector field

$$\xi = H(\tau, y)\, \partial_\phi + \alpha\, \nabla^a H \partial_a, \tag{3.164}$$

where the function $H(\tau, y)$ is the same as the one defined in (3.136). The perturbation generated by ξ is $\mathcal{L}_\xi g$. It is straightforward to check that it is traceless. Moreover, its divergence reads

$$-\nabla^\mu \left(\nabla_\mu \xi_\nu + \nabla_\nu \xi_\mu\right) = (2r_0 + 4\alpha)\ \nabla_\nu H. \tag{3.165}$$

Hence we see that ξ with $\alpha = -\frac{r_0}{2}$ is indeed a zero mode, since it is a pure (large) diffeomorphism satisfying the gauge condition.

At this point, it is appropriate to comment on the choice of ensemble. The rotational zero-modes written above, as well as the ones in the previous section, naturally arise in a fixed charge ensemble. They affect the normalizable mode, but keep the non-normalizable mode in the gauge field (which only in 2d controls the charge) unchanged. These modes also contribute to the grand canonical ensemble in the following way. While in higher dimensions the grand canonical ensemble corresponds to fixing the holonomy of a gauge field, that is not the case in the near-horizon geometry. It is easy to see this from the 2d perspective. Consider a gauge field A_μ in two dimensions. It was shown in [40, 41, 47] that a fixed-holonomy boundary condition in the full geometry translates to a mixed boundary condition in the throat with

$$\delta(\mathsf{A}_\mu - c\, n^\nu \mathsf{F}_{\mu\nu}) = 0, \tag{3.166}$$

where c is a coefficient determined by the details of how the throat is glued to the exterior, and is proportional to the quantity $1/T_q^{\mathrm{U}(1)}$ introduced below. This means that a fluctuation mode that affect the normalizable piece of A is consistent with the 2d grand canonical boundary condition only if one supplements it with a shift in the charge that keeps (3.166) fixed. In all cases relevant to this chapter, the effect from the small change in the charge is subleading and can be neglected in the evaluation of the action. This manifests itself in two dimensions

in the fact that the Yang-Mills coupling is always suppressed by factors of G_N, reducing the Yang-Mills theory to an effective BF model with mixed boundary conditions. This implies that the modes written in the previous paragraph should also contribute to the grand canonical ensemble.

Assuming these rotational modes can be regularized by turning on the temperature, we would find out that it produces an additional factor of $T^{1/2}$ to the total graviton one-loop determinant. This stands in stark contrast both with the heat-kernel method and our results on the spectrum of the Lichnerowicz operator from section 3.1.1. But the conclusion that there should be an additional $T^{1/2}$ factor is too naive for two reasons:

- First, it is not guaranteed that a zero-mode that exists in the near-horizon region will extend to the full (in this case asymptotically AdS_3) geometry. Indeed, while this might not be completely evident from our analysis in section 3.1.1, the Schwarzian modes found in that section are the only ones that exist in the full geometry with an action that vanishes linearly with the temperature. This conclusion can be extracted from the thorough analysis of the eigenfunctions of the Lichnerowicz operator in [122, 123]. This is not surprising; for example, it is not guaranteed that a mode in the throat, when extended to the full geometry, remains normalizable. The fact that no rotational modes are found in the analysis of [122, 123] suggests this is the case. In fact, the main purpose of this chapter is to verify in non-trivial examples that the Schwarzian modes always successfully extend to the full geometry.

- The rotational zero-modes would produce a factor of $T^{1/2}$ only if their eigenvalue with a fine-temperature regulator is linear with the temperature. But what is the coefficient of proportionality? The Schwarzian modes eigenvalues are always proportional to T/T_q setting the temperature scale at which they become strongly coupled. This scale can be

identified from the classical thermodynamics, see for example [116], through the relation

$$T_q = 4\pi^2 \frac{1}{\frac{\partial S}{\partial T}\big|_{T=0}}. \tag{3.167}$$

In other words, the Schwarzian coupling is the coefficient in the linear-in-temperature term in the classical entropy, viz., it is determined by the specific heat at extremality. This temperature scale is of order $\mathcal{O}(G_N)$ in the semiclassical limit. Similar scales can be defined for any gauge mode $T_q^{\mathrm{U}(1)}$ below which the gauge sector nearly zero-modes become strongly coupled. As explained in [116] (or in [41, Section 3.4]) this scale can again be extracted from classical thermodynamics

$$T_q^{\mathrm{U}(1)} = \frac{1}{K}\,, \qquad K = \left.\frac{\partial Q}{\partial \mu}\right|_{T=0}. \tag{3.168}$$

This applies to any gauge mode and can be generalized also to non-Abelian ones. The coefficient K is the charge susceptibility (but is referred to as the compressibility of the system in the condensed matter literature). Similarly, the rotational modes also are governed by the angular momentum susceptibility

$$T_q^{\mathrm{rot}} = \frac{1}{K}\,, \qquad K = \left.\frac{\partial J}{\partial \Omega}\right|_{T=0}. \tag{3.169}$$

This separation between Schwarzian and gauge-mode scales is usually unimportant since all these quantities are finite and of the same order of magnitude $\mathcal{O}(G_N)$, but something special happens for BTZ. An extremal rotating BTZ black hole satisfies $\Omega(J, T = 0) = 1$ regardless of the angular momentum. This means that the angular momentum susceptibility diverges! This implies that the finite-temperature action of the would-be U(1) modes diverges, essentially removing them from the spectrum. This is not independent of the previous bullet point; the finite-temperature action of the throat zero-modes arises precisely from the way the throat is glued to the exterior spacetime. Both perspectives imply that

such gluing is problematic for the rotational modes.

Taking these two observations into account, the situation becomes clear; the rotational modes of BTZ that one finds in the near-extremal solution near the horizon are not physical. They do not exist in the full geometry. Further evidence for this assertion is provided by the fact that the other one-loop effect, viz., $\log S_0$ correction to the black hole entropy, is reproduced from the near-horizon analysis by the Schwarzian modes alone.

A general lesson can be drawn from this specific case. We propose that whenever the zero temperature susceptibility associated to a gauge symmetry or background isometry (extracted from the classical thermodynamical analysis) is singular, this symmetry does not lead to any physical light mode at low temperatures.[38]

A singular limit of the susceptibility arising from gravitational solutions is not uncommon. Besides the BTZ black hole, an example is provided by the prototypical case of the asymptotically flat Reissner-Nordström black hole. In the case of a flat space black hole, in the conventions of section 3.1.3, the extremal chemical potential is simply $\mu = 1$ irrespective of the charge.[39] This leads to a singular charge susceptibility $K \to \infty$. This singularity is regulated by the presence of a cosmological constant, leading to

$$\mu = \sqrt{\frac{1}{2} + \sqrt{\frac{1}{4} + \frac{3\,Q^2}{\ell_{\rm AdS}^2}}} \quad \Rightarrow \quad K = \frac{\ell_{\rm AdS}^2}{3\,|Q|} + \cdots \,. \tag{3.170}$$

Our general guess, together with the expression above for K in the large $\ell_{\rm AdS}$ limit, predicts the rate at which the U(1) eigenvalues should diverge in the flat space limit. In particular, we expect $\lambda \sim (\mu - 1)^{-1}$ as we approach the asymptotically flat solution. This is indeed what we see from our numerical analysis, as already explained in section 3.1.3, see fig. 3.11. Based on this numerical analysis, we would like to argue that gauge fields which source the background

[38]For black holes with non-compact spatial horizon cross-section, like the planar AdS or hyperbolic AdS black holes, the Schwarzian contribution is likewise suppressed because the specific heat is proportional to the spatial volume.

[39]This might not be surprising. If the U(1) gauge field arises from a five-dimensional Kaluza-Klein reduction, as is usually the case in string theory, the near-horizon geometry is $\mathrm{AdS}_2 \times \mathbf{S}^1 \times \mathbf{S}^2$ with the first two factors being precisely the same as the BTZ throat.

charge do not contribute to quantum effects for the asymptotically flat Reissner-Nordström spacetime.

3.4 Discussion

In this chapter, we constructed off-shell modes in the full higher-dimensional asymptotically flat (or AdS) metric that behave in the near-extremal limit precisely like the Schwarzian modes present near the horizon in the AdS_2 description. Our results confirm that the modes identified in previous work on quantum corrections to the near-extremal black hole spectrum and dynamics, relying on the analysis of quantum effects in the throat using two-dimensional gravity techniques, are indeed physical and relevant in higher dimensions. We end with some open questions which are left for future work.

- To carry out our analysis we had to rely on numerics to find the Schwarzian modes in the full geometry. It would be desirable to find the profiles analytically. This is hopeless to achieve for the full spectrum of metric fluctuations, but the Schwarzian modes have special properties that might make this possible.

- It would be interesting to find the extension of the Schwarzian modes for the Kerr black hole in AdS_4, or even in flat space to the full spacetime. This would have to be tackled after using a gauge-fixing term which does not suffer the drawbacks of the harmonic gauge in Ricci-flat spacetimes. This would be an interesting exercise to undertake, although one also needs to address the role that superradiance plays near extremality.

- Likewise, it would be interesting to extend some of these results to supergravity. It was recently uncovered how to perform the gravitational computation of the index in the full geometry, where one works at a finite temperature and identifies a complex Euclidean saddle associated with a particular value of chemical potential, cf. [97, 131, 132, 133, 134, 135, 136, 137, 81, 138]. The index is, of course, temperature independent and thus are no

logarithmic corrections of the kind discussed herein. However, at low temperatures, the Schwarzian modes play a non-trivial role in correcting the density of states.

- Since we focused on evaluating the determinant by working in Euclidean signature, it sufficed for us to extract off-shell eigenmodes of the quadratic fluctuation operator. The determinant can, however, be expressed as a product over physical on-shell quasinormal (and their conjugate, anti-quasinormal) modes [139]. These are on-shell in Lorentz signature. It would be interesting to understand how to interpret the analysis herein in terms of these quasinormal modes [140].

- Finally, analogs of the Schwarzian modes appear in the evaluation of the wavefunction of the universe with a positive cosmological constant and with spatial $\mathbf{S}^1 \times \mathbf{S}^2$ topology [141]. When the size of the circle is much larger than the size of the sphere, there is a long period of dS_2 inflation and similar light modes were shown to arise. In that case, the role of quantum effects was to make the wavefunction normalizable. It would be interesting to find those modes in the full inflating geometry.

Chapter 4

Charged particle emission by near-extremal black holes

The goal of this chapter will be to extend the analysis of [60]. Their quantum treatment of the neutral emission rates using the wave method described in the Introduction, and the rates found for charged radiation using the seemingly disparate instanton method, and finally the application of these in deriving the evaporation history of a large near-extremal black hole motivate the following questions, which form the basis of this chapter.

- Can the quantum-corrected evaporation rates for a charged field be computed in an analogous manner to the neutral rates, i.e. by solving the charged field scattering problem and using this as input for the effective quantum theory? This would result in a unified treatment of neutral and charged radiation based on the wave method. Furthermore, can this be done for any combination of the background and field parameters, not just for the large black holes, which were needed to justify the use of the instanton method?

- For large black holes, does this quantum-corrected rate reduce to the semi-classical one, regardless of the energy regime, as the instanton calculation suggests, and does this semi-classical rate further reduce to the same exponentially suppressed Schwinger-like result the instanton method gives when the black hole is taken to be very large? The latter

question was already partially answered by Gibbons in [51], where it was shown that for a large black hole the exponentially suppressed rate can be obtained from the wave equation using the approximate technique of WKB theory.[1] Our goal will be to fully solve the wave equation and to show that the WKB result is obtained in the appropriate limit.

- Using these quantum-corrected evaporation rates, we will be able to derive the evaporation history of a charged black hole of any size. Do these rates lead to a history different from the one that semi-classical theory would predict, at least for some combination of the parameters?

We will also consider the evaporation of a near-extremal Kerr black hole. As in the case of Reissner-Nordström, the near-horizon region of the Kerr spacetime is well approximated by the NHEK (Near-Horizon-Extremal-Kerr) geometry [70], which also contains AdS_2 with the sphere fibered over it. As we will see, the (radial part of the) wave equation of a neutral field of any spin in the near-extremal Kerr geometry has the same form as that of a charged field in Reissner-Nordström, which in part has to do with the fact that both have an AdS_2 factor in their near-horizon region. To make this more obvious, the gravity plus matter theory on this spacetime can be dimensionally reduced on the sphere, causing the metric to break up into an AdS_2 metric and a U(1) gauge potential corresponding to the SO(2) symmetry of Kerr and NHEK. The modes of any field in the original 4D background act as massive AdS_2 fields that are charged under this gauge potential, with the charge being the azimuthal angular momentum of the original mode. This motivates the following question.

- Given the close analogy between near-extremal Reissner-Nordström and Kerr, is a parallel treatment of the two possible, and what does it imply for the evaporation rates and history of near-extremal Kerr?

In this chapter, we will address all of these questions. Recent work on the first question includes [142, 143], and on the fourth includes [142]. We will indicate where our results

[1] In fact, this was the first work to derive this rate in the context of black holes, and the instanton calculations came later.

recover or differ from the results of those works. We will also mention where our results reproduce the results of [60] and the classic results of Gibbons, Starobinskii, and Press & Teukolsky in certain limits.

One distinctive feature of charged radiation is the phenomenon of superradiance. This was first discovered in the context of black hole scattering in [144, 145], specifically for Kerr in [52, 53] and discussed for Reissner-Nordström in [51]. It can be defined as follows. For charged radiation, for frequencies below a certain threshold frequency, an incident wave can be amplified, meaning that it is reflected with an amplitude higher than the incident one. Later in the text, we will give a definition more suited to a black hole spontaneously emitting radiation. For now, we only mention the most important property of superradiance for our analysis, which is the fact that, unlike for neutral radiation, the evaporation rate of modes with superradiant frequencies does not go to zero as the temperature of the black hole is taken to zero, instead it goes to a constant. This implies that no matter how low the temperature is, there is always a constant flux of charged radiation in this range of frequencies. The same is true for field modes with angular momentum in the Kerr background. We will see that the fact that superradiance exists introduces an additional scale into the problem of charged radiation, which will give it a richer spectrum of solutions than was found for neutral radiation.

Before turning to our results, one comment is in order. A large Reissner-Nordström black hole, no matter at what energy it starts at, naturally approaches extremality, both in the original semi-classical calculation [51] and in the quantum-corrected one of [60]. This is a consequence of the fact that the charged particle emission is highly suppressed such that the neutral radiation has enough time to lower the temperature close enough to zero before the next charged particle is emitted. For small charged black holes, and for Kerr, this is not the case, both neutral and charged radiation is continuously being emitted. Whether the black hole moves towards or away from extremality depends on the ratio of energy emitted to charge/angular momentum emitted. In [57, 58, 59] it was shown that for the

entire evaporation history of both of these, charged emission drives the black hole away from extremality. Therefore, if there is any chance of seeing quantum corrections for these black holes, it would be for one starting as close to extremality as possible, as once it has left this region, it never comes back. This motivates the following two additional questions related to the third one listed above. First, do the quantum-corrected evaporation rates give a different ratio of emitted energy to charge than the semi-classical ones, and does it possibly drive the black hole towards extremality? We will find that the ratio is different, but it still drives the black hole away. Secondly, does the black hole spend more or less time in the near-extremal regime than the semi-classical theory predicts? This also touches upon a question raised in Chapter 2 of how the time scale associated with the quantum corrections to the thermodynamics of a near-extremal black hole compares with the time it has to spend near extremality. Once the black hole has left the near-extremal regime, the subsequent evolution is just that of [57, 58, 59].

We now turn to an overview of this chapter and a presentation of the main results. For Reissner-Nordström emitting a nearly[2] massless charged scalar field, the scattering problem is defined by three parameters: the size of the black hole determined by its charge $r_{\rm h} = \sqrt{G}Q$, a measure of near-extremality taken to be either its temperature T or the energy above extremality E, and the charge of the quanta being emitted e. We only assume that the black hole is near-extremal, which means that T and E are small. We solve the wave equation for any allowed combination of these parameters and compute both the semi-classical Hawking and the quantum-corrected JT/Schwarzian emission rate.

We define small black holes as those with $e \leq Q \leq \frac{1}{2e}$ and large black holes as those with $Q \geq \frac{1}{2e}$. We will see that this determines whether the conformal dimension[3] Δ, a key parameter in the wave equation, which further determines the character of the spectra, is

[2]For most of this work, we will take $m = 0$ for simplicity, but to obtain the Gibbons exponential suppression result, we will need $m \neq 0$.

[3]We note that Δ plays two roles in this work. First, it is just a parameter in the 4D wave equation, which will take a set of possible values, for each of which the wave equation gives sensible physical solutions. Second, it can be though of as the usual conformal dimension of the $\mathrm{AdS}_2/\mathrm{CFT}_1$ correspondence, where we have to be careful with what value it takes.

purely real or both real and complex on the interval of available frequencies. For small black holes, the semi-classical and quantum emission rates of a mode with frequency ω and angular momentum l, m_l can be found in equations (4.71) and (4.95), respectively. For large black holes, the semi-classical emission rate is given by (4.71) only for the frequencies with real Δ and by (4.155) for the rest.

The two parameters Q and e further define two energy scales, the breakdown scale $E_{\rm b} = \frac{1}{\sqrt{G}Q^3}$, and the superradiant scale $\omega_{\rm sr} = \frac{eQ}{r_+} \approx \frac{e}{\sqrt{G}}$. The breakdown scale defines where the quantum regime starts, i.e. where the quantum evaporation rate starts deviating from the semi-classical one. When at least one of the other two scales E and $\omega_{\rm sr}$ is above $E_{\rm b}$, the quantum evaporation rate to leading order reduces to the semi-classical, so it is safe to compute only the latter in this regime. When both of the other two scales are below $E_{\rm b}$, the quantum rate gives different predictions for the spectra from the semi-classical. In this case we will compute both rates and compare them. We will find that all large black holes and some of the small ones always have $\omega_{\rm sr} > E_{\rm b}$, which implies that they are always in the semi-classical regime. The remainder of small black holes is where the novel quantum behavior will be found. A summary of the different sizes and corresponding regimes can be found in figure 4.1.

The superradiant scale determines the superradiant frequencies; all modes below are superradiant, and all above are not. Depending on how the scales E and $\omega_{\rm sr}$ compare to each other, the emission spectra will either be dominated by non-superradiant frequencies or dominated by superradiant ones. For the non-superradiant-dominated radiation, we will find the spectra to be similar to neutral radiation and will therefore also refer to it as neutral-like.

If we assume a separation between these three scales, $E_{\rm b}$, E, and $\omega_{\rm sr}$, the emission rates simplify significantly. For any choice of these scales, we will have a black hole that is either small or large, with an emission spectrum that is either semi-classical or quantum, and neutral-like or superradiant-dominated (see table 4.1 for a summary). We proceed with the results for each regime. Starting with small black holes $e \leq Q \leq \frac{1}{2e}$ with $\omega_{\rm sr} \ll E_{\rm b} \ll E$

or $E_{\rm b} \ll \omega_{\rm sr} \ll E$, which defines the semi-classical neutral-like regime, the emission rate is found to be

$$\left.\frac{dE}{dt}\right|_{\rm sc} = \sum_{l=0}^{\infty} C_l \left(\frac{\sqrt{G}E}{Q}\right)^{2l+2} \frac{1}{r_{\rm h}^2}\,, \tag{4.1}$$

with the unitless numerical C_l given by equation (4.112). This equation can be safely approximated by the contribution of the dominant $l = 0$ mode. The rate is written in the microcanonical (Q, E) variables rather than the standard canonical (Q, T) for easier comparison with the quantum rate. The emission rate of small black holes with $\omega_{\rm sr} \ll E \ll E_{\rm b}$, which defines the quantum neutral-like regime, is found to be

$$\left.\frac{dE}{dt}\right|_{\rm q} = \sum_{l=0}^{\infty} \hat{C}_l \left(\frac{\sqrt{G}E}{Q}\right)^{2l+2} \left(\frac{E}{E_{\rm b}}\right)^{\frac{3}{2}} \frac{1}{r_{\rm h}^2}\,, \tag{4.2}$$

with the coefficients $\hat{C}_l$ given in (4.118). The semi-classical and quantum rates have the same form, with different numerical coefficients of roughly the same size. The main difference comes from the extra suppression factor in the quantum rate, first found for neutral radiation by [60]. We note that for neutral-like radiation, near-extremality implies that the parameter $eQ \ll 1$, causing it to fully drop out in the equations above.

Turning to superradiant emission, for small black holes with $E \ll E_{\rm b} \ll \omega_{\rm sr}$ or $E_{\rm b} \ll E \ll \omega_{\rm sr}$, which defines the semi-classical superradiant-dominated regime, the emission rate is

$$\left.\frac{dE}{dt}\right|_{\rm sc} = \sum_{l=0}^{\infty} G_l(eQ) \frac{1}{r_{\rm h}^2} \xrightarrow{eQ \ll 1} \sum_{l=0}^{\infty} D_l \,(eQ)^{4l+4} \frac{1}{r_{\rm h}^2}\,, \tag{4.3}$$

where the coefficient functions $G_l(eQ)$ and numerical coefficients D_l can be found in equations (4.125) and (4.128), respectively. For small black holes with $E \ll \omega_{\rm sr} \ll E_{\rm b}$, which defines the quantum superradiant-dominated regime, is

$$\left.\frac{dE}{dt}\right|_{\rm q} = \sum_{l=0}^{\infty} \hat{D}_l \,(eQ)^{4l+4} \left(\frac{\sqrt{G}E_{\rm b}}{e}\right)^{2l+\frac{1}{2}} \frac{1}{r_{\rm h}^2}\,, \tag{4.4}$$

where the coefficients $\hat{D}_l$ can be found in (4.134). This is our first main result. It turns out that in the quantum superradiant regime $eQ \ll 1$. Therefore, we can only compare the low charge limit of (4.3) to this equation, and we find that they have the same form up to the extra ratio in the quantum rate, which now results in it being enhanced compared to the semi-classical one. Furthermore, unlike the neutral-like rate, both (4.3) and (4.4) have the property that they give a constant flux at extremality, which is a signature of superradiant emission.

For large black holes $Q \geq \frac{1}{2e}$, as mentioned above, the quantum rate always reduces to the semi-classical one, so we only compute the latter. Furthermore, since neutral-like emission requires $eQ \ll 1$, we only consider superradiant-dominated emission. The emission rate is found to be

$$\left.\frac{dE}{dt}\right|_{\text{sc}} = \sum_{l=0}^{\infty} \Big(G_l(eQ) + G'_l(eQ)\Big) \frac{1}{r_{\text{h}}^2} \xrightarrow{eQ \gg 1} e^{-2\pi Q\left(e-\sqrt{e^2-m^2}\right)} \frac{1}{r_{\text{h}}^2}\,, \tag{4.5}$$

where there are now two coefficient functions $G_l(eQ)$ and $G'_l(eQ)$, which can be found in (4.170) and (4.171). The first comes from the subset of frequencies where the conformal dimension Δ is real and is computed using equation (4.71), and the second comes from the frequencies with a complex Δ and is found using equation (4.155). Furthermore, in equation (4.159), we take the $eQ \gg 1$ limit of the spectrum and show that it concentrates around the superradiant bound $\omega = e$ with its size determined by the Schwinger-like exponential suppression found in [51] using the WKB approximation. This is our second main result. We also plot the emission spectrum for different values of eQ in figure 4.5 where we can explicitly see how the rate transitions into the Gibbons result as eQ is turned up.

For near-extremal Kerr, where the scattering problem is defined by the black hole angular momentum J and the temperature T or energy above extremality E, we solve the wave equation and compute the semi-classical emission rate for the scalar, photon, and graviton in equation (4.209). We argue that for any combination of these parameters, the quantum

rate would reduce to the semi-classical, so we only compute the latter. Note that there is no analogous parameter to e, so there is no notion of small versus large black holes, but it turns out that the conformal dimension Δ can be complex for certain modes, and it turns out that it is so for the most dominant ones. Finally, we will argue that all modes, at all temperatures, as long as the black hole is near-extremal, must be in the superradiant-dominated regime, and therefore there is no neutral-like regime. Putting this all together, the emission rate of a spin-s field is found to be

$$\left.\frac{dE}{dt}\right|_{\rm sc}^{(s)} = \sum_{l,m} \left(H_{slm} + H'_{slm}\right) \frac{1}{GJ}\,, \tag{4.6}$$

where the coefficients H_{slm} and H'_{slm} are given in (4.216) and (4.229). The first term comes from the set of frequencies for which Δ is real and the second from frequencies where it is complex, if such frequencies exist for that mode. We will see that the dominant contributions comes from the $l = m$ modes, and that they fall off with growing l, but slowly, implying that for the full rate we need to compute and add up the first few modes if we want any precision (for the real part, see tables 4.3, 4.4 and 4.5, and for the complex, see 4.6, 4.7 and 4.8).

Outline of the chapter: We start by introducing the Reissner-Nordström background metric and gauge potential, and its near-extremal region in subsection 4.1.1. We then solve the wave equation for real Δ in 4.1.2 by breaking it up into an equation in a near region and one in a far region, then solve these two equations, and match their solutions in the overlapping region to obtain a full solution. In 4.1.3 we use this solution to compute the greybody factor and the semi-classical evaporation rate. In 4.1.4 we introduce the effective string formalism, which is used to compute the quantum-corrected evaporation rate based on Schwarzian theory. Putting this together with additional input from the wave equation, we compute the quantum evaporation rate. In subsection 4.2.1, we define small versus large black holes and their relationship to Δ. Then, we define the quantum and semi-classical regimes, and the neutral-like and superradiant-dominated regimes. In 4.2.2 and 4.2.3 we

compute the evporation rates of small black holes in the neutral-like and superradiant-dominated regimes, respectively. In subsection 4.3.1, we review the WKB computation of the exponentially suppressed rate of a very large black hole, which does not require us to solve the wave equation. Then, in 4.3.2 we solve the wave equation for complex Δ, compute the semi-classical evaporation rate, and show that it reduces to the Gibbons result in the very large limit. In section 4.4, we repeat the analysis for the Kerr black hole, starting with the geometry in 4.4.1, then turning to the wave equation for a spin-s field and resulting evaporation rate in 4.4.2, and ending with a calculation of the emission rates in 4.4.3 and 4.4.4. In 4.5, we use the rates to discuss the evaporation histories for the different types of black holes. We end with a discussion of some potential future directions for our work.

4.1 Emission by a Reissner-Nordström black hole

4.1.1 Near-extremal Reissner-Nordström background

The Reissner-Nordström solution of the Einstein-Maxwell system of equations describes a charged black hole with mass M and charge Q. The gravitational field is described by the metric, which is given by

$$ds^2_{\rm RN} = -f(r)\,dt^2 + \frac{dr^2}{f(r)} + r^2\,d\Omega_2^2\,, \tag{4.7}$$

where

$$f(r) = 1 - \frac{2GM}{r} + \frac{GQ^2}{r^2}\,. \tag{4.8}$$

We will set $G = 1$ everywhere, until we reach our final results. An alternative parameterization of the metric is in terms of the roots of $f(r)$

$$r_\pm = M \pm \sqrt{M^2 - Q^2}\,, \tag{4.9}$$

which are the radii of the inner and outer horizons. So, we can also write

$$f(r) = \frac{(r - r_+)(r - r_-)}{r^2} \,. \tag{4.10}$$

The electromagnetic field is described by the gauge potential, which is given by

$$A_\mu \, dx^\mu = \left(\frac{Q}{r} - \frac{Q}{r_+} \right) dt \,, \tag{4.11}$$

from which the field strength can be calculated. The constant term is chosen such that a finite answer is obtained once we zoom into the near-horizon region later on.

The parameters M and Q must satisfy the following bound

$$M \geq Q \,. \tag{4.12}$$

An near-extremal black hole is defined as one that nearly saturates this bound, $M \approx Q$. As can be seen from (4.9), at extremality, the inner and outer horizons meet at the extremal horizon

$$r_{\rm h} = Q \,. \tag{4.13}$$

For most of this work, we will parameterize the background in terms of the extremal horizon and a small parameter

$$\delta r = r_+ - r_- \,, \tag{4.14}$$

which is a measure of how much the black hole deviates from extremality.

For a near-extremal black hole, we can zoom into the near-horizon region using the

following shift plus rescaling of the time and radial coordinates

$$\begin{aligned} t &= \frac{2r_+^2}{\delta r}\,\tau \\ r &= r_+ + \delta r\, x\,. \end{aligned} \tag{4.15}$$

Plugging into (4.7) and ignoring terms of higher order in $\delta r\, x$ results in the near-horizon metric

$$ds^2_{\rm NHR} = r_+^2\left(-4x(x+1)\,d\tau^2 + \frac{dx^2}{x(x+1)}\right) + r_+^2\,d\Omega_2^2\,. \tag{4.16}$$

We can see that the near-horizon spacetime factorizes into an AdS_2 factor (one can check that it has $\mathcal{R}_{\rm Ricci} = -1/r_+^2$) and a sphere, both having radius r_+. This metric approximates the original background well up to a cut-off radius x_c, which has to satisfy the following two inequalities

$$1 \ll x_c\,, \qquad \frac{\delta r\, x_c}{r_+} \ll 1\,. \tag{4.17}$$

The first says that the cut-off radius can be taken to be large, i.e., it covers the full AdS_2, while the second says that when x is multiplied by δr, this has to result in a small quantity, as this is the size of the terms we ignored to obtain (4.16). Outside of this radius, we would need to include terms higher-order in $\delta r\, x$ to obtain the original metric. Under this coordinate transformation, the gauge potential reduces to

$$A_\tau\,d\tau = -2r_+ x\,d\tau\,. \tag{4.18}$$

To define the thermodynamics of the black hole, we introduce the temperature and entropy, both of which can be identified with geometric quantities as follows. The temperature can be written in terms of the surface gravity at the outer horizon

$$T = \frac{\kappa}{2\pi} = \frac{f'(r_+)}{4\pi} = \frac{r_+ - r_-}{4\pi r_+^2}\,. \tag{4.19}$$

The entropy is given by the famous Bekenstein-Hawking formula which gives it in terms of the area of the outer horizon

$$S = \frac{A}{4}\,. \tag{4.20}$$

We also introduce the conjugate variable to the black hole charge, the electric potential at the outer horizon

$$\Phi = A_t(r = r_+) = \frac{Q}{r_+}\,. \tag{4.21}$$

Finally, for convenience, instead of the full energy we will use the energy above extremality defined as follows

$$E = M - Q\,. \tag{4.22}$$

In addition to $(Q, \delta r)$, we will parameterize the black hole using the microcanonical variables (Q, E) or the canonical (Q, T). From (4.22) and (4.19) we see that E and T are also small quantities for a near-extremal black hole, which we can now use to give a more precise definition of near-extremality

$$\frac{E}{Q} \ll 1\,, \qquad QT \ll 1\,. \tag{4.23}$$

The following equations relate these quantities and will be used in later calculations

$$\begin{aligned} \delta r &= 4\pi Q^2 T\,, \\ E &= 2\pi^2 Q^3 T^2\,. \end{aligned} \tag{4.24}$$

Note that these are only correct to leading order in T. Finally, we define a breakdown energy scale

$$E_{\rm b} = \frac{1}{Q^3}\,, \tag{4.25}$$

below which the thermodynamics of the black hole "breaks down" in the sense of [29]. Below this scale, the earlier mentioned effective quantum theory gives important corrections to the thermodynamics. This is also where corrections to the emission spectra of neutral radiation show up [60].

4.1.2 Solving the wave equation

The Klein-Gordon wave equation for a mass m scalar field with charge e is given by

$$\left((\nabla_\mu - ieA_\mu)\,(\nabla^\mu - ieA^\mu) + m^2\right)\Phi = 0\,. \tag{4.26}$$

This equation is separable in the Reissner-Nordström metric (4.7), and given the time-translation and spherical symmetry, the solution takes the following form

$$\Phi(t, r, \theta, \phi) = e^{-i\omega t}\, R(r)\, Y_{lm}(\theta, \phi)\,, \tag{4.27}$$

where $Y_{lm}(\theta, \phi)$ are the standard spherical harmonics. Therefore, solving the wave equation amounts to solving the resulting radial equation

$$\frac{d}{dr}\left(\Delta \frac{dR}{dr}\right) + \left(\frac{(\omega - eQ/r)^2\, r^4}{\Delta} - l(l+1) - m^2 r^2\right) R = 0\,, \tag{4.28}$$

where we have introduced the function $\Delta(r) = r^2 f(r)$ for easier comparison with the Kerr wave equation (4.187).

For Hawking radiation, we need to find the transmission coefficient from this equation with the following boundary conditions - an incident wave approaching the potential from the horizon is scattered, producing a reflected wave that goes back into the black hole and a transmitted wave that escapes to infinity. An alternative scattering problem has the incident wave come in from infinity, producing a reflected wave going back to infinity and a transmitted wave that goes into the black hole. Given that these two problems yield the same transmission coefficient, we will solve the latter, because it is more convenient. We start by transforming the radial equation into a one-dimensional Schrodinger-like equation. At asymptotic infinity $r \to \infty$, we expect spherical waves, which have amplitude proportional to inverse radial distance. To obtain plane-wave-like solutions, we factor out this radial

dependence by introducing the wavefunction

$$S(r) = \frac{R(r)}{r}\,. \tag{4.29}$$

Furthermore, to remove the first derivative term from the resulting equation for $S(r)$, we require that $dr_* = \frac{dr}{f(r)}$, which defines the tortoise coordinate given by

$$r_* = r + \frac{r_+^2}{\delta r}\log(r - r_+) - \frac{r_-^2}{\delta r}\log(r - r_-)\,. \tag{4.30}$$

The original radial coordinate has a range from the outer horizon at r_+ to ∞, which means that r_* goes from $-\infty$ to $+\infty$. These transformations result in a Schrodinger-like equation

$$\frac{d^2S}{dr_*^2} + V_{\text{eff}}(r_*)\,S = 0\,, \tag{4.31}$$

with the following effective potential, which we write in terms of r, as $r_* = r_*(r)$ cannot be inverted in terms of elementary functions,

$$V_{\text{eff}}(r) = \left(\omega - \frac{eQ}{r}\right)^2 - \frac{f(r)\,(\,l(l+1) + m^2r^2 + rf'(r)\,)}{r^2}\,. \tag{4.32}$$

The boundary conditions for (4.31) in our scattering problem are now given by the following

$$S(r_*) = \begin{cases} C_{\text{trans}}\,e^{-i\omega_{\text{eff}}r_*}\,, & r_* \to r_*(r_+) = -\infty \\ C_{\text{inc}}\,e^{-ik_\infty r_*} + C_{\text{refl}}\,e^{+ik_\infty r_*}\,, & r_* \to r_*(+\infty) = +\infty\,. \end{cases} \tag{4.33}$$

This defines the amplitudes of the three waves C_{inc}, C_{refl}, and C_{trans}. Our goal will be to find a relationship between these amplitudes which can then be used to compute the reflection and transmission coefficients. The wavenumber at asymptotic infinity is given by

$$k_\infty = \sqrt{V_{\text{eff}}(\infty)} = \sqrt{\omega^2 - m^2}\,, \tag{4.34}$$

whereas the wavenumber at the horizon, which we will also refer to as the effective near-horizon frequency, is given by

$$\omega_{\text{eff}} = \sqrt{V_{\text{eff}}(r_+)} = \omega - \frac{eQ}{r_+}\,. \tag{4.35}$$

This equation defines another energy scale $\omega_{\text{sr}} = \frac{eQ}{r_+}$ which we will refer to as the superradiant scale. Note that ω_{eff} can be negative, depending on how ω compares to ω_{sr}. The significance of this scale and the sign of ω_{eff} will further be discussed in subsection 4.1.3.

We will solve this scattering problem using the conventional technique [52] of splitting up spacetime into a near region and a far region. In each of these regions, the wave equation then simplifies to a near and far equation, which can then be solved and their asymptotics is matched in an in-between region. This works only for a specific range of parameters, which we will discuss at the end of this subsection. Beyond this range, this scattering problem was recently solved by [146] using a different technique, which we will refer to as the CFT_2 technique. We present this solution in appendix 5.3, where we also show that it ends up taking the same form as the one found using the conventional technique. We have opted to present the conventional technique in the main text, as the near equation also plays an important role in the calculation of the quantum emission rate in 4.1.4.

Starting with the equation in the near region, we first perform the coordinate transformation

$$r = r_+ + \delta r\, x\,. \tag{4.36}$$

The radial equation in this coordinate takes the following form

$$\frac{d}{dx}\left(x(x+1)\frac{dR}{dx}\right) + \left(\frac{(\omega - eQ/(r_+ + \delta r x))^2\,(r_+ + \delta r x)^4}{\delta r^2\, x\,(x+1)} - l(l+1) - m^2(r_+ + \delta r\, x)^2\right) R = 0\,. \tag{4.37}$$

In the near region, we treat $\delta r\, x$ as a small quantity and ignore terms that are higher-order in $\delta r\, x$, as we did when obtaining the metric in (4.16). Note that in the m^2 term, we can ignore

the terms that are first and second order in $\delta r\, x$, but in the ω term, we can only ignore the terms that are third and fourth order in $\delta r\, x$, since there is an extra δr^2 in the denominator, and x by itself is not necessarily small. This results in the following equation

$$\frac{d^2R}{dx^2} + \frac{(2x+1)}{x\,(x+1)}\,\frac{dR}{dx} + \frac{a_0 + a_1 x + a_2 x^2}{x^2\,(x+1)^2}\,R = 0\,, \tag{4.38}$$

with coefficients

$$\begin{aligned} a_0 &= \frac{r_+^4 \omega_{\text{eff}}^2}{\delta r^2}\,, \\ a_1 &= \frac{2eQr_+^2\omega_{\text{eff}}}{\delta r} - l(l+1) - m^2 r_+^2\,, \\ a_2 &= e^2Q^2 - l(l+1) - m^2 r_+^2 + 6r_+\omega_{\text{eff}}(r_+\omega_{\text{eff}} + eQ)\,. \end{aligned} \tag{4.39}$$

This equation has three regular singular points, 0, -1 and ∞. The solutions can therefore be written in terms of ordinary hypergeometric functions ${}_2F_1(a,\, b;\, c;\, x)$ (defined in appendix 5.2), where the a, b, and c are determined by the parameters a_0, a_1 and a_2. These parameters assemble into the following three combinations

$$\begin{aligned} F &= \sqrt{a_0}\,, \\ \mu &= \sqrt{a_0 - a_1 + a_2} - \sqrt{a_0}\,, \\ \beta &= \sqrt{\tfrac{1}{4} - a_2}\,. \end{aligned} \tag{4.40}$$

If we expand to sub-leading order in δr the first square root in μ, we obtain the following

$$\begin{aligned} F &= \frac{r_+^2\,\omega_{\text{eff}}}{\delta r} = \frac{\omega_{\text{eff}}}{4\pi T}\,, \\ \mu &= -eQ - 2r_+\omega_{\text{eff}}\,, \\ \beta &= \sqrt{\tfrac{1}{4} + l(l+1) + m^2 r_+^2 - e^2Q^2 - 6r_+\omega_{\text{eff}}(r_+\omega_{\text{eff}} + eQ)}\,. \end{aligned} \tag{4.41}$$

Notice that β can be real or imaginary, but we will not impose any restrictions on it, for now. The general solution to our equation can be written in terms of the following two independent

hypergeometric functions

$$R(x) = \sum_{\pm} A_{\mp}\, x^{\mp iF}\, (1+x)^{\pm i(F+\mu)}\, {}_2F_1\left(\tfrac{1}{2} - \beta \pm i\mu,\, \tfrac{1}{2} + \beta \pm i\mu;\, 1 \mp 2iF;\, -x\right) . \tag{4.42}$$

To impose the ingoing boundary conditions at the horizon as defined in (4.33), we need to change coordinates in our solution to r_* and expand it around the horizon. The r_* coordinates written in terms of x near the horizon and to leading order in δr is given by

$$\frac{\delta r}{Q^2} r_* = \log x\,. \tag{4.43}$$

Using the small argument limit of the hypergeometric function (5.15), we can expand our solution around the horizon as follows

$$R(x \to 0) = A_{\mp}\, x^{\mp ip} = A_{\mp}\, e^{\mp i \frac{\delta r}{Q^2}\, p\, r_*} = A_{\mp}\, e^{\mp i\, \omega_{\text{eff}}\, r_*}\,. \tag{4.44}$$

Comparing to (4.33), we see that the function with the A_- coefficient is the ingoing wave at the horizon, and the A_+ function is the outgoing. Therefore, we will set $A_+ = 0$. Relabeling $A_- \to A$, the solution to the near equation is given by

$$R(x) = A\, x^{-iF}\, (1+x)^{+i(F+\mu)}\, F\left(\tfrac{1}{2} - \beta + i\mu,\, \tfrac{1}{2} + \beta + i\mu;\, 1 - 2iF;\, -x\right) . \tag{4.45}$$

In (4.41), when we took the square roots and expanded in δr, we assumed that $\omega \geq \frac{eQ}{r_+}$. If we had assumed the opposite, we would have had an extra minus sign ($\omega_{\text{eff}} = -|\omega_{\text{eff}}|$), but then the boundary conditions would eliminate the opposite function in our solution, which would effectively cancel this minus sign. Therefore, the solution to the near equation (4.45) is valid for all ω, with F and μ as defined in (4.41).

Turning to the far region, we perform the following coordinate shift

$$r = r_+ + y\,. \tag{4.46}$$

Taking y to be large, and expanding the parameters in the radial equation to second order results in the following equation

$$R_{yy} + \frac{2}{y}R_y + \frac{b_0 + b_1\,y + b_2\,y^2}{y^2}R = 0\,, \tag{4.47}$$

with coefficients

$$\begin{aligned} b_0 &= -l(l+1) + e^2Q^2 - m^2r_+^2 - 6r_+\omega\,(eQ - r_+\omega) \\ &\quad + 2\omega\,(eQ - 2r_+\omega)\;\delta r + \omega^2\,\delta r^2\,, \\ b_1 &= \;(4r_+ - \delta r)\;\omega^2 - 2Qe\omega - 2r_+m^2\,, \\ b_2 &= \omega^2 - m^2\,. \end{aligned} \tag{4.48}$$

The solutions can be written in terms of the Kummer confluent hypergeometric function $M(a,b;x)$ (defined in appendix 5.2). The parameters b_0, b_1 and b_2 assemble into the following three combinations

$$\begin{aligned} \beta &= \sqrt{\tfrac{1}{4} - b_0}\,, \\ \alpha &= \frac{b_1}{2\sqrt{b_2}}\,, \\ k &= \sqrt{b_2}\,. \end{aligned} \tag{4.49}$$

Expanding to leading order in δr, these simplify to

$$\begin{aligned}\beta &= \sqrt{\tfrac{1}{4} + l(l+1) + m^2 r_+^2 - e^2Q^2 + 6r_+\omega(eQ - r_+\omega)}\,,\\ \alpha &= \frac{(2r_+\omega^2 - Qe\omega - r_+m^2)}{\sqrt{\omega^2 - m^2}}\,,\\ k &= \sqrt{\omega^2 - m^2}\,.\end{aligned} \tag{4.50}$$

The last parameter is just the earlier defined wavenumber at asymptotic infinity (4.34). Furthermore, notice that in the near-extremal limit, the β parameters defined in the near region (4.40) and in the far region (4.49) are equal. The general solution to the far equation can be written as follows

$$R(y) = e^{-iky} \sum_{\pm} C_\pm\, y^{-1/2\pm\beta}\, M\left(\tfrac{1}{2} \pm \beta + i\alpha, 1 \pm 2\beta, 2iky\right)\,. \tag{4.51}$$

We can check that this solution has the right spherical wave behavior at infinity by using the asymptotic expansion for the confluent hypergeometric function (5.18). This gives four terms, two of which are

$$\left(C_+ \frac{\Gamma(1{+}2\beta)}{\Gamma(\frac{1}{2}{+}\beta{+}i\alpha)}(2ik)^{-1/2-\beta+i\alpha} + C_- \frac{\Gamma(1{-}2\beta)}{\Gamma(\frac{1}{2}{-}\beta{+}i\alpha)}(2ik)^{-1/2+\beta+i\alpha}\right)\frac{e^{+iky}}{y} y^{+i\alpha}\,, \tag{4.52}$$

which together form the outgoing or reflected wave as defined in (4.33) ($r_* = r = y$ to leading order). The remaining two terms are the ingoing or incident wave

$$\left(C_+ \frac{\Gamma(1{+}2\beta)}{\Gamma(\frac{1}{2}{+}\beta{-}i\alpha)}(-2ik)^{-1/2-\beta-i\alpha} + C_- \frac{\Gamma(1{-}2\beta)}{\Gamma(\frac{1}{2}{-}\beta{-}i\alpha)}(-2ik)^{-1/2+\beta-i\alpha}\right)\frac{e^{-iky}}{y} y^{-i\alpha}\,. \tag{4.53}$$

The extra position-dependent phase shift $y^{\pm i\alpha} = e^{\pm i\alpha \ln y}$ is characteristic for potentials that at infinity have a $1/r$ fall-off and will not contribute to the reflection and transmission coefficients.

We now match the two solutions in the in-between region to find the relationship between

the coefficients A, C_+, and C_-. We expand the near solution at large distances and the far solution at small. Starting with the former, we use the large argument expansion of the hypergeometric function, which is given by (5.16). Applying this to the near solution results in

$$R(x \to \infty) = \sum_{\pm} A \, \frac{\Gamma\left(\pm 2\beta\right) \, \Gamma\left(1 - 2iF\right)}{\Gamma\left(\frac{1}{2} \pm \beta + i\mu\right) \, \Gamma\left(\frac{1}{2} \pm \beta - 2iF - i\mu\right)} \, x^{-\frac{1}{2} \pm \beta} \, . \tag{4.54}$$

Then, for the far solution we use the small argument limit of the confluent hypergeometric functions (5.17), which gives

$$R(y \to 0) = \sum_{\pm} C_{\pm} \, y^{-1/2 \pm \beta} \, . \tag{4.55}$$

As mentioned earlier, the power β in these two solutions is only equal if we have a near-extremal black hole. Using the fact that $y = \delta r \, x$, we match the solutions in (4.54) and (4.55) and obtain the following relationship between the coefficients

$$C_{\pm} = \frac{\Gamma(\pm 2\beta) \, \Gamma(1 - 2iF)}{\Gamma\left(\frac{1}{2} \pm \beta + i\mu\right) \, \Gamma\left(\frac{1}{2} \pm \beta - 2iF - i\mu\right)} \, \delta r^{+\frac{1}{2} \mp \beta} \, A \, . \tag{4.56}$$

To take the limit of the far equation, we need $ky \ll 1$. At the same time, we also need to stay in the far region, which means $y \gg r_+$. These two conditions are both possible only if $r_+ k \ll 1$. Furthermore, even though the solutions have the same power law behavior, the near and far regions do not overlap. If the wave equation in the in-between region can be simplified to one that has as its solution this same power law, then the matching is complete (see for example Appendix A of [60] for how this works out for the neutral case). Both of these conditions are satisfied if we assume that $r_+ \omega_{\text{eff}} \sim r_+ T \ll 1$ and $eQ \ll 1$. As we mentioned earlier, the transmission coefficient that we will derive will be valid outside of this range, but to show that we would need the techniques of appendix 5.3.

The solutions given by equations (4.45) and (4.51) together with the matching conditions

(4.56) represent a full solution of the wave equation. Once $C_\pm$ are eliminated from this solution, we are left with only one undetermined constant, the overall normalization A.

We also note that our wave equation includes the neutral scalar as a special case. In the limit of $e = 0$, the equation in the near region has $\mu = 0$, which gives real parameters a and b in the hypergeometric functions. If we further assume a massless field $m = 0$, these parameters become integers, which means that the hypergeometric function reduces to the Jacobi polynomials. In the far region, the two confluent hypergeometric functions reduce to the spherical Bessel functions. For work on higher spin ($s = 1, 2$) neutral fields and their spectra, see [60].

4.1.3 Semiclassical emission rate

The number of quanta of a given field emitted by the black hole per unit time is found using the Hawking formula [10]

$$\left.\frac{dN}{dt}\right|_{\text{semi-classical}} = \frac{1}{2\pi}\sum_{l,m_l}\int_0^\infty d\omega\,\frac{\Gamma(\omega)}{e^{\omega_{\text{eff}}/T}-1}\,. \tag{4.57}$$

We will refer to this quantity as the emission or evaporation rate, whereas the integrand we will refer to as the spectral (per unit frequency) emission rate. This formula was obtained by treating the quantum fields in a fixed curved background provided by the black hole, so we will also refer to this as the semi-classical rate, as opposed to the quantum-corrected one that we will derive in the next subsection. The rate of emitting other quantities that the quanta carry, such as charge or angular momentum, is found by simply multiplying this integral by that quantity. The energy emitted, or energy flux, is found by multiplying the integrand in (4.57) by the energy ω of a quantum before integrating

$$\left.\frac{dE}{dt}\right|_{\text{semi-classical}} = \frac{1}{2\pi}\sum_{l,m_l}\int_0^\infty d\omega\,\frac{\omega\,\Gamma(\omega)}{e^{\omega_{\text{eff}}/T}-1}\,. \tag{4.58}$$

In these equations, T is the black hole temperature given by (4.19). ω_{eff} is the effective frequency introduced in (4.35). The sum goes over angular momentum modes. $\Gamma(\omega)$ is the greybody factor, a measure of how much the black hole emission spectrum deviates from that of a blackbody. It is equal to the transmission coefficient of the scattering problem set up in the previous subsection.

The transmission and reflection coefficients are defined as follows

$$\mathcal{R} = \left|\frac{C_{\text{refl}}}{C_{\text{inc}}}\right|^2 , \qquad \mathcal{T} = \frac{\omega_{\text{eff}}}{k}\left|\frac{C_{\text{trans}}}{C_{\text{inc}}}\right|^2 . \tag{4.59}$$

Before computing these two, we first discuss the sign of the transmission coefficient, which is related to the phenomenon of superradiance. As mentioned earlier, ω_{eff} can be negative, which implies that the transmission coefficient can be negative. The unitarity condition

$$\mathcal{R} + \mathcal{T} = 1 \, , \tag{4.60}$$

implies that when this is the case, the reflection coefficient has to be greater than one i.e. the reflected wave comes out with a higher amplitude than the incident. This is the definition of superradiance. The transmitted wave in equation (4.33) looks like it has a negative phase velocity meaning that it is actually moving away from the horizon, but it turns out that the group velocity is positive, which implies that a physical disturbance moves towards the horizon (see [147] for a detailed review).

An inspection of the emission rate (4.58) gives an idea of the role of superradiance in black hole evaporation. Consider a black hole at low temperature, which is when superradiance becomes significant. Equation (4.58) shows that for non-superradiant modes, i.e. those with $\omega_{\text{eff}} > 0$, the spectral emission rate is exponentially suppressed. We will see that this implies that the emission rate is proportional to a power of temperature, which means that no non-superradiant quanta are emitted at zero temperature. For the superradiant modes, the opposite is true, the exponential in (4.58) goes to zero at low temperatures, and, as we

shall see, the rest of the integrand goes to a constant. Therefore, at low temperatures, the spectrum of the black hole is fully superradiant. Note that when $\omega_{\text{eff}} < 0$, the statistical factor in (4.58) is negative, but this is also when the transmission coefficient (4.59) is negative, so the emission rate is always positive. A more careful analysis of the integral in the emission rate in the low temperature limit is left for subsection 4.2.1.

To compute the reflection and transmission coefficients, we will need the amplitudes of the incident, reflected, and transmitted waves defined in equation (4.33). The amplitude of the transmitted wave can be found by expanding the solution of the near equation around the horizon, which was done in (4.44). Comparing to (4.33) gives

$$C_{\text{trans}} = r_+ A \,, \tag{4.61}$$

where the r_+ comes from the relationship between $R(r)$ and $S(r)$ at the horizon. The amplitudes of the incident and reflected waves can be found by expanding the solution of the far equation at asymptotic infinity, which was done in equations (4.52) and (4.53). From the matching equation (4.56), we can see that that C_-/C_+ is of the order of $\delta r^{2\beta}$, which is very small for near-extremal black holes, and therefore C_- can be safely ignored relative to C_+ in both the incident and reflected wave amplitudes. For the incident wave we have

$$C_{\text{inc}} = C_+ \frac{\Gamma(1+2\beta)}{\Gamma(\frac{1}{2}+\beta-i\alpha)} (-2ik)^{-1/2-\beta-i\alpha} \,, \tag{4.62}$$

and for the reflected wave we find

$$C_{\text{refl}} = C_+ \frac{\Gamma(1+2\beta)}{\Gamma(\frac{1}{2}+\beta+i\alpha)} (2ik)^{-1/2-\beta+i\alpha} \,. \tag{4.63}$$

In these two equations, C_+ can further be written in terms of A using the matching equation (4.56). The next step is to square these three expressions. As mentioned earlier, β can be real or imaginary, and this will lead to very different expressions after the squaring. For now,

we will focus on the case of real β for all frequencies, and then in subsection 4.2.1, we will discuss under what conditions this is true, and finally in 4.3.2, we will rederive the reflection and transmission coefficients for imaginary β. To square the amplitudes, we will use the following identity

$$|\pm i^{i\alpha}| = |e^{(\pm i\frac{\pi}{2})(i\alpha)}| = e^{\mp\frac{\pi\alpha}{2}}\,. \tag{4.64}$$

We find for the incident wave

$$\begin{aligned}|C_{\rm inc}|^2 = \delta r^{+1-2\beta}\,(2k)^{-1-2\beta}\,\frac{\Gamma(1+2\beta)^2\,\Gamma(2\beta)^2}{|\Gamma(\frac{1}{2}+\beta-i\alpha)|^2\,|\Gamma(\frac{1}{2}+\beta+i\mu)|^2}\,e^{-\pi\alpha}\\ \frac{|\Gamma(1-2iF)|^2}{|\Gamma(\frac{1}{2}+\beta-2iF-i\mu)|^2}\,|A|^2\,,\end{aligned} \tag{4.65}$$

and for the reflected wave

$$\begin{aligned}|C_{\rm refl}|^2 = \delta r^{+1-2\beta}\,(2k)^{-1-2\beta}\,\frac{\Gamma(1+2\beta)^2\,\Gamma(2\beta)^2}{|\Gamma(\frac{1}{2}+\beta+i\alpha)|^2\,|\Gamma(\frac{1}{2}+\beta+i\mu)|^2}\,e^{-\pi\alpha}\\ \frac{|\Gamma(1-2iF)|^2}{|\Gamma(\frac{1}{2}+\beta-2iF-i\mu)|^2}\,|A|^2\,.\end{aligned} \tag{4.66}$$

The final step is to plug into equation (4.59) which for the reflected coefficient gives

$$\mathcal{R} = 1\,. \tag{4.67}$$

This is the answer to leading order in δr, and it tells us that most of the incident wave is reflected. To find the correction, we would have had to include the C_- terms in the amplitudes. For the transmission coefficient we find

$$\begin{aligned}\mathcal{T} = 2^{2\beta+1}\,\delta r^{2\beta-1}\,r_+^2\,k^{2\beta}\,\omega_{\rm eff}\,\frac{|\Gamma(\frac{1}{2}+\beta-i\alpha)|^2\,|\Gamma(\frac{1}{2}+\beta+i\mu)|^2}{\Gamma(2\beta+1)^2\,\Gamma(2\beta)^2}\\ \frac{|\Gamma(\frac{1}{2}+\beta-2iF-i\mu)|^2}{|\Gamma(1-2iF)|^2}\,e^{\pi\alpha}\,.\end{aligned} \tag{4.68}$$

The greybody factor is equal to the transmission coefficient. We will rewrite δr in (4.68) in terms of T using equation (4.24). Furthermore, for easier comparison to the quantum-corrected

rate, we introduce the conformal dimension

$$\Delta = \tfrac{1}{2} + \beta \,, \tag{4.69}$$

which we will use instead of β, going forward. In the next subsection, in the calculation of the quantum-corrected rate, this parameter will play the role of an operator conformal dimension in the sense of $\mathrm{AdS}_2/\mathrm{CFT}_1$, but it is important to note that in this subsection, in the context of the semi-classical emission rate, its role is just that of a parameter in the wave equation. With these changes, the greybody factor is found to be

$$\begin{aligned}\Gamma\left(Q,T\,;m,e\,;\omega,l,m_l\right) = 2^{6\Delta-4}\,\pi^{2\Delta-2}\,Q^{4\Delta-2}\,T^{2\Delta-2}k^{2\Delta-1}\,\omega_{\text{eff}}\,\frac{\left|\Gamma(\Delta-i\alpha)\right|^2\left|\Gamma(\Delta+i\mu)\right|^2}{\Gamma(2\Delta)^2\,\Gamma(2\Delta-1)^2} \\ \frac{\left|\Gamma(\Delta-2iF-i\mu)\right|^2}{\left|\Gamma(1-2iF)\right|^2}\,e^{\pi\alpha}\,.\end{aligned} \tag{4.70}$$

We have explicitly listed all the variables that determine the greybody factor; (Q,T) label the black hole state, (m,e) define the field being radiated, and (ω,l,m_l) the mode which it is being emitted (the equation is independent of m_l, but it has been included for completeness). We can now put this together with the remaining factors in the Hawking formula to obtain the final formula for the semi-classical spectral evaporation rate

$$\begin{aligned}\left.\frac{d^2E}{d\omega\,dt}\right|_{\text{sc}} = 2^{6\Delta-5}\,\pi^{2\Delta-3}\,Q^{4\Delta-2}\,T^{2\Delta-2}\,\frac{\left|\Gamma(\Delta-i\alpha)\right|^2\left|\Gamma(\Delta+i\mu)\right|^2}{\Gamma(2\Delta)^2\,\Gamma(2\Delta-1)^2}\,e^{\pi\alpha} \\ \frac{\omega\,\omega_{\text{eff}}\,k^{2\Delta-1}}{e^{\omega_{\text{eff}}/T}-1}\,\frac{\left|\Gamma(\Delta-2iF-i\mu)\right|^2}{\left|\Gamma(1-2iF)\right|^2}\,.\end{aligned} \tag{4.71}$$

The parameters F,μ,Δ,α can be found in equations (4.41) and (4.50), which are all frequency-dependent in general. A systematic analysis of this equation is left for section 4.2.

We note that this equation was recently derived in [143]. If we set $\mu = 0$ in our result (4.71), we find agreement with theirs. The non-zero value of μ comes from keeping subleading (in δr) terms in (4.40), which we believe should be kept, because we can see that they do not

go away in the $\delta r \ll 1$ limit in the final result.

This rate can also be compared to the one found in [51] for small black holes (the one for large will be recovered in 4.3.2), where non-extremal black holes were studied, but the radiation was taken to have low frequencies. Therefore, for comparison, we need to take the low frequency limit of our rate and the near-extremal limit of the rate in [51] (which can be found in equation 4.33). For a small black hole, we can ignore μ and set $\Delta = l + 1$, which gives

$$\left.\frac{d^2E}{d\omega\, dt}\right|_{\rm sc} = 2^{6l+1}\,\pi^{2l-1}\,Q^{4l+2}\,T^{2l}\,\frac{|\Gamma(l+1-i\alpha)|^2\,\Gamma(l+1)^2}{\Gamma(2l+2)^2\,\Gamma(2l+1)^2}\,e^{\pi\alpha} \\ \frac{\omega\,\omega_{\rm eff}\,k^{2l+1}}{e^{\omega_{\rm eff}/T}-1}\,\frac{|\Gamma(l+1-2iF)|^2}{|\Gamma(1-2iF)|^2}\,. \tag{4.72}$$

Using the Gamma function identities from appendix 5.2, we find that this can be further rewritten as follows

$$\left.\frac{d^2E}{d\omega\, dt}\right|_{\rm sc} = \frac{2^{6l+1}\,\pi^{2l-1}\,l!^4}{(2l+1)!^2\,(2l)!^2}\,\frac{Q^{4l+2}\,T^{2l}\,\omega\,\omega_{\rm eff}\,k^{2l+1}}{e^{\omega_{\rm eff}/T}-1}\,e^{\pi\alpha}\,\frac{\pi\alpha}{\sinh\pi\alpha}\,\prod_{j=1}^{l}\left(j^2+\alpha^2\right)\left(1+\frac{4F^2}{j^2}\right)\,. \tag{4.73}$$

This agrees with equations 4.33 from [51] after writing the δr in their result in terms of T. For the comparison, note that our α is negative of theirs.

4.1.4 Quantum-corrected emission rate

To compute the quantum-corrected evaporation rate, we will follow the effective string approach used to calculate black hole greybody factors [148, 149, 150, 151, 152, 153, 154]. It was first applied to 4D near-extremal black holes using JT gravity as the effective theory by [61, 60].

We will treat both the black hole and the quantum field as two quantum systems that are coupled through an interaction Hamiltonian. This coupling enables spontaneous decay of the

black hole from higher energy states to lower ones through the emission of field quanta. The setup is completely analogous to the atom-electromagnetic field system, where the coupling (e.g. dipole) comes in the form of the product of two operators, one acting on the Hilbert space of the atom, and having non-zero matrix elements between two energy eigenstates (e.g. the position operator), and the other, a creation/annihilation operator acting on the radiation space.[4]

Once the interaction Hamiltonian is specified, we can use perturbation theory to compute the probability that a transition between two energy states will happen. Since the interaction has a time dependence coming from the radiation field, we need to use time-dependent perturbation theory, which for a harmonic perturbation (a single mode of the field) gives the rate of transition in the form of Fermi's golden rule as follows. For a transition between two black hole states with energies $E_{\rm i}$ and $E_{\rm f}$, through the emission of a single field quantum with energy ω,

$$|E_{\rm i}\rangle^{\rm BH} \otimes |\Omega\rangle^{\rm rad} \to |E_{\rm f}\rangle^{\rm BH} \otimes |\omega\rangle^{\rm rad}\,, \tag{4.74}$$

where Ω represents the vacuum states in the radiation space, the transition rate is given by

$$\Gamma_{i\to f} = 2\pi\,|\langle E_f, \omega|\hat{H}_{\rm int}|E_i\rangle|^2\,\delta(E_f - E_i - \omega)\,, \tag{4.75}$$

where $\hat{H}_{\rm int}$ is the interaction Hamiltonian, which enables this transition in the quantum theory. The δ-function ensures energy conservation in this process. For perturbation theory to be applicable, the matrix element of $\hat{H}_{\rm int}$ has to be small. Once the transition rate is computed, we can find the total quantum-corrected evaporation rate by summing over all

[4]This also provides a framework for the study of quantum black hole scattering, where an incoming coherent wave, represented as a classical expectation value of the field operator, causes the processes of absorption and stimulated emission of quanta. For recent work, see [155, 156].

final states of both the black hole and radiation[5]

$$\left.\frac{dN}{dt}\right|_{\text{quantum-corrected}} = \sum_{l,m_l} \int d\omega \int dE_f\, \rho(E_f)\, \Gamma_{i\to f}\,, \tag{4.76}$$

which can further be used to find the emission rate of any quantity such as charge and angular momentum. Multiplying the rate with the energy of a quantum ω before integrating gives the energy flux

$$\left.\frac{dE}{dt}\right|_{\text{quantum-corrected}} = \sum_{l,m_l} \int d\omega\, \omega \int dE_f\, \rho(E_f)\, \Gamma_{i\to f}\,. \tag{4.77}$$

In these equations, $\rho(E)$ is the density of states of the system, which is the product of the densities of both the black hole and the radiation.

Before we have a well-defined problem and the equations from above can be applied, we need to address two questions. First, how do we describe the energy states of the black hole, and find the matrix elements of operators between these states. And second, what operator do we use, in particular, what is the interaction Hamiltonian of the black hole-radiation system? To answer both of these questions, we will use $\text{AdS}_2/\text{CFT}_1$. A near-extremal Reissner-Nordström black hole can be dimensionally reduced in its near horizon region, which results in a 2D theory, JT gravity. The dynamics of the 2D metric is captured by a strongly-coupled boundary mode called the Schwarzian mode. This mode can be quantized, and the resulting 1D quantum mechanics can be exactly solved [158, 159, 160, 161, 38]. This mode describes the low-temperature quantum dynamics of the near-extremal black hole. Solving this quantum mechanics gives a continuous spectrum[6] with a density of states given by

$$\rho(E) = \frac{e^{S_0}}{2\pi^2 E_{\text{b}}}\, \sinh\left(2\pi\sqrt{2E/E_{\text{b}}}\right)\, \Theta(E)\,, \tag{4.78}$$

[5]We will be computing the emission rates in the microcanonical ensemble. For a discussion of both the microcanonical and canonical ensemble in this context, see [157].

[6]It is commonly accepted that this theory actually describes an ensemble of theories of gravity. This is reflected in the fact that the density of states in this theory is continuous, instead of being discrete, which is what we would expect from a true bound quantum system like an atom for instance.

where $E_{\rm brk}$ is the breakdown scale introduced in (4.25). Furthermore, owing to the reparameterization invariance of this theory, operators can be classified by their conformal dimension Δ, which also fully determines their matrix elements between the energy eigenstates[7]. These are given by

$$|\langle E_f|\mathcal{O}_\Delta|E_i\rangle|^2 = \frac{E_{\rm b}^{2\Delta}\, e^{-S_0}}{2^{2\Delta-1}\,\Gamma(2\Delta)}\,\Gamma\left(\Delta \pm i\sqrt{2E_f/E_{\rm b}} \pm i\sqrt{2E_i/E_{\rm b}}\right)\,, \tag{4.79}$$

where the two $\pm$ signs are shorts for multiplying four Γ-functions with all possible combinations of the signs. The four Gamma functions combine into two pairs of complex conjugates, so this matrix element is manifestly real. This covers the part of Schwarzian theory that we will have use for. Higher point matrix elements, which would appear for instance in higher-order perturbation theory, can be found in the references above.

To address the second question from above, note that in addition to the Schwarzian mode, the 2D near-horizon region also includes a modes coming from the dimensional reduction of the radiation field. Each of these modes represents a field in the 2D theory which interacts with the Schwarzian mode. The interaction term is given by a deformation of the 1D Schwarzian action by

$$I_{\rm int} = \int dt\,\phi(t)\,\mathcal{O}(t)\,, \tag{4.80}$$

where $\phi(t)$ is the boundary value field, which can be thought of as a source and $\mathcal{O}(t)$ is its dual operator in the usual AdS/CFT sense. The conformal dimension of this operator, which we will need for the Schwarzian matrix element, is determined by the effective mass of the 2D field or, equivalently, it is the power of the non-normalizable mode in the asymptotic expansion of the solution to the 2D wave equation. From (4.80) we find the interaction

[7]This conformal dimension has to be frequency-independent. As we saw in the previous subsection, the Δ parameter that shows up in the wave equation is in general frequency-dependent. Usually for charged radiation in AdS_2, we zoom into the frequencies near the superradiant bound, i.e. take $\omega_{\rm eff} \sim T$, which makes the wave equation Δ frequency-independent, allowing for a dual CFT interpretation. Furthermore, if we also take $eQ \ll 1$, then all modes of interest will have a constant Δ, not just those close to the superradiant bound. In the next section, we will see that this small charge limit is exactly what we will be interested in when computing the quantum-corrected emission rate.

Hamiltonian to be

$$\hat{H}_{\text{int}} = \hat{\phi}_0 \, \hat{\mathcal{O}} \, . \tag{4.81}$$

We only need the $t = 0$ value of this operator, as the rest of the time dependence has been accounted for by Fermi's rule. Once this interaction Hamiltonian is plugged into the transition rate, the matrix elements breaks up into a matrix element between the black hole states given by (4.79) and a matrix element in radiation space, which we turn to next.

To quantize the 4D radiation field, we start by canonically normalizing the classical field modes of the scalar field as follows

$$\phi(t = 0, r, \theta, \phi) \sim a_{\text{far}} \, \frac{r_+}{\sqrt{4\pi k}} \, \frac{e^{-ikr}}{r} \, r^{-i\alpha} \, Y_{lm_l}(\theta, \phi) \, . \tag{4.82}$$

Once these operators are quantized, the creation $\hat{a}^\dagger$ and annihilation $\hat{a}$ operators define states with a definite number of field quanta at asymptotic infinity (past or future), and they satisfy the unit normalized commutation relations, which implies that the following matrix element gives one

$$\left| \langle \omega | \hat{a}^\dagger_{\text{far}} | \Omega \rangle \right|^2 = 1 \, . \tag{4.83}$$

Since the interaction Hamiltonian (4.81) requires the matrix element of the 2D field, we need to dimensionally reduce the 4D field on the sphere of the Reissner-Nordström near-horizon region. We will canonically normalize the 2D fields by requiring that at AdS_2 infinity they behave as follows

$$\phi_{lm_l}(t = 0, r) \sim a_{\text{near}} \left(\frac{r_+^2}{r - r_+} \right)^{1-\Delta} + b_{\text{near}} \left(\frac{r_+^2}{r - r_+} \right)^{\Delta} , \tag{4.84}$$

where Δ is the conformal dimension of the dual operator $\mathcal{O}$, as mentioned above. Since we solved the 4D equation by breaking it up into a near and far region, we already have the solution to the 2D equation, which is just the near equation. Comparing the asymptotic behavior of our near solution (4.54) to the equation from above, we see that they agree. As

we argued in subsection 4.1.3, the coefficient b_{near} can be ignored compared to a_{near} for a near-extremal black hole. Furthermore, this comparison confirms that $\Delta = \frac{1}{2} + \beta$ as defined in subsection 4.1.3.

We can now evaluate the radiation space matrix element. Since the states are defined at asymptotic infinity and the field operator at AdS_2 infinity, there is no reason to expect this to be one. Since $\hat{a}^\dagger_{\text{near}}$ and $\hat{a}^\dagger_{\text{far}}$ are linear combinations of each other, in fact they're proportional to each other when $b_{\text{near}} = 0$, we can calculate the matrix element as follows

$$\left|\langle\omega|\hat{a}^\dagger_{\text{near}}|\Omega\rangle\right|^2 = |\mathcal{N}|^2\,|\phi_0|^2\,\left|\langle\omega|\hat{a}^\dagger_{\text{far}}|\Omega\rangle\right|^2 = |\mathcal{N}|^2\,|\phi_0|^2\,, \tag{4.85}$$

where ϕ_0 is this proportionality constant. The normalization constant $\mathcal{N}$ we introduce when quantizing these fields such as to make the interaction term (4.80) unit normalized. To find ϕ_0 we proceed as follows. The $\hat{a}^\dagger_{\text{near}}$ and $\hat{a}^\dagger_{\text{far}}$ operators will both be written in terms of A from subsection 4.1.2, which is now also an operator, and then compared. First, by comparing equations (4.82) and (4.52), we find that $\hat{a}^\dagger_{\text{far}}$ is related to the coefficient of the reflected wave as follows

$$\hat{a}^\dagger_{\text{far}} = \frac{\sqrt{4\pi k}}{r_+}\,\frac{\Gamma(1+2\beta)}{\Gamma(\frac{1}{2}+\beta+i\alpha)}\,(2ik)^{-1/2-\beta+i\alpha}\,\hat{C}_+\,, \tag{4.86}$$

which can further be written in terms of $\hat{A}$ using the matching equation (4.56)

$$\hat{a}^\dagger_{\text{far}} = \frac{\sqrt{4\pi k}}{r_+}\,\frac{\Gamma(1+2\beta)\Gamma(2\beta)\Gamma(1-2iF)(2ik)^{-1/2-\beta+i\alpha}}{\Gamma(\frac{1}{2}+\beta+i\alpha)\Gamma(\frac{1}{2}+\beta+i\mu)\Gamma(\frac{1}{2}+\beta-2iF-i\mu)}\delta r^{+1/2-\beta}\hat{A}\,. \tag{4.87}$$

Similarly, comparing equations (4.84) and (4.54) gives us $\hat{a}_{\text{near}}$ in terms of $\hat{A}$ as follows

$$\hat{a}^\dagger_{\text{near}} = r_+^{-1+2\beta}\,\frac{\Gamma(2\beta)\,\Gamma(1-2iF)}{\Gamma(\frac{1}{2}+\beta+i\mu)\,\Gamma(\frac{1}{2}+\beta-2iF-i\mu)}\,\delta r^{+1/2-\beta}\hat{A}\,. \tag{4.88}$$

Comparing $\hat{a}_{\text{near}}$ and $\hat{a}_{\text{near}}$, we can find the proportionality constant, which after some

simplifying is given by

$$|\phi_0|^2 = \frac{1}{\pi}\, 2^{2\Delta-2}\, r_+^{4\Delta-2}\, k^{2\Delta-1}\, \frac{|\Gamma(\Delta+i\alpha)|^2}{\Gamma(2\Delta)^2}\, e^{\pi\alpha}\,. \tag{4.89}$$

We will find the normalization constant $\mathcal{N}$ once we have calculated the quantum-corrected evaporation rate by taking the limit of the quantum rate and comparing to the semi-classical rate.

Before we can plug the black hole and radiation matrix elements into the transition rate, we need to account for one more effect peculiar to charged radiation. The E in the Schwarzian equations stands for energy above extremality, but when a charged particle is emitted, the black hole charge also drops, which results in the extremal energy dropping as well. If the black hole started out with total energy $M_{\rm i}$, and emits a quantum with energy ω (measured at asymptotic infinity), then it will end up with total energy $M_{\rm f}$ which satisfies

$$M_{\rm i} = M_{\rm f} + \omega\,. \tag{4.90}$$

This can be rewritten in terms of energy above extremality as follows

$$E_{\rm i} = E_{\rm f} + (\omega - e)\,, \tag{4.91}$$

Plugging this into the transition rate (4.75) results in

$$\Gamma_{i\to f} = 2\pi\, |\mathcal{N}|^2\, |\phi_0|^2\, \left|\langle E_{\rm f}|\mathcal{O}|E_{\rm i}\rangle\right|^2\, \delta\left(E_{\rm f} - E_{\rm i} - (\omega - e)\right)\,. \tag{4.92}$$

The Delta function implies that the range of frequencies for charged radiation goes from 0 up to the biggest available energy which is $E_{\rm i} + e$, not just $E_{\rm i}$, with the extra energy coming from the drop in extremal energy. Note that $\omega - e$ is equal to $\omega_{\rm eff}$ once the extremal limit of the superradiant bound is taken $\omega_{\rm sr} = \frac{eQ}{r_+} = e$, i.e., once the subleading temperature

corrections are ignored. The $\mathrm{AdS}_2/\mathrm{CFT}_1$ analysis does not see this temperature correction, whereas the wave analysis does. It is important to distinguish between these two quantities when comparing the semi-classical and quantum rates, as there are equations in which the temperature correction in ω_{eff} cannot be ignored, for example, the ω_{eff}/T. term in the statistical factor of the Hawking formula.

We can now find the spectral evaporation rate from the transition rate by integrating over the final states. This results in

$$\left.\frac{d^2E}{d\omega\, dt}\right|_{\text{q}} = 2\pi\,\omega\,|\mathcal{N}|^2\,|\Phi_0|^2\,\rho(E+e-\omega)\;|\langle E+e-\omega|\mathcal{O}_\Delta|E\rangle|^2\;, \tag{4.93}$$

where we are labeling the initial black hole energy with E. The final step is to find the normalization constant $|\mathcal{N}|^2$ by comparing the quantum-corrected evaporation rate that we just found to the semi-classical rate (4.71). To do this, we need to take the high-energy/temperature limit. This means take $|E-\omega_{\text{eff}}| \gg E_{\text{b}}$, and then zoom in on $\omega \ll E+\omega_{\text{sr}}$. This calculation is straightforward, but technical, so we leave it for appendix 5.4. The following is obtained

$$|\mathcal{N}|^2 = \frac{1}{\pi}\,2^{2\Delta-2}\,\frac{\Gamma(2\Delta)}{\Gamma(2\Delta-1)^2}\;|\Gamma(\Delta+i\mu)|^2\;e^{+\pi\mu}\,. \tag{4.94}$$

Plugging this into equation (4.93), we find the final formula for the quantum-corrected spectral evaporation rate

$$\begin{aligned}\left.\frac{d^2E}{d\omega\, dt}\right|_{\text{q}} = \frac{1}{\pi^3}\,2^{2\Delta-3}\,Q^{4\Delta-2}\,E_{\text{b}}^{2\Delta-1}\,\frac{|\Gamma(\Delta+i\alpha)|^2\;|\Gamma(\Delta+i\mu)|^2}{\Gamma(2\Delta)^2\,\Gamma(2\Delta-1)^2}\,e^{\pi(\alpha+\mu)} \\ \omega\,k^{2\Delta-1}\,\sinh\left[2\pi\left(2\frac{E+e-\omega}{E_{\text{b}}}\right)^{\frac{1}{2}}\right] \\ \Gamma\left[\Delta\pm i\left(2\frac{E+e-\omega}{E_{\text{b}}}\right)^{\frac{1}{2}}\pm i\left(\frac{2E}{E_{\text{b}}}\right)^{\frac{1}{2}}\right]\,.\end{aligned} \tag{4.95}$$

As mentioned earlier, the frequency range in this equation goes from zero to $E+e$. The parameters μ, Δ, α are the same as before and can be found in equations (4.41) and (4.50).

In the following section, we will compute this rate in different energy regimes and compare it to the semi-classical rate.

This equation was recently derived in [143]. As mentioned earlier, if we set $\mu = 0$ in our result, we find agreement with theirs.

4.2 Radiation from small charged black holes

The conformal dimension for a massive charged scalar field being radiated by a near-extremal Reissner-Nordström black hole is given by

$$\Delta(\omega) = \tfrac{1}{2} + \sqrt{\tfrac{1}{4} + l(l+1) - e^2Q^2 + m^2Q^2 + 6\omega(e-\omega)Q^2}\,. \tag{4.96}$$

For simplicity, we will consider a massless field in this section. Depending on the relationship between Q and e, this will either be real for all frequencies, or real for only a subset of frequencies and complex for the rest (it is never complex for all frequencies). The character of the greybody factor, and therefore the evaporation rate strongly depends on whether Δ is real or complex. In this section, we will study radiation with real Δ. Inspecting the quadratic under the square root, we find that it is positive for all frequencies when[8]

$$eQ \leq \tfrac{1}{2} + l\,. \tag{4.97}$$

Note that for all black holes, their charge has to be greater than the charge of the particles they are emitting, so we also have $Q \geq e$. These two conditions imply that $e \leq Q \leq\ (\frac{1}{2}+l)\frac{1}{e}$, so we will refer to these black holes as small[9] (Q can be equally thought of as the radius of the horizon, the charge, or the mass of the black hole). For large black holes, those with

[8]Even for $eQ \leq \frac{1}{2} + l$ there will be a large frequency beyond which Δ goes complex, so here we really mean not all frequencies, but those between 0 and $e + E$, with E being a small number. In the semi-classical rate, the integral does go from 0 to ∞, but the contribution from the larger frequencies is negligible. We will explicitly see that this is true later in this section.

[9]l can be arbitrarily high, but we will see that higher angular momentum modes contribute significantly less than the lowest one, and therefore it is safe to focus on the lowest one and take $l = 0$ in equation (4.97).

$Q \geq (\frac{1}{2} + l)\frac{1}{e}$, the quadratic under the square root in (4.96) will still be positive on a subset of the available frequencies, so the equations that will be derived in this section will still hold on this subset. The rest of the frequency range will be covered in the next section.

4.2.1 Classification of charged radiation

We start with a discussion of the energy scales involved in the problem. For neutral radiation, if we look at the quantum-corrected evaporation rates, there are two scales, the initial energy of the black hole E (which in the semi-classical rate is more naturally thought of as the initial temperature) and the breakdown energy $E_{\rm b}$. In the rate equation ($e = 0$ limit of (4.95)), these two scales appear in the following combination

$$\frac{E - \omega}{E_{\rm b}}\,, \tag{4.98}$$

with the frequency being at most E. Requiring that this number be either very big or very small, [60] introduced two energy regimes, the semi-classical $E_{\rm b} \ll E$, where the quantum-corrected rate reduces to the semi-classical, and the quantum regime $E \ll E_{\rm b}$, where the quantum-corrected rate simplifies, but is not equal to the semi-classical. Therefore, the latter regime is where we should search for the corrections from JT/Schwarzian theory.

Our goal will be to define a quantum regime for charged radiation, and then to compare the two rates in this regime. For charged radiation, there is an additional energy scale, the superradiant bound e, which makes the analysis of the energy regimes more involved. From (4.95), we see that these three scales appear in the combination

$$\frac{(E + e) - \omega}{E_{\rm b}}\,, \tag{4.99}$$

with the frequency now being at most equal to $e + E$. Requiring this to be either big or small, we define the semi-classical regime to have $E_{\rm b}$ smaller than *either* (*or both*) E and e, and the quantum regime to have $E_{\rm b}$ greater than *both* E and e.

Independently, in either regime, we can further require a separation between E and e, which defines two more cases. When $e \gg E$, most of the emitted frequencies will be below the superradiant bound, so this will be referred to as the superradiant-dominated regime, while $e \ll E$ will be referred to as the neutral-like regime, since the character of the radiation, as we will see, will be the same as that found for neutral radiation in [60] for both the semi-classical and quantum rates. All six possible permutations of these three energies, and the corresponding energy regimes are summarized in the following table.

	Semi-Classical	Quantum
Neutral-Like	$e \ll E_{\rm b} \ll E$ $E_{\rm b} \ll e \ll E$	$e \ll E \ll E_{\rm b}$
Superradiant-Dominated	$E \ll E_{\rm b} \ll e$ $E_{\rm b} \ll E \ll e$	$E \ll e \ll E_{\rm b}$

Table 4.1: A summary of the possible energy regimes for the emission of charged radiation from Reissner-Nordström.

For the left column, it is safe to use the semi-classical rate (4.71), as the quantum rate would just reduce to it, as shown in Appendix 5.4, while for the right column, the semi-classical (4.71) and quantum (4.95) rates give different answers. Note that $E_{\rm b}$ is grayed out in the left column, since it is not "seen" by the semi-classical rate, so its position relative to the other two scales is irrelevant, as long as it is smaller than one of them. In the canonical ensemble, which is more convenient for computing semi-classical rates, the neutral regime will have $e \ll T$, and the superradiant regime will have $T \ll e$.

Choosing the scales $E_{\rm b} = \frac{1}{Q^3}$ and the superradiant e amounts to choosing a charge for the black hole Q and the particle it is radiating e. But, as we saw at the beginning of this section, there are further constraints on these two parameters, first $Q \geq e$, and second $eQ \lesssim 1$ (we are ignoring numbers of order one here) for the conformal dimension to be real. All possible

values of these two parameters and the corresponding energy and Δ regimes they define are summarized in the following figure.

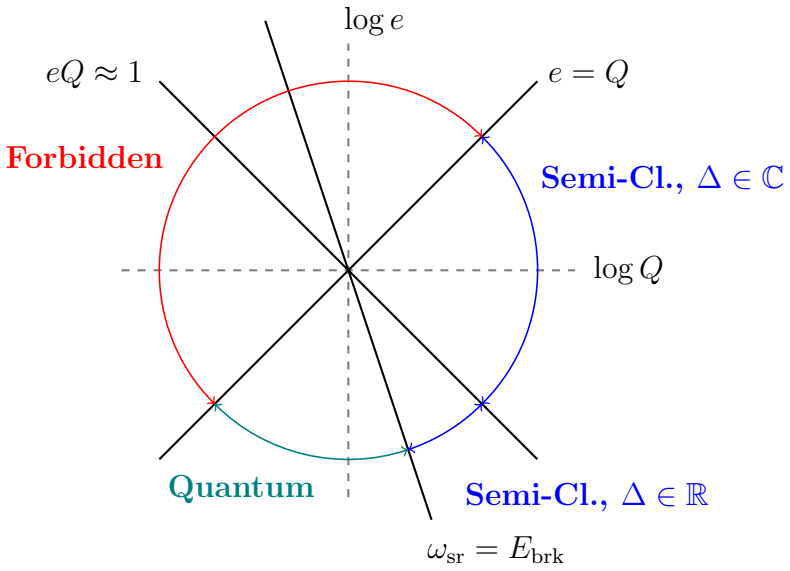


Figure 4.1: A diagram of $\log Q$ vs. $\log e$ parameter space for radiation from a Reissner-Nordström black hole. In the allowed region ($Q \geq e$), the bottom two wedges (small black holes) always have real Δ, the top wedge (large) has both real and complex Δ. The top two wedges always have the quantum rate (4.95) reduce to the semi-classical formula (4.71), while the bottom wedge can have (and this further depends on the size of E which is not on this diagram) the quantum rate give different predictions from the semi-classical.

Only points under $e = Q$ are possible. Everything under $eQ \approx 1$ are the small black holes[10] with real Δ (the subject of this section), and everything above are large black holes with complex Δ (section 4.3). Everything below the $e = E_{\rm b}$ line ($e = Q^{-3}$) is possibly in the quantum regime (if E is low enough), and everything above is in the semi-classical regime. At each available (Q, e) point on this plot, we still need to independently choose E (or T), which, depending on how it compares to $\omega_{\rm sr}$, will further determine whether we are in the neutral-like or superradiant-dominated regime.

There are a number of conclusions that we can draw from this diagram. First, large black holes (the top wedge) necessarily radiate in the semi-classical regime. Therefore, we will not

[10]We will sometimes refer to the middle wedge in the figure as mid-sized black holes and the bottom as small, when we need to distinguish between them. The main difference is that the former always produce semi-classical radiation, while the latter can also radiate in the quantum regime.

need to consider the quantum evaporation rates for these black holes in the next section. Second, in the neutral regime $e \ll T$, which together with the near-extremal conditions $QT \ll 1$ implies that we should always take the limit $eQ \ll 1$ in this regime. This further implies that large black holes, those with $eQ \geq 1/2$, always radiate in the superradiant regime. Third, if we consider black holes in the quantum regime, we can see that we will always have $eQ \ll 1$, which significantly simplifies the formulae in both the neutral and superradiant regime, but does not mean that they give the same answer. This also explains why the conformal dimension is frequency-independent, as it effectively sets to zero the last term in (4.96). Finally, we can apply this analysis to our Universe where the smallest charged particle is the positron with $e = 0.0854$. All near-extremal black holes then sit on a horizontal line slightly below the abscissa ($e = 1$). This implies that the quantum-corrections would only appear for microscopic black holes which would at most have a charge roughly double the positron.

The three parameters (Q, T, e), or equivalently the three energy scales $(E_{\rm b}, E, e)$ define a unique emission spectrum in one of the four energy regimes given in table 4.1. In the next two subsections, our goal will be to compute, analyze, and compare the spectra and rates in these regimes. Before turning to the details, we first point out some general features of the neutral-like and superradiant-dominated regimes. We start with the semi-classical evaporation rates. The integral in equation (4.58), which goes from 0 to ∞ can be split up into superradiant ($\omega \leq \omega_{\rm sr}$) and non-superradiant frequencies ($\omega \geq \omega_{\rm sr}$) frequencies. In each of the two regimes, superradiant with $T \ll e$ and neutral-like with $e \ll T$, each of these two integrals can be estimated as follows. Starting with the lower frequencies in the superradiant regime, we only copy the temperature and frequency-dependent part of the semi-classical evaporation rate (4.71) (ignoring the frequency-dependence of the parameters Δ, μ, α as these

are irrelevant for the size of the integrals) which gives

$$I^{\rm SD}_{\omega\leq\omega_{\rm sr}} \sim T^{2\Delta-2}\int_0^e d\omega\,\frac{\omega_{\rm eff}\,\omega^{2\Delta}\,\gamma(\omega_{\rm eff}/T)}{e^{\omega_{\rm eff}/T}-1} \sim T^{2\Delta-2}\int_0^e d\omega\,|\omega_{\rm eff}|\,\omega^{2\Delta}\,\left(\frac{\omega_{\rm eff}}{T}\right)^{2(\Delta-1)} \sim e^{4\Delta}\,. \tag{4.100}$$

$\gamma(\omega_{\rm eff}/T)$ consists of the F-dependent part of (4.71) (the last fraction), and given that $F=\omega_{\rm eff}/4\pi T$, it is a function of $\omega_{\rm eff}/T$. In the second equality, we ignored the exponential as $|\omega_{\rm eff}|\leq e$ and $e\gg T$. We also used the fact that $\gamma(\omega_{\rm eff}/T)$ reduces to the fraction in the third integral in this limit, which we will explicitly show in subsection 4.2.3. As a result, the temperature dependence cancels out. In the third equality, we performed the integral to get the final estimate, which is true to leading order in T/e. For the higher frequencies, we have the following

$$I^{\rm SD}_{\omega\geq\omega_{\rm sr}} \sim T^{2\Delta-2}\int_e^\infty d\omega\frac{\omega_{\rm e}\omega^{2\Delta}\gamma(\omega_{\rm e}/T)}{e^{\omega_{\rm e}/T}-1} \sim T^{2\Delta-2}\int_0^\infty d\omega'\frac{\omega'(\omega'+e)^{2\Delta}\gamma(\omega'/T)}{e^{\omega'/T}-1} \sim e^{4\Delta}\left(\frac{T}{e}\right)^{2\Delta}\,. \tag{4.101}$$

In the second equality, we shifted the frequency variable $\omega'=\omega-e$. In the resulting integral, all frequencies beyond $\omega'=T$ experience exponential suppression, and can be ignored, which means that ω' is at most of order T. As a result, in the third equality, we ignored ω' in $(\omega'+e)$, and did the integral to obtain the final estimate. What this analysis shows, is that, in this regime, the non-superradiant modes are strongly suppressed compared to the superradiant modes, and can therefore be ignored. In the neutral-like regime, we can perform an analogous analysis. Starting with the lower frequencies, we have

$$I^{\rm NL}_{\omega\leq e} \sim T^{2\Delta-2}\int_0^e d\omega\frac{\omega_{\rm e}\,\omega^{2\Delta}\,\gamma(\omega_e/T)}{e^{\omega_e/T}-1} \sim T^{2\Delta-2}\int_0^e d\omega\,\frac{|\omega_e|\,\omega^{2\Delta}}{\frac{|\omega_e|}{T}} \sim T^{4\Delta}\,\left(\frac{e}{T}\right)^{2\Delta+1}\,. \tag{4.102}$$

In the second equality, we approximated the denominator in the left integral to lowest order using the fact that $e\ll T$. We then did the integral. For the higher frequencies, we have

$$I^{\rm NL}_{\omega\geq e} \sim T^{2\Delta-2}\int_0^\infty d\omega'\,\frac{\omega'\,(\omega'+e)^{2\Delta}\,\gamma(\omega'/T)}{e^{\omega'/T}-1} \sim T^{4\Delta}\,, \tag{4.103}$$

where we have performed the same shift as before. Here, we ignore e in $(\omega' + e)$ and do the integral to find the final estimate. We find the opposite conclusion in this regime, the superradiant frequencies are suppressed compared to the non-superradiant ones.

For the quantum-corrected evaporation rate, the integral in equation (4.77) goes from 0 to $e + E$, with the superradiant modes from 0 to e, and the non-superradiant ones from e to $e + E$. The emitted frequencies in the neutral-like ($e \ll E$) and superradiant-dominated ($E \ll e$) regimes parallel what we found for the semi-classical rate, which here is more straightforward to show. When $e \ll E$, the range of superradiant frequencies is very small and can be ignored, and when $E \ll e$, the opposite is true.

We also point out that in the quantum regime ($E + e \ll E_{\rm b}$), we can make the following two approximations in the quantum-corrected evaporation rate. The sinh function in the density of states simplifies as follows

$$\sinh\left(2\pi\sqrt{2\frac{E+e-\omega}{E_{\rm b}}}\right) = 2\pi\sqrt{2\frac{E+e-\omega}{E_{\rm b}}}\,, \tag{4.104}$$

and the frequency-dependent part of the matrix element given by the four Gamma functions reduces to

$$\left|\Gamma\left(\Delta + i\sqrt{2\frac{E+e-\omega}{E_{\rm b}}} \pm i\sqrt{2\frac{E}{E_{\rm b}}}\right)\right|^2 = \Gamma(\Delta)^4\,. \tag{4.105}$$

Finally, we comment on the parameters Δ, α, μ, which are all functions of frequency in general, but simplify in some of the energy regimes. First, for massless radiation, we have the following

$$\mu = -\alpha = -Q(2\omega - 1)\,. \tag{4.106}$$

Then, in the neutral-like regime, as we saw, the superradiant frequencies can be ignored, and the frequency is at most $\omega \sim T$, which is small for a near-extremal black hole. This means that all terms of the order $Q\omega \sim QT \ll 1$ can be ignored, which gives Δ, α, μ the following

frequency-independent values

$$\begin{aligned}\Delta_e &= \tfrac{1}{2} + \sqrt{\tfrac{1}{4} + l(l+1) - e^2\,Q^2}\,,\\ \alpha_e &= -\mu_e = -eQ\,.\end{aligned} \tag{4.107}$$

But as we said, we must have $eQ \ll 1$ in the neutral regime, which means that these further simplify to

$$\begin{aligned}\Delta_0 &= l + 1\,,\\ \alpha_0 &= \mu_0 = 0\,.\end{aligned} \tag{4.108}$$

In the superradiant regime, the frequency is of order $\omega \sim e$, so terms such as $Q\omega \sim eQ$ cannot necessarily be ignored, and the full frequency-dependent form of Δ, α, μ must be taken

$$\begin{aligned}\Delta(\omega) &= \tfrac{1}{2} + \sqrt{\tfrac{1}{4} + l(l+1) - e^2Q^2 + 6\omega(e-\omega)Q^2}\,,\\ \alpha(\omega) &= -\mu(\omega) = Q(2\omega - e)\,.\end{aligned} \tag{4.109}$$

For quantum superradiant emission, we must have $eQ \ll 1$, so these again reduce to (4.108).

4.2.2 Neutral-like regime

We start with the semi-classical regime, where the quantum-corrected evaporation rate would reduce to the semi-classical rate, and therefore we can just use equation (4.71). In the previous subsection, we showed that in the neutral regime we only need to consider the non-superradiant frequencies where in the integral we can effectively drop e in ω_{eff} (see equation (4.103)). Furthermore, we argued that $eQ \ll 1$, so we can use the (4.108) for

$\alpha = -\mu$ and Δ. Under these assumptions, the evaporation rate is given by

$$\left.\frac{dE}{dt}\right|_{\rm sc} = \sum_{l,m_l} 2^{6\Delta_0-5}\,\pi^{2\Delta_0-3}\,Q^{4\Delta_0-2}\,T^{2\Delta_0-2}\,\frac{|\Gamma(\Delta_0)|^4}{\Gamma(2\Delta_0)^2\,\Gamma(2\Delta_0-1)^2} \int_0^\infty d\omega\,\frac{\omega^{2\Delta_0+1}}{e^{\omega/T}-1}\left|\frac{\Gamma(\Delta_0-i\omega/2\pi T)}{\Gamma(1-i\omega/2\pi T)}\right|^2, \tag{4.110}$$

where we have pulled out all the frequency-independent terms in front of the integral. The only frequency dependence comes from the $k = \omega$ and $\omega_{\rm eff} = \omega$ terms. Performing a change of variables $x = \omega/T$ under the integral, and writing T in terms of E using (4.24), gives our final result for the semi-classical neutral-like evaporation rate

$$\left.\frac{dE}{dt}\right|_{\rm sc} = \sum_{l=0}^{\infty} C_l\,\left(\frac{E}{Q}\right)^{2l+2}\frac{1}{Q^2}\,, \tag{4.111}$$

where we can see that the $E-$dependence factored out of the integral after changing variables. The remaining numerical factors are collected into the following coefficient

$$C_l = \frac{2^{4l-1}\,\pi^{-2l-5}\,l!^4}{(2l+1)!\,(2l)!^3}\int_0^\infty dx\frac{x^{2l+3}}{e^x-1}\prod_{j=1}^{l}\left(j^2+\frac{x^2}{4\pi^2}\right). \tag{4.112}$$

The conformal dimension $\Delta_0 = l+1$ is an integer, and therefore the ratio of Gamma functions under the integral reduces to a polynomial in x using the Gamma function identities from Appendix 5.2. For a given l, the product can be expanded into a sum and each term can be solved using the integral formula for the Zeta function, but there is no simple closed form expression for writing this product in terms of a sum for arbitrary l. In equation (4.111), we can reintroduce units by inserting factors of G as follows. Replace $E/Q \to \sqrt{G}E/Q$, which gives a unitless energy ratio, and $1/Q^2 \to 1/GQ^2$, which has units of energy squared, which is the right unit for an emission rate.

From this formula it is clear that higher angular momentum modes are proportional to higher powers of temperature, and therefore contribute less to the evaporation rate. As an

example, we compute the dominant lowest $l = 0$ mode using (4.111). Setting $l = 0$ and doing the integral gives

$$\left.\frac{dE}{dt}\right|_{\rm sc}^{(l=0)} = \frac{1}{30\pi}\left(\frac{E}{Q}\right)^2 \frac{1}{Q^2}\,. \tag{4.113}$$

This agrees with the neutral rate found in [60]. For completeness and the purposes of later discussion, we also compute the rate of emission of charge in this limit for this dominant mode. By replacing one power of ω with a factor e in the derivation from above, it is straightforward to show that the following is obtained for the emission rate of charge

$$\left.\frac{dQ}{dt}\right|_{\rm sc}^{(l=0)} = \frac{\sqrt{2}\,\zeta(3)}{\pi^4}\left(\frac{E}{Q}\right)^{\frac{3}{2}} \frac{e}{Q}\,. \tag{4.114}$$

We now turn to the quantum neutral-like regime, where we have $e \ll E \ll E_{\rm b}$. Using the two approximations introduced in the previous subsection, equations (4.104) and (4.105) and the fact that α and Δ are given by (4.108) when $eQ \ll 1$, we find that the quantum rate given by equation (4.95) reduces to

$$\begin{aligned}\left.\frac{dE}{dt}\right|_{\rm q} = \sum_{l,m_l} \frac{1}{\pi^2}\, 2^{2\Delta_0-3/2}\, Q^{4\Delta_0-2}\, E_{\rm b}^{2\Delta_0-3/2} \frac{|\Gamma(\Delta_0)|^4\,\Gamma(\Delta_0)^4}{\Gamma(2\Delta_0)^2\,\Gamma(2\Delta_0-1)^2} \\ \int_0^E d\omega\,\omega^{2\Delta_0}\,(E-\omega)^{1/2}\,.\end{aligned} \tag{4.115}$$

After performing a change of variables $x = \omega/E$, we obtain our final result for the quantum neutral-like evaporation rate

$$\left.\frac{dE}{dt}\right|_{\rm q} = \sum_{l=0}^{\infty} \hat{C}_l \left(\frac{E}{Q}\right)^{2l+2} \left(\frac{E}{E_{\rm b}}\right)^{\frac{3}{2}} \frac{1}{Q^2}\,. \tag{4.116}$$

The same $E-$dependence factors out with an extra factor of $(E/E_{\rm b})^{3/2}$. The rest of the rate is collected into the following coefficient

$$\hat{C}_l = (2l+1)\,\frac{1}{\pi^2}\,2^{2\Delta_0-3/2}\,\frac{|\Gamma(\Delta_0)|^4\,\Gamma(\Delta_0)^4}{\Gamma(2\Delta_0)^2\,\Gamma(2\Delta_0-1)^2}\int_0^1 dx\,x^{2\Delta_0}\,(1-x)^{1/2}\,. \tag{4.117}$$

This integral can be performed using the Beta function integral, which can then be written in terms of Gamma functions, and then further simplified using the Gamma function duplication formula. The following is obtained

$$\hat{C}_l = \frac{2^{6l+6+1/2}\, l!^8\, (2l+2)!\, (2l+3)!\, (2l+1)^3}{\pi^2\, (2l+1)!^4\, (4l+7)!}\,. \tag{4.118}$$

As an example, we evaluate this formula for the dominant $l = 0$ mode. This gives the following

$$\left.\frac{dE}{dt}\right|_{\rm q}^{(l=0)} = \frac{16\sqrt{2}}{105\,\pi^2}\,\left(\frac{E}{Q}\right)^2\,\left(\frac{E}{E_{\rm b}}\right)^{\frac{3}{2}}\frac{1}{Q^2}\,. \tag{4.119}$$

This agrees with what was found in [60] for neutral scalar radiation. For completeness, we also give the charge emission rate

$$\left.\frac{dQ}{dt}\right|_{\rm q}^{(l=0)} = \frac{8}{15\pi}\,\left(\frac{E}{Q}\right)^{\frac{3}{2}}\left(\frac{E}{E_{\rm b}}\right)\,\frac{e}{Q}\,. \tag{4.120}$$

When we compare the semi-classical and quantum emission rates, equations (4.111) and (4.116), we find that the answers differ by the following ratio of scales

$$\frac{\left.\dfrac{dE}{dt}\right|_{\rm q}}{\left.\dfrac{dE}{dt}\right|_{\rm sc}} \sim \left(\frac{E}{E_{\rm b}}\right)^{3/2}\,, \tag{4.121}$$

which is true up to an order one numerical factor. This means that the quantum rate for neutral-like charged radiation is suppressed compared to the semi-classical rate at low energies, meaning that the black hole emits less than we would have found using the semi-classical Hawking formula.

Finally, we can address the question of whether perturbation theory, which was used to derive the quantum rate, is valid for charged radiation in the neutral regime. Since the evaporation rate is proportional to a power of E/Q times a power of $E/E_{\rm b}$, both of which

are small quantities in this regime, it is safe to say that perturbation theory is valid.

4.2.3 Superradiant-dominated regime

We start with the semi-classical regime at finite values of eQ, leaving the small charge limit for later. In subsection 4.2.1, we show that the non-superradiant frequencies can be ignored, leaving us with an integral from 0 and e. Furthermore, given that $|F| = |\omega_{\text{eff}}|/4\pi T \sim e/T \gg 1$, the following approximation can be applied to the F-dependent Gamma functions (using the asymptotic expansion for the complex argument Gamma function (5.22))

$$\left|\frac{\Gamma(\Delta + i(2|F| - \mu))}{\Gamma(1 + 2i|F|)}\right|^2 \sim \left(\frac{\omega_{\text{eff}}}{2\pi T}\right)^{2(\Delta-1)} e^{\pi\mu}\,, \tag{4.122}$$

Note that for the superradiant frequencies $\omega_{\text{eff}} < 0$, so $F = -|F|$, which then determines the relative sign between F and μ, which is important for evaluating the absolute value in the asymptotic expansion formula. Using (4.122), the rate simplifies as follows

$$\left.\frac{dE}{dt}\right|_{\text{sc}} = \sum_{l,m_l} \int_0^e 2^{4\Delta-3}\,\pi^{-1}\,Q^{4\Delta-2}\,\frac{|\Gamma(\Delta + i\alpha)|^4}{\Gamma(2\Delta)^2\,\Gamma(2\Delta-1)^2}\,\omega^{2\Delta}\,\omega_{\text{eff}}^{2\Delta-1}\,. \tag{4.123}$$

Note that the temperature dependence drops out, as we mentioned under equation (4.101). Furthermore, to simplify the exponential functions, we used the fact that $\mu = -\alpha$.[11] Performing a change of variables $x = \omega/e$ gives our final result for the semi-classical superradiant-dominated evaporation rate

$$\left.\frac{dE}{dt}\right|_{\text{sc}} = \sum_{l=0}^{\infty} G_l(eQ)\,\frac{1}{Q^2}\,, \tag{4.124}$$

[11]We are working with massless radiation $m = 0$, which gives us $\alpha = -\mu$. When we take the limit of $\omega \to 0$, we get $\alpha \to -eQ$. If we took $m \neq 0$, and we zoomed in onto the lower range of the frequencies $\omega \to m$, we would find that $\alpha \to -\infty$, which implies that there is an order of limits issue with α. This doesn't cause any issues in the evaporation rate, since at $\omega \to m$ we have $|\Gamma(\Delta + i\alpha)|^2 \sim 2\pi\alpha^{2\Delta-1}\,e^{-\pi|\alpha|}$, which when $m \to 0$ is taken gives zero for the evaporation rate, which is exactly what we get if we take $m = 0$ from the start, and then take $\omega \to 0$.

where the coefficient function is given by the following integral

$$G_l(eQ) = \frac{2l+1}{\pi}\int_0^1 dx\, 2^{4\Delta-3}\,(eQ)^{4\Delta}\,\frac{|\Gamma(\Delta+i\alpha)|^4}{\Gamma(2\Delta)^2\,\Gamma(2\Delta-1)^2}\,x^{2\Delta}\,(1-x)^{2\Delta-1}\,, \tag{4.125}$$

and the parameters Δ, and α are now functions of x and eQ

$$\begin{aligned}\Delta(x,eQ) &= \tfrac{1}{2} + \sqrt{\tfrac{1}{4} + l(l+1) - (eQ)^2 + 6(eQ)^2\,x\,(1-x)}\,,\\ \alpha(x,eQ) &= eQ\,(2x-1)\,.\end{aligned} \tag{4.126}$$

Without further approximation, these integrals cannot be performed in terms of elementary functions. In the left panel of figure 4.2, we plot the spectral evaporation rate at different values of eQ for the $l = 0$ mode. In the right panel, we also plot the integrated rate as a function of eQ.

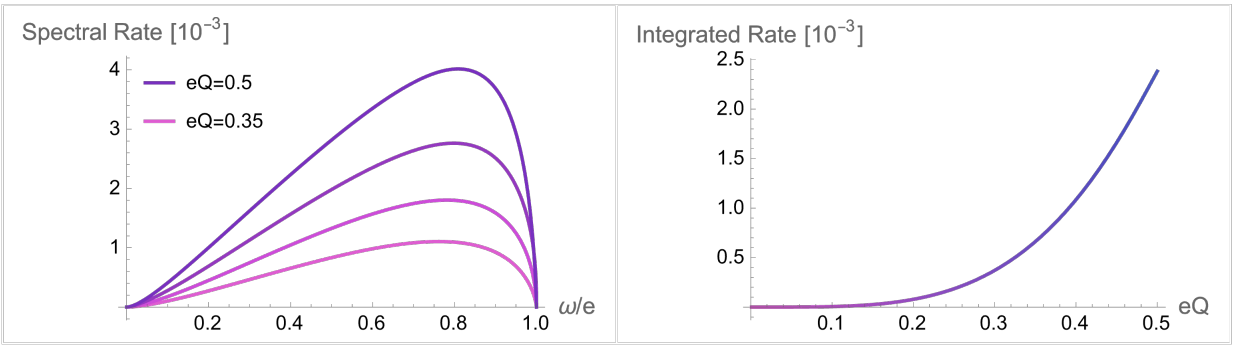


Figure 4.2: (Left) Spectral evaporation rate in quantum superradiant-dominated regime at four different values of eQ between 0.5 and 0.35, in equal increments. (Right) Integrated evaporation rate as a function of eQ.

These plots show that the rate grows with eQ. In the next section, we will see what happens beyond $eQ = \frac{1}{2}$. We also mention that the right boundary of the plot in the left panel is not actually zero. In deriving the rate, we assumed (4.122), which does not hold in a small interval near $\omega = e$. This was not important for integrating, as it gives a small temperature-dependent correction, but it does show up in the plots.

To further simplify these expressions, and for comparison with the quantum rate, we now

take the small charge limit $eQ \ll 1$, but staying within $T \ll e$. Using the (4.108) limit of Δ and α, the rate in (4.124) simplifies to

$$\left.\frac{dE}{dt}\right|_{\rm sc} = \sum_{l=0}^{\infty} D_l \, (eQ)^{4l+4} \, \frac{1}{Q^2} \,, \tag{4.127}$$

The integral in the coefficient can be performed in terms of the Beta function which results in

$$D_l = \frac{1}{\pi} \, \frac{2^{4l+1} \, l!^4 \, (2l+1)^3}{(2l+1)!^4} \, \frac{(2l+2)! \, (2l+1)!}{(4l+4)!} \,. \tag{4.128}$$

As an example, we use this equation to compute the contribution from the dominant $l = 0$ mode. The following is found for the energy flux

$$\left.\frac{dE}{dt}\right|_{\rm sc}^{(l=0)} = \frac{1}{6\pi} \, (eQ)^4 \, \frac{1}{Q^2} \,. \tag{4.129}$$

We also compute the charge emission rate, by repeating the procedure from above and replacing one power of frequency with a factor of e. This gives

$$\left.\frac{dQ}{dt}\right|_{\rm sc}^{(l=0)} = \frac{1}{3\pi} \, (eQ)^3 \, \frac{e}{Q} \,. \tag{4.130}$$

In the quantum superradiant-dominated regime, we have $E \ll e \ll E_{\rm b}$ and $eQ \ll 1$. The calculation for the rate proceeds as before, but now the frequency range goes from zero to e. Using the approximate form of the density of states and matrix element, equations (4.104) and (4.105), and (4.108) for Δ an α, we find

$$\begin{aligned} \left.\frac{dE}{dt}\right|_{\rm q} = \sum_{l,m_l} 2^{2\Delta_0 - 3/2} \, \pi^{-2} \, Q^{4\Delta_0 - 2} \, E_{\rm b}^{2\Delta_0 - 3/2} \, \frac{|\Gamma(\Delta_0)|^4 \, \Gamma(\Delta_0)^4}{\Gamma(2\Delta_0)^2 \, \Gamma(2\Delta_0 - 1)^2} \\ \int_0^e d\omega \, \omega^{2\Delta_0} \, (e - \omega)^{1/2} \,. \end{aligned} \tag{4.131}$$

Note that the E dependence drops out. Performing a change of variables $x = \omega/e$ under the

integral gives our final result for the quantum superradiant-dominated evaporation rate

$$\left.\frac{dE}{dt}\right|_{\rm q} = \sum_{l=0}^{\infty} \hat{D}_l \, (eQ)^{4l+4} \, \left(\frac{E_{\rm b}}{e}\right)^{2l+1/2} \, \frac{1}{Q^2} \,, \tag{4.132}$$

with the coefficient given by

$$\hat{D}_l = \frac{2l+1}{\pi^2} 2^{2\Delta-3/2} \, \frac{\left|\Gamma(\Delta+i\alpha)\right|^4 \, \Gamma(\Delta)^4}{\Gamma(2\Delta)^2 \, \Gamma(2\Delta-1)^2} \, \int_0^1 dx \, x^{2\Delta} \, (1-x)^{1/2} \,. \tag{4.133}$$

The integral can be done, which results in

$$\hat{D}_l = \frac{1}{\pi^2} \, 2^{6l-7+1/2} \, \frac{l!^8 \, (2l+1)^3}{(2l+1)!^4} \, \frac{(2l+2)! \, (2l+3)!}{(4l+7)!} \,. \tag{4.134}$$

As an example, we calculate the quantum energy flux of the dominant $l = 0$ mode

$$\left.\frac{dE}{dt}\right|_{\rm q}^{(l=0)} = \frac{16\sqrt{2}}{105\,\pi^2} \, (eQ)^4 \, \left(\frac{E_{\rm b}}{e}\right)^{1/2} \, \frac{1}{Q^2} \,, \tag{4.135}$$

and the charge emission rate, which we find to be

$$\left.\frac{dQ}{dt}\right|_{\rm q}^{(l=0)} = \frac{4\sqrt{2}}{15\pi^2} \, (eQ)^3 \, \left(\frac{E_{\rm b}}{e}\right)^{1/2} \, \frac{e}{Q} \,. \tag{4.136}$$

The overall size of the quantum emission rate is determined by two unitless parameters in equation (4.132), eQ and the ratio $E_{\rm b}/e$, the first of which, in the quantum regime, is a small quantity and the second a large one. The product of these two simplifies as follows

$$(eQ)^{4l+4} \, \left(\frac{E_{\rm b}}{e}\right)^{2l+2} = \left(\frac{e}{Q}\right)^{2l+2} \,. \tag{4.137}$$

This implies that as long as the black hole charge is reasonably greater than the particle it is radiating, which is true for most of parameter space, the emission rate is a small quantity, and the use of perturbation theory is valid in this regime as well. This addresses another

concern. Based on equation (4.132), we could worry that higher angular momentum modes would contribute more, given that $E_{\rm b}/e$ is raised to higher and higher powers of l. But since the product of eQ and $E_{\rm b}/e$ is actually a small number, this does not happen.

Comparing the semi-classical (4.127) and quantum (4.132) emission rates in the small charge limit $eQ \ll 1$, we find

$$\frac{\left.\frac{dE}{dt}\right|_{\rm q}}{\left.\frac{dE}{dt}\right|_{\rm sc}} \sim \left(\frac{E_{\rm b}}{e}\right)^{2l+1/2} . \tag{4.138}$$

This shows that the quantum rate is enhanced compared to the semi-classical by a power of $\frac{E_{\rm b}}{e}$. This agrees with what was reported in [142, 143] from their analysis of emission spectra plots. This also implies that higher modes are more strongly enhanced, which does not mean that higher modes radiate at a large rate, just that when the two rates are compared mode by mode, a higher enhancement is found at higher l.

4.3 Radiation from large charged black holes

Large black holes were defined in the previous section as those having[12]

$$eQ \geq \tfrac{1}{2} + l \,, \tag{4.139}$$

which is the condition for the conformal dimension $\Delta(\omega)$ to have complex values on some subset of the available frequencies $[0, e+E]$. As we argued in the previous section, there is no neutral-like regime when we don't have $eQ \ll 1$, so we only consider the superradiant regime in this section. Using the fact that $T \ll e$, and inspecting the quadratic under the square root in (4.96), we find the following behavior, as we vary eQ from small to large values. At very small eQ, it starts out flat and positive. As eQ approaches 1/2, it starts bending

[12]Our definition of small versus large black holes is related to the definition used in [51], but not the same. There, large black holes were defined as those with $M \gg m$, which made the effective potential large, allowing for a WKB treatment. Here, the same Schwinger-like result will appear for $eQ \gg 1$, which is only a limiting case of all large black holes $eQ \geq \frac{1}{2}$.

downward. At $eQ = 1/2$, the roots are exactly at 0 and e. Beyond $eQ = 1/2$, the roots, given by (for the dominant $l = 0$)

$$\omega_{\pm} = \tfrac{1}{2}\left(1 \pm \sqrt{\tfrac{1}{3} + \tfrac{1}{6e^2Q^2}}\right) e\,, \tag{4.140}$$

start moving inward and approaching the limiting values of $\frac{1}{2}(1 \pm 1/\sqrt{3})e$. Therefore, for large black holes, $\Delta(\omega)$ is real for frequencies inside of an interval bounded by $[\omega_-, \omega_+]$, and complex outside of this interval $[0, \omega_-]$ and $[\omega_+, \omega_{\rm sr}]$.

In subsection 4.2.1, using figure 4.1, we showed that we always have $E_{\rm b} \gg e$ for large black holes, which implies that they are never in the quantum regime. Therefore, even if we calculate the quantum-corrected emission rate, we would expect it to reduce to the semi-classical formula, so we will only consider this rate in this section.

The greybody factor that we computed in subsection 4.1.3 assumed that β and Δ are real. This result can still be used in the middle frequency interval for large black holes, but on the left and right intervals, where Δ is complex, and β is imaginary, we will have to recompute the greybody factor, which we will find to be very different.

We will find significant simplification in our results, if we take the limit of very large black holes, those with $eQ \gg 1$. The greybody factor in this limit was derived in [51] where a Schwinger-like exponential suppression was found. This result was obtained using WKB theory, which does not require solving the wave equation. We will start by repeating this calculation, and then we will show that our greybody factor, which is valid on the full range of eQ, reduces to the Gibbons result in the large eQ limit.

4.3.1 Greybody factor from WKB theory

We will repeat the large black hole calculation done in [51]. For the rest of this section, we will consider a nearly massless scalar, as a non-zero m, no matter how small, will be required to give us the right results in the $eQ \gg 1$ limit.

In 1D quantum mechanics, if the potential in a "tunneling through the barrier" scattering problem is large, the transmission coefficient can be found using the quasi-classical approximation or WKB theory as follows

$$\Gamma = \exp\left(-2\int_{x_1}^{x_2} dx\sqrt{V(x)}\right), \tag{4.141}$$

where the integral goes over the classically-forbidden region, which is defined by $x_{1,2}$, the roots of $V(x)$. As we can see, this does not require solving the Schrodinger equation.

In the 1D scattering problem set up in subsection 4.1.2, when we set $\delta r = 0$ in $f(r)$ and take $eQ \gg 1$, the effective potential (4.32) is large and given by

$$V_{\text{eff}}(r) = \left(\omega - \frac{eQ}{r}\right)^2 - m^2\,\frac{(r-Q)^2}{r^2}\,, \qquad r_\pm = \frac{e \mp m}{\omega \mp m}\,, \tag{4.142}$$

where we have ignored the term involving $f'(r)$ as it is subleading in eQ. We have also included the roots $r_\pm$ of the potential, which we can see would coincide, if we had not taken $m \neq 0$, so there would be no classically-forbidden region, and the WKB approximation would not be possible. Plugging into (4.141) and integrating gives

$$\Gamma = \exp\left(-2\int_{r_{*,-}}^{r_{*,+}} dr_*\sqrt{V_{\text{eff}}(r_*)}\right) = \exp\left(-2\pi Q\left(2\omega - 1 - \tfrac{2\omega^2-\omega-m^2}{\sqrt{\omega^2-m^2}}\right)\right). \tag{4.143}$$

Note that the 1D scattering problem is in terms of the coordinate r_*, but to solve the integral, it is much more convenient to change to r. Following [51], the final step is to evaluate this expression at $\omega = e$, which results in the Gibbons greybody factor

$$\Gamma = e^{-2\pi Q(e-\sqrt{e^2-m^2})}\,. \tag{4.144}$$

Note that if we had taken $\omega = e$ before evaluating the integral, the roots of the potential $r_\pm$ would be equal and WKB theory could not be applied. We can take a further limit of

(4.144) for $m \ll e$, which results in the classical Schwinger result

$$\Gamma = e^{-\frac{\pi Q m^2}{e}} \,. \tag{4.145}$$

Both of these equations, (4.144) and (4.145), tell us that there is a large suppression of charged radiation for very large black holes. Without assuming the size of m, equation (4.144) tells us that the suppression rate is exponentially suppressed at $eQ \gg 1$. When $m \ll e$, (4.145) tells us that there is suppression when $eQ\,\frac{m^2}{e^2} \gg 1$, which defines even larger black holes given by

$$eQ \geq eQ_* = \frac{e^2}{\pi m^2} \,. \tag{4.146}$$

Taking $\omega = e$ can be justified on the basis of this formula being exponentially peaked at $\omega = e$ on the subset of superradiant frequencies. There are two caveats that apply to this statement. First, equation (4.143) does not actually peak, but continues to grow beyond $\omega = e$. Second, the transmission coefficient given by (4.141) is only true if the incident and transmitted waves have the same k on the two sides of the potential, which, as we saw in (4.33), is not true. Incorporating this difference in k is what led to the ω_{eff}/k factor in the transmission coefficient in (4.59). This would imply that our greybody factor is not (4.144) but zero at $\omega = e$. Both of these are resolved if instead we consider the full Hawking emission rate (4.58). Then, the statistical factor reduces to $1/\omega_{\text{eff}}$ when $\omega = e$, canceling the ω_{eff} in the greybody factor, resulting in a non-zero rate. Furthermore, beyond $\omega = e$, the statistical factor thermally suppresses the greybody factor, giving an emission rate that truly peaks around $\omega = e$ with a value determined by the exponential factor in (4.144). We will show this explicitly in the next subsection.

Finally, if one could solve the wave equation and compute the exact transmission coefficient in terms of a parameter λ that controls the size of the potential, then at large λ, the transmission coefficient can be quasi-classically expanded into a series in $\exp(-\lambda)$. On general grounds, it can be argued that the coefficient of the first term is given by unity, which recovers

the WKB result (4.141) (see, for example, chapter 52 of [162]). One of the goals of the next subsection will be to confirm that this is true, by solving the wave equation, deriving the greybody factor, and showing that at $eQ \gg 1$ it reduces to exponential in (4.144), with the coefficient exactly equal to one.

4.3.2 Wave equation with complex Delta

We proceed as follows. We first derive the greybody factor and emission rate for all $eQ \geq 1/2$. Then, we take the large charge limit and derive the Gibbons result. We end by plotting the emission rate for finite $eQ \geq 1/2$.

The solution to the wave equation, given by equations (4.45), (4.51) and (4.56) is valid for both real and imaginary β, which can be found in (4.41). To make the imaginary value of β manifest, we will make the following replacement $\beta \to i\beta$, which amounts to pulling out a minus sign from the square root, which means that all the terms in the square root of the original β will have their sign flipped. A first attempt at recomputing the transmission coefficient would be to make the same replacement in its already derived equation (4.68), but this would not work for the following reason. In deriving this equation, we ignored C_- compared to C_+, because they were proportional to different powers, determined by β, of δr, a small quantity, as can be seen in the matching conditions (4.56). Since β is now imaginary, the coefficients C_+ and C_- take the following form

$$C_\pm = \frac{\Gamma(\pm 2i\beta)\,\Gamma(1-2iF)}{\Gamma(\frac{1}{2}\pm i\beta+i\mu)\,\Gamma(\frac{1}{2}\pm i\beta-2iF-i\mu)}\,\delta r^{+1/2\mp i\beta}\,A\,, \tag{4.147}$$

where we can see that after squaring, this will give the same power of δr, and we cannot assume that one is small compared to the other in general. Therefore, we will have to use both when computing the transmission coefficient. The coefficient of the incident wave will

now have a contribution from both given by

$$C_{\text{inc},\,\pm} = \frac{\Gamma(1 \pm 2i\beta)}{\Gamma(\frac{1}{2} \pm i\beta - i\alpha)} \, (-2ik)^{-1/2 \mp i\beta - i\alpha} \, C_{\pm} \,, \tag{4.148}$$

Squaring each term gives

$$|C_{\text{inc},\,\pm}|^2 = \frac{\delta r}{2k} \, \frac{|\Gamma(1 + 2i\beta)|^2 \, |\Gamma(2i\beta)|^2 \, |\Gamma(1 - 2iF)|^2}{|\Gamma(\frac{1}{2} \pm i\beta - i\alpha)|^2 \, |\Gamma(\frac{1}{2} \pm i\beta + i\mu)|^2 \, |\Gamma(\frac{1}{2} \pm i\beta - 2iF - i\mu)|^2} \, e^{\pi(\mp\beta - \alpha)} \, |A|^2 \,. \tag{4.149}$$

Comparing to the squared incident coefficient (4.65) from before, we see that in addition to replacing $\beta \to i\beta$, the powers of δr and k are different, and there is an extra β term in the exponential function (coming from $i^{i\beta}$).[13] Using (5.19) and (5.20), we can further simplify these coefficients to the following

$$|C_{\text{inc},\,\pm}|^2 = \frac{\delta r \, 2F}{2k} \, \frac{\cosh \pi(\pm\beta - \alpha) \, \cosh \pi(\pm\beta + \mu) \, \cosh \pi(\pm\beta - 2F - \mu)}{\sinh^2 \pi(2\beta) \, \sinh \pi(2F)} \, e^{\pi(\mp\beta - \alpha)} \, |A|^2 \,. \tag{4.150}$$

Squaring the full $|C_{\text{inc}}|^2$ would also produce the following cross term

$$|C_{\text{inc},\,+}| \, |C_{\text{inc},\,+}| \, \cos(\psi) \,, \tag{4.151}$$

where ψ is the relative phase between the two terms $C_{\text{inc},\,\pm}$. This term has the following odd property, the relative phase has a term proportional to $\ln \delta r$ coming from the $\delta r^{\mp i\beta}$ in (4.147), which implies that as we take the black hole closer to extremality, the cross-term oscillates indefinitely. This odd behavior was first observed in [52, 53] in the context of the

[13] Note that we need to be careful when moving β from the real part of the argument inside the Gamma functions to the imaginary part. In the transmission coefficient we have $|\Gamma(x + \beta + iy)|^2$ and we can freely change the sign of y, while in C_{inc} we just have $\Gamma(x + \beta + iy)$, so, when moving β to $i\beta$, we have to use the exact sign of β that was found from solving the wave equation, which would give $\Gamma(x + i\beta + iy)$. Once this is squared, then we can change the overall sign of $i(\beta + y)$. In other words, we have to be careful with the order of these operations, otherwise we would end up with the wrong relative sign between β and y.

Kerr black hole. In [54, 55, 56], also in the context of Kerr, an argument was given for why this cross term can be ignored to high accuracy, eliminating this odd behavior. We will use that argument here, and also in the next section for Kerr, to argue-away the crossterm. As we shall see below, when $eQ \gg 1$, which is the limit we are interested in, each of the two $|C_{\text{inc},\,\pm}|$ will be exponentially small/large in eQ, with a different prefactor, which implies that one will always be dominant. Depending on where we are in the frequency range, a different term will dominate, which means that we cannot ignore one of them once and for all, instead we should keep both $|C_{\text{inc},\,\pm}|$, but what we can do, is ignore the cross term, as it will always be subdominant to one of $|C_{\text{inc},\,\pm}|$. In fact, even for finite $eQ \geq 1/2$, this is a very good approximation. Each Gamma function in (4.149) is either a sinh or cosh, which is a sum of exponential functions with arguments of the form $\pi eQ f(\omega/e)$, where f is of order one. For most ω, this is a small/big number, which again implies that the cross-term can be ignored. Therefore, for all $eQ \geq 1/2$, the following holds to high accuracy

$$|C_{\text{inc}}|^2 = |C_{\text{inc},\,+}|^2 + |C_{\text{inc},\,-}|^2 \ . \tag{4.152}$$

The amplitude of the transmitted wave C_{trans} remains unchanged when β is imaginary, and is given by equation (4.61). To find the greybody factor, we combine the incident and transmitted waves using (4.59), which gives

$$\Gamma = \frac{\sinh^2 \pi(2\beta)\, \sinh \pi(2F)}{\sum_{\pm} \cosh \pi(\pm\beta - \alpha)\, \cosh \pi(\pm\beta + \mu)\, \cosh \pi(\pm\beta - 2F - \mu)\, e^{\pi(\mp\beta - \alpha)}} \ . \tag{4.153}$$

Substituting into the Hawking formula (4.58) and using the fact that the statistical factor can be rewritten as follows

$$\frac{1}{e^{\omega_{\text{eff}}/T} - 1} = \frac{e^{-2\pi F}}{2 \sinh 2\pi F} \ , \tag{4.154}$$

we find the final formula for the semi-classical spectral emission rate for complex Δ in the

superradiant regime

$$\left.\frac{d^2E}{d\omega\,dt}\right|_{\rm sc} = \frac{1}{4\pi}\frac{\omega\,\sinh^2\pi(2\beta)\,e^{-\omega_{\rm eff}/2T}}{\sum_\pm \cosh\pi(\pm\beta-\alpha)\,\cosh\pi(\pm\beta+\mu)\,\cosh\pi(\pm\beta-2F-\mu)\,e^{\pi(\mp\beta-\alpha)}}\,. \quad (4.155)$$

The parameters μ, β, α can be found in equations (4.41) and (4.50) (with β having all signs flipped under the square root). These expression are only true for frequencies $\omega < e_-$ and $\omega > e_+$, while (4.71) applies in between. Note that, as mentioned in the previous subsection, the greybody factor goes to zero, but the emission rate doesn't at $\omega = e$.

We will now use these formulae to analyze the spectrum at finite eQ and to take the $eQ \gg 1$ limit. Starting with the latter, the $eQ \gg 1$ limit will result in a different answer in each of the three frequency intervals $[0, \omega_-]$, $[\omega_-, \omega_+]$, and $[\omega_+, e]$. Each sinh and cosh function in the emission rate will be approximated by an exponential function, and to compare these, we will need to know how the parameters α, β, and μ compare along this range. We graph these in the figure below. The vertical asymptote in α comes from having non-zero m. Furthermore, note that β is always smaller than α and μ, in terms of absolute value, along the $[0, e]$ interval. Beyond $\omega = e$, $\beta \geq \alpha = |\mu|$.

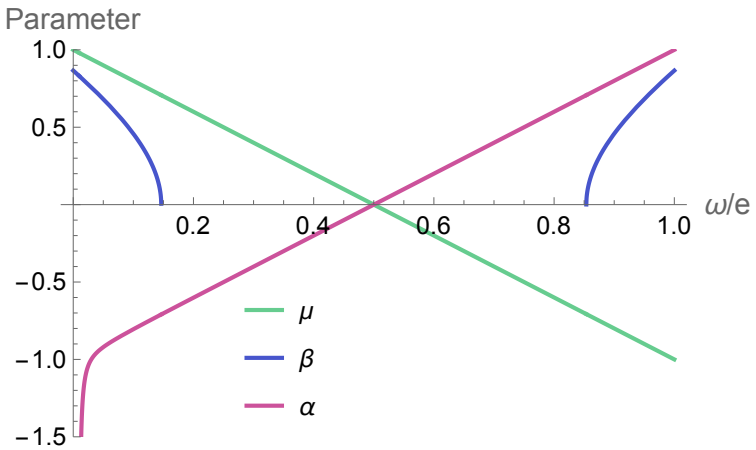


Figure 4.3: Parameters μ, β, and α as a function of ω in units of e.

Starting with $[\omega_+, e]$, which is where the Gibbons result lies, we have $\alpha \geq 0$ and $-\mu = |\mu| \geq 0$, and also $\alpha \geq \beta$ and $|\mu| \geq \beta$. Going back to the incident wave amplitude, we replace

$\mu = -|\mu|$ in (4.150). Focusing on the terms that differ between $|C_{\text{inc, }+}|$ and $|C_{\text{inc, }-}|$, we find

$$\sum_{\pm} \cosh \pi(\alpha \mp \beta) \, \cosh \pi(|\mu| \mp \beta) \, \cosh \pi(\pm\beta - 2F + |\mu|) \, e^{\pi(\mp\beta - \alpha)} \, . \tag{4.156}$$

We can now take the $eQ \gg 1$ limit of this equation. Using (5.23), we can replace each hyperbolic function with its asymptotic exponential. In the following equation, we summarize what we get (5.23)

$$e^{\pi(\alpha \mp \beta)} \, e^{\pi(|\mu| \mp \beta)} \, e^{\pi(\mp\beta - \alpha)} \, . \tag{4.157}$$

Note that we are not yet approximating the cosh with F inside of it. Due to the absolute value in (5.23), the signs of the exponents crucially depend on the relative size of the parameters β, μ, α. (4.157) simplifies to the following

$$e^{\pi(|\mu| \mp 3\beta)} \, . \tag{4.158}$$

We can clearly see that the second term is larger than the first. The extra suppression is given by $e^{-6\pi\beta}$, which is very small when $eQ \gg 1$. Therefore, the greybody factor in this limit is given by

$$\left. \frac{d^2 E}{d\omega \, dt} \right|_{\text{sc}} = \frac{\omega}{2\pi} \, \frac{1}{e^{2\pi(|\mu| - \beta)} + e^{\omega_{\text{eff}}/T}} \, , \tag{4.159}$$

with the sum of exponentials coming from the one remaining cosh function we did not approximate. When $\omega > e$, the first term in the denominator is exponentially small, because $|\mu| < \beta$, so the whole result reduces to exponential thermal suppression. When $\omega < e$, the second term is exponentially small and the result reduces to

$$\left. \frac{d^2 E}{d\omega \, dt} \right|_{\text{sc}} = \frac{\omega}{2\pi} \, e^{-2\pi(|\mu| - \beta)} \, , \tag{4.160}$$

which is strongly peaked at $\omega = e$. When evaluated at this value, it exactly reproduces the

Gibbons result found earlier

$$\left.\frac{d^2E}{d\omega\, dt}\right|_{\rm sc} = \frac{e}{2\pi}\, e^{-2\pi Q\left(e-\sqrt{e^2-m^2}\right)}\,. \tag{4.161}$$

We can see that the coefficient in front of the exponential, if we ignore the $\omega = e$ and the 2π from the Hawking emission formula, is exactly one, as required by WKB theory. To complete this analysis, we still need to check that the rest of the frequency interval gives corrections that can be ignored compared to this. We also point out that this type of result has been obtained in [163, 164] by working directly in the Reissner-Nordström near-horizon region, which does not account for the full frequency range, but only the superradiant frequency.

In $\omega \leq \omega_-$, we can perform the same type of calculation, but now we have $-\alpha = |\alpha| \geq 0$ and $\mu \geq 0$. Given that we are in the superradiant regime, and we are safely away from $\omega = e$, we can make the following approximation. Using the fact that $e \gg T$, which implies that $|\omega_{\rm eff}|/T \gg 1$, the F-dependent Gamma functions in (4.149) can be approximated as follows

$$\frac{|\Gamma(1-2iF+i\mu)|^2}{|\Gamma(\frac{1}{2}\pm i\beta-2iF)|^2} = \frac{|\Gamma(1+2i|F|+i\mu)|^2}{|\Gamma(\frac{1}{2}\pm i\beta+2i|F|)|^2} = 2|F|\, e^{\pi(-\mu\pm\beta)}\,. \tag{4.162}$$

Plugging this into the incident wave amplitude and replacing $\alpha = -|\alpha|$ results in the following

$$|C_{\rm inc,\,\pm}|^2 = \frac{\delta r\,|F|}{k}\,\frac{\cosh\pi(|\alpha|\pm\beta)\,\cosh\pi(\mu\pm\beta)}{\sinh^2 2\pi\beta} e^{\pi(-\mu+|\alpha|)}\,|A|^2\,. \tag{4.163}$$

At $eQ \gg 1$ these two reduce to

$$\begin{aligned} |C_{\rm inc,\,+}|^2 &= \frac{\delta r\,|F|}{k}\, e^{\pi(2|\alpha|-2\beta)}\,|A|^2\,, \\ |C_{\rm inc,\,-}|^2 &= \frac{\delta r\,|F|}{k}\, e^{\pi(2|\alpha|-6\beta)}\,|A|^2\,. \end{aligned} \tag{4.164}$$

The first coefficient is less suppressed, so we ignore the second. This results in

$$\left.\frac{d^2E}{d\omega\, dt}\right|_{\rm sc} = \frac{\omega}{2\pi} e^{-2\pi(|\alpha|-\beta)}\,, \tag{4.165}$$

Note that the statistical factor reduces to -1 in this part of the frequency interval. This looks like the Gibbons result due to the fact that $|\alpha| = |\mu|$ on most of the frequency interval, but there is a caveat. When $\omega \to m$, we have $|\alpha| \to \infty$, which means that the emission rate quickly goes to zero, not a constant as we had at $\omega = e$. Therefore, the dominant contribution from this interval is not at $\omega = 0$, but at some small, but non-zero ω, and this is exponentially smaller than the dominant contribution from the right interval, which allows us to ignore it. This was only possible because of the asymmetry between α and μ (see figure 4.3), which is only true when $m \neq 0$. If we had $m = 0$, then $\alpha = -\mu$, which would result in the left and right frequency intervals giving the same contribution.

Finally, in $e_- < \omega < e_+$, we have to use the emission rate with real β. In the superradiant limit, this was obtained in equation (4.124), which we copy here

$$\left.\frac{d^2E}{d\omega\, dt}\right|_{\rm sc} = \frac{1}{\pi}\, 2^{4\Delta-3}\, (eQ)^{4\Delta-2}\, \frac{|\Gamma(\Delta + i\alpha)|^4}{\Gamma(2\Delta)^2\, \Gamma(2\Delta-1)^2}\, x^{2\Delta}\, (1-x)^{2\Delta-1}\,, \tag{4.166}$$

where $x = \omega/e$. The parameters Δ and α are found by taking the large eQ limit of equation (4.126), which gives

$$\begin{aligned} \Delta(x) &= eQ\, \sqrt{-1 + 6\, x\, (1-x)}\,, \\ \alpha(x) &= eQ\, (2x-1)\,. \end{aligned} \tag{4.167}$$

Also note that we can use $\mu = -\alpha$ in this interval, since their difference only appears near $\omega = 0$ (see figure 4.3). We can take the large eQ limit of the Gamma functions in the (4.166) using Stirling's approximation (5.21) for the ones in the denominator, and (5.22) for the one

in the numerator. This gives

$$\left.\frac{d^2E}{d\omega\, dt}\right|_{\rm sc} = \frac{x}{2\pi}\left(\frac{e^2\,(2x-1)}{12\sqrt{x(1-x)}}\right)^{4\Delta-2} e^{-2\pi|\alpha|}\,. \tag{4.168}$$

The second factor is a function of $x \in [x_-, x_+]$ raised to a very large power. One can check that this function never crosses 1 on this interval, which implies that the greybody factor is at least exponentially suppressed in $e^{-2\pi|\alpha|}$, which is a much higher degree of suppression than the contributions from the left (4.160) and right (4.165) intervals. This completes the argument that the dominant emission comes from $\omega = e$ when $eQ \gg 1$.

We now turn to the finite values of $eQ \geq 1/2$. Using equation (4.124) for the spectral rate on the inner interval and equation (4.155) for the outer intervals, and after changing variables to $x = \omega/e$, we find our final result for the semi-classical superradiant-dominated evaporation rate for large black holes

$$\left.\frac{dE}{dt}\right|_{\rm sc} = \sum_{l=0}^{\infty}\left(G_l(eQ) + G'_l(eQ)\right)\frac{1}{Q^2}\,, \tag{4.169}$$

where the coefficient functions are given by the following two integrals. For the first we have

$$G_l(eQ) = \frac{2l+1}{\pi}\int_{x_-}^{x_+} dx\, 2^{4\Delta-3}\,(eQ)^{4\Delta}\,\frac{|\Gamma(\Delta+i\alpha)|^4}{\Gamma(2\Delta)^2\,\Gamma(2\Delta-1)^2}\,x^{2\Delta}\,(1-x)^{2\Delta-1}\,, \tag{4.170}$$

where the bounds of integrations now go between $x_\pm = \omega_\pm/e$. And the second term is given by

$$G'_l(eQ) = \frac{2l+1}{2\pi}(eQ)^2\int_{x\in I_\pm} dx \frac{x\sinh^2 2\pi\beta}{\cosh\pi(\alpha-\beta)\cosh\pi(\mu+\beta)+\cosh\pi(\alpha+\beta)\cosh\pi(\mu-\beta)}e^{-\pi(\mu+\alpha)}\,, \tag{4.171}$$

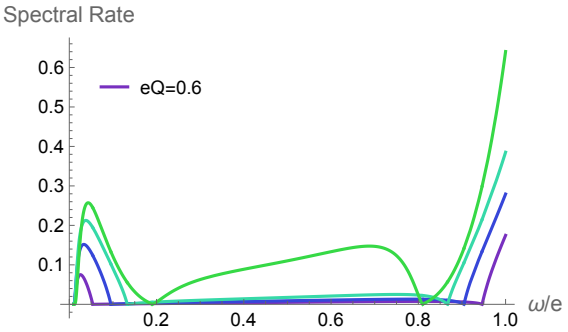
where the integration interval is given by $I_\pm = [0,\omega_-]\cup[\omega_+, e]$. The parameters Δ, α, β are

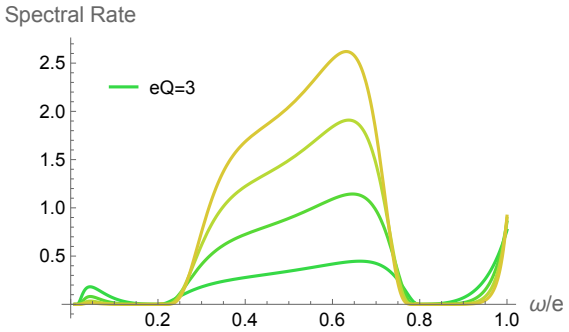
given by

$$\begin{aligned}\Delta(x,eQ) &= \tfrac{1}{2} + \sqrt{\tfrac{1}{4} + l(l+1) - (eQ)^2 + 6(eQ)^2\, x\,(1-x)}\,,\\ \alpha(x,eQ) &= eQ\,(2x-1)\,,\\ \beta(x,eQ) &= \sqrt{-\tfrac{1}{4} - l(l+1) + (eQ)^2 - 6(eQ)^2\, x\,(1-x)}\,.\end{aligned} \tag{4.172}$$

Note the sign flip in the square root in Δ and β!

We plot these rates in figure 4.5 for a broad range of $eQ \geq 1/2$. Starting with the top left panel at eQ close to $1/2$, we can see that the $eQ = 0.6$ spectrum, with maximum value of ~ 0.01 nicely matches onto to $eQ = 0.5$ found in figure 4.2, which has a maximum value of ~ 0.005. We can also clearly see that the interval is broken up into three regions, and that the rate is zero at $x_\pm$ as this is where $\Delta = 1/2$. As we start increasing eQ, the spectral rate starts rising on all three intervals, and the $x_\pm$ start moving inward and eventually settle at the limiting value, which agrees with (4.140). In the top right panel, we see that the rate on the middle interval keeps growing, while the left and right intervals start approaching zero, attaining their maxima at $\omega \approx 0$ for the left interval (4.165), and at $\omega = e$ for the right interval (4.160), which is the Gibbons result.





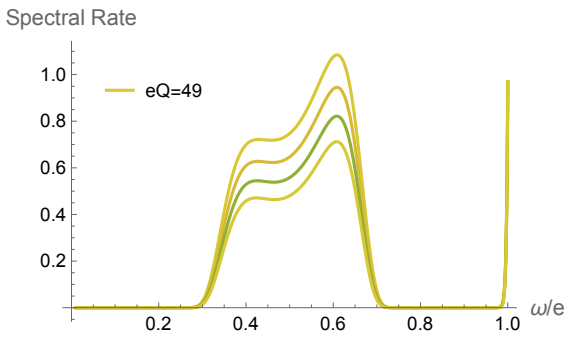


Figure 4.5: Spectral evaporation rate of a large black hole in the semi-classical superradiant-dominated regime at different values of eQ. Top left panel, eQ is goes from 0.6 to 1.8. Top right, eQ is between 3 and 9. Bottom, eQ is between 49 and 55. The mass of the particle is $m = 0.01e$.

On the bottom panel, we can see that eventually the rate on the middle interval also starts going towards zero. Notice that the rate on the right end appears to have reached a limiting value, which is slightly below one. This number is given by $\exp\left(-\pi eQ\frac{m^2}{e^2}\right)$. It is one on our plots, as the black hole eQ is still not large enough to overcome the small mass ratio $\frac{m^2}{e^2}$. If we kept increasing eQ, we would reach $Q = Q_* = \frac{e}{\pi m^2}$, equation (4.146), and this part of the rate would also start approaching zero.

4.4 Emission by a Kerr black hole

We repeat the same analysis for the near-extremal Kerr black hole, starting with the wave equation, which will have the same form. We will find that there are two important differences. First, the parameters μ and α in the solution of the wave equation will also have an imaginary spin-dependent part for both real and complex Δ. Secondly, the equation for the transmission coefficient for the fields with spin will be more involved.

4.4.1 Near-extremal Kerr Background

The Kerr solution describes a rotating black hole with mass M and angular momentum J. It is conventional to use the rotational parameter $a = J/M$ instead of J. The metric is found

to be

$$ds^2_{\rm Kerr} = -\frac{\rho^2\,\Delta}{\Xi}dt^2 + \frac{\rho^2}{\Delta}\,dr^2 + \rho^2\,d\theta^2 + \frac{\Xi}{\rho^2}\,\sin^2\theta\left(d\phi - \frac{2aMr}{\Xi}\,dt\right)^2\,, \tag{4.173}$$

with the functions given by

$$\begin{aligned} \Delta = r^2 - 2Mr + a^2\,, \qquad \rho^2 = r^2 + a^2\,\cos^2\theta\,, \\ \Xi = (r^2+a^2)^2 - a^2\,\Delta\,\sin^2\theta\,. \end{aligned} \tag{4.174}$$

The radii of the inner and outer horizons are given by

$$r_\pm = M \pm \sqrt{M^2 - a^2}\,. \tag{4.175}$$

To define an extremal and near-extremal Kerr black hole, we start with the extremality bound involving the mass and rotational parameter given by the following

$$M \geq a\,, \tag{4.176}$$

from which the story proceeds as before. The extremal horizon and the horizon measure of near-extremality are given by

$$\begin{aligned} r_h &= a\,, \\ \delta r &= r_+ - r_-\,. \end{aligned} \tag{4.177}$$

We can zoom into the near-horizon region using

$$\begin{aligned} r &= r_+ + \delta r\,x\,, \\ t &= \frac{r_+^2}{\delta r}\,\tau\,, \\ \phi &= \phi_{\rm NHR} + \frac{a}{r_+^2 + a^2}\frac{r_+^2}{\delta r}\,\tau\,, \end{aligned} \tag{4.178}$$

which when plugged into (4.173) and expanded in δr leads to the NHEK metric (Near-Horizon Extremal Kerr)

$$ds^2_{\rm NHR} = 2a^2\,\Omega^2(\theta)\,\left(-4x(x+1)\,d\tau^2 + \frac{dx^2}{x(x+1)} + d\theta^2 + \Lambda(\theta)\,(d\phi_{\rm NHR} + 2x\,dt)^2\right)\,, \quad (4.179)$$

with functions given by

$$\Omega^2(\theta) = \frac{1+\cos^2\theta}{2}\,, \qquad \Lambda(\theta) = \frac{2\sin\theta}{1+\cos^2\theta}\,. \quad (4.180)$$

We can see that when $\theta = \frac{\pi}{2}$, the metric reduces to AdS_2 with size $l_{\rm AdS} = 2a^2$. At arbitrary θ, the sphere is fibered over the factor of AdS_2.

We can define the thermodynamics of the Kerr black hole starting with the temperature and entropy which are defined as follows

$$\begin{aligned} T &= \frac{r_+ - r_-}{4\pi\,(a^2 + r_+^2)}\,, \\ S &= \pi(r_+^2 + a^2)\,. \end{aligned} \quad (4.181)$$

The parameter conjugate to the angular momentum is the angular velocity of the horizon and is given by

$$\Omega = \frac{a}{r_+^2 + a^2}\,. \quad (4.182)$$

The energy above extremality is given by

$$E = M - a\,. \quad (4.183)$$

The parameters δr, E and T are all small, if the black hole is near-extremal. They are related

as follows

$$\begin{aligned} \delta r &= 8\pi a^2 T\,, \\ E &= 8\pi^2 a^3 T^2\,. \end{aligned} \tag{4.184}$$

For the Kerr black hole, the thermodynamic breakdown scale is given by

$$E_{\rm b} = \frac{1}{2a^3}\,. \tag{4.185}$$

4.4.2 Wave equation and emission rate

Our goal is to solve the wave equation for a spin$-s$ field, and to compute the transmission coefficient. This was done by Press & Teukolsky [54, 55, 56] using the Newman-Penrose formalism, which works as follows. Out of our spin$-s$ field, a curvature invariant is built, which we will label with ψ for any spin. ψ satisfies a wave equation, which is separable. If one can solve this equation, the original spin$-s$ field perturbation can be extracted from the invariant, at least in principle. We will not repeat how the scalars ψ are related to the original spin$-s$ field perturbation and how the transmission coefficient of the spin$-s$ field is calculated from the perturbation. Both of these can be found in [54, 55, 56]. Instead, we will only solve the equation for ψ, and then directly quote how the transmission coefficient for the spin$-s$ field is written in terms of ψ.

We will also not repeat the full partial differential equation satisfied by the scalar ψ, which can also be found in these references. Instead, we will write down the ordinary differential equations that it separates into. Given the time translation and axial symmetries of the background, the solution to this equation has the following form

$$\psi(t, r, \theta, \phi) = e^{i\omega t}\, R(r)\, S_{slm}(\theta)\, e^{im\phi}\,. \tag{4.186}$$

This results in the following equation for the radial function

$$\Delta\frac{d^2R}{dr^2}+(s+1)\frac{d\Delta}{dr}\frac{dR}{dr}+\left(\frac{K^2-2is(r-M)K}{\Delta}+2am\omega-K_{slm}(a\omega)+4is\omega r\right)R=0\,,$$
$$K=(r^2+a^2)\,\omega-am\,. \tag{4.187}$$

The angular functions, known as the spin-weighted spheroidal harmonics, satisfy the following equation

$$\frac{1}{\sin\theta}\frac{d}{d\theta}\left(\sin\theta\frac{d}{d\theta}S_{slm}\right)+\left(K_{slm}(a\omega)-\frac{(m+s\cos\theta)^2}{\sin^2\theta}-(a\omega)^2\sin^2\theta-2a\omega s\cos\theta+s\right)S_{slm}=0\,, \tag{4.188}$$

where $K_{slm}(a\omega)=2ma\omega+\lambda_{slm}(a\omega)$, with $\lambda_{slm}(a\omega)$ being the eigenvalues associated with these functions[14]. The $(s+1)$ factor in the first derivative term of (4.187) can be removed with the following change of variable

$$\rho(r)=\Delta(r)^{s/2}\,R(r)\,. \tag{4.189}$$

which results in the following radial equation

$$\Delta\frac{d^2\rho}{dr^2}+\frac{d\Delta}{dr}\frac{d\rho}{dr}+\left(\frac{K^2-2is(r-M)K}{\Delta}+2am\omega-K_{slm}(a\omega)+4is\omega r-\frac{s^2\,\Delta'^2}{4\,\Delta}-\frac{s}{2}\,\Delta''\right)\rho=0\,. \tag{4.190}$$

We will solve this equation for near-extremal Kerr, for which we first have to set up the boundary conditions. A tortoise-like variable can be introduced using $dr_*=(r^2+a^2)\,dr/\Delta(r)$. Integrating this relationship gives

$$r_*=r+\frac{r_+^2+a^2}{\delta r}\ln(r-r_+)-\frac{r_-^2+a^2}{\delta r}\ln(r-r_-)\,, \tag{4.191}$$

[14]This follows the conventions defined in Press & Teukolsky. We will use the Mathematica package Black Hole Perturbation Toolkit [165] to calculate $\lambda_{slm}(a\omega)$ with the command "SpinWeightedSpheroidalEigenvalue$[s,l,m,a\omega]$".

with r_* going from $-\infty$ to $+\infty$. Following Press & Teukolsky, we will define the boundary conditions in the scattering problem by requiring the following asymptotic behavior for the radial function[15]

$$R(r_*) = \begin{cases} \frac{Y_{\rm trans}}{\Delta^s}\, e^{-i\omega_{\rm eff} r_*}\,, & r_* \to r_*(r_+) = -\infty \\ \frac{Y_{\rm inc}}{r}\, e^{-i\omega r_*} + \frac{Y_{\rm refl}}{r}\, \frac{1}{(\omega r)^{2s}}\, e^{+i\omega r_*}\,, & r_* \to r_*(+\infty) = +\infty \end{cases} \tag{4.192}$$

This also defines the amplitudes of the incident, reflected and transmitted waves $Y_{\rm inc}, Y_{\rm refl}, Y_{\rm trans}$. The wave number at the horizon is given by

$$\omega_{\rm eff} = \omega - \frac{ma}{r_+^2 + a^2}\,. \tag{4.193}$$

Given that $\omega_{\rm eff}$ can be negative, we find that the Kerr black hole can also emit superradiant modes. The threshold frequency defines the Kerr superradiant scale

$$\omega_{\rm sr} = \frac{ma}{r_+^2 + a^2} \approx \frac{m}{2a}\,, \tag{4.194}$$

where we have also included its near-extremal value.

In both the near and far regions, equation (4.190) reduces to exactly the same equations we had in subsection 4.1.2, equation (4.37) in the near region and (4.47) in the far. We will not repeat these here, but instead we will just give the solution parameters p, q (or

[15] If we were just dealing with a scalar field, we would further transform this equation into a 1D Schrodinger-like equation by defining a wavefunction $S(r)$ as follows $R(r) = S(r)/\sqrt{r^2 + a^2}$. Then, we could just use the 1D transmission coefficient equation (4.59). We will not go down this route, as our goal is to use the spin$-s$ transmission coefficient equations from Press & Teukolsky.

equivalently F and μ), β (or equivalently Δ), and α. These are summarized in the following

$$\begin{aligned} F &= F_{\rm r} + iF_{\rm i} = \frac{\omega_{\rm eff}}{4\pi T} - \tfrac{1}{2}is\,, \\ \mu &= \mu_r + i\mu_i = -2a\omega + is\,, \\ \beta &= \sqrt{\tfrac{1}{4} + K_{slm}(a\omega) + s(s+1) - 8a^2\omega^2}\,, \\ \Delta &= \tfrac{1}{2} + \beta\,, \\ \alpha &= \alpha_r + i\alpha_i = 2a\omega + is\,. \end{aligned} \tag{4.195}$$

Note the extra imaginary terms. It turns out that for certain combinations of the (s, l, m) mode numbers, β can be imaginary for on a subinterval of the frequencies. In the next subsection, we will discuss which modes have only real β and which have both. The near equation has the following solution after implementing the boundary conditions

$$\rho(x) = A\, x^{-iF_r - s/2}\,(1+x)^{+i(F_r+\mu_r)-s/2}\,{}_2F_1\left(\tfrac{1}{2}-\beta-s+i\mu_r,\, \tfrac{1}{2}+\beta-s+i\mu_r;\, 1-s-2iF_r;\, -x\right)\,. \tag{4.196}$$

We can check that this solution has the correct behavior near the horizon as follows. First, we can expand ρ near the horizon taking x to be small, then we can relate this to R using (4.189) and the fact that $\Delta(x) \sim \delta r^2\, x$ at small x, and finally we can write r in terms of r_* using (4.191) and evaluating this near the horizon. This results in

$$R(x \to 0) = \frac{A}{\delta r^s\, x^s}\, x^{-ip_r} = \frac{A\,\delta r^s}{\Delta^s}\, e^{-i\omega_{\rm eff}\, r_*}\,, \tag{4.197}$$

which we can see agrees with the expected behavior defined in (4.192). The equation in the far region has the following solution

$$\rho(y) = e^{-i\omega y} \sum_{\pm} C_\pm\, y^{-1/2\pm\beta}\, M\Big(\tfrac{1}{2} \pm \beta - s + i\alpha_r, 1 \pm 2\beta, 2i\omega y\Big)\,. \tag{4.198}$$

We can use the asymptotics of the confluent hypergeoemtric function (5.18), and the fact that far away $\Delta(y) \sim y^2$, to find the following behavior for $R(r)$ at infinity

$$R(y \to \infty) = C_-^\infty \, \frac{e^{-i\omega y}}{y} \, y^{+s-s} \, y^{-i\alpha_r} + C_+^\infty \, \frac{e^{+i\omega y}}{y} \, y^{i\alpha_r} \, y^{-s-s} \, . \tag{4.199}$$

which agrees with the boundary conditions defined in (4.192) with the first term being the incident and the second the reflected. In equation (4.199), we have introduced the following coefficients

$$C_\pm^\infty = C_+ \frac{\Gamma(1+2\beta)}{\Gamma(\frac{1}{2}+\beta\mp s\pm i\alpha_r)} (\pm 2i\omega)^{-1/2-\beta\mp s\pm i\alpha_r} + C_- \frac{\Gamma(1-2\beta)}{\Gamma(\frac{1}{2}-\beta\mp s\pm i\alpha_r)} (\pm 2i\omega)^{-1/2+\beta\mp s\pm i\alpha_r} \, . \tag{4.200}$$

The two solutions for $\rho(r)$ in the near (4.196) and far (4.198) regions can be matched in the overlapping region. Adding the extra $s-$dependent terms to what was found in equation (4.56) results in

$$C_\pm = \frac{\Gamma(\pm 2\beta)\, \Gamma(1-s-2iF_r)}{\Gamma(\frac{1}{2}\pm\beta-s+i\mu_r)\, \Gamma(\frac{1}{2}\pm\beta-2iF_r-i\mu_r)} \, \delta r^{+1/2\mp\beta} \, A \, . \tag{4.201}$$

Having solved the wave equation, we can proceed to compute the transmission coefficients or the greybody factors. From Press & Teukolsky, we quote the greybody factor for a spin$-s$ field (with $s = 0, 1, 2$), which can be found in equations (4.26), (4.32), and (4.44) of [56]. These are given in terms of the Kerr parameters M and a, and the amplitudes of the incoming and transmitted waves, which are defined in (4.192). Using the fact that we have a near-extremal black hole, so $M \approx a$, their equations can be written as follows

$$\begin{aligned} \Gamma_{s=0} &= 2a^2 \, \frac{\omega_{\text{eff}}}{\omega} \left| \frac{Y_{\text{trans}}}{Y_{\text{inc}}} \right|^2_{s=0} , \qquad \Gamma_{s=1} = 2a^2 \, \frac{\omega_{\text{eff}}}{\omega} \, \frac{\omega^2}{4a^4\omega_{\text{eff}}^2} \left| \frac{Y_{\text{trans}}}{Y_{\text{inc}}} \right|^2_{s=1} , \\ \Gamma_{s=2} &= 2a^2 \, \frac{\omega_{\text{eff}}}{\omega} \, \frac{\omega^4}{(4a^4)^2\omega_{\text{eff}}^2(\omega_{\text{eff}}^2 + (4\pi T)^2)} \left| \frac{Y_{\text{trans}}}{Y_{\text{inc}}} \right|^2_{s=2} . \end{aligned} \tag{4.202}$$

These can further be rewritten in terms of the geometric factors δr and F and brought under

the same product as follows

$$\Gamma_s = 2a^2\,\frac{\omega_{\rm eff}}{\omega}\,\frac{2^{2s}\,\omega^{2s}}{(\delta r)^{2s}\,\prod_{j=0}^{s-1}\left(j^2+(2F_r)^2\right)}\,\left|\frac{Y_{\rm trans}}{Y_{\rm inc}}\right|_s^2\,, \tag{4.203}$$

with the product absent when $s=0$.

To compute the greybody factors, we will need to square the wave amplitudes which, as we saw in 4.3, depends on whether β is real or imaginary. For the rest of this section, we will assume real β, and we will work out the factor for imaginary β in 4.4.4. Comparing equations (4.192) with (4.197), we find the amplitude of the transmitted wave to be[16]

$$Y_{\rm trans} = \delta r^s\,A\,, \tag{4.204}$$

which can then straightforwardly be squared. For the incident wave, we can ignore C_- relative to C_+ as it is subleading in δr. Comparing equation (4.192) with (4.199), we find that the amplitude of the incident wave is given by

$$Y_{\rm inc} = \frac{\Gamma(1+2\beta)}{\Gamma(1/2+\beta+s-i\alpha_r)}\,(-2i\omega)^{-1/2-\beta+s-i\alpha_r}\,C_+\,. \tag{4.205}$$

This can be further written in terms of A using the matching equation (4.201). Squaring the incident then gives

$$\begin{aligned}|Y_{\rm inc}|^2 = 2^{-2\Delta+2s}\,\delta r^{-2\Delta+2}\,\omega^{-2\Delta+2s}\,\frac{\Gamma(2\Delta)^2\,\Gamma(2\Delta-1)^2}{|\Gamma(\Delta+s-i\alpha_r)|^2\,|\Gamma(\Delta-s+i\mu_r)|^2}\\ \frac{|\Gamma(1-s-2iF_r)|^2}{|\Gamma(\Delta-2iF_r-i\mu_r|^2}\,e^{-\pi\alpha_r}\,.\end{aligned} \tag{4.206}$$

In the last fraction, we can factor out the spin dependence as follows

$$\frac{|\Gamma(1-s-2iF_r)|^2}{|\Gamma(\Delta-2iF_r-i\mu_r)|^2} = \frac{|\Gamma(1-2iF_r)|^2}{|\Gamma(\Delta-2iF_r-i\mu_r)|^2}\,\prod_{j=0}^{s-1}\frac{1}{j^2+4F_r^2}\,, \tag{4.207}$$

[16]Note that, for the scalar, this is different from the transmitted wave amplitude for Reissner-Nordström (4.61) due to the different way of defining the boundary conditions in (4.33) and (4.192).

where we have used some of the Gamma function identities (5.19) and (5.20). Plugging the incident amplitude (4.206) and the transmitted amplitude (4.204) into the greybody factor (4.203) and using this identity, we find the greybody factor for a spin-s field to be

$$\Gamma^{(s)}(a,T;\omega,l,m_l) = 2^{8\Delta-5}\pi^{2\Delta-2}a^{4\Delta-2}T^{2\Delta-2}\omega^{2\Delta-1}\omega_{\text{eff}}\frac{|\Gamma(\Delta+s-i\alpha_r)|^2\,|\Gamma(\Delta-s+i\mu_r)|^2}{\Gamma(2\Delta)^2\,\Gamma(2\Delta-1)^2} \\ \frac{|\Gamma(\Delta-2iF_r-i\mu_r)|^2}{|\Gamma(1-2iF_r)|^2}\,e^{\pi\alpha_r}\,, \tag{4.208}$$

where we have also written β in terms of Δ, and δr in terms of T. Note that the spin-dependent products has canceled. This can now be plugged into the Hawking formula (4.58), which gives the final emission rate for a massless spin-s field being radiated by a near-extremal Kerr black hole

$$\frac{d^2E}{d\omega\,dt}\Big|^{(s)}_{\text{sc}} = 2^{8\Delta-6}\,\pi^{2\Delta-3}\,a^{4\Delta-2}\,T^{2\Delta-2}\,\frac{|\Gamma(\Delta+s-i\alpha_r)|^2\,|\Gamma(\Delta-s+i\mu_r)|^2}{\Gamma(2\Delta)^2\,\Gamma(2\Delta-1)^2}\,e^{\pi\alpha_r} \\ \frac{\omega^{2\Delta}\,\omega_{\text{eff}}}{e^{\omega_{\text{eff}}/T}-1}\,\frac{|\Gamma(\Delta-2iF_r-i\mu_r)|^2}{|\Gamma(1-2iF_r)|^2}\,. \tag{4.209}$$

The parameters μ_r, Δ and α_r can be found in (4.195). When we set $s=0$ and compare with the Reissner-Nordström rate (4.71), there is an extra $2^{2\Delta-2}$ from the extra factor of 2 in δr, and there is an extra factor of 2 in the greybody factor flux (4.203). We will find it convenient to write the spin-s evaporation rate in terms of the spin-0 rate as follows

$$\frac{d^2E}{d\omega\,dt}\Big|^{(s)}_{\text{sc}} = \frac{|\Gamma(\Delta+s-i\alpha_r)|^2\,|\Gamma(\Delta-s+i\mu_r)|^2}{|\Gamma(\Delta-i\alpha_r)|^2\,|\Gamma(\Delta+i\mu_r)|^2}\,\frac{d^2E}{d\omega\,dt}\Big|^{(0)}_{\text{sc}}\,. \tag{4.210}$$

We can take the small frequency limit of this equation and check that it reproduces known results from the literature. In this limit, the spin-weighted spheroidal harmonic eigenvalues reduce to the following

$$K_{slm}(a\omega=0) = \lambda_{slm}(a\omega=0) = l(l+1)-s(s+1)\,, \tag{4.211}$$

so $\Delta = l + 1$. Furthermore, μ_r, $\alpha_r = 0$. We first consider the $s = 0$ rate and plug these parameters into (4.209), which results in

$$\left.\frac{d^2E}{d\omega\, dt}\right|_{\rm sc}^{(0)} = 2^{8l+2}\,\pi^{2l-1}\,a^{4l+2}\,T^{2l}\,\frac{l!^4\cdot l!^2}{(2l)!^2\,(2l+1)!^2}\,\frac{\omega^{2l+2}\,\omega_{\rm eff}}{e^{\omega_{\rm eff}/T}-1}\prod_{j=1}^{l}\left(1+\left(\frac{\omega_{\rm eff}}{2j\pi T}\right)^2\right)\,. \quad (4.212)$$

After using the double factorial identity, this result exactly matches what was found in [52], after taking the $M \approx a$ in their paper. For the case of $s = 1, 2$, we only need to evaluate the extra spin-dependent factor in (4.210) in this limit. This results in

$$\left.\frac{d^2E}{d\omega\, dt}\right|_{\rm sc}^{(s)} = \frac{(l+s)!^2\,(l-s)!^2}{l!^4}\left.\frac{d^2E}{d\omega\, dt}\right|_{\rm sc}^{(0)}\,, \quad (4.213)$$

which matches what was found in [53].

One could ask why the wave equation has the same form for the Reissner-Nordström and Kerr black holes. As mentioned in the opening of this chapter, the near wave equation is determined by the symmetries of the near-horizon region, which for both black holes is given by the enhanced AdS_2 symmetry. It was explicitly shown[17] in [70] for the scalar and [78, 77] for higher spin fields that the radial equation in NHEK (4.179) has the same form as that in the near-horizon region of Reissner-Nordström (4.16). For the far equation, it is easy to see that if one expands the Kerr metric (4.173) at large distance, it is has the same form as Reissner-Nordström (4.7), with the leading order term given by the Schwarzschild black hole.

4.4.3 Real Delta

Before turning to the evaporation rate, we first present a discussion of the types of near-extremal Kerr radiation in the spirit of subsection 4.2.1. We start with the conformal dimension. For certain combinations of the mode numbers s, l, and m, Δ can be complex

[17]These references fully worked in NHEK, which amounts to setting the frequency to the superradiant bound. We also point out that in the context of Kerr/CFT [72], the wave equation was solved in the full near-extremal Kerr geometry (not just NHEK) by breaking it up into a near and far region, but still at frequencies approximately equal to the superradiant bound [166, 167].

on a subset of the frequency range. It turns out that this is almost always the case for the modes with $l = m$, but there are modes where Δ is complex when $l \neq m$ and there are also modes where it is not complex when $l = m$. As we will see, the $l = m$ modes will be the dominant ones, which means that we always have to consider both real and complex Δ for the Kerr black hole.[18] In other words, here there is no notion of small versus large black holes. In this subsection, we will only compute the rates for the frequencies with real Δ, leaving the remainder for the next subsection.

As mentioned before, each mode that carries angular momentum m can be thought of as a charged particle with charge m, but there is one important difference between this "charged" particle and the particles in Reissner-Nordström, and that is the fact that we do not get to choose m as we did e, instead modes with all possible values of angular momentum need to be considered. In this sense, we have one less free parameter for Kerr, which leads to less diversity in the possible energy regimes and their emission spectra. Keeping this in mind, we can still plot $\log m$ versus $\log a$, which will tell us how $\omega_{\rm sr}$ compares to $E_{\rm b}$ for different combinations of a and m. This is done in figure 4.6 which has the $\frac{m}{2a} = \omega_{sr} = E_{\rm b} = \frac{1}{2a^3}$ line and two addition constraints. First, the black hole must have more angular momentum than the mode it is emitting, so $\sqrt{a} = J \geq m$. And secondly, the smallest angular momentum that can be emitted is $m = 1$. This second constraint we did not have in Reissner-Nordström.

[18] Since the conformal dimension depends on the spheroidal harmonic eigenvalue, which itself depends on and monotonically decreases with the frequency, one only needs to check the value of the spheroidal eigenvalue at $\omega_{\rm sr}$ to determine whether a mode has real or complex Δ. For scalar fields, this was done in [70] for the lowest few modes. We will repeat this for the photon and graviton.

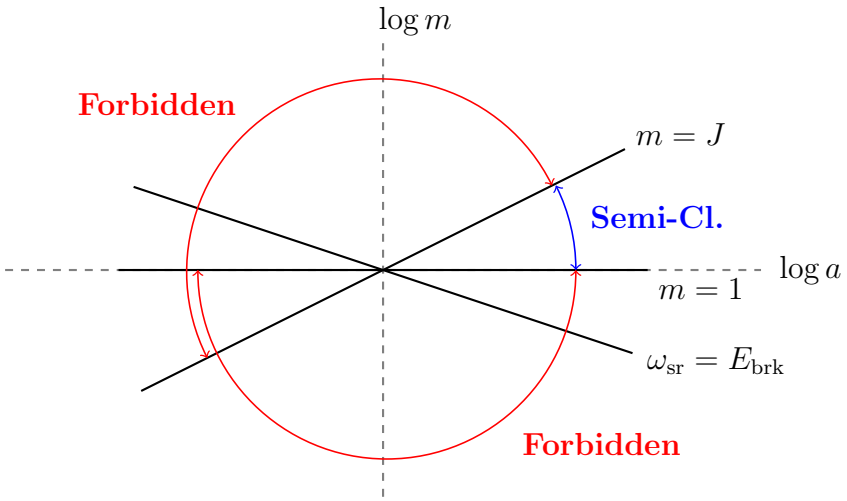


Figure 4.6: A diagram of $\log m$ vs. $\log a$ parameter space showing the available regions for radiation from a Kerr black hole. In the only available wedge, the emission rate is always given by the semi-classical formula (4.209). Δ can be both real and complex, depending on the mode.

What we find is that all of the allowed combinations of a and m must have $\omega_{\rm sr} \gg E_{\rm b}$, which by the arguments of 4.2.1 means that the energy ratio in the quantum evaporation rate (4.99) is always greater than one, regardless of the size of E, which then implies that the quantum rate, even if we computed it, would always reduce to the semi-classical formula, which is why we will only consider the semi-classical rate (4.209) for Kerr.

There is one more important difference between Reissner-Nordström and Kerr, which is the fact that for near-extremal Kerr there is only a superradiant-dominanted regime. To see this, for the semi-classical rate we need to check how the temperature T compares to the superradiant scale $\omega_{\rm sr}$. We are treating T as an independent parameter, but for a near-extremal black hole, it still has to be small, meaning $aT \ll 1$. Comparing $aT \ll 1$ to $a\omega_{\rm sr} = \frac{m}{2}$ which is at best an order one number, we find that $T \ll \omega_{\rm sr}$, which implies that near-extremal Kerr always radiates in the superradiant regime. Therefore, we only need to consider the range of frequencies $0 \leq \omega \leq \omega_{sr}$ as shown with equations (4.100) and (4.101).

This also implies that we have to consider both photon and graviton radiation. If there were a neutral-like regime, we would have $\Delta = l + 1$, and the photon would dominate, as it

has $l = 1$ as its lowest mode, while the graviton has $l = 2$, which would be suppressed due to a higher Δ. We will see that in the superradiant regime, both fields will have roughly the same Δ and produce comparable amounts of radiation. Furthermore, we can ignore "neutral" radiation, that is, modes with $m = 0$, since their evaporation rates are proportional to a power of temperature, while the rates for the "charged" modes will be constant.

To summarize, for near-extremal Kerr, the dominant modes in the emission specturm are those with $l = m$, most of these having both a real and complex Δ, while all other modes can be ignored, including $m = 0$. The spectrum will be given by the semi-classical Hawking formula and will be dominated by the superradiant frequencies. With that in mind, we can turn to computing the evaporation rate.

In the superradiant regime, we can approximate the $F-$dependent Gamma functions in the semi-classical rate (4.209) expanding in large $|F|$ as in (4.122). Furthermore, we can ignore the last factor in (4.209) at large $|F|$. The rate then reduces to

$$\left.\frac{d^2E}{d\omega dt}\right|_{\rm sc}^{(s)} = 2^{8\Delta-6}\pi^{2\Delta-3}a^{4\Delta-2}T^{2\Delta-2}\frac{|\Gamma(\Delta+s-i\alpha_r)|^2\,|\Gamma(\Delta-s-i\alpha_r)|^2}{\Gamma(2\Delta)^2\,\Gamma(2\Delta-1)^2}\omega^{2\Delta}|\omega_{\rm eff}|\left(\frac{\omega_{\rm eff}}{2\pi T}\right)^{2(\Delta-1)}\,, \tag{4.214}$$

where we used the fact that $\mu_r = -\alpha_r$ to cancel the exponential functions. We perform a change of variables $x = a\omega$, which gives our final result for the Kerr emission rate of a spin$-s$ field for frequencies with real Δ

$$\left.\frac{dE}{dt}\right|_{\rm sc}^{(s)} = H_{slm}\,\frac{1}{a^2}\,, \tag{4.215}$$

where the coefficients H_{slm} are now just numbers, not functions, and are given by the following integral

$$H_{slm} = \frac{1}{\pi}\int_0^{x_*} dx\, 2^{6\Delta-4}\,x^{2\Delta}\,\left(\tfrac{m}{2}-x\right)^{2\Delta-1}\,\frac{|\Gamma(\Delta-s+2ix)|^2\,|\Gamma(\Delta+s+2ix)|^2}{\Gamma(2\Delta)^2\,\Gamma(2\Delta-1)^2}\,, \tag{4.216}$$

where the frequency-dependent conformal dimension written as a function of x is given by

$$\Delta_{slm}(x) = \tfrac{1}{2} + \sqrt{\tfrac{1}{4} + K_{slm}(x) + s(s+1) - 2m^2x^2}\,. \tag{4.217}$$

If $\Delta(x)$ is real on the entire frequency range $0 \leq x \leq x_{\rm sr} = a\omega_{\rm sr} = m/2$, then $x_* = m/2$ and (4.215) covers the entire evaporation rate. If $\Delta(x)$ turns complex at some frequency, then the upper bound of integration x_* is the point where this happens, that is where $\beta(x)^2 = 0$ (the expression under the square root in $\Delta(x)$). In that case, (4.215) covers only a part of the evaporation rate and the remaining part we leave for the next subsection. To compute the numerical values of $K_{slm}(x)$ we use the Mathematica package Black Hole Perturbation Toolkit [165].

We can now compute the evaporation rate for $s = 0, 1, 2$, for the lowest few modes. One can check that for the scalar, the dominant $l = m$ modes have complex Δ starting at $l = m = 2$, while for the photon and graviton complex Δ starts at the lowest $l = m$ mode. Starting with the scalar, we numerically evaluate (4.216) for $l = 1, 2, 3$ and all possible $m \neq 0$. The results are summarized in the following table

	$l=m$	$l=m-1$	$l=m-2$
$l=1$	$0.0483\cdot10^{-3}$	/	/
$l=2$	$0.0729\cdot10^{-3}$	$\sim10^{-9}$	/
$l=3$	$0.0334\cdot10^{-3}$	$\sim10^{-9}$	$\sim10^{-14}$

Table 4.2: Table of energy and angular momentum emission rates for lowest few modes of a scalar field ($s = 0$) being radiated by a near-extremal Kerr black hole, obtained by evaluating the integrals in equation (4.216). This only account for the frequencies with real Δ.

This shows that at a given l, the rates for the modes with different m fall off very quickly with decreasing m. The trend continues if we go to higher l. This implies that it is safe to ignore modes with $l \neq m$, unless extremely high precision is required. Furthermore, this

shows that the contribution of the $l = m$ modes does not drop very quickly,[19] which implies that a number of these must be taken for any reasonable degree of precision, and therefore there is no single dominant mode for near-extremal Kerr radiation.

We can also write down an equation for the angular momentum emission rate, which takes the following form

$$\left.\frac{dJ}{dt}\right|_{\rm sc}^{(s)} = H^J_{slm}\,\frac{1}{a}\,. \tag{4.218}$$

To compute the coefficients H^J_{slm}, we replace a power of ω in (4.214) with a factor of m and then changing variables, which is straightforward and will not be explicitly shown here. We can now proceed to evaluate the energy and angular momentum emission rates for further scalar $l = m$ modes. These are given in the following table

$l = m$	1	2	3	4	5	6	7	8
$H^E_{0lm}\,[10^{-3}]$	0.0483	0.0729	0.0334	0.0115	0.0034	0.0010	0.0003	0.0001
$H^J_{0lm}\,[10^{-3}]$	0.1450	0.2007	0.0940	0.0328	0.0099	0.0028	0.0007	0.0002

Table 4.3: Table of energy and angular momentum emission rates for the most dominant modes, those with $l = m$, of a scalar field ($s = 0$) being radiated by a near-extremal Kerr black hole, obtained by evaluating the integrals in equation (4.216). This only account for the frequencies with real Δ.

This table should give a better sense of how quickly the contributions of subsequent modes drop. For the photon and graviton, the same patterns are observed. We compute the energy and angular momentum emission rates for the lowest eight modes, which are given in the following two tables.

[19] From this table it looks like the rate for the $l = m$ modes grows and then drops, but this is only true for the $l = m = 1$ mode of the scalar.

$l=m$	1	2	3	4	5	6	7	8
$H^E_{1lm}\,[10^{-3}]$	0.6022	0.2622	0.0832	0.0236	0.0063	0.0016	0.0004	0.0001
$H^J_{1lm}\,[10^{-3}]$	1.7135	0.7534	0.2412	0.0687	0.0183	0.0047	0.0012	0.0003

Table 4.4: Table of energy and angular momentum emission rates for the electromagnetic field ($s=1$). This only accounts for the frequencies with real Δ.

$l=m$	2	3	4	5	6	7	8	9
$H^E_{2lm}\,[10^{-3}]$	5.0565	0.9008	0.1690	0.0335	0.0068	0.0014	0.0003	0.0001
$H^J_{2lm}\,[10^{-3}]$	17.557	2.8857	0.5250	0.1024	0.0208	0.0043	0.0009	0.0002

Table 4.5: Table of energy and angular momentum emission rates for the gravitational field ($s=2$). This only accounts for the frequencies with real Δ.

Note that there is no $l=m=1$ mode for a spin-2 field. As mentioned before, all modes except for the scalar $l=m=1$ mode have Δ go complex on an upper part of the frequency range. Once we have computed the contribution from that part of the range, we will sum over all modes to obtain the full evaporation rate for a given spin.

4.4.4 Complex Delta

To compute the rate at complex Δ, we need to make the appropriate modifications to the solution of the wave equation and then rederive the greybody factor and evaporation rate. Most of this section will involve the same kinds of arguments used in section 4.3.2.

The first step is to make the replacement $\beta \to i\beta$ in the Kerr matching equation (4.201), which results in

$$C_\pm = \frac{\Gamma(\pm 2i\beta)\,\Gamma(1-s-2iF_r)}{\Gamma(\frac{1}{2}-s\pm i\beta+i\mu_r)\,\Gamma(\frac{1}{2}\pm i\beta-2iF_r-i\mu_r)}\,\delta r^{+1/2\mp i\beta}\,A\,. \tag{4.219}$$

We need to keep both $C_\pm$, since they involve the same (real) power of the small quantity δr, and one cannot be ignored relative to the other. Then, the same replacement is made in the

amplitude of the incident wave, which gives

$$Y_{\text{inc, }\pm} = \frac{\Gamma(1 \pm 2i\beta)}{\Gamma(\frac{1}{2} + s \pm i\beta - i\alpha_r)} \, (-2i\omega)^{-1/2+s\mp i\beta - i\alpha_r} \, C_{\pm} \, . \tag{4.220}$$

Plugging the matching condition (4.219) into this equation and squaring results in

$$\begin{aligned} |Y_{\text{inc, }\pm}|^2 = \frac{\delta r}{(2\omega)^{1-2s}} \frac{|\Gamma(1+2i\beta)|^2 \, |\Gamma(2i\beta)|^2}{|\Gamma(\frac{1}{2} + s \pm i\beta - i\alpha_r)|^2 \, |\Gamma(\frac{1}{2} - s \pm i\beta + i\mu_r)|^2} \\ \frac{|\Gamma(1 - s - 2iF_r)|^2}{|\Gamma(\frac{1}{2} \pm i\beta - 2iF_r - i\mu_r)|^2} \, e^{\pi(\mp\beta - \alpha_r)} \, |A|^2 \, . \end{aligned} \tag{4.221}$$

Since we only need to consider the superradiant regime, we can simplify the fractions that involve F as we did in equation (4.162). This gives

$$\frac{|\Gamma(1 - s - 2iF_r)|^2}{|\Gamma(\frac{1}{2} \pm i\beta - 2iF_r - i\mu_r)|^2} = e^{\pi(-\mu_r \pm \beta)} \prod_{j=0}^{s-1} \frac{1}{j^2 + (2F_r)^2} \, . \tag{4.222}$$

The spin product can be extracted using (5.19) and (5.20). Note that there is no μ_r next to the $2F$ in the product as in (4.207) since we are in the large F regime. Plugging this into equation (4.221) and using that fact that $-\mu_r = +\alpha_r \geq 0$, we have

$$|Y_{\text{inc, }\pm}|^2 = \frac{\delta r \, |F_r|}{2^{-2s}\omega^{1-2s}} \frac{|\Gamma(1+2i\beta)|^2 \, |\Gamma(2i\beta)|^2}{|\Gamma(1/2 \pm i\beta - i\alpha_r)|^4} \prod_{j=0}^{s-1} \frac{1}{j^2 + (2F_r)^2} \, |A|^2 \, . \tag{4.223}$$

Expanding the Gamma functions in terms of hyperbolic trigonometric functions, we find that this simplifies to

$$|Y_{\text{inc, }\pm}|^2 = \frac{\delta r \, |F_r|}{2^{-2s}\omega^{1-2s}} \frac{\cosh^2 \pi(\alpha_r \mp \beta)}{\sinh^2 2\pi\beta} \prod_{j=0}^{s-1} \frac{1}{j^2 + (2F_r)^2} \, |A|^2 \, . \tag{4.224}$$

This equation, together with the amplitude of the transmitted wave (4.204), can be plugged

into the greybody equation (4.203), which results in

$$\Gamma^{(s)} = -\frac{\sinh^2 2\pi\beta}{\cosh^2 \pi\left(\alpha_r + \beta\right) + \cosh^2 \pi\left(\alpha_r - \beta\right)} \,. \tag{4.225}$$

Even though the spin-dependent products canceled, there is still spin dependence hidden in $\beta(\omega)$.

As in 4.3.2, we omitted the cross-term between $Y_{\text{inc}+}$ and $Y_{\text{inc}-}$ when squaring, but for Kerr we do not have a parameter like eQ which we can tune to make one of these terms dominate. It turns out that $\alpha \geq \beta$ is true for almost all modes, and for those that it isn't they are still approximately equal. This means that the first term in the denominator will always dominate the second, and therefore we do get to omit the cross term, as well as the second term in the denominator. The greybody factor then simplifies to

$$\Gamma^{(s)} = -e^{-2\pi(\alpha_r - \beta)} \,. \tag{4.226}$$

After evaluating at $\omega = \omega_{\text{sr}}$ and ignoring the cross-term, equation (4.225) agrees with Starobinskii [52], who considered an extremal black hole and frequencies around the superradiant bound. Note that this is different from the limit in equation (4.212). Press & Teukolsky in [54, 55, 56] performed the same calculation for near-extremal Kerr. If we had not made the large $|F|$ approximation in (4.221) we would have recovered their result. They also took the extremal limit and recovered the Starobinskii result. It is not surprising that taking the superradiant large $|F|$ limit or the extremal limit gives the same result, since at extremality, all frequencies that are being radiated are superradiant.

The greybody factor can now be plugged into the Hawking formula, which in the superradiant regime amounts to multiplying by $-1/2\pi$. After a changing of variables $x = a\omega$, we obtain our final result for the Kerr emission rate of a spin$-s$ field for frequencies with

complex Δ

$$\left.\frac{dE}{dt}\right|_{\text{sc}}^{(s)} = H'_{slm}\,\frac{1}{Ga^2}\,. \tag{4.227}$$

If we use equation (4.226) for the greybody factor, we obtain the following for the H'_{slm} coefficients

$$H'_{slm} = \frac{1}{2\pi}\int_{x_*}^{\frac{m}{2}} dx\, x\, e^{-2\pi(x-\beta)}\,. \tag{4.228}$$

If we want higher precision, we can use equation (4.225), which would result in

$$H'_{slm} = \frac{1}{2\pi}\int_{x_*}^{\frac{m}{2}} dx\, x\, \frac{\sinh^2 2\pi\beta}{\cosh^2\pi\,(2x+\beta)+\cosh^2\pi\,(2x-\beta)}\,, \tag{4.229}$$

but this would still not give the exact answer, since the cross-terms are missing. The parameter β as a function of x is given by

$$\beta = \sqrt{2m^2x^2 - \tfrac{1}{4} - K_{slm}(\tfrac{mx}{2}) - s(s+1)}\,. \tag{4.230}$$

Note the flipped sign under the square root. The lower bound of integration x_* is given by $\beta(x_*) = 0$ as explained in the previous subsection. We can also compute the emission rate of angular momentum as in 4.4.3.

We compute the coefficients $H'_{sl;m}$ by numerically performing the integral in equation (4.228) for the scalar, photon, and graviton. The $l \neq m$ modes are again highly suppressed compared to the dominant $l = m$ modes whose contribution can be found in the following three tables.

$l=m$	1	2	3	4	5	6	7	8
$H^E_{0lm}\,[10^{-3}]$	0	0.0045	0.0115	0.0108	0.0076	0.0047	0.0027	0.0014
$H^J_{0lm}\,[10^{-3}]$	0	0.0092	0.0235	0.0222	0.0156	0.0095	0.0054	0.0029

Table 4.6: Table of energy and angular momentum emission rates for the most dominant modes, those with $l = m$, of a scalar field ($s = 0$) being radiated by a near-extremal Kerr black hole, obtained by evaluating the integrals in equation (4.229). This only account for the frequencies with complex Δ.

$l=m$	1	2	3	4	5	6	7	8
$H^E_{1lm}\,[10^{-3}]$	0.0141	0.0809	0.0675	0.0420	0.0232	0.0121	0.0061	0.0030
$H^J_{1lm}\,[10^{-3}]$	0.0285	0.1664	0.1387	0.0860	0.0475	0.0247	0.0124	0.0061

Table 4.7: Table of energy and angular momentum emission rates for the electromagnetic field ($s = 1$). This only accounts for the frequencies with complex Δ.

$l=m$	2	3	4	5	6	7	8	9
$H^E_{2lm}\,[10^{-3}]$	11.5373	3.6450	1.2039	0.4235	0.1566	0.0601	0.0237	0.0096
$H^J_{2lm}\,[10^{-3}]$	24.2331	7.5508	2.4756	0.8668	0.3196	0.1224	0.0482	0.0194

Table 4.8: Table of energy and angular momentum emission rates for the gravitational field ($s = 2$). This only accounts for the frequencies with complex Δ.

Note that there is no contribution from the $l = m = 1$ mode for the scalar since it has real Δ on the full frequency range. Another pattern can be observed if we compare these three tables with the ones from the previous subsection. The H'_{slm} start to be significantly bigger than the H_{slm} after a certain mode, which parallels what we found for charged radiation, where the frequencies with complex Δ (at least for the right half of the frequency interval) dominated the emission spectrum at large charge (see figure 4.5).

We can now add up the contribution from the H_{slm} and H'_{slm} coefficients for each spin to find the total emission rate. The following is found for the energy and angular momentum emission rates to the third digit.

	$H^E\,[10^{-3}]$	$H^J\,[10^{-3}]$
$s=0$	0.215	0.577
$s=1$	1.23	3.32
$s=2$	23.2	56.7

Table 4.9: Table of the total energy and angular momentum emission rates for the scalar ($s = 0$), electromagnetic ($s = 1$) and gravitational ($s = 2$) fields being radiated by a near-extremal Kerr black hole, obtained by adding up the contributions of all modes and all frequencies (those with real and complex Δ).

4.5 Discussion

Summary of Reissner-Nordström

The semi-classical and quantum-corrected evaporation rates are uniquely specified by the three parameters Q, E, and e. A choice of Q and e places us somewhere in figure 4.1 and determines whether we are dealing with a small black hole (bottom two wedges in 4.1) and we use equation (4.71) for the semi-classical and (4.95) for the quantum-corrected evaporation rate, as Δ is real across the entire frequency range, or a large black hole (top wedge in 4.1) where we use equation (4.71) for the semi-classical rate for frequencies with real Δ and (4.155) for frequencies with complex Δ. Q and e also determine the two energy scales $E_{\rm b}$ and $\omega_{\rm sr}$. Depending on how these two scales compare, we can distinguish two more cases. When $E_{\rm b} \ll \omega_{\rm sr}$, the radiation will always be semi-classical (top two wedges in figure 4.1), and when $\omega_{\rm sr} \ll E_{\rm b}$ (bottom wedge in figure 4.1), the radiation can be either semi-classical or quantum, depending on whether $E_{\rm b} \ll E$ or $E \ll E_{\rm b}$, respectively. Semi-classical radiation has the quantum-corrected formula reduce to the semi-classical one to leading order, whereas for quantum radiation, the quantum rate gives genuinely different predictions from the semi-classical formula. Furthermore, depending on how E compares to $\omega_{\rm sr}$, the radiation will come out as neutral-like or superradiant-dominated. The different ways of ordering

these three energy scales and the corresponding regimes they define are summarized in table 4.1. The rates for small black holes are given in (4.111) (semi-classical neutral-like), (4.116) (quantum neutral-like), (4.124) (semi-classical superradiant-dominated) and (4.132) (quantum superradiant-dominated), and for large black holes in (4.169). When the black hole starts at any combination of these three parameters, as it emits radiation, it is driven away from extremality, which means that E grows. This implies that it will move through possibly a number of these regimes during its evolution towards non-extremality. We now turn to a discussion of this evaporation history for each type of black hole.

Evaporation history of near-extremal Reissner-Nordström

For the remainder of the discussion, we reintroduce G into our formulas. We start with the smallest black holes, those with $\omega_{\rm sr} \ll E_{\rm b}$, or $Q \leq \frac{1}{\sqrt[3]{e}}$ (bottom wedge of figure 4.1). We will also have the black hole start arbitrarily close to extremality, which means that it starts with $E \ll \omega_{\rm sr} \ll E_{\rm b}$, the quantum superradiant-dominated regime, with its evaporation rate captured by the dominant $l = 0$ mode and given by

$$\frac{dE}{dt} = \frac{32\sqrt{2}}{105\,\pi^2}\,(eQ)^4 \left(\frac{\sqrt{G}E_{\rm b}}{e}\right)^{\frac{1}{2}} \frac{1}{GQ^2}\,. \tag{4.231}$$

We remind the reader that eQ is small in most of this wedge, so we can use the small charge limit of our equations. As the black holes moves away from extremality, the energy eventually surpasses the superradiant scale and the black hole crosses into the quantum neutral-like regime with $\omega_{\rm sr} \ll E \ll E_{\rm b}$ where the dominant contribution to the rate is given by

$$\frac{dE}{dt} = \frac{16\sqrt{2}}{105\,\pi^2} \left(\frac{\sqrt{G}E}{Q}\right)^2 \left(\frac{E}{E_{\rm b}}\right)^{\frac{3}{2}} \frac{1}{GQ^2}\,. \tag{4.232}$$

The energy continues to rise, and eventually the semi-classical regime with $\omega_{\rm sr} \ll E_{\rm b} \ll E$ is reached, where the evaporation rate just reduces to the semi-classical answer

$$\frac{dE}{dt} = \frac{1}{30\pi}\left(\frac{\sqrt{G}E}{Q}\right)^2 \frac{1}{GQ^2}\,. \tag{4.233}$$

Eventually, the black hole leaves the region of extremality $\frac{\sqrt{G}E}{Q} \ll 1$. We can see that the evaporation history, at least while it is in the near-extremal region, is significantly different from the one predicted by the semi-classical formula - it starts out emitting superradiant radiation that is enhanced compared to the semi-classical answer, then it emits neutral-like radiation that is suppressed compared to semi-classical, and finally it exits the quantum regime. Given that the quantum superradiant-dominated rate is strongly suppressed compared to the neutral-like rate (their ratio goes like $(\frac{e}{E})^{7/2} \ll 1$), most of the time in the near-extremal regime is spent emitting superradiant radiation, and since this is enhanced compared to semi-classical rate, the black hole spends overall less time in the near-extremal regime than would be expected based on semi-classical theory.

In the above, we assumed that charged emission drives the black hole away from extremality. We can check that this is indeed the case using the energy and charge emission rates. In the black hole parameter space (M, Q), the extremal line is given by $M = Q$. As long as the slope of the evaporation trajectory in this space has a slope smaller than one (the black hole moves towards smaller Q and M), the black hole will be moving away from this line, away from extremality. This slope can be found from the energy and charge emission rates as follows[20]

$$\frac{dM}{dQ} = \frac{dE}{dt}\Big/\frac{dQ}{dt} \leq 1\,. \tag{4.234}$$

In the quantum superradiant regime, these rates are given by (4.135) and (4.136), which

[20]Note the misleading use of notation. M stands for the total black hole energy, E stands for energy above extremality, and dE/dt does not stand for the derivative of E, but M!

gives the following value for the slope

$$\frac{dM}{dQ} = \frac{4}{7}\,. \tag{4.235}$$

This proves that the black hole is driven away from extremality in this regime. For both the quantum and semi-classical neutral-like regimes, we can see from equations (4.120) and (4.114) that dQ/dt has one less power of E/Q than dE/dt, which implies that the slope dM/dQ is of the order of $E/Q \ll 1$. Therefore, it is nearly horizontal and the black hole moves away from the extremal line.

In addition to charged radiation, the black hole also emits neutral radiation. If we assume this is a universe like ours where there is no (massless) neutral scalar, but there is a photon-like particle in addition to the graviton, we can use the results of [60] for the evaporation rates of these particles. In the quantum superradiant regime, due to the fact that $E \ll e$, neutral radiation, which is of the order of a power of E/Q, is completely suppressed compared to charged radiation, which is proportional to eQ. In the two neutral-like regimes that follow, both charged and neutral radiation are proportional to a power of E, which is determined by the conformal dimension Δ. For the dominant $l = 0$ mode, for our charged scalar, $\Delta = \frac{1}{2} + \sqrt{\frac{1}{4} - (eQ)^2} \approx 1$ when $eQ \ll 1$. For the photon and graviton, [60] found the dominant modes to have $\Delta = l + 1 = 2$ and $\Delta = 3$ for the photon and graviton, respectively.[21] This means that they can also be safely ignored relative to the emission of charged particles. If there are also heavier charged particles that the black hole can emit, their emission rates will also be suppressed because the conformal dimension grows with mass.

For completeness, we comment on the mid-sized black holes (middle wedge in figure 4.1), where the quantum rates for charged radiation just reduce to the semi-classical in all available energy regimes. A mid-sized black hole is one with $E_{\rm b} \ll \omega_{\rm sr}$ and $Q \leq \frac{1}{2e}$, so $\frac{1}{\sqrt[3]{e}} \leq Q \leq \frac{1}{2e}$.

[21] In fact, if the black hole has zero angular momentum, it cannot radiate single photons/gravitons, as they carry away angular momentum. Instead it has to radiation two photons/gravitons at once with equal and opposite angular momentum. Quantum-mechanically this process is highly suppressed, which results in an even higher suppression in temperature for the evaporation rate.

If we start very close to extremality, the black hole goes from the $E \ll E_{\rm b} \ll \omega_{\rm sr}$ regime to $E_{\rm b} \ll E \ll \omega_{\rm sr}$. Both of these are semi-classical superradiant-dominated regimes. As the energy keeps growing, the semi-classical neutral-like regime $E_{\rm b} \ll \omega_{\rm sr} \ll E$ is reached, and then eventually the black hole leaves the near-extremal region. Note that something new happens for these black holes. As the black hole emits radiation, it also loses charge, which means that its trajectory in figure 4.1 is a leftward straight line. Therefore, if the black hole starts in the middle wedge, there is a possibility that it crosses into the bottom wedge, while still in the near-extremal regime. For the process we considered, we assumed that it leaves extremality before reaching the bottom wedge, but one could also imagine a more complicated evaporation history, where the initially mid-sized black hole becomes small while still in the near-extremal region, passing along the way through a richer sequence of energy regimes, some of which are possibly quantum.

Finally, for large black holes, those with $Q \geq \frac{1}{2e}$, when eQ is not too big, the story is similar to the mid-sized black holes. In the limit that eQ is big, the Gibbons suppression kicks in for charged emission and the black hole, through neutral emission, has sufficient time to re-enter the near-extremal region, once it has left it. This is just the story of the black holes studied in [60], and was also briefly summarized in the opening of this chapter.

Evaporation history of near-extremal Kerr

For near-extremal Kerr radiation, we argued that for all modes the superradiant scale is always above the breakdown scale, and therefore the quantum-corrected rate is to leading order always given by the semi-classical formula (4.209). We also argued that emission is dominated by the superradiant frequencies for all modes. We saw that the dominant modes are those with $l = m$, and for almost all of these we found that the conformal dimension Δ can be both real and complex on the frequency range $0 \leq \omega \leq \omega_{\rm sr}$. The evaporation rates are computed by equations (4.215) (Δ is real) and (4.227) (Δ is complex) for single modes. The summed evaporation rate (over the first 10 or so modes) can be found in table 4.9. For our

Universe, where we just have a photon and graviton, the evaporation rate is given by

$$\left.\frac{dE}{dt}\right|^{(\mathrm{ph+gr})} = 0.0244\,\frac{1}{Ga^2}\,. \tag{4.236}$$

We did not explicitly include the "neutral" $m = 0$ mode, since it scales with T and can be ignored. Using 4.9, we can also find the ratio of photon versus graviton radiation for near-extremal Kerr. For the emitted energy and angular momentum we find the following ratio

$$\begin{aligned} \text{energy:}\ & 5.0\%\ \ \text{photon}\ \ \text{vs.}\ \ 95.0\%\ \ \text{graviton}\,, \\ \text{ang.\,mom.:}\ & 5.5\%\ \ \text{photon}\ \ \text{vs.}\ \ 94.5\%\ \ \text{graviton}\,. \end{aligned} \tag{4.237}$$

We can check that these rates drive the black hole away from extremality, the $M = a$ line in M vs. a parameter space, which is true if

$$\frac{dM}{da} \leq 1\,. \tag{4.238}$$

We can rewrite the left side using $a = J/M$ in terms of the ratio of the energy and angular momentum flux

$$\frac{dM}{da} = \frac{M\,\frac{dM}{dJ}}{1 - a\,\frac{dM}{dJ}}\,. \tag{4.239}$$

Plugging this into (4.238) and using the near-extremal condition $M \approx a$ gives the following bound for dM/dJ

$$\frac{dM}{dJ} \leq \frac{1}{2\sqrt{GJ}}\,. \tag{4.240}$$

Using the rates from table 4.9, we find for the scalar, photon and graviton the following

$$\frac{dM}{dJ} = 0.373\,\frac{1}{\sqrt{GJ}}\,, \qquad \frac{dM}{dJ} = 0.371\,\frac{1}{\sqrt{GJ}}\,, \qquad \frac{dM}{dJ} = 0.409\,\frac{1}{\sqrt{GJ}}\,, \tag{4.241}$$

which confirms that the emission of each of these fields drives the black hole away from

extremality confirming the numerical results of [58].

Note that even though the evaporation rate is not corrected, the Schwarzian theory still gives corrections to the thermodynamics, as long as the black hole is below the breakdown scale as shown in Chapter 2. These evaporation rates can be used to address the following question, which was raised in that chapter. The time scale associated with these quantum corrections to the thermodynamics is given by the inverse of the breakdown scale, so $t_{\text{thermo}} \sim a^3$. The question was whether the black hole spends enough time below the breakdown scale for these corrections to be noticeable. Integrating the rates found in table 4.9 from $E = 0$ to $E = E_{\text{b}}$, we find the time to be of order $t_{\text{evap}} \sim 1/a$, which is very short compared to the thermodynamic time scale.

Instanton in the near-horizon region

As mentioned in the opening of this chapter, an alternative way of deriving the emission rate of charged particles, is using the instanton method [63, 64, 65]. This amounts to computing the rate of decay of the black hole to a lower energy state, through the emission of a particle-antiparticle pair. The rate is given in terms of the on-shell Euclidean action of a geometry called the instanton, which consists of the black hole geometry corrected by the worldline of the pair [168]. The instanton associated with the emission of a light charged particle from a large near-extremal Reissner-Nordström black hole was found in the full 4D geometry by [60], which resulted in the same exponentially suppressed Gibbons decay rate found from the wave equation. One benefit of doing the gravitational instanton calculation is that it incorporates the gravitational backreaction to the pair production process, which leads to terms that correct the decay rate.

To lay some groundwork for a future analysis of this effect, we point out an alternative way of doing the calculation. One can work directly in the AdS_2 part of the near-horizon region, where the instanton was found in [168]. In Appendix B of [169], it was shown that the decay rate corresponding to this instanton also gives the Gibbons result. We suggest

checking whether other geometrical properties of the instanton (its radius, conical angle, etc.) agree with the ones found from the 4D calculation in the near-extremal limit, as these quantities play an important role in the analysis of quantum fluctuations on top of this geometry, including those coming from the Schwarzian mode. The advantage of doing the 2D calculation over the 4D one is that it can easily be adapted to the near-horizon region of Kerr, which also has an AdS_2 structure, and where the 4D calculation would be significantly harder. In fact, we saw in subsection 4.4.4 that at complex Δ we obtain a Gibbons-like exponential suppression with the same form for the emission rate in Kerr (4.226) as in Reissner-Nordström, which provides further motivation for the study of instantons.

Future directions

For the "mid-sized" and large black holes in Reissner-Nordström (upper two wedges in figure 4.1) and for all Kerr black holes, we argued that the quantum-corrected evaporation rate (4.95) to leading order is always given by the semi-classical formula (4.71). It would be interesting to find the quantum corrections to this semi-classical leading order term in the relevant expansion parameter, which for the neutral-like radiation was $E/E_{\rm b}$, and for the superradiant-dominated radiation was $\omega_{\rm sr}/E_{\rm b}$. Furthermore, the evaporation rate was obtained using the first-order term in a perturbative expansion. This expansion involves the same three energy scales and relies on a certain combination to be small. Therefore, one would also need to check whether the second order term in this perturbative expansion would be comparable to the sub-leading quantum correction at first order perturbation theory. Going to higher order in perturbation theory would also allow us to compute processes involving the emission of two or more quanta, such as the di-photon/graviton emission studied in [60].

In the same spirit, a more interesting question is the following. For large Reissner-Nordström black holes and for certain Kerr modes, we found that Δ was complex on a subset of frequencies. We only argued that for these modes, the superradiant scale is always above the breakdown scale, which implies that the leading order term is always captured by

the semi-classical formula, and therefore we were able to get away without computing the quantum-corrected rate, but only the semi-classical, which only relies on the wave equation, where Δ is just another parameter, and it being complex does not represent a problem. But we could still ask how would the quantum-corrected rate be computed in this case, i.e. how would Schwarzian theory with a complex Δ work in the effective string formalism? A complex Δ is a sign of instabilities in the 2D theory in the AdS_2 part of the near-horizon region. These are closely related to the instanton calculation mentioned earlier (see e.g. [169, 170]). It would be interesting to revisit this instanton calculation with the goal of developing a better understanding of complex Δ in Schwarzian theory. We plan to explore this question in future work.

Chapter 5

Appendix

5.1 Rotational zero mode: compensating diffeomorphism

According to [27], the zero modes of the extremal Kerr black hole geometry are associated to large diffeomorphisms that act on the boundary of the throat. Their concrete profile in the bulk is sensitive to gauged diffeomorphisms that fall off fast enough near the boundary. Therefore, the precise profile of the zero modes is uniquely determined only after a choice of gauge fixing term in the action. The naive zero modes are associated to the isometries of the AdS_2 factor in the geometry, namely the tensor modes analyzed in section 2.2.3, and to the rotation around φ. The purpose of this Appendix is to show that, working in harmonic gauge as in Eq. (2.37), the rotational (would-be) zero mode has actually a non-zero action even at zero temperature. This is the puzzle explained in section 2.2.3.

We shall begin with some general comments that will simplify the analysis below. The Einstein-Hilbert action including the Gibbons-Hawking-York boundary term can be expanded to quadratic order around a solution of the equations of motion. We denote the kernel by

$\widetilde{\Delta}_L$, such that

$$-\int \mathrm{d}^4x\sqrt{g}\,R - 2\oint \mathrm{d}^3x\sqrt{\gamma}\,K = I_{\text{classical}} + \int \mathrm{d}^4x\,\sqrt{g}\,\frac{1}{4}\,\widetilde{h}^{\mu\nu}\widetilde{\Delta}_L\,h_{\mu\nu} + \mathcal{O}(h^3) \tag{5.1}$$

The relation between this operator and the one defined through (2.39) is

$$\Delta_L h_{\mu\nu} = \widetilde{\Delta}_L h_{\mu\nu} - \underbrace{2\nabla_\mu\nabla_\rho h^\rho{}_\nu + \nabla_\mu\nabla_\nu h^\rho{}_\rho + g_{\mu\nu}\left(\nabla_\rho\nabla_\sigma h_{\rho\sigma} - \frac{1}{2}\nabla_\rho\nabla^\rho h^\sigma{}_\sigma\right)}_{\text{From Gauge-Fixing Term}}. \tag{5.2}$$

One can check explicitly that $\widetilde{\Delta}_L\nabla_\mu\xi_\nu = 0$ as expected from a diffeomorphism invariant action. The rest of the right hand side comes purely from the gauge fixing term $I_{\text{gf}} = \frac{1}{32\pi G_N}\int \mathrm{d}^4x\,\sqrt{g}\,\mathsf{GF}_\mu\mathsf{GF}^\mu$, where for convenience we defined

$$\mathsf{GF}_\mu \equiv \nabla_\rho h^\rho{}_\mu - \frac{1}{2}\nabla_\mu h^\rho{}_\rho. \tag{5.3}$$

Instead of finding the zero modes of Δ_L, in this section we will look for diffeomorphism ξ such that $\mathsf{GF}_\mu = 0$, which automatically implies that

$$\mathsf{GF}_\mu = 0 \implies \Delta_L\nabla_\mu\xi_\nu = 0. \tag{5.4}$$

After these preliminaries we can start our analysis. First, we shall remind the reader that the naive rotational vector zero mode is generated by a linear combination of diffeomorphisms

$$\textit{Ansatz 1:} \qquad \xi^\mu_R = e^{\mathrm{i}n\tau} f(y)\,(\partial_\varphi)^\mu\,. \tag{5.5}$$

In analogy with the Schwarzian modes we expect $f(y) \propto (\frac{y-1}{y+1})^{\frac{n}{2}}$. Our main observation is that this transformation is not in the harmonic gauge since

$$\mathsf{GF}_y = e^{\mathrm{i}n\tau}\frac{4n\sin^2\theta}{(y^2-1)(1+\cos^2\theta)^2}f(y), \quad \Rightarrow \quad f(y) = 0. \tag{5.6}$$

This implies that there is no diffeomorphism taking the form (5.5) that is a zero mode of $\Delta_L h_{\mu\nu}$. The second option we could try is

$$\textit{Ansatz 2:} \qquad \xi^\mu_R = e^{in\tau}\left(f_1(y)\,\frac{\partial}{\partial y} + f_2(y)\frac{\partial}{\partial t} + f_3(y)\frac{\partial}{\partial \varphi}\right). \tag{5.7}$$

Nevertheless, we already proved in section 2.2.3 that the only diffeomorphism of this form that generates a zero mode of $\Delta_L h_{\mu\nu}$ are the Schwarzian modes themselves and not the new rotational zero mode we are looking for. Next, we consider a generalization

$$\textit{Ansatz 3:} \qquad \xi^\mu_R = e^{in\tau} f_\mu(y)\,\frac{\partial}{\partial x^\mu}. \tag{5.8}$$

This adds a (y,τ)-dependent generator along θ compared to the previous case. When evaluating the gauge fixing term we find $(\sin^2\theta\,\mathsf{GF}_\theta)|_{\theta\to 0} = -e^{in\tau} f_\theta(y)$ and therefore $f_\theta(y) = 0$, getting us back to the previous case (5.7).

Since we find no (y,τ)-dependent diffeomorphism that produces a zero mode, we next allow for θ-dependence along some coordinates. We assume adding a dependence with φ will never result in a zero mode. A reasonable generalization of our ansatz since we know the wave equation around the Kerr geometry to be separable is therefore

$$\textit{Ansatz 4:} \qquad \xi^\mu_R = e^{in\tau}\left(\alpha(\theta) f_1(y)\,\frac{\partial}{\partial y} + \alpha(\theta) f_2(y)\frac{\partial}{\partial t} + f_3(y)\frac{\partial}{\partial \varphi}\right). \tag{5.9}$$

One can show once again no such diffeomorphism exists such that $\mathsf{GF} = 0$. The procedure is a bit more involved, so we will only outline it. First, we look at $\mathsf{GF}_\theta = 0$ which determines $f_2(y)$ in terms of $f_1(y)$. Next we evaluate GF_y in an expansion around $\theta = 0$. We find that in order for $\mathsf{GF}_y = 0$ order by order in θ we need to impose $\alpha'(0) = 0$, $\alpha''(0) = \alpha(0)/2$, and $\alpha'''(0) = \alpha''''(0) = 0$ but the equations that determine $\alpha^{(4)}(0)$ and $\alpha^{(6)}(0)$ are incompatible leaving $\alpha^{(n)}(0) = 0$ as the only solution for $n = 0, \ldots, 6$. Carrying this out to higher orders we expect the only solution to be $\alpha(\theta) = 0$. At that point we are back to one of the previous

cases.

Instead of following this route to try and generalize the angle dependence, we found the following choice to simplify the result. Take the diffeomorphism to be

$$\textit{Ansatz 5:} \qquad \xi^\mu_R = e^{\mathrm{i}n\tau} f_4(y) \left(\frac{\partial}{\partial\varphi}\right)^\mu + \xi^\mu_H\,, \quad \xi^H_\mu \,\mathrm{d}x^\mu = e^{\mathrm{i}n\tau}(f_1(y)\mathrm{d}y + f_2(y)\mathrm{d}\tau + f_3(y)\mathrm{d}\varphi). \tag{5.10}$$

This combination of the naive rotational zero mode proportional to ∂_φ and a compensating diffeomorphism. The latter is presented in terms of its dual one-form to simplify the evaluation of GF_μ. When the components are written down explicitly, this choice introduces dependence on θ through the metric factor needed to raise the index of ξ_H. After some tedious calculation we can show that the only solution is $f_1(y) = f_2(y) = f_3(y) = f_4(y) = 0$. To see this first determine $f_2(y)$ from $\mathsf{GF}_\theta = 0$. Then $f_3(y)$ can be determined from $\mathsf{GF}_\varphi(\theta = 0) = 0$. From $\mathsf{GF}_y(\theta = 0) = 0$ and smoothness at the horizon we can find $f_1(y)$ and finally $f_4(y)$ from $\mathsf{GF}_y(\theta = \frac{\pi}{2}) = 0$. After this we can verify the solution is not in the harmonic gauge unless all f's vanish.

Finally, we try the last ansatz, using which we do find a solution. This is the one quoted in section 2.2.3, which happens to be singular.

$$\textit{Ansatz 6:} \qquad \xi^\mu_R = e^{\mathrm{i}n\tau} f_4(y)\frac{\partial}{\partial\varphi} + \xi^\mu_H, \qquad \xi^H_\mu \,\mathrm{d}x^\mu = e^{\mathrm{i}n\tau}\alpha(\theta)(f_1(y)\mathrm{d}y + f_2(y)\mathrm{d}\tau). \tag{5.11}$$

This solution can be ruled out using similar tricks as in the previous cases. Nevertheless, this gets the closest to a possible solution, provided we are willing to live with a singularity on the axis. For example, using the ansatz

$$f_4(y) = c\left(\frac{y-1}{y+1}\right)^{\frac{n}{2}}\,, \quad f_1(y) = \partial_y f(y)\,, \quad f_2(y) = \mathrm{i}\,n\, f(y)\,, \quad f(y) \equiv \left(\frac{y-1}{y+1}\right)^{\frac{n}{2}}\,, \tag{5.12}$$

where c is an arbitrary coefficient, we can put this diffeomorphism in the harmonic gauge as

long as

$$\alpha(\theta) = c_1 + c_2 \left(\cos\theta + 2 \log\tan\frac{\theta}{2} \right) + 4 \log\sin\theta \,. \tag{5.13}$$

This is the result quoted in section 2.2.3. There is no choice of c_1 and c_2 such that $\alpha(\theta)$ is smooth along the sphere. We tried adding a component along θ to the compensating diffeomorphism $\xi^H_\mu \, \mathrm{d}x^\mu \to \xi^H_\mu \, \mathrm{d}x^\mu + e^{\mathrm{i}n\tau} \, \beta(\theta) \, (\frac{y-1}{y+1})^{\frac{n}{2}} \, \mathrm{d}\theta$ but found $\beta(\theta) = 0$ to be the only smooth solution regardless of $\alpha(\theta)$.

Incidentally, if we only seek a compensating vector field ξ_H that brings our guess $\xi^\mu_R = \left(\frac{y-1}{y+1}\right)^{\frac{n}{2}} \, e^{\mathrm{i}n\tau} \, \frac{\partial}{\partial\varphi}$ to harmonic gauge, we can do so in a slightly simpler manner. Demanding that $\mathsf{GF}_\mu = 0$ for a diffeomorphism along $\xi_R + \xi_H$, implies that ξ_H satisfy

$$\nabla_\mu \nabla^\mu \xi^H_\rho = \frac{4\, g_2}{g_1} \left(\partial_y f \, \mathrm{d}y + i \, n \, f \, \mathrm{d}\tau \right), \tag{5.14}$$

with $f(y)$ given in (5.12). This equation can be solved directly to recover the vector field quoted in the main text in section 2.2.3. This is, of course, no different from what was described above, but it is helpful to note that the compensating diffeomorphism satisfies an inhomogeneous Laplace equation.

To summarize the discussion, we were unable to find a compensating diffeomorphism that puts the naive rotational zero mode, that generates AdS_2 dependent translations along φ, in harmonic gauge. Nevertheless, we should stress we cannot rule out the possibility of a complicated solution which is not part of the ansatz explored above, although we find it unlikely.

5.2 Wave equation: hypergeometric and gamma functions

The ordinary hypergeometric function is defined as follows

$$F(a,b,c;z) = \sum_{n=0}^{\infty} \frac{(a)_n\,(b)_n}{(c)_n}\frac{z^n}{n!}\,, \tag{5.15}$$

where $(a)_n$ is the rising Pochhammer symbol. For our purposes z is a negative real number, and for the combination of parameters a, b, c that we encounter, this series is convergent. The asymptotics of this functions is given by

$$F(a,b,c;-x) \to \frac{\Gamma(b-a)\,\Gamma(c)}{\Gamma(b)\,\Gamma(c-a)}\,x^{-a} + \frac{\Gamma(a-b)\,\Gamma(c)}{\Gamma(a)\,\Gamma(c-b)}\,x^{-b}\,, \qquad x \gg 1\,. \tag{5.16}$$

The confluent hypergeometric function is defined as follows

$$M(a,b;z) = \sum_{n=0}^{\infty} \frac{(a)_n}{(b)_n}\frac{z^n}{n!}\,. \tag{5.17}$$

For our purposes z is a positive imaginary number. The series is convergent everywhere, as long as b is not zero or a negative integer, which for us is the case. The asymptotics of this functions is given by

$$M(a,b,z) \sim \frac{\Gamma(b)}{\Gamma(a)}\,z^{a-b}\,e^z + \frac{\Gamma(b)}{\Gamma(b-a)}\,(-z)^{-a}\,, \qquad |z| \gg 1\,. \tag{5.18}$$

Turning to the gamma function, when it has a complex argument with an integer real part, it simplifies as follows

$$|\Gamma(1+n+ib)|^2 = \frac{\pi b}{\sinh(\pi b)}\prod_{k=1}^{n}(k^2+b^2)\,, \quad |\Gamma(-n+ib)|^2 = \frac{\pi}{b\,\sinh(\pi b)}\prod_{k=1}^{n}(k^2+b^2)^{-1}\,, \tag{5.19}$$

Similarly, when the real part is a half-integer we have

$$|\Gamma(\tfrac{1}{2} \pm n + ib)|^2 = \frac{\pi}{\cosh(\pi b)} \prod_{k=1}^{n} \left((k - \tfrac{1}{2})^2 + b^2\right)^{\pm 1} \,. \tag{5.20}$$

The product is absent when $n = 0$ in both of the above equations. The asymptotic expansion of the Gamma function when the argument is real is given by the Stirling approximation

$$\Gamma(x) \sim \sqrt{2\pi x}\, x^{(x-1)}\, e^{-(x-1)}\,, \qquad x \gg 1\,. \tag{5.21}$$

The asymptotics of the absolute value when the argument is complex, and the imaginary part is large is given by

$$|\Gamma(x + iy)|^2 = 2\pi\, |y|^{2x-1}\, e^{-\pi|y|}\,, \qquad |y| \gg 1\,. \tag{5.22}$$

This is from the NIST Digital Library of Mathematical Functions [171]. The asymptotics of the hyperbolic trigonometric functions is given by

$$\sinh(x) \sim \operatorname{sgn}(x)\, e^{|x|}\,, \qquad \cosh(x) \sim 2\, e^{|x|}\,, \qquad |x| \gg 1\,, \tag{5.23}$$

which appears as a special case of the previous equation.

5.3 Wave equation: alternative solution using the $\mathbf{CFT_2}$ technique

In this appendix, we will present an alternative derivation of the transmission coefficient based on [146], which applied this to the Kerr solution, and [142] who generalized it to Kerr-Newman. We will only quote the main formulae needed to understand their final equation for the transmission coefficient, without going into the derivation. We will then

show is the same as ours.

We start by rewriting the radial equation. First, we introduce a new coordinate

$$z = \frac{r - r_-}{r_+ - r_-} \,. \tag{5.24}$$

Then we introduce a new radial wavefunction function

$$\psi = \Delta^{\frac{1+s}{2}} \, R \,. \tag{5.25}$$

This results in a Heun equation with the following potential

$$V(z) = \frac{1}{z^2(z-1)^2} \sum_{i=0}^{4} A_i \, z^i \,. \tag{5.26}$$

We map the parameters of our radial equation $(A_0, A_1, A_2, A_3, A_4)$ into a new set of parameters $(E, a_1, a_2, m_3, \Lambda)$ as follows

$$\begin{aligned} A_0 &= \tfrac{1}{4} - a_1^2 \,, \\ A_1 &= -\tfrac{1}{4} + E + a_1^2 - a_2^2 - m_3 \, \Lambda \,, \\ A_2 &= \tfrac{1}{4} - E + 2 \, m_3 \, \Lambda - \frac{\Lambda^2}{4} \,, \\ A_3 &= -m_3 \, \Lambda + \frac{\Lambda^2}{2} \,, \\ A_4 &= -\frac{\Lambda^2}{4} \,. \end{aligned} \tag{5.27}$$

These equations will be inverted in the next two subsections. We introduce one more parameter a, which is implicitly defined in terms of the others as follows

$$E = a^2 - \Lambda \, \partial_\Lambda \, \mathcal{F}^{\text{inst}} \,. \tag{5.28}$$

So far everything was exact. At this point, we will take the $\Lambda \ll 1$ limit.[1] As we will see,

[1] Λ is an imaginary number, so we really mean $|\Lambda| \ll 1$.

$\Lambda = -2ik(r_+ - r_-)$, which is small for a near-extremal black hole, as long as the frequency is less than $1/\delta r$, which is well beyond any frequency range considered in this work. In this limit, we have

$$\mathcal{F}^{\text{inst}} = -\frac{\frac{1}{4} - a^2 - m_1\, m_2}{\frac{1}{2} - 2a^2}\, m_3\, \Lambda + \mathcal{O}(\Lambda^2)\,, \tag{5.29}$$

where

$$\begin{aligned} m_1 &= a_1 + a_2\,, \\ m_2 &= a_2 - a_1\,. \end{aligned} \tag{5.30}$$

We can use this to invert (5.28), which to leading order in Λ reads

$$a(E) = \sqrt{E} - \frac{\frac{1}{4} - E + a_1^2 - a_2^2}{\sqrt{E}\,(1-4E)}\, m_3\, \Lambda + \mathcal{O}(\Lambda^2)\,. \tag{5.31}$$

Finally, the transmission coefficient is given by

$$\mathcal{T} = \frac{\omega_{\text{eff}}}{2\pi T}\, \frac{1}{|\phi(a) + \phi(-a)|^2}\,, \tag{5.32}$$

with

$$\phi(a) = \frac{\Gamma(1+2a)\,\Gamma(2a)\,\Gamma(1+2a_2)\,\Lambda^{-a+m_3}\, e^{\Lambda/2}}{\Gamma(\frac{1}{2}+a+m_3)\,\Gamma(\frac{1}{2}+a+a_1+a_2)\,\Gamma(\frac{1}{2}+a-a_1+a_2)} \exp\left(\frac{\partial \mathcal{F}^{\text{inst}}}{\partial a_1}\right)\Bigg|_{\substack{a_1=+a \\ a_2=-a}}\,. \tag{5.33}$$

This is an exact equation in Λ, but we will only take the leading order piece. Our equation for the transmission coefficient is given by

$$\mathcal{T} = \frac{\omega_{\text{eff}}}{k}\, \frac{r_+^2\, |A|^2}{|C_{\text{inc},\,+} + C_{\text{inc},\,-}|^2}\,. \tag{5.34}$$

Comparing equations (5.32) and (5.34), we can see that as long as we can show that

$$\phi(\pm a) = \left(\frac{2k}{\delta r}\right)^{1/2} \frac{C_{\text{inc}\,\pm}}{A}\,, \tag{5.35}$$

these two equations will give the same transmission coefficient.

5.3.1 Reissner-Nordström wave equation

Inverting (5.27) for the Reissner-Nordström radial equation results in

$$\begin{aligned} E &= \tfrac{1}{4} + l(l+1) + m^2 r_+^2 - e^2Q^2 + 2eQ\omega(2r_+ + r_-) - \omega^2(3r_+^2 + 2r_+r_- + r_-^2)\,, \\ a_1 &= i\frac{r_-(eQ - r_-\omega)}{r_+ - r_-}\,, \\ a_2 &= i\frac{r_+(eQ - r_+\omega)}{r_+ - r_-}\,, \\ m_3 &= i\frac{-2M\omega^2 + eQ\omega + Mm^2}{k}\,, \\ \Lambda &= -2ik(r_+ - r_-)\,. \end{aligned} \tag{5.36}$$

Comparing to equations (4.41) and (4.50) we find that these parameters are related to our (β, F, μ, α) parameters as follows

$$\begin{aligned} a &= \sqrt{E} = \beta\,, \\ a_1 &= -i(F + \mu)\,, \\ a_2 &= -iF\,, \\ m_3 &= -i\alpha\,. \end{aligned} \tag{5.37}$$

Note that a_2 is exact and a_1 is found by keeping subleading terms in δr in (5.36). Plugging this into (5.33) and using the following

$$\Lambda^{-a+m_3} = (-2ik\delta r)^{-\beta - i\alpha} = (2k\delta r)^{-\beta}\,(-i)^{-\beta}\,(-i)^{-\alpha}\,, \tag{5.38}$$

gives

$$\phi(\pm a) = \frac{\Gamma(1 \pm 2\beta)\,\Gamma(\pm 2\beta)\,\Gamma(1 - 2iF)}{\Gamma(\frac{1}{2} \pm \beta - i\alpha)\,\Gamma\left(\frac{1}{2} \pm \beta - 2iF - i\mu\right)\,\Gamma\left(\frac{1}{2} \pm \beta + i\mu\right)}\,(-2ik\delta r)^{\mp\beta - i\alpha}\,, \tag{5.39}$$

after discarding a factor of $(-i)^{-1/2}\,\delta r^{+i\alpha}$, which would not matter after taking the square. Comparing to $C_{\text{inc},\,\pm}$ found in equations (4.53) and (4.56) shows that (5.35) is exactly satisfied. This completes the derivation of the transmission coefficient with the only constraint on the wave equation parameters being that $\Lambda \ll 1$.

5.3.2 Kerr wave equation

Inverting (5.27) for the Kerr wave equation results in

$$\begin{aligned} E &= \tfrac{1}{4} + \lambda + s(s+1) + a^2\omega^2 - 8M^2\omega^2 - (2M\omega^2 + is\omega)(r_+ - r_-)\,, \\ a_1 &= -i\frac{\omega_{\text{eff}}}{4\pi T} + \frac{s}{2} + 2iM\omega\,, \\ a_2 &= -i\frac{\omega_{\text{eff}}}{4\pi T} - \frac{s}{2}\,, \\ m_3 &= -2iM\omega + s\,, \\ \Lambda &= -2i\omega(r_+ - r_-)\,. \end{aligned} \tag{5.40}$$

The rest of the derivation proceeds analogously to Reissner-Nordström.

5.4 Emission rate: determining the normalization constant in the quantum rate

To determine the normalization constant $|\mathcal{N}|^2$, we start by isolating the energy-dependent part of evaporation rate (4.93), which comes from the density of states and the matrix element

$$\sinh\!\left(2\pi\sqrt{2E_{\text{f}}/E_{\text{b}}}\right)\left|\Gamma\left(\Delta + i\sqrt{2E_{\text{f}}/E_{\text{b}}} + i\sqrt{2E_{\text{i}}/E_{\text{b}}}\right)\right|^2\left|\Gamma\left(\Delta + i\sqrt{2E_{\text{f}}/E_{\text{b}}} - i\sqrt{2E_{\text{i}}/E_{\text{b}}}\right)\right|^2\,, \tag{5.41}$$

where $E_{\text{i}} = E$ and $E_{\text{f}} = E + e - \omega$. We will be taking two limits in the calculation, the high energy limit $|E + e - \omega| \gg E_{\text{b}}$ and $E \gg E_{\text{b}}$, and the low frequency limit $\omega \ll E + e$. We will

break up the calculation into three parts, each focusing on one factor in (5.41). We start with

$$\mathcal{A} = \sinh\Big(2\pi\sqrt{2E_{\rm f}/E_{\rm b}}\Big)\left|\Gamma\Big(1{+}i\sqrt{2E_{\rm f}/E_{\rm b}}{+}i\sqrt{2E_{\rm i}/E_{\rm b}}\Big)\right|^2\left|\Gamma\Big(1{+}i\sqrt{2E_{\rm f}/E_{\rm b}}{-}i\sqrt{2E_{\rm i}/E_{\rm b}}\Big)\right|^2 , \tag{5.42}$$

which is what we would have had if $\Delta = 1$. The Gamma functions can be written in terms of hyperbolic trigonometric functions using (5.19) as follows

$$\mathcal{A} = -\frac{2\pi^2(\omega-e)}{E_{\rm b}}\frac{\sinh\Big(2\pi\sqrt{2(E_{\rm f}/E_{\rm b}}\Big)}{\sinh\Big(\pi\sqrt{2E_{\rm f}/E_{\rm b}}{+}\pi\sqrt{2E_{\rm i}/E_{\rm b}}\Big)\sinh\Big(\pi\sqrt{2E_{\rm f}/E_{\rm b}}{-}\pi\sqrt{2E_{\rm i}/E_{\rm b}}\Big)} , \tag{5.43}$$

Using a trigonometric product identity, the denominator can be rewritten as follows

$$\mathcal{A} = \frac{4\pi^2(\omega-e)}{E_{\rm b}}\frac{\sinh\Big(2\pi\sqrt{2(E+e-\omega)/E_{\rm b}}\Big)}{\cosh\Big(2\pi\sqrt{2E/E_{\rm b}}\Big)-\cosh\Big(2\pi\sqrt{2(E+e-\omega)/E_{\rm b}}\Big)} . \tag{5.44}$$

We take the high energy limit and simplify, which gives

$$\mathcal{A} = \frac{4\pi^2(\omega-e)}{E_{\rm b}}\frac{1}{\exp\Big(2\pi\sqrt{2E/E_{\rm b}}-2\pi\sqrt{2(E+e-\omega)/E_{\rm b}}\Big)\ -\ 1} . \tag{5.45}$$

In the low frequency limit, we can expand the square root, and rewrite E in terms of T using equation (4.24), which gives

$$\mathcal{A} = \frac{4\pi^2(\omega-e)}{E_{\rm b}}\frac{1}{e^{(\omega-e)/T}-1} . \tag{5.46}$$

This can further be rewritten as follows

$$\mathcal{A} = \frac{4\pi^2}{E_{\rm b}}\frac{\omega-e}{2\sinh\frac{\omega-e}{2T}}e^{-(\omega-e)/2T} . \tag{5.47}$$

For easier comparison to the semi-classical rate, we can use the fact that

$$\frac{\omega - e}{2T} = \frac{\omega_{\text{eff}}}{2T} + \pi\mu\,, \tag{5.48}$$

to find

$$\mathcal{A} = \frac{4\pi^2}{E_{\text{b}}} \frac{\omega - e}{2\sinh\frac{\omega-e}{2T}} e^{-\omega_{\text{eff}}/2T}\, e^{-\pi\mu}\,. \tag{5.49}$$

The next factor in (5.41) is given by

$$\mathcal{B} = \frac{\left|\Gamma\left(\Delta + i\sqrt{2(E+e-\omega)/E_{\text{b}}} + i\sqrt{2E/E_{\text{b}}}\right)\right|^2}{\left|\Gamma\left(1 + i\sqrt{2(E+e-\omega)/E_{\text{b}}} + i\sqrt{2E/E_{\text{b}}}\right)\right|^2}\,. \tag{5.50}$$

In the low frequency limit, this simplifies to

$$\mathcal{B} = \frac{\left|\Gamma\left(\Delta + 2i\sqrt{2E/E_{\text{b}}}\right)\right|^2}{\left|\Gamma\left(1 + 2i\sqrt{2E/E_{\text{b}}}\right)\right|^2}\,. \tag{5.51}$$

Using the asymptotic Gamma function expansion (5.22), we can take the high energy limit, which gives

$$\mathcal{B} = \left(\frac{2\sqrt{2E}}{\sqrt{E_{\text{b}}}}\right)^{2(\Delta-1)}\,, \tag{5.52}$$

where we rewrote E in terms of T using (4.24), and used the fact that $Q^3 = 1/E_{\text{b}}$. We note that we also could've taken the limit in the opposite order, which would've resulted in the same expression. The third factor in (5.41) is given by

$$\mathcal{C} = \frac{\left|\Gamma\left(\Delta + i\sqrt{2(E+e-\omega)/E_{\text{b}}} - i\sqrt{2E/E_{\text{b}}}\right)\right|^2}{\left|\Gamma\left(1 + i\sqrt{2(E+e-\omega)/E_{\text{b}}} - i\sqrt{2E/E_{\text{b}}}\right)\right|^2} \tag{5.53}$$

In the low frequency limit, we can expand the square root, which gives

$$\mathcal{C} = \frac{\left|\Gamma\left(\Delta - i\sqrt{2}\,(\omega - e)\,/\sqrt{E_{\rm b}E}\right)\right|^2}{\left|\Gamma\left(1 - i\sqrt{2}\,(\omega - e)\,/\sqrt{E_{\rm b}E}\right)\right|^2}\,. \tag{5.54}$$

Using (5.48), this further simplifies as follows

$$\mathcal{C} = \frac{2T\sinh\frac{\omega-e}{2T}}{\omega - e}\left|\Gamma\left(\Delta - 2iF - i\mu\right)\right)\right|^2, \tag{5.55}$$

where we used (4.24) to write T in terms of E.

Before comparing to the semi-classical rate (4.71), we also rewrite some of the terms in that equation as follows

$$\frac{\omega_{\rm eff}/T}{e^{\omega_{\rm eff}/T} - 1}\,\frac{|\Gamma(\Delta - 2iF - i\mu)|^2}{|\Gamma(1 - 2iF)|^2} = |\Gamma(\Delta - 2iF - i\mu)|^2\, e^{-\omega_{\rm eff}/2T}\,. \tag{5.56}$$

Plugging $\mathcal{A}, \mathcal{B}, \mathcal{C}$ into the quantum rate and comparing to the semi-classical gives the normalization constant

$$|\mathcal{N}|^2 = \frac{1}{\pi}\,2^{2\Delta-2}\,\frac{\Gamma(2\Delta)}{\Gamma(2\Delta-1)^2}\,\left|\Gamma(\Delta + i\mu)\right|^2\, e^{+\pi\mu}\,. \tag{5.57}$$

References

[1] Ilija Rakic, Mukund Rangamani, and Gustavo J. Turiaci. "Thermodynamics of the near-extremal Kerr spacetime". In: *JHEP* 06 (2024), p. 011. DOI: 10.1007/JHEP06(2024)011. arXiv: 2310.04532 [hep-th].

[2] Maciej Kolanowski et al. "Looking at extremal black holes from very far away". In: *JHEP* 04 (2025), p. 020. DOI: 10.1007/JHEP04(2025)020. arXiv: 2409.16248 [hep-th].

[3] Ilija Rakic and Lorenzo Toni. "One-loop determinants in AdS_3 supergravity with extended supersymmetry". In: *JHEP* 07 (2026), p. 257. DOI: 10.1007/JHEP07(2026)257. arXiv: 2508.15701 [hep-th].

[4] Ilija Rakic. "The evaporation of near-extremal black holes through charged particle emission". In: (Dec. 2025). arXiv: 2512.18895 [hep-th].

[5] G. W. Gibbons and S. W. Hawking. "Action Integrals and Partition Functions in Quantum Gravity". In: *Phys. Rev. D* 15 (1977), pp. 2752–2756. DOI: 10.1103/PhysRevD.15.2752.

[6] James M. Bardeen, B. Carter, and S. W. Hawking. "The Four laws of black hole mechanics". In: *Commun. Math. Phys.* 31 (1973), pp. 161–170. DOI: 10.1007/BF01645742.

[7] J. D. Bekenstein. "Black holes and the second law". In: *Lett. Nuovo Cim.* 4 (1972), pp. 737–740. DOI: 10.1007/BF02757029.

[8] Jacob D. Bekenstein. "Black holes and entropy". In: *Phys. Rev. D* 7 (1973), pp. 2333–2346. DOI: 10.1103/PhysRevD.7.2333.

[9] S. W. Hawking. "Black hole explosions?" In: *Nature* 248 (1974), pp. 30–31. DOI: https://doi.org/10.1038/248030a0.

[10] S. W. Hawking. "Particle Creation by Black Holes". In: *Commun.Math.Phys.* 43 (1975), pp. 199–220. DOI: https://doi.org/10.1007/BF02345020.

[11] J. B. Hartle and S. W. Hawking. "Path Integral Derivation of Black Hole Radiance". In: *Phys. Rev. D* 13 (1976), pp. 2188–2203. DOI: 10.1103/PhysRevD.13.2188.

[12] Gerard 't Hooft. "Dimensional reduction in quantum gravity". In: *Conf. Proc. C* 930308 (1993), pp. 284–296. arXiv: gr-qc/9310026.

[13] Leonard Susskind. "The World as a hologram". In: *J. Math. Phys.* 36 (1995), pp. 6377–6396. DOI: 10.1063/1.531249. arXiv: hep-th/9409089.

[14] Raphael Bousso. "The Holographic principle". In: *Rev. Mod. Phys.* 74 (2002), pp. 825–874. DOI: 10.1103/RevModPhys.74.825. arXiv: hep-th/0203101.

[15] Juan Martin Maldacena. "The Large N limit of superconformal field theories and supergravity". In: *Adv. Theor. Math. Phys.* 2 (1998), pp. 231–252. DOI: 10.4310/ATMP.1998.v2.n2.a1. arXiv: hep-th/9711200.

[16] S. S. Gubser, Igor R. Klebanov, and Alexander M. Polyakov. "Gauge theory correlators from noncritical string theory". In: *Phys. Lett. B* 428 (1998), pp. 105–114. DOI: 10.1016/S0370-2693(98)00377-3. arXiv: hep-th/9802109.

[17] Edward Witten. "Anti de Sitter space and holography". In: *Adv. Theor. Math. Phys.* 2 (1998), pp. 253–291. DOI: 10.4310/ATMP.1998.v2.n2.a2. arXiv: hep-th/9802150.

[18] Ofer Aharony et al. "Large N field theories, string theory and gravity". In: *Phys. Rept.* 323 (2000), pp. 183–386. DOI: 10.1016/S0370-1573(99)00083-6. arXiv: hep-th/9905111.

[19] S. W. Hawking. "Breakdown of Predictability in Gravitational Collapse". In: *Phys. Rev. D* 14 (1976), pp. 2460–2473. DOI: 10.1103/PhysRevD.14.2460.

[20] Don N. Page. "Average entropy of a subsystem". In: *Phys. Rev. Lett.* 71 (1993), pp. 1291–1294. DOI: 10.1103/PhysRevLett.71.1291. arXiv: gr-qc/9305007.

[21] Don N. Page. "Information in black hole radiation". In: *Phys. Rev. Lett.* 71 (1993), pp. 3743–3746. DOI: 10.1103/PhysRevLett.71.3743. arXiv: hep-th/9306083.

[22] Ahmed Almheiri et al. "The entropy of Hawking radiation". In: *Rev. Mod. Phys.* 93.3 (2021), p. 035002. DOI: 10.1103/RevModPhys.93.035002. arXiv: 2006.06872 [hep-th].

[23] Ashoke Sen. "Entropy Function and AdS(2) / CFT(1) Correspondence". In: *JHEP* 11 (2008), p. 075. DOI: 10.1088/1126-6708/2008/11/075. arXiv: 0805.0095 [hep-th].

[24] Ashoke Sen. "Quantum Entropy Function from AdS(2)/CFT(1) Correspondence". In: *Int. J. Mod. Phys. A* 24 (2009), pp. 4225–4244. DOI: 10.1142/S0217751X09045893. arXiv: 0809.3304 [hep-th].

[25] Shamik Banerjee, Rajesh Kumar Gupta, and Ashoke Sen. "Logarithmic Corrections to Extremal Black Hole Entropy from Quantum Entropy Function". In: *JHEP* 03 (2011), p. 147. DOI: 10.1007/JHEP03(2011)147. arXiv: 1005.3044 [hep-th].

[26] Ashoke Sen. "Logarithmic Corrections to N=2 Black Hole Entropy: An Infrared Window into the Microstates". In: *Gen. Rel. Grav.* 44.5 (2012), pp. 1207–1266. DOI: 10.1007/s10714-012-1336-5. arXiv: 1108.3842 [hep-th].

[27] Ashoke Sen. "Logarithmic Corrections to Rotating Extremal Black Hole Entropy in Four and Five Dimensions". In: *Gen. Rel. Grav.* 44 (2012), pp. 1947–1991. DOI: 10.1007/s10714-012-1373-0. arXiv: 1109.3706 [hep-th].

[28] Hari K. Kunduri, James Lucietti, and Harvey S. Reall. "Near-horizon symmetries of extremal black holes". In: *Class. Quant. Grav.* 24 (2007), pp. 4169–4190. DOI: 10.1088/0264-9381/24/16/012. arXiv: 0705.4214 [hep-th].

[29] John Preskill et al. “Limitations on the statistical description of black holes”. In: *Mod. Phys. Lett.* A6 (1991), pp. 2353–2362. DOI: 10.1142/S0217732391002773.

[30] Jeremy Michelson and Marcus Spradlin. “Supergravity spectrum on AdS(2) x S**2”. In: *JHEP* 09 (1999), p. 029. DOI: 10.1088/1126-6708/1999/09/029. arXiv: hep-th/9906056 [hep-th].

[31] Don N. Page. “Thermodynamics of near extreme black holes”. In: *Proceedubgs of the 10th Workshop on General Relativity and Gravitation in Japan (JGRG10)*. Sept. 2000. arXiv: hep-th/0012020.

[32] R. Jackiw. “Lower Dimensional Gravity”. In: *Nucl. Phys. B* 252 (1985). Ed. by R. Baier and H. Satz, pp. 343–356. DOI: 10.1016/0550-3213(85)90448-1.

[33] C. Teitelboim. “Gravitation and Hamiltonian Structure in Two Space-Time Dimensions”. In: *Phys. Lett. B* 126 (1983), pp. 41–45. DOI: 10.1016/0370-2693(83)90012-6.

[34] Ahmed Almheiri and Joseph Polchinski. “Models of AdS_2 backreaction and holography”. In: *JHEP* 11 (2015), p. 014. DOI: 10.1007/JHEP11(2015)014. arXiv: 1402.6334 [hep-th].

[35] Kristan Jensen. “Chaos in AdS_2 Holography”. In: *Phys. Rev. Lett.* 117.11 (2016), p. 111601. DOI: 10.1103/PhysRevLett.117.111601. arXiv: 1605.06098 [hep-th].

[36] Julius Engelsöy, Thomas G. Mertens, and Herman Verlinde. “An investigation of AdS_2 backreaction and holography”. In: *JHEP* 07 (2016), p. 139. DOI: 10.1007/JHEP07(2016)139. arXiv: 1606.03438 [hep-th].

[37] Juan Maldacena, Douglas Stanford, and Zhenbin Yang. “Conformal symmetry and its breaking in two dimensional Nearly Anti-de-Sitter space”. In: *PTEP* 2016.12 (2016), p. 12C104. DOI: 10.1093/ptep/ptw124. arXiv: 1606.01857 [hep-th].

[38] Thomas G. Mertens and Gustavo J. Turiaci. "Solvable models of quantum black holes: a review on Jackiw–Teitelboim gravity". In: *Living Rev. Rel.* 26.1 (2023), p. 4. DOI: 10.1007/s41114-023-00046-1. arXiv: 2210.10846 [hep-th].

[39] Douglas Stanford and Edward Witten. "Fermionic Localization of the Schwarzian Theory". In: *JHEP* 10 (2017), p. 008. DOI: 10.1007/JHEP10(2017)008. arXiv: 1703.04612 [hep-th].

[40] Animik Ghosh, Henry Maxfield, and Gustavo J. Turiaci. "A universal Schwarzian sector in two-dimensional conformal field theories". In: *JHEP* 05 (2020), p. 104. DOI: 10.1007/JHEP05(2020)104. arXiv: 1912.07654 [hep-th].

[41] Luca V. Iliesiu and Gustavo J. Turiaci. "The statistical mechanics of near-extremal black holes". In: *JHEP* 05 (2021), p. 145. DOI: 10.1007/JHEP05(2021)145. arXiv: 2003.02860 [hep-th].

[42] Subir Sachdev. "Bekenstein-Hawking Entropy and Strange Metals". In: *Phys. Rev. X* 5 (4 Nov. 2015), p. 041025. DOI: 10.1103/PhysRevX.5.041025. URL: https://link.aps.org/doi/10.1103/PhysRevX.5.041025.

[43] Ahmed Almheiri and Byungwoo Kang. "Conformal Symmetry Breaking and Thermodynamics of Near-Extremal Black Holes". In: *JHEP* 10 (2016), p. 052. DOI: 10.1007/JHEP10(2016)052. arXiv: 1606.04108 [hep-th].

[44] Pranjal Nayak et al. "On the Dynamics of Near-Extremal Black Holes". In: *JHEP* 09 (2018), p. 048. DOI: 10.1007/JHEP09(2018)048. arXiv: 1802.09547 [hep-th].

[45] Upamanyu Moitra, Sandip P. Trivedi, and V. Vishal. "Extremal and near-extremal black holes and near-CFT_1". In: *JHEP* 07 (2019), p. 055. DOI: 10.1007/JHEP07(2019)055. arXiv: 1808.08239 [hep-th].

[46] Upamanyu Moitra et al. "Jackiw-Teitelboim Gravity and Rotating Black Holes". In: *JHEP* 11 (2019), p. 047. DOI: 10.1007/JHEP11(2019)047. arXiv: 1905.10378 [hep-th].

[47] Luca V. Iliesiu, Sameer Murthy, and Gustavo J. Turiaci. "Revisiting the Logarithmic Corrections to the Black Hole Entropy". In: (Sept. 2022). arXiv: 2209.13608 [hep-th].

[48] Sergio Hernández-Cuenca. "Entropy and spectrum of near-extremal black holes: semiclassical brane solutions to non-perturbative problems". In: *JHEP* 05 (2025), p. 020. DOI: 10.1007/JHEP05(2025)020. arXiv: 2407.20321 [hep-th].

[49] Stefano Antonini et al. "Black Hole Airy Tail". In: *Phys. Rev. Lett.* 135.19 (2025), p. 191501. DOI: 10.1103/ft96-b212. arXiv: 2507.10657 [hep-th].

[50] Stefano Antonini et al. "Living on the edge: a non-perturbative resolution to the negativity of bulk entropies". In: *JHEP* 03 (2026), p. 035. DOI: 10.1007/JHEP03(2026)035. arXiv: 2509.15295 [hep-th].

[51] G. W. Gibbons. "Vacuum Polarization and the Spontaneous Loss of Charge by Black Holes". In: *Commun.Math.Phys.* 44 (1975), pp. 245–264. DOI: https://doi.org/10.1007/BF01609829.

[52] A. A. Starobinskii. "Amplification of waves during reflection from a rotating "black hole"". In: *Zh. Eksp. Teor. Fiz.* 64 (1973), pp. 48–57.

[53] A. A. Starobinskii and S. M. Churilov. "Amplification of electromagnetic and gravitational waves scattered by a rotating "black hole"". In: *Zh. Eksp. Teor. Fiz.* 65 (1973), pp. 3–11.

[54] S. A. Teukolsky. "Perturbations of a rotating black hole. 1. Fundamental equations for gravitational electromagnetic and neutrino field perturbations". In: *Astrophys. J.* 185 (1973), pp. 635–648. DOI: 10.1086/152444.

[55] W. H. Press and S. A. Teukolsky. "Perturbations of a Rotating Black Hole. II. Dynamical Stability of the Kerr Metric". In: *Astrophys. J.* 185 (1973), pp. 649–674. DOI: 10.1086/152445.

[56] S. A. Teukolsky and W. H. Press. "Perturbations of a rotating black hole. III. Interaction of the hole with gravitational and electromagnetic radiation." In: *Astrophys. J.* 193 (1974), pp. 443–461. DOI: 10.1086/153180.

[57] D. N. Page. "Particle emission rates from a black hole: Massless particles from an uncharged, nonrotating hole". In: *Phys. Rev. D* 13 (1976), pp. 198–206. DOI: https://doi.org/10.1103/PhysRevD.13.198.

[58] D. N. Page. "Particle emission rates from a black hole. II. Massless particles from a rotating hole". In: *Phys. Rev. D* 14 (1976), pp. 3260–3273. DOI: https://doi.org/10.1103/PhysRevD.14.3260.

[59] D. N. Page. "Particle emission rates from a black hole. III. Charged leytons from a nonrotating hole". In: *Phys. Rev. D* 16 (1977), pp. 2402–2411. DOI: https://doi.org/10.1103/PhysRevD.16.2402.

[60] A. R. Brown et al. "The evaporation of charged black holes". In: (). DOI: 10.48550/arXiv.2411.03447. arXiv: 2411.03447 [hep-th].

[61] Y. Bai and M. Korwar. "Near-Extremal Charged Black Holes: Greybody Factors and Evolution". In: *JHEP* 2023 (2023). DOI: 10.1007/JHEP03(2023)151. arXiv: 2301.07739 [hep-th].

[62] Guanda Lin, Luca V. Iliesiu, and Mykhaylo Usatyuk. "The evaporation of black holes in supergravity". In: *Journal of High Energy Physics* 2025 (2025), p. 220. DOI: 10.1007/JHEP08(2025)220. arXiv: 2504.21077 [hep-th].

[63] Sidney Coleman. "Fate of the false vacuum: Semiclassical theory". In: *Phys. Rev. D* 15 (10 May 1977), pp. 2929–2936. DOI: 10.1103/PhysRevD.15.2929. URL: https://link.aps.org/doi/10.1103/PhysRevD.15.2929.

[64] Curtis G. Callan and Sidney Coleman. "Fate of the false vacuum. II. First quantum corrections". In: *Phys. Rev. D* 16 (6 Sept. 1977), pp. 1762–1768. DOI: 10.1103/PhysRevD.16.1762. URL: https://link.aps.org/doi/10.1103/PhysRevD.16.1762.

[65] Sidney Coleman and Frank De Luccia. "Gravitational effects on and of vacuum decay". In: *Phys. Rev. D* 21 (12 June 1980), pp. 3305–3315. DOI: 10.1103/PhysRevD.21.3305. URL: https://link.aps.org/doi/10.1103/PhysRevD.21.3305.

[66] Julian Schwinger. "On Gauge Invariance and Vacuum Polarization". In: *Phys. Rev.* 82 (5 June 1951), pp. 664–679. DOI: 10.1103/PhysRev.82.664. URL: https://link.aps.org/doi/10.1103/PhysRev.82.664.

[67] Daniel Kapec et al. "Logarithmic Corrections to Kerr Thermodynamics". In: (Oct. 2023). arXiv: 2310.00848 [hep-th].

[68] Sabyasachi Maulik et al. "Universality in logarithmic temperature corrections to near-extremal rotating black hole thermodynamics in various dimensions". In: *JHEP* 06 (2024), p. 034. DOI: 10.1007/JHEP06(2024)034. arXiv: 2401.16507 [hep-th].

[69] Jan Boruch et al. "BPS and near-BPS black holes in AdS_5 and their spectrum in $\mathcal{N} = 4$ SYM". In: (Mar. 2022). arXiv: 2203.01331 [hep-th].

[70] James M. Bardeen and Gary T. Horowitz. "The Extreme Kerr throat geometry: A Vacuum analog of AdS(2) x S**2". In: *Phys. Rev. D* 60 (1999), p. 104030. DOI: 10.1103/PhysRevD.60.104030. arXiv: hep-th/9905099.

[71] Matthew Heydeman et al. "The statistical mechanics of near-BPS black holes". In: *J. Phys. A* 55.1 (2022), p. 014004. DOI: 10.1088/1751-8121/ac3be9. arXiv: 2011.01953 [hep-th].

[72] Monica Guica et al. "The Kerr/CFT Correspondence". In: *Phys. Rev. D* 80 (2009), p. 124008. DOI: 10.1103/PhysRevD.80.124008. arXiv: 0809.4266 [hep-th].

[73] Alejandra Castro and Finn Larsen. "Near Extremal Kerr Entropy from AdS(2) Quantum Gravity". In: *JHEP* 12 (2009), p. 037. DOI: 10.1088/1126-6708/2009/12/037. arXiv: 0908.1121 [hep-th].

[74] Geoffrey Compère. "The Kerr/CFT correspondence and its extensions". In: *Living Rev. Rel.* 15 (2012), p. 11. DOI: 10.1007/s41114-017-0003-2. arXiv: 1203.3561 [hep-th].

[75] Ashoke Sen. "Logarithmic Corrections to Schwarzschild and Other Non-extremal Black Hole Entropy in Different Dimensions". In: *JHEP* 04 (2013), p. 156. DOI: 10.1007/JHEP04(2013)156. arXiv: 1205.0971 [hep-th].

[76] Nabamita Banerjee and Muktajyoti Saha. "Revisiting leading quantum corrections to near extremal black hole thermodynamics". In: *JHEP* 07 (2023), p. 010. DOI: 10.1007/JHEP07(2023)010. arXiv: 2303.12415 [hep-th].

[77] Aaron J. Amsel et al. "No Dynamics in the Extremal Kerr Throat". In: *JHEP* 09 (2009), p. 044. DOI: 10.1088/1126-6708/2009/09/044. arXiv: 0906.2376 [hep-th].

[78] Oscar J. C. Dias, Harvey S. Reall, and Jorge E. Santos. "Kerr-CFT and gravitational perturbations". In: *JHEP* 08 (2009), p. 101. DOI: 10.1088/1126-6708/2009/08/101. arXiv: 0906.2380 [hep-th].

[79] Temple He et al. "The timbre of Hawking gravitons: an effective description of energy transport from holography". In: *JHEP* 09 (2022), p. 092. DOI: 10.1007/JHEP09(2022)092. arXiv: 2202.04079 [hep-th].

[80] J. David Brown, Erik A. Martinez, and James W. York Jr. "Complex Kerr-Newman geometry and black hole thermodynamics". In: *Phys. Rev. Lett.* 66 (1991), pp. 2281–2284. DOI: 10.1103/PhysRevLett.66.2281.

[81] Yiming Chen and Gustavo J. Turiaci. "Spin-Statistics for Black Hole Microstates". In: (Sept. 2023). arXiv: 2309.03478 [hep-th].

[82] J. David Brown and James W. York Jr. "The Microcanonical functional integral. 1. The Gravitational field". In: *Phys. Rev. D* 47 (1993), pp. 1420–1431. DOI: 10.1103/PhysRevD.47.1420. arXiv: gr-qc/9209014.

[83] M. J. Duff. "Observations on Conformal Anomalies". In: *Nucl. Phys. B* 125 (1977), pp. 334–348. DOI: 10.1016/0550-3213(77)90410-2.

[84] S. M. Christensen and M. J. Duff. "New Gravitational Index Theorems and Supertheorems". In: *Nucl. Phys. B* 154 (1979), pp. 301–342. DOI: 10.1016/0550-3213(79)90516-9.

[85] S. M. Christensen and M. J. Duff. "Quantizing Gravity with a Cosmological Constant". In: *Nucl. Phys. B* 170 (1980), pp. 480–506. DOI: 10.1016/0550-3213(80)90423-X.

[86] M. J. Duff and P. van Nieuwenhuizen. "Quantum Inequivalence of Different Field Representations". In: *Phys. Lett. B* 94 (1980), pp. 179–182. DOI: 10.1016/0370-2693(80)90852-7.

[87] D. V. Vassilevich. "Heat kernel expansion: User's manual". In: *Phys. Rept.* 388 (2003), pp. 279–360. DOI: 10.1016/j.physrep.2003.09.002. arXiv: hep-th/0306138.

[88] R. Camporesi and A. Higuchi. "Spectral functions and zeta functions in hyperbolic spaces". In: *J. Math. Phys.* 35 (1994), pp. 4217–4246. DOI: 10.1063/1.530850.

[89] Alejandra Castro et al. "Gravitational perturbations from NHEK to Kerr". In: *JHEP* 07 (2021), p. 218. DOI: 10.1007/JHEP07(2021)218. arXiv: 2102.08060 [hep-th].

[90] Upamanyu Moitra, Sunil Kumar Sake, and Sandip P. Trivedi. "Jackiw-Teitelboim gravity in the second order formalism". In: *JHEP* 10 (2021), p. 204. DOI: 10.1007/JHEP10(2021)204. arXiv: 2101.00596 [hep-th].

[91] Harry W. Braden et al. "Charged black hole in a grand canonical ensemble". In: *Phys. Rev.* D42 (1990), pp. 3376–3385. DOI: 10.1103/PhysRevD.42.3376.

[92] S. W. Hawking and Simon F. Ross. "Duality between electric and magnetic black holes". In: *Phys. Rev.* D52 (1995), pp. 5865–5876. DOI: 10.1103/PhysRevD.52.5865. arXiv: hep-th/9504019 [hep-th].

[93] Sayantani Bhattacharyya, Binata Panda, and Ashoke Sen. "Heat Kernel Expansion and Extremal Kerr-Newmann Black Hole Entropy in Einstein-Maxwell Theory". In: *JHEP* 08 (2012), p. 084. DOI: 10.1007/JHEP08(2012)084. arXiv: 1204.4061 [hep-th].

[94] Gustavo J. Turiaci. "New insights on near-extremal black holes". In: (July 2023). arXiv: 2307.10423 [hep-th].

[95] Ashoke Sen. "Logarithmic Corrections to N=2 Black Hole Entropy: An Infrared Window into the Microstates". In: *Gen. Rel. Grav.* 44.5 (2012), pp. 1207–1266. DOI: 10.1007/s10714-012-1336-5. arXiv: 1108.3842 [hep-th].

[96] B. Carter. "Hamilton-Jacobi and Schrodinger separable solutions of Einstein's equations". In: *Commun. Math. Phys.* 10.4 (1968), pp. 280–310. DOI: 10.1007/BF03399503.

[97] Alejandro Cabo-Bizet et al. "Microscopic origin of the Bekenstein-Hawking entropy of supersymmetric AdS_5 black holes". In: *JHEP* 10 (2019), p. 062. DOI: 10.1007/JHEP10(2019)062. arXiv: 1810.11442 [hep-th].

[98] Sunjin Choi et al. "Large AdS black holes from QFT". In: (Oct. 2018). arXiv: 1810.12067 [hep-th].

[99] Francesco Benini and Elisa Milan. "Black Holes in 4D $\mathcal{N}$=4 Super-Yang-Mills Field Theory". In: *Phys. Rev. X* 10.2 (2020), p. 021037. DOI: 10.1103/PhysRevX.10.021037. arXiv: 1812.09613 [hep-th].

[100] Thomas Hartman et al. "CFT Duals for Extreme Black Holes". In: *JHEP* 04 (2009), p. 019. DOI: 10.1088/1126-6708/2009/04/019. arXiv: 0811.4393 [hep-th].

[101] Marina David et al. “Non-topological logarithmic corrections in minimal gauged supergravity”. In: *JHEP* 08 (2022), p. 043. DOI: 10.1007/JHEP08(2022)043. arXiv: 2112.09444 [hep-th].

[102] Thomas G. Mertens and Gustavo J. Turiaci. “Defects in Jackiw-Teitelboim Quantum Gravity”. In: *JHEP* 08 (2019), p. 127. DOI: 10.1007/JHEP08(2019)127. arXiv: 1904.05228 [hep-th].

[103] Rajesh Kumar Gupta, Sameer Murthy, and Manya Sahni. “Quantum entropy of BMPV black holes and the topological M-theory conjecture”. In: *JHEP* 06 (2022), p. 053. DOI: 10.1007/JHEP06(2022)053. arXiv: 2104.02634 [hep-th].

[104] Hari K. Kunduri and James Lucietti. “Classification of near-horizon geometries of extremal black holes”. In: *Living Rev. Rel.* 16 (2013), p. 8. DOI: 10.12942/lrr-2013-8. arXiv: 1306.2517 [hep-th].

[105] Pau Figueras et al. “Extremal vacuum black holes in higher dimensions”. In: *Phys. Rev. D* 78 (2008), p. 044042. DOI: 10.1103/PhysRevD.78.044042. arXiv: 0803.2998 [hep-th].

[106] Sridip Pal and Jiaxin Qiao. “Lightcone Modular Bootstrap and Tauberian Theory: A Cardy-like Formula for Near-extremal Black Holes”. In: (July 2023). arXiv: 2307.02587 [hep-th].

[107] Gary T. Horowitz et al. “Extremal Kerr Black Holes as Amplifiers of New Physics”. In: *Phys. Rev. Lett.* 131.9 (2023), p. 091402. DOI: 10.1103/PhysRevLett.131.091402. arXiv: 2303.07358 [hep-th].

[108] Stefanos Aretakis. “Stability and Instability of Extreme Reissner-Nordström Black Hole Spacetimes for Linear Scalar Perturbations I”. In: *Commun. Math. Phys.* 307 (2011), pp. 17–63. DOI: 10.1007/s00220-011-1254-5. arXiv: 1110.2007 [gr-qc].

[109] Vitor Cardoso and Oscar J. C. Dias. “Small Kerr-anti-de Sitter black holes are unstable”. In: *Phys. Rev. D* 70 (2004), p. 084011. DOI: 10.1103/PhysRevD.70.084011. arXiv: hep-th/0405006.

[110] Seok Kim et al. "'Grey Galaxies' as an endpoint of the Kerr-AdS superradiant instability". In: (May 2023). arXiv: 2305.08922 [hep-th].

[111] G. W. Gibbons, S. W. Hawking, and M. J. Perry. "Path Integrals and the Indefiniteness of the Gravitational Action". In: *Nucl. Phys. B* 138 (1978), pp. 141–150. DOI: 10.1016/0550-3213(78)90161-X.

[112] Donald Marolf and Jorge E. Santos. "The canonical ensemble reloaded: the complex-stability of Euclidean quantum gravity for black holes in a box". In: *JHEP* 08 (2022), p. 215. DOI: 10.1007/JHEP08(2022)215. arXiv: 2202.11786 [hep-th].

[113] Xiaoyi Liu, Donald Marolf, and Jorge E. Santos. "Stability of saddles and choices of contour in the Euclidean path integral for linearized gravity: dependence on the DeWitt parameter". In: *JHEP* 05 (2024), p. 087. DOI: 10.1007/JHEP05(2024)087. arXiv: 2310.08555 [hep-th].

[114] Edward Witten. "SL(2,Z) action on three-dimensional conformal field theories with Abelian symmetry". In: *From Fields to Strings: Circumnavigating Theoretical Physics: A Conference in Tribute to Ian Kogan*. July 2003, pp. 1173–1200. arXiv: hep-th/0307041.

[115] Donald Marolf and Simon F. Ross. "Boundary Conditions and New Dualities: Vector Fields in AdS/CFT". In: *JHEP* 11 (2006), p. 085. DOI: 10.1088/1126-6708/2006/11/085. arXiv: hep-th/0606113.

[116] Subir Sachdev. "Universal low temperature theory of charged black holes with AdS_2 horizons". In: *J. Math. Phys.* 60.5 (2019), p. 052303. DOI: 10.1063/1.5092726. arXiv: 1902.04078 [hep-th].

[117] Maximo Banados, Claudio Teitelboim, and Jorge Zanelli. "The Black hole in three-dimensional space-time". In: *Phys. Rev. Lett.* 69 (1992), pp. 1849–1851. DOI: 10.1103/PhysRevLett.69.1849. arXiv: hep-th/9204099.

[118] J. David Brown and M. Henneaux. "Central Charges in the Canonical Realization of Asymptotic Symmetries: An Example from Three-Dimensional Gravity". In: *Commun. Math. Phys.* 104 (1986), pp. 207–226. DOI: 10.1007/BF01211590.

[119] Simone Giombi, Alexander Maloney, and Xi Yin. "One-loop Partition Functions of 3D Gravity". In: *JHEP* 08 (2008), p. 007. DOI: 10.1088/1126-6708/2008/08/007. arXiv: 0804.1773 [hep-th].

[120] Phil Saad, Stephen H. Shenker, and Douglas Stanford. "JT gravity as a matrix integral". In: (2019). arXiv: 1903.11115 [hep-th].

[121] Luca V. Iliesiu, Sameer Murthy, and Gustavo J. Turiaci. "Black hole microstate counting from the gravitational path integral". In: (Sept. 2022). arXiv: 2209.13602 [hep-th].

[122] Shouvik Datta and Justin R. David. "Higher Spin Quasinormal Modes and One-Loop Determinants in the BTZ black Hole". In: *JHEP* 03 (2012), p. 079. DOI: 10.1007/JHEP03(2012)079. arXiv: 1112.4619 [hep-th].

[123] Alejandra Castro, Cynthia Keeler, and Phillip Szepietowski. "Tweaking one-loop determinants in AdS_3". In: *JHEP* 10 (2017), p. 070. DOI: 10.1007/JHEP10(2017)070. arXiv: 1707.06245 [hep-th].

[124] Roberto Emparan and Javier M. Magan. "Tearing down spacetime with quantum disentanglement". In: *JHEP* 03 (2024), p. 078. DOI: 10.1007/JHEP03(2024)078. arXiv: 2312.06803 [hep-th].

[125] Lloyd N Trefethen. *Spectral methods in MATLAB*. SIAM, 2000.

[126] Óscar J. C. Dias, Jorge E. Santos, and Benson Way. "Numerical Methods for Finding Stationary Gravitational Solutions". In: *Class. Quant. Grav.* 33.13 (2016), p. 133001. DOI: 10.1088/0264-9381/33/13/133001. arXiv: 1510.02804 [hep-th].

[127] Dieter Brill. "Splitting of an extremal Reissner-Nordstrom throat via quantum tunneling". In: *Phys. Rev. D* 46 (1992), pp. 1560–1565. DOI: 10.1103/PhysRevD.46.1560. arXiv: hep-th/9202037.

[128] Fay Dowker et al. "On pair creation of extremal black holes and Kaluza-Klein monopoles". In: *Phys. Rev. D* 50 (1994), pp. 2662–2679. DOI: 10.1103/PhysRevD.50.2662. arXiv: hep-th/9312172.

[129] Ricardo Monteiro and Jorge E. Santos. "Negative modes and the thermodynamics of Reissner-Nordstrom black holes". In: *Phys. Rev. D* 79 (2009), p. 064006. DOI: 10.1103/PhysRevD.79.064006. arXiv: 0812.1767 [gr-qc].

[130] Alexander Maloney and Edward Witten. "Quantum Gravity Partition Functions in Three Dimensions". In: *JHEP* 02 (2010), p. 029. DOI: 10.1007/JHEP02(2010)029. arXiv: 0712.0155 [hep-th].

[131] Davide Cassani and Lorenzo Papini. "The BPS limit of rotating AdS black hole thermodynamics". In: *JHEP* 09 (2019), p. 079. DOI: 10.1007/JHEP09(2019)079. arXiv: 1906.10148 [hep-th].

[132] Nikolay Bobev and P. Marcos Crichigno. "Universal spinning black holes and theories of class $\mathcal{R}$". In: *JHEP* 12 (2019), p. 054. DOI: 10.1007/JHEP12(2019)054. arXiv: 1909.05873 [hep-th].

[133] Nikolay Bobev, Anthony M. Charles, and Vincent S. Min. "Euclidean black saddles and AdS_4 black holes". In: *JHEP* 10 (2020), p. 073. DOI: 10.1007/JHEP10(2020)073. arXiv: 2006.01148 [hep-th].

[134] Finn Larsen and Siyul Lee. "Microscopic entropy of AdS_3 black holes revisited". In: *JHEP* 07 (2021), p. 038. DOI: 10.1007/JHEP07(2021)038. arXiv: 2101.08497 [hep-th].

[135] Luca V. Iliesiu, Murat Kologlu, and Gustavo J. Turiaci. "Supersymmetric indices factorize". In: *JHEP* 05 (2023), p. 032. DOI: 10.1007/JHEP05(2023)032. arXiv: 2107.09062 [hep-th].

[136] Pietro Benetti Genolini, Alejandro Cabo-Bizet, and Sameer Murthy. "Supersymmetric phases of AdS_4/CFT_3". In: *JHEP* 06 (2023), p. 125. DOI: 10.1007/JHEP06(2023)125. arXiv: 2301.00763 [hep-th].

[137] A. H. Anupam, Chandramouli Chowdhury, and Ashoke Sen. "Revisiting logarithmic correction to five dimensional BPS black hole entropy". In: *JHEP* 05 (2024), p. 070. DOI: 10.1007/JHEP05(2024)070. arXiv: 2308.00038 [hep-th].

[138] Jan Boruch et al. "New forms of attraction: Attractor saddles for the black hole index". In: (Oct. 2023). arXiv: 2310.07763 [hep-th].

[139] Frederik Denef, Sean A. Hartnoll, and Subir Sachdev. "Black hole determinants and quasinormal modes". In: *Class. Quant. Grav.* 27 (2010), p. 125001. DOI: 10.1088/0264-9381/27/12/125001. arXiv: 0908.2657 [hep-th].

[140] Hewei Frederic Jia and Mukund Rangamani. "work in progress". In: (2024).

[141] Juan Maldacena, Gustavo J. Turiaci, and Zhenbin Yang. "Two dimensional Nearly de Sitter gravity". In: *JHEP* 01 (2021), p. 139. DOI: 10.1007/JHEP01(2021)139. arXiv: 1904.01911 [hep-th].

[142] S. Maulik, X. Meng, and L. A. Pando Zayas. "Quantum-Corrected Hawking Radiation from Near Extremal Kerr-Newman Black Holes". In: (). DOI: 10.48550/arXiv.2501.08252. arXiv: 2501.08252 [hep-th].

[143] P. Betzios, O. Papadoulaki, and Y. Zhou. "Near-extremal quantum cross-section for charged fields and superradiance". In: (). DOI: 10.48550/arXiv.2507.13896. arXiv: 2507.13896 [hep-th].

[144] Ya. B. Zel'Dovich. "Generation of Waves by a Rotating Body". In: *Soviet Journal of Experimental and Theoretical Physics Letters* 14 (Aug. 1971), p. 180.

[145] Ya. B. Zel'Dovich. "Amplification of Cylindrical Electromagnetic Waves Reflected from a Rotating Body". In: *Soviet Journal of Experimental and Theoretical Physics* 35 (Jan. 1972), p. 1085.

[146] G. Bonelli et al. "Exact solution of Kerr black hole perturbations via CFT_2 and instanton counting. Greybody factor, Quasinormal modes and Love numbers". In: *Phys. Rev. D* 105 (2022). DOI: 10.1103/PhysRevD.105.044047. arXiv: 2105.04483 [hep-th].

[147] Richard Brito, Vitor Cardoso, and Paolo Pani. "Superradiance: New Frontiers in Black Hole Physics". In: *Lect. Notes Phys.* 906 (2015), pp.1–237. DOI: 10.1007/978-3-319-19000-6. arXiv: 1501.06570 [gr-qc].

[148] Sumit R. Das and Samir D. Mathur. "Comparing decay rates for black holes and D-branes". In: *Nucl. Phys. B* 478 (1996), pp. 561–576. DOI: 10.1016/0550-3213(96)00453-1. arXiv: hep-th/9606185.

[149] S. S. Gubser and Igor R. Klebanov. "Emission of charged particles from four-dimensional and five-dimensional black holes". In: *Nucl. Phys. B* 482 (1996), pp. 173–186. DOI: 10.1016/S0550-3213(96)00496-8. arXiv: hep-th/9608108.

[150] Steven S. Gubser and Igor R. Klebanov. "Four-dimensional grey body factors and the effective string". In: *Phys. Rev. Lett.* 77 (1996), pp. 4491–4494. DOI: 10.1103/PhysRevLett.77.4491. arXiv: hep-th/9609076.

[151] Steven S. Gubser. "Absorption of photons and fermions by black holes in four-dimensions". In: *Phys. Rev. D* 56 (1997), pp. 7854–7868. DOI: 10.1103/PhysRevD.56.7854. arXiv: hep-th/9706100.

[152] Juan Martin Maldacena and Andrew Strominger. "Black hole grey body factors and d-brane spectroscopy". In: *Phys. Rev. D* 55 (1997), pp. 861–870. DOI: 10.1103/PhysRevD.55.861. arXiv: hep-th/9609026.

[153] Juan Martin Maldacena and Andrew Strominger. "Universal low-energy dynamics for rotating black holes". In: *Phys. Rev. D* 56 (1997), pp. 4975–4983. DOI: 10.1103/PhysRevD.56.4975. arXiv: hep-th/9702015.

[154] Curtis G. Callan Jr. et al. "Absorption of fixed scalars and the D-brane approach to black holes". In: *Nucl. Phys. B* 489 (1997), pp. 65–94. DOI: 10.1016/S0550-3213(97)00013-8. arXiv: hep-th/9610172.

[155] Roberto Emparan. "Quantum cross-section of near-extremal black holes". In: *Journal of High Energy Physics* 2025 (2025), p. 122. DOI: 10.1007/JHEP04(2025)122. arXiv: 2501.17470 [hep-th].

[156] Roberto Emparan and Stefano Trezzi. "Quantum transparency of near-extremal black holes". In: *Journal of High Energy Physics* 2025 (2025), p. 23. DOI: 10.1007/JHEP10(2025)023. arXiv: 2507.03398 [hep-th].

[157] Anna Biggs. "Following the state of an evaporating charged black hole into the quantum gravity regime". In: (Mar. 2025). arXiv: 2503.02051 [hep-th].

[158] Thomas G. Mertens, Gustavo J. Turiaci, and Herman L. Verlinde. "Solving the Schwarzian via the conformal bootstrap". In: *Journal of High Energy Physics* 2017.8, 136 (Aug. 2017), p. 136. DOI: 10.1007/JHEP08(2017)136. arXiv: 1705.08408 [hep-th].

[159] Zhenbin Yang. "The Quantum Gravity Dynamics of Near Extremal Black Holes". In: *JHEP* 05 (2019), p. 205. DOI: 10.1007/JHEP05(2019)205. arXiv: 1809.08647 [hep-th].

[160] Alexei Kitaev and S. Josephine Suh. "Statistical mechanics of a two-dimensional black hole". In: *JHEP* 05 (2019), p. 198. DOI: 10.1007/JHEP05(2019)198. arXiv: 1808.07032 [hep-th].

[161] S. Josephine Suh. "Dynamics of black holes in Jackiw-Teitelboim gravity". In: *JHEP* 03 (2020), p. 093. DOI: 10.1007/JHEP03(2020)093. arXiv: 1912.00861 [hep-th].

[162] Lev Davidovich Landau and E. M. Lifshits. *Quantum Mechanics: Non-Relativistic Theory*. Vol. v.3. Course of Theoretical Physics. Oxford: Butterworth-Heinemann, 1991. ISBN: 978-0-7506-3539-4. DOI: 10.1016/C2013-0-02793-4.

[163] Chiang-Mei Chen et al. "Spontaneous pair production in Reissner-Nordström black holes". In: *Phys. Rev. D* 85 (12 June 2012), p. 124041. DOI: 10.1103/PhysRevD.85.124041. URL: https://link.aps.org/doi/10.1103/PhysRevD.85.124041.

[164] Chiang-Mei Chen et al. "Pair production in near extremal Kerr-Newman black holes". In: *Phys. Rev. D* 95 (4 Feb. 2017), p. 044043. DOI: 10.1103/PhysRevD.95.044043. URL: https://link.aps.org/doi/10.1103/PhysRevD.95.044043.

[165] *Black Hole Perturbation Toolkit*. (bhptoolkit.org).

[166] Irene Bredberg et al. "Black hole superradiance from Kerr/CFT". In: *Journal of High Energy Physics* 2010, 19 (Apr. 2010), p. 19. DOI: 10.1007/JHEP04(2010)019. arXiv: 0907.3477 [hep-th].

[167] Thomas Hartman, Wei Song, and Andrew Strominger. "Holographic derivation of Kerr-Newman scattering amplitudes for general charge and spin". In: *Journal of High Energy Physics* 2010 (2010), p. 118. DOI: 10.1007/JHEP03(2023)151. arXiv: 0908.3909 [hep-th].

[168] J.David Brown and Claudio Teitelboim. "Neutralization of the cosmological constant by membrane creation". In: *Nuclear Physics B* 297.4 (1988), pp. 787–836. ISSN: 0550-3213. DOI: https://doi.org/10.1016/0550-3213(88)90559-7. URL: https://www.sciencedirect.com/science/article/pii/0550321388905597.

[169] Boris Pioline and Jan Troost. "Schwinger pair production in AdS2". In: *Journal of High Energy Physics* 2005.03 (Apr. 2005), p. 043. DOI: 10.1088/1126-6708/2005/03/043. URL: https://doi.org/10.1088/1126-6708/2005/03/043.

[170] Sang Pyo Kim and Don N. Page. "Schwinger pair production in dS_2 and AdS_2". In: *Phys. Rev. D* 78.10, 103517 (Nov. 2008), p. 103517. DOI: 10.1103/PhysRevD.78.103517. arXiv: 0803.2555 [hep-th].

[171] *NIST Digital Library of Mathematical Functions*. https://dlmf.nist.gov/, Release 1.2.4 of 2025-03-15. F. W. J. Olver, A. B. Olde Daalhuis, D. W. Lozier, B. I. Schneider, R. F. Boisvert, C. W. Clark, B. R. Miller, B. V. Saunders, H. S. Cohl, and M. A. McClain, eds. URL: https://dlmf.nist.gov/.